

INORGANIC-ORGANIC SOL-GEL DERIVED HYBRID MATERIALS AS ABRASION RESISTANT COATINGS

Chenghong Li

Dissertation submitted to the Faculty of the
Virginia Polytechnic Institute and State University
in partial fulfillment of the requirements for the degree of

Doctor of Philosophy
in
Chemistry

Garth L. Wilkes, Chairman
Judy S. Riffle, Co-Chair
Richey M. Davis
John G. Dillard
Thomas C. Ward

August 1, 1999
Blacksburg, Virginia

Keywords: Abrasion Resistant Coatings, Sol-Gel Processes, Inorganic-
Organic Hybrid Materials, Optical Plastics

Copyright 1999, Chenghong Li

INORGANIC ORGANIC SOL-GEL DERIVED HYBRID MATERIALS AS ABRASION RESISTANT COATINGS

Chenghong Li

[Abstract]

Inorganic-organic hybrid materials have been developed using sol-gel reactions of a trialkoxysilylated organic compound and a metal or semi-metal alkoxide and applied as coatings on polymeric or metallic substrates. Many of these coatings have demonstrated good to excellent abrasion resistance.

Abrasion resistant coatings were prepared by hydrolysis and condensation of mixtures of a triethoxysilylated diethylenetriamine (f-DETA), tetramethoxysilane (TMOS), water and an alcohol in the presence of an acid catalyst (a one-step hydrolysis approach). The influences of many formulation and processing variables on the gelation time, optical properties, hardness and abrasion resistance were investigated. An aminolysis mechanism was also proposed to explain the adhesion between sol-gel derived coatings and polycarbonate substrates promoted by a 3-aminopropyltriethoxysilane (3-APS) primer. FT-IR, GPC, ^1H and ^{13}C NMR, XPS experiments were conducted to support this mechanism.

The f-DETA/TMOS system is essentially a binary system of an alkyltriethoxysilane (T) and a tetraalkoxysilane (Q). At pH 0-2 and pH 4-5, the relative condensation reactivities of the T and Q species in this system were compared using ^{29}Si NMR spectroscopy. After thermal curing, ^{13}C or ^{29}Si solid state NMR spectroscopy was used to estimate the extent of hydrolysis of the urea linkages in f-DETA, the concentration of residual alkoxysilane groups, and the extent of condensation for both T and Q species. The dependence of the morphology of f-DETA/TMOS gels on the pH and the water concentration was also investigated using AFM, SEM and SAXS.

Many other trialkoxysilylated organic compounds containing urea, urethane, epoxy and siloxane linkages were also synthesized and utilized to prepare abrasion resistant coatings via a one-step hydrolysis approach, a two-step hydrolysis approach or a moisture-curing approach. Coatings derived from many of these systems or approaches demonstrated abrasion resistance comparable to that of the f-DETA/TMOS coating. Thin coatings were also derived from cubic octasilicate monomers via hydrosilylation or sol-gel reactions. These coatings were very transparent but unfortunately lacked abrasion resistance.

DEDICATION

To

my wife Yan Yang

my son Roy Young Li

my parents Wanglin Li & Fenglan Cheng

and my sisters Qiaoming Li and Qiaoyan Li

for their sacrifices, encouragement, and all-out support.

ACKNOWLEDGEMENTS

I feel deeply indebted to my graduate advisor Dr. Garth L. Wilkes. Due to his timely and valuable guidance, encouragement, respect, and financial support, I have made important progress not only in my academic capabilities, but also in English language and communication. I would also like to thank Dr. Judy S. Riffle for serving as my co-advisor and the permission to use her laboratory for some of the synthesis work. Thanks are also extended to other graduate committee members for their help and permission to use their equipment.

I will always remember my colleagues in Dr. Wilkes' lab and Dr. Riffle's lab for the great moments I have enjoyed with them. Thanks are given to colleagues in Dr. Wilkes' lab for instrumental training and stimulating discussions, especially, Mr. Kurt J. Jordens for a quick introduction to sol-gel chemistry and abrasion resistant coatings, Mr. Christopher G. Robertson for instrument training, and Mr. Brayn D. Kaushiva for help conducting the SAXS experiments.

Special thanks are given to Mr. Thomas E. Glass for his help with the NMR training and some NMR experiments, Mr. Stephen McCartney for help with AFM experiments, Dr. James E. McGrath and Dr. William Velander for permission to use their equipment, and the secretaries in Department of Chemical Engineering-Sandy Simpkins, Carol Stables, and Karen Bowles for many little but indispensable things to my research work.

LIST OF ABBREVIATIONS

3-APS	3-aminopropyltriethoxysilane
3-GPTMS:	3-glycidoxypropyltrimethoxysilane
3-ICPTES:	3-isocyanatopropyltriethoxysilane
3-MPTMS:	3-methacryloxypropyltrimethoxysilane
AFM	atomic force microscopy
BAPI	bis(3-aminopropyl)imine
bis-A PC	bisphenol-A polycarbonate
CPMAS	cross-polarization magic angle spinning
CR39	diallyl diglycol polycarbonate
DETA:	diethylenetriamine
DISIL	1,3-bis(3-aminopropyl)-1,1,3,3-tetramethyldisiloxane
DLCA	diffusion limited cluster-cluster aggregation
DLMCA	diffusion limited monomer-cluster aggregation
D_{mass}	fractal dimension of mass fractal objects
DMF	N,N-dimethylformamide
DTA	differential thermal analysis
EtOH	ethanol
F-BAPI	the reaction product of bis(3-aminopropyl)imine (1 mole) and 3-isocyanatopropyltriethoxysilane (3 moles)
F-DETA:	the reaction product of diethylenetriamine (1 mole) and 3-isocyanatopropyltriethoxysilane (3 moles)
F-DISIL	the reaction product of 1,3-bis(3-aminopropyl)-1,1,3,3-tetramethyldisiloxane (1 mole) with 3-isocyanatopropyltriethoxysilane (2 moles)
F-EPXY:	the reaction product of ethylenediamine (1mole) with 3-glycidoxypropyltrimethoxysilane (4 moles)
F-ISOP	the reaction product of isophorone diisocyanate (1 mole) with 3-aminopropyltriethoxysilane (2 mole)
F-TEA	the reaction product of triethanolamine (1 mole) and 3-isocyanatopropyltriethoxysilane (3 moles)
F-THPDEA	the reaction product of N, N, N', N'-tetrakis(2-hydroxypropyl)ethylenediamine (1 mole) and 3-isocyanatopropyltriethoxysilane (4 moles)
FT-IR	Fourier transformed infrared spectroscopy
GPC	gel permeation chromatography
IEP	isoelectrical point of colloidal particles
ⁱ PrOH	2-propanol
ISOP	isophorone diisocyanate

MeOH	methanol
M ^H 8Q8	dimethylsilyl cubic octasilicate
MTMS	methyltrimethoxysilane
M ^V 8Q8	vinyltrimethylsilyl cubic octasilicate
NMR	nuclear magnetic resonance
PMMA	poly(methyl methacrylate)
POSS	polyhedral organosilsequioxane
PZC	point of zero surface charge of colloidal particles
Q	Si(OR) _x (OH) _y (OH) _z
Q ^z	Si(OR) _x (OH) _y (OH) _z
Q ^z (x,y)	Si(OR) _x (OH) _y (OH) _z
r	the equivalent ratio of water to alkoxy silane
RLCA	reaction limited cluster-cluster aggregation
RLMCA	reaction limited monomer-cluster aggregation
SAXS	small angle x-ray scattering
SEM	scanning electron microscopy
T	SiR(OR) _x (OH) _y (OH) _z , R is an alkyl group
T4D4	1,3,5,7-tetra(2-trimethoxysilyl)ethyl-1,3,5,7-tetramethyl cyclotetrasiloxane
T4M4Q	tetra((2-tri(methoxy)silyl)ethyl)dimethylsilyl silicate
TEA	triethanolamine
TEOS	tetraethoxysilane
TG	thermogravimetry
THF	tetrahydrofuran
THPDEA	N, N, N', N'-tetrakis(2-hydroxypropyl)ethylenediamine
TiO ⁱ Pr	titanium tetra(2-propoxide)
TMA8Q8	tetramethylammonium cubic octasilicate
TMOS	tetramethoxysilane
T ^{OEt} 8M8Q8	octakis(2-triethoxysilylethyl)dimethylsilyl cubic octasilicate
TS	transition state
T ^z	SiR(OR) _x (OH) _y (OH) _z , R is an alkyl group
T ^z (x,y)	SiR(OR) _x (OH) _y (OH) _z , R is an alkyl group
XPS	x-ray photoelectron spectroscopy

TABLE OF CONTENTS

LIST OF ABBREVIATIONS	v
TABLE OF CONTENTS	vii
TABLE OF FIGURES	xi
LIST OF TABLES	xvii
PREFACE	1
CHAPTER 1. INTRODUCTION	5
1.1. The Sol-Gel Process	5
1.1.1. Sol-Gel Reactions	5
1.1.2. Mechanisms of Sol-Gel Reactions	9
1.1.2.1. Hydrolysis	11
1.1.2.2. Condensation.....	14
1.1.2.3. Alkoxysilane/Silanol Condensations by Metal Salt Catalysts	19
1.1.3. Relevant Concepts of Fractal Analysis and Their Application in the Sol-Gel Process	20
1.1.4. Gelation	26
1.1.5. Structural Evolution Prior to Gelation	27
1.1.5.1. Computer Simulation of Cluster Growth.....	28
1.1.5.2. The pH-Dependence of Sol-Gel Reactions.....	30
1.1.5.3. The pH-Dependence of Cluster Structures	31
1.1.6. Structural Evolution after Gelation	35
1.1.6.1. Aging of Gels	36
1.1.6.2. Drying of Gels.....	37
1.1.7. Advantage and Disadvantages of the Sol-Gel Process	43
1.2. Inorganic-Organic Hybrid Materials.....	44
1.2.1. Embedment of Nanometer Particles into Polymer Matrices.....	44
1.2.2. Co-Hydrolysis & Condensation Methods	45
1.2.3. Impregnation of Polymers into Porous Ceramics	46
1.2.4. In-Site Formation of Metal Oxides in Polymer Networks.....	46
1.3. Abrasion Resistant Coatings	47
1.3.1. Wear Phenomena	47
1.3.2. Approaches for Controlling Polymer Wear	53

1.3.3. Abrasion Resistant Coatings	54
1.3.3.1. Coatings by Plasma Treatment/Polymerization.....	54
1.3.3.2. Inorganic-Organic Hybrid Coatings.....	55
1.3.4. Summary	62
CHAPTER 2. PREPARATION AND CHARACTERIZATION OF ABRASION RESISTANT COATINGS.....	64
2.1. Introduction	64
2.2. Triethoxysilylation of Diethylenetriamine	70
2.3. Formulation of F-DETA/TMOS Coating recipes	71
2.3.1. General Approaches for Coating Formulation.....	71
2.3.2. Nomenclature	75
2.3.3. Examples of Coating Recipes	76
2.3.3.1. F-DETA31TMOS31W5-HCL27	76
2.3.3.2. F-DETA26TMOS26W19-HPO23	77
2.3.3.3. F-DETA22TMOS22W31-HAC140.....	77
2.4. Surface Treatment of Substrates	77
2.5. Coating Formation	78
2.5.1. Spin-Coating	79
2.5.2. Dip-Coating.....	81
2.6. Thermal Curing	83
2.7. Characterization of the Coating	83
2.7.1. Measurement of Coating Thickness.....	83
2.7.2. Evaluation of Adhesion.....	86
2.7.3. Evaluation of Abrasion Resistance	88
2.7.3.1. Standard Taber Abrasion Test.....	88
2.7.3.2. Standard Optical Test for Abrasion Resistance of Transparent Plastics.....	89
2.7.3.3. Evaluation of Abrasion Resistance in this Work	91
2.7.3.4. Microscopy Methods for Evaluation of Abrasion Resistance	94
2.7.3.4.1. Optical Microscopy.....	95
2.7.3.4.2. Scanning Electron Microscopy.....	98
CHAPTER 3. ABRASION RESISTANT COATINGS DERIVED FROM TRIETHOXYSILYLATED DIETHYLENETRIAMINE AND TETRAMETHOXYSILANE. 103	
3.1. Introduction	103
3.2. Experimental	104
3.2.1. Materials and Surface Treatments.....	104
3.2.2. Formulation of Coating Recipe.....	105
3.2.3. Preparation of Abrasion Resistant Coatings	106
3.2.4. Characterization	107
3.3. Results and Discussion.....	109
3.3.1. Optical Properties.....	109
3.3.2. Thermal Curing of the Coatings.....	110

3.3.3. Influences of Formulation and Processing Variables on the Hardness and Abrasion Behavior	115
3.3.4. Abrasion Resistant Coatings on Metal Substrates	124
3.4. Conclusions	126
CHAPTER 4. THE MECHANISM FOR 3-APS TO STRENGTHEN THE INTERFACE BETWEEN POLYCARBONATE AND SOL-GEL HYBRID COATINGS.....	128
4.1. Introduction	128
4.2. Experimental and Characterization Procedures	131
4.3. Results and Discussion.....	133
4.3.1. Solution NMR Experiments.....	133
4.3.2. Surface Analyses for Polymers Treated with 3-APS	137
4.4. Conclusions	140
CHAPTER 5. NMR STUDIES OF SOL-GEL COATING MATERIALS BASED ON TRIETHOXYSILYLATED DIETHYLENTRIAMINE AND TETRAMETHOXYSILANE. 142	142
5.1. Introduction	142
5.2. Experimental	143
5.2.1. Chemicals and Coating Preparations	143
5.2.2. Characterization	145
5.3. Results and Discussions	146
5.3.1. Solution ²⁹ Si NMR Analyses	148
5.3.2. Solid State ¹³ C NMR Analyses	154
5.3.3. ²⁹ Si Solid State NMR Analyses.....	160
5.4. Conclusions	167
CHAPTER 6. MORPHOLOGY OF F-DETA/TMOS GELS..... 169	169
6.1. INTRODUCTION.....	169
6.2. Experimental	171
6.2.1. Materials and Surface Treatments.....	171
6.2.2. Characterization	172
6.3. Results and Discussions	173
6.3.1. The pH-Dependence of Condensation Reactivity for T and Q.....	173
6.3.2. The Influence of pH on the Morphology	176
6.3.3. The Influence of the Water Concentration on Gel Morphology.....	181
6.3.4. The Influence of Drying Speed on the Morphology	187
6.4. Conclusions	189
CHAPTER 7. INORGANIC-ORGANIC HYBRID MATERIALS AND THEIR POTENTIAL AS ABRASION RESISTANT COATINGS. 190	190
7.1. Introduction	190
7.2. Experimental	191
7.2.1. Characterization	191

7.2.2. Chemicals and Preparation.....	192
7.2.2.1. Preparation of F-DETA and F-BAPI (Reference Systems).....	195
7.2.2.1.1. F-DETA	195
7.2.2.1.2. F-BAPI.....	195
7.2.2.2. Preparation of T4M8Q and T4D4.....	196
7.2.2.2.1. T4M4Q.....	196
7.2.2.2.2. M4D4	196
7.2.2.3. Preparation of f-TEA	198
7.2.2.4. Preparation of f-THPDEA	198
7.2.2.5. Preparation of f-DISIL	199
7.2.2.6. Preparation of f-ISOP.....	199
7.2.2.7. Preparation of f-EPXY.....	199
7.2.3. Sol-Gel Coatings by One-Step Hydrolysis	200
7.2.4. Sol-Gel Coatings by Two-Step Hydrolysis.....	203
7.2.4.1. The MTMS/Metal Oxide System.....	204
7.2.4.2. The f-DETA/Silica System	205
7.2.4.3. The f-EPXY System.....	205
7.2.5. Sol-Gel Coatings By Moisture Vulcanization	206
7.3. Results and Discussion.....	207
7.3.1. Optical Properties.....	207
7.3.2. Morphology.....	209
7.3.3. Hardness and Abrasion Resistance	214
7.4. Conclusions	223
CHAPTER 8. COATINGS DERIVED FROM SPHEREOSILICATES.....	224
8.1. Introduction	224
8.2. Experimental	227
8.2.1. Characterization	227
8.2.2. Chemicals and Preparation.....	227
8.2.2.1. Tetramethylammonium Cubic Octasilicate (TMA8Q8).....	227
8.2.2.2. Vinyltrimethylsilyl Cubic Octasilicate (M^V8Q8).....	228
8.2.2.3. Dimethylsilyl Cubic Octasilicate (M^H8Q8)	229
8.3. Coatings through Hydrosilylation	232
8.4. Coatings through the Sol-Gel Approach.....	236
8.4.1. Octakis(2-triethoxysilylethyldimethylsilyl) Cubic Octasilicate ($T^{OEt}8M8Q8$).....	236
8.4.2. Sol-gel Coatings Derived from $T^{OEt}8M8Q8$	238
8.5. Conclusions	240
CHAPTER 9. RECOMMENDATIONS FOR FUTURE WORK	241
BIBLIOGRAPHY.....	244
VITA	256

TABLE OF FIGURES

Fig. 0.1.	Molecular structure of triethoxysilylated diethylenetriamine (f-DETA).....	3
Fig. 1.1.	Silicon derivatives formed during the sol-gel process of a tetraalkoxysilane.	8
Fig. 1.2.	The S_N2 -type reaction mechanism for acid-catalyzed hydrolysis	12
Fig. 1.3.	The two transition state mechanism for the base-catalyzed hydrolysis.....	13
Fig. 1.4.	The one transition state mechanism for the acid-catalyzed condensation for silanetriol.	16
Fig. 1.5.	The two transition state mechanism for the base-catalyzed condensation of silanetriol.	17
Fig. 1.6.	The activation of organotin dicarboxylate in moisture vulcanization	20
Fig. 1.7.	The mechanism of silanol/alkoxysilane condensation in the presence of titanium catalyst.	20
Fig. 1.8.	A schematic Log I(s) vs Log s profile for small angle x-ray scattering for a dilute macromolecular solution.	23
Fig. 1.9.	The experimental scattering curve I(s) resulting from the product of the form factor P(s) and the structure factor S(s) for a system of interacting charged micelles	25
Fig. 1.10.	Simulated structures resulting from various kinetic growth models	29
Fig. 1.11.	Schematic representation of the influences of pH on the rates of hydrolysis (H), condensation (C) and dissolution (D).....	30
Fig. 1.12.	Polymerization behavior of aqueous silica.....	32
Fig. 1.13.	Porod plots of silicate solutions prepared by: (A) two-step acid-catalyzed TEOS system; (B) two-step acid and base-catalyzed TEOS system; (C) one-step base-catalyzed TEOS system ($r=1$); (D) one-step base-catalyzed TEOS system ($r=2$); (E) aqueous silicate system Ludox	35
Fig. 1.14.	Dissolution and reprecipitation cause the growth of necks between particles, increasing the strength and stiffness of the gel.....	37
Fig. 1.15.	Illustration showing three stages of solvent evaporation from gel.....	38
Fig. 1.16.	Illustration showing the liquid/vapor interfaces during different drying stages.....	39
Fig. 1.17.	Schematic representations for drying of a gel obtained by acid catalysis (a) and base catalysis (b), and aging of a particulate silica gel under conditions of high (c) or low (d) solubility	41
Fig. 1.18.	A film gel undergoing a drying process from both surfaces.	42
Fig. 1.19.	Tribological interactions of polymers.....	50
Fig. 1.20.	The mechanisms for abrasive wear.....	51
Fig. 1.21.	A deformation map of MRF80 polycarbonate.....	53

Fig. 2.1.	The one-step approach, two-step approach and moisture vulcanization approach used for preparation of f-DETA/TMOS sol-gel coatings.....	65
Fig. 2.2.	A flowchart showing the six fundamental steps of the one-step approach for preparation of the f-DETA/TMOS sol-gel inorganic-organic hybrid coatings.	68
Fig. 2.3.	Inorganic-organic hybrid materials based on triethoxysilylated diethylenetriamine and tetramethoxysilane.	69
Fig. 2.4.	The f-DETA-TMOS-water- ¹ PrOH quaternary system showing the sections f-DETA47 ¹ PrOH53-TMOS-Water and f-DETA-water- ¹ PrOH.	73
Fig. 2.5.	The compositions of f-DETA/TMOS coating recipes studied in this dissertation..	74
Fig. 2.6.	The compositions of f-DETA gels studied in this dissertation.....	75
Fig. 2.7.	Different stages of the spin coating process	79
Fig. 2.8.	Different stages of the dip coating process: (A-E) Batch; (F) Continuous.	81
Fig. 2.9.	The estimation of coating thickness by scanning electron microscopy.....	84
Fig. 2.10.	Principal components in a Metricon 2021 instrument.....	85
Fig. 2.11.	Measurement of refractive index and thickness of a f-DETA22TMOS22W31-HAC140 coating (n=ca. 1.506) on aluminum foil.....	86
Fig. 2.12.	Illustration of the Taber abrasion test.	89
Fig. 2.13.	Light scattering from the surface of Taber abrasion tracks	90
Fig. 2.14.	Absorbance or transmittance measurement of a Taber wear track.....	92
Fig. 2.15.	Absorbance curves obtained by scanning of a 420 nm and a 633 nm light beam of $0.2 \times 1 \text{ mm}^2$ in size across a Taber track on bis-A PC substrate with a f-DETA100 coating.....	93
Fig. 2.16.	Absorbance curves obtained by scanning 420 nm light beams of $0.2 \times 1 \text{ mm}^2$, $0.4 \times 0.4 \text{ mm}^2$, $0.4 \times 10 \text{ mm}^2$, and $0.4 \times 16 \text{ mm}^2$ in sizes across the Taber track mentioned in Fig. 2.15.....	94
Fig. 2.17.	The transmittance of Taber tracks as a function of the number of abrasion cycles. The substrates for these tests were bis-A PC.....	96
Fig. 2.18.	Mechanisms for material removal[Gahr, 1987 #336].	97
Fig. 2.19.	Transmission optical micrographs of the Taber tracks on an uncoated bis-A PC substrate after 50 (A), 150 (B), 300 (C) and 500 (D) cycles of abrasion	99
Fig. 2.20.	Transmission optical micrographs for the Taber tracks on a bis-A PC substrate with a f-DETA26TMOS26W19-HPO24 coating after 50 (A), 150 (B), 300 (C), and 500 (D) cycles of abrasion.....	100
Fig. 2.21.	Reflection optical micrographs of Taber tracks on bis-A PC substrates with f-DETA22TMOS22W31-HAC140 coatings. Test conditions were (A) CS10F wheels, 500 cycles; (B) CS10 wheels, 500 cycles; (C) CS10F wheels, 1000 cycles; and (D) CS10 wheels, 1000 cycles.....	101

Fig. 2.22.	Reflection optical micrographs and secondary electron micrographs of Taber tracks on bis-A PC substrates: (A) and (C): uncoated, 20 cycles of abrasion; (B) and (D), with f-DETA58Ludox42 coating, 500 cycles of abrasion.....	102
Fig. 3.1.	Molecular structure of bisphenol TMC (1,1-bis(4-hydroxyphenyl)-3,3,5-trimethyl-cyclohexane).....	105
Fig. 3.2.	UV/Vis spectra of free sol-gel films based on gels f-DETA/TMOS and f-DETA/Ludox silica.....	109
Fig. 3.3.	Refractive index of the f-DETA/TMOS coatings obtained using an acetic acid catalyst and cured under different conditions.....	110
Fig. 3.4.	Isothermal TG scans for gel f-DETA22TMOS22W31-HAC140 at various temperatures.....	111
Fig. 3.5.	Isothermal gravimetric diagrams of f-DETA/TMOS gels formulated using different acid catalysts and water concentrations.	112
Fig. 3.6.	The thermal gravimetric profile of gel f-DETA22TMOS22W31-HAC140 obtained at a temperature ramp of 10°C/min.....	113
Fig. 3.7.	Vickers microhardness of f-DETA22TMOS22W31-HAC139 coatings cured at different conditions.....	116
Fig. 3.8.	Dependence of Vickers hardness on the concentration of TMOS.....	117
Fig. 3.9.	Transmission optical micrographs for wear tracks on bis-A PC substrates: (A) uncoated after 150 cycles; (B) coated with f-DETA28TMOS28W10-HPO27 after 500 cycles; (C) coated with f-DETA22TMOS22W31-HAC139 after 500 cycles.	117
Fig. 3.10.	The transmittance of the wear track after 500 cycles of abrasion for 1:1 f-DETA/TMOS coatings on bis-A PC with different ratio of OH/OR	119
Fig. 3.11.	The transmittance through the wear track after 500 cycles for f-DETA26 TMOS26W19 coatings on bis-A PC using HPO or HAC catalysts.....	120
Fig. 3.12.	Transmittance of the wear track after 500 cycles for f-DETA22TMOS22W31-HAC140 coatings on bis-A PC substrates.....	121
Fig. 3.13.	Optical transmittance of APEC-HT9353 [®] polycarbonate coated with f-DETA56TMOS44 sol-gel coatings following the Taber abrasion test	123
Fig. 3.14.	Reflection optical micrographs of aluminum substrates: (A) uncoated and unabraded; (B) uncoated and abraded for 25 cycles; (C) coated with recipe f-DETA26 TMOS26W19-HPO23 and abraded for 500 cycles; (D) coated with recipe f-DETA22 TMOS22W31-HAC140 abraded for 500 cycles.....	125
Fig. 3.15.	Reflectance optical micrographs of (A) uncoated brass surface (unabraded); (B) uncoated brass surfaces after 50 cycles of abrasion; (C) aluminum substrate coated with f-DETA26TMOS26W19-HPO23 after 500 cycles of abrasion	126
Fig. 4.1.	Proposed chemical bonding of 3-APS to a polycarbonate substrate	130
Fig. 4.2.	GPC scans for a bis-A PC sample and a mixture of the polymer with 3-APS.....	133

Fig. 4.3.	^1H NMR spectra for the bis-A PC (A), a mixture of the polymer with 3-APS (B) and 3-APS alone (C).....	134
Fig. 4.4.	The proposed reaction of 3-APS with bisphenol-A polycarbonate	135
Fig. 4.5.	The ^{13}C NMR spectra for a bis-A PC (A) and a mixture of the polymer with 3-APS (B).....	136
Fig. 4.6.	The dispersion FT-IR spectra for a bis-A PC surface with and without treatment by 3-APS.....	137
Fig. 4.7.	The XPS scan for a bis-A PC sample treated with 3-APS and heated at 145°C for 30 min.	140
Fig. 5.1.	^{29}Si NMR spectra acquired at the specified hydrolysis time for 3-MPTES25 TMOS25W18-HAC150, 3-MPTES31TMOS31W5-HCL27, UREA25TMOS25 W18-HAC150 and UREA31TMOS31W5-HCL27.....	150
Fig. 5.2.	Concentration changes of major T^z & Q^z during sol-gel reactions of UREA22 TMOS22W31-HCL140.	151
Fig. 5.3.	Concentration changes of major T & Q during sol-gel reactions of f-DETA22TOS22W31-HAC140.	153
Fig. 5.4.	The ^{13}C NMR spectrum for a f-DETA solution in 2-propanol.....	155
Fig. 5.5.	The ^{13}C CPMAS NMR spectra (contact time=1 ms) for gels f-DETA ^A 31TMOS31 W5-HCL27, f-DETA ^A 22TMOS22W31-HAC140 and f-DETA ^B 22 TMOS22 W31-HAC140.....	156
Fig. 5.6.	The ^{13}C CPMAS NMR spectra acquired at a series of contact times for gel f-DETA22 ^A TMOS22W31-HAC140.....	158
Fig. 5.7.	The relationship between the observed NMR signal I(t) and contact time for gel f-DETA22 ^A TMOS22W31-HAC140.....	158
Fig. 5.8.	The ^{29}Si CPMAS solid state NMR spectra for several f-DETA/TMOS gels prepared under different conditions.....	161
Fig. 5.9.	Intensity of each silicon species as a function of contact time in ^{29}Si CPMAS NMR spectra for gels f-DETA22TMOS22W31-HAC140 and f-DETA31TMOS31W5-HCL27.	163
Fig. 5.10.	^{29}Si MAS NMR spectra (Single-Pulse) for f-DETA31TMOS31W5-HCL27, f-DETA22TMOS22W31-HCL20, f-DETA28TMOS28W10-HPO25, f-DETA22TMOS22W31-HAC140, f-DETA22TMOS22W31-HAC140, and f-DETA22TMOS22W31-HAC140.....	167
Fig. 6.1.	The suggested approximate pH-dependence of the condensation rates for TMOS (①), $\text{EtSi}(\text{OEt})_3$ (②) and f-DETA (③).	175
Fig. 6.2.	Small angle x-ray scattering profiles (arbitrarily shifted along the y-axis) for 0.2-0.3 mm thick f-DETA/TMOS films derived from different acid catalysts.	177
Fig. 6.3.	AFM tapping mode images showing surface features of a f-DETA22TMOS22W31-HCL20 coating.....	180

Fig. 6.4.	AFM tapping mode images showing surface features of a f-DETA22TMOS22W31-HCL20 coating.....	180
Fig. 6.5.	AFM tapping mode images showing surface features of a f-DETA22TMOS22W31-HAC140 coating.....	181
Fig. 6.6.	SEM micrographs of f-DETA gels derived in 2-propanol using HCL catalyst at pH ~0-2. (a) $r = 0.47$, (b) $r=0.93$, (c) $r=1.86$, (d) $r= 3.72$ (e) $r=7.44$, and (f) $r= 14.9$..	184
Fig. 6.7.	SEM micrographs of f-DETA gels derived in ethanol using HCL catalyst at pH ~0-2. (a) $r = 0.47$, (b) $r=0.93$, (c) $r=1.86$, (d) $r= 3.72$ (e) $r=7.44$, and (f) $r= 14.9$	185
Fig. 6.8.	SEM micrographs for gel f-DETA23W33-HAC138 ($r=2.2$) (a) the gel surface; (b) internal fracture surface of the gel.	186
Fig. 6.9.	SEM micrograph for the fracture surface of gel f-DETA26TMOS26W19-HCL24 ($r=2.2$).....	186
Fig. 6.10.	A sectional view of a 0.9-mm thick gel of f-DETA43W8-HCL38 gel showing a structurally compact surface layer.	188
Fig. 7.1.	The ^{13}C NMR spectrum for tetrakis((2-triethoxysilylethyl)dimethylsilyl)tetramethylcyclotetrasiloxane	197
Fig. 7.2.	The ^{29}Si NMR spectrum for tetrakis((2-triethoxysilylethyl)dimethylsilyl)-tetramethylcyclotetrasiloxane. B'=cyclotrisiloxane, B''=cyclopentasiloxane, and A' is due to β -hydrosilylation.	197
Fig. 7.3.	The ^1H NMR spectrum for tetrakis((2-triethoxysilylethyl)dimethylsilyl)tetramethylcyclotetrasiloxane. The Si-CH(CH ₃)-Si linkage is caused by β -hydrosilylation	198
Fig. 7.4.	The GPC chromatograms for f-EPXY after the sample was stored in chloroform for the specified time.....	200
Fig. 7.5.	UV/Vis/Infrared spectra of several sol-gel coatings.....	208
Fig. 7.6.	The relationship between the refractive index and the concentration of silica or zirconia.	209
Fig. 7.7.	SAXS profiles for sol-gel coatings containing Ludox TM-50 silica. (A) Linear plot, (B) Double logarithm plot.	212
Fig. 7.8.	SAXS profiles for sol-gel coatings involving f-EPXY and titanium butoxide	213
Fig. 7.9.	SAXS profiles for the f-EPXY coatings containing titanium butoxide.....	213
Fig. 7.10.	SAXS profiles for RT moisture vulcanized f-DETA sol-gel coatings	214
Fig. 7.11.	Transmission optical micrographs of Taber wear tracks for bis-A PC substrates: (A) Uncoated (20 cycles), (B) coated with f-TEA100 (500 cycles), (C) coated with f-TEA65TMOS35 (500 cycles), (D) coated with f-TEA50TMOS50 (500 cycles).	218
Fig. 7.12.	Transmission optical micrographs of Taber wear tracks on bis-A PC substrates: (A) Uncoated (20 cycles), (B) coated with f-THPDEA100 (500 cycles), (C) coated with f-THPDEA65TMOS35 (500 cycles), (D) coated with f-THPDEA 50TMOS50 (500 cycles).....	219

Fig. 7.13.	Reflection optical micrographs of Taber wear tracks on bis-A PC substrates: (A) Uncoated (20 cycles), (B) coated with f-DETA74Silica26 (500 cycles), (C) coated with f-DETA58Silica42 (500 cycles), (D) coated with f-DETA48Silica52 (500 cycles).....	220
Fig. 7.14.	Reflection optical micrographs for Taber wear tracks on aluminum substrates: (A) coated with f-DETA-Ti (B) coated with f-DETA-Ti, (C) coated with f-DETA-Ti36. Coatings were cured by RT moisture vulcanization for ca. 4 weeks.....	221
Fig. 7.15.	Reflection optical micrographs for Taber tracks on bis-A PC substrates coated with: (A) f-DETA50TMOS50, (B) f-BIPA50TMOS50, (C) MTMS60Silica40, (D) f-ISOP44TMOS66, (E) f-THPDEA50TMOS50, (F) f-DISIL50 TMOS50.....	222
Fig. 8.1.	Molecular structures of POSS and sphereosilicates	225
Fig. 8.2.	Synthetic approaches for TMA8Q8, M ^V 8Q8 and M ^H 8Q8	226
Fig. 8.3.	The solid state ²⁹ Si NMR spectrum for TMA8Q8 crystals	228
Fig. 8.4.	The ¹ H NMR spectrum for octakis(vinyldimethylsilyl) cubic octasilicate	230
Fig. 8.5.	The ²⁹ Si NMR spectrum for octakis(vinyldimethylsilyl) cubic octasilicate.....	230
Fig. 8.6.	The ¹ H NMR spectrum of octakis(dimethylsilyl) cubic octasilicate.....	231
Fig. 8.7.	The ²⁹ Si NMR spectrum of octakis(dimethylsilyl) cubic octasilicate	231
Fig. 8.8.	Preparation of a M ^V 8Q8/M ^H 4Q/ M ^V OM ^V silicone resin by hydrosilylation.	233
Fig. 8.9.	TGA curve (10°C/min) for the M ^V 8Q8/M ^H 4Q/ M ^V OM ^V silicone resin.	234
Fig. 8.10.	DSC curve (10°C/min) for the M ^V 8Q8/M ^H 4Q/ M ^V OM ^V silicone resin.....	234
Fig. 8.11.	Dispersion IR spectrum for the M ^V 8Q8/M ^H 4Q/ M ^V OM ^V silicone resin.....	235
Fig. 8.12.	²⁹ Si CPMAG NMR spectra for the M ^V 8Q8/M ^H 4Q/ M ^V OM ^V silicone resin.....	235
Fig. 8.13.	A synthetic approach for Triethoxysilylation of octakis(vinyldimethylsilyl) cubic octasilicate	236
Fig. 8.14.	The ¹ H NMR spectrum for T8M8Q8.....	237
Fig. 8.15.	The ²⁹ Si NMR spectrum for T ^{OEt} 8M8Q8	237
Fig. 8.16.	The GPC curves for M ^V 8Q8 (before reaction) and T ^{OEt} 8M8Q8 (after reaction) ..	238
Fig. 8.17.	²⁹ Si CPMAS NMR spectra for T ^{OEt} 8M8Q8 gels cured by hydrochloric acid and acetic acid catalysts.....	239

LIST OF TABLES

Table 1.1.	Porod slopes for various structures.....	24
Table 1.2.	Abrasion resistant coatings based on methylsilsesquioxane and silica	56
Table 1.3.	Scratch and Abrasion Tests of different coatings	57
Table 1.4.	Inorganic-organic hybrid coatings and their abrasion resistance reported in reference.	60
Table 1.5.	Typical coatings which have percent transmittance beyond 90% in Taber test with CS-10 abrasers and 500 cycles/500 g.....	61
Table 2.1.	Some chemical reactions that were utilized to attach $-\text{Si}(\text{OR})_3$ groups to organic compounds.....	67
Table 2.2.	Classification of Adhesion Test Results.....	87
Table 2.3.	Adhesion of f-DETA/TMOS coatings on bis-A PC substrates	87
Table 3.1.	F-DETA/TMOS coating recipes and their gelation times and pH.	106
Table 3.2.	Curve-fitting parameters and estimated extent of curing for four f-DETA/TMOS gels.....	114
Table 3.3.	Abrasion resistance of f-DETA/TMOS coatings cured at difference conditions..	122
Table 4.1.	A comparison of chemical shifts for the corresponding carbon atoms in 3-APS and in a mixture of the bis-A PC with 3-APS	136
Table 4.2.	Binding Energies of N 1s electrons for polymer surfaces treated with 3-APS	139
Table 4.3.	Binding energies of N 1s electrons for a few nitrogen containing compounds relative to a saturated hydrocarbon.....	139
Table 5.1.	Compositions of samples, their pH values and reaction times during which NMR spectra were acquired.	149
Table 5.2.	Chemical shifts, cross polarization transfer constants, proton spin-lattice relaxation constants and absolute peak intensities of carbon signals in gel f-DETA ^A 22 TMOS22W31-HAC140.....	159
Table 5.3.	The ratio of unhydrolyzed SiO^iPr and extent of urea hydrolysis for three gels....	160
Table 5.4.	Curve fitting parameters for ²⁹ Si CPMAS NMR spectra of gels f-DETA31 TMOS31W5-HCL27 and of f-DETA22TMOS22W31-HAC140.....	164
Table 5.5.	The distribution of T in gels f-DETA31TMOS31W5-HCL27, f-DETA26TMOS26 W19-HPO23 and f-DETA22TMOS22W31-HAC140.	165
Table 5.6.	The distribution of Q in f-DETA50TMOS50 gels prepared using different acid catalysts and equivalent ratios of water to alkoxysilane.....	166

Table 6.1.	F-DETA50TMOS50 recipes formulated using different catalysts.....	176
Table 7.1.	Chemical structures and abbreviations of compounds containing multiple trialkoxysilyl groups	194
Table 7.2.	Concentrations and particle sizes of silica, zirconia and alumina	195
Table 7.3.	Formulation of T4M4Q/TMOS sol-gel coatings.....	201
Table 7.4.	Formulation of T4D4/TMOS/DMDMS sol-gel coatings	201
Table 7.5.	Formulation of f-THPDEA/TMOS sol-gel coatings	202
Table 7.6.	Formulation of f-TEA/TMOS sol-gel coatings	202
Table 7.7.	Formulation of f-DISIL and f-ISOP sol-gel coatings.....	203
Table 7.8.	Formulation of f-EPXY/TMOS sol-gel coatings.....	203
Table 7.9.	Formulation of f-DETA/Silica coatings	205
Table 7.10.	Preparation of f-EPXY derived sol-gel coatings.	206
Table 7.11.	Formulation of f-DETA derived moisture-curing sol-gel coatings	207
Table 7.12.	Sol-gel coatings and their curing conditions, hardness and abrasion resistance ...	217

PREFACE

Many optical polymers have excellent transparency, lower densities, and better toughness than inorganic glasses and hence are ideal candidates for glazing. Among them, several polycarbonates are extremely tough and can be potentially utilized as glazing for automobiles, trains and airplanes. According to Bayer AG, Germany, and GE Plastics, USA¹⁻³, “the main advantages of polycarbonate glazing materials over glass windows include not only a high degree of design freedom and high resistance to impact and forced entry, but also a weight saving of up to 40 percent. Consequently, replacing glass windows with polycarbonate glazing for automobiles should improve fuel efficiency, lower emission, and reduce the risk of injuries of occupants of vehicles in cases of side impact and roll-over accidents”. However, polycarbonates also have a fatal weakness—very poor wear resistance. Without protection, the material can suffer from severe surface damage and lose transparency quickly during daily use and maintenance. One possible solution to this problem is to apply a thin layer of a hard and tough protective coating. On June 15, 1997, Bayer AG and GE Plastics announced the founding of a joint venture in the field of abrasion-resistant, coated polycarbonate automobile windows¹⁻³. The 50-50 joint venture will invest about \$40 million in research, technology, and equipment during the next few years to develop new abrasion resistant coatings as well as the application and process technologies required to enable broad use of polycarbonate windows in advanced vehicle designs. On March 9, 1998, Bayer AG and GE Plastics announced that they have completed creation of the joint venture and the new company, ExatecTM L.L.C. will be headquartered at Wixom, Mich., with the European headquarters at Cologne, Germany.

Prior to the founding of ExatecTM L.L.C., many acrylate and urethane abrasion resistant coatings were developed for various applications. One of the important applications of these coatings is to protect polymer lenses for the eye-glass industry. Nevertheless, these coatings cannot meet the standard of abrasion resistance for automobile plastic windows. As abrasion resistant coatings for automobile windows, the coating should be nearly comparable to inorganic glasses in abrasion resistance, weatherability and optical clarity. Organic abrasion resistant

coatings have consistently failed to meet the requirements of abrasion resistance. By the Taber abrasion test, a qualified coating should maintain a haze of less than 2% after 1000 cycles of abrasion using a pair of CS10F wheels and a 500-gram load per wheel. Although ceramic coatings can offer this level of abrasion resistance, these coatings are often prepared by chemical vapor deposition (CVD), physical vapor deposition (PVD), surface nitrogeneration, etc., which are not applicable to polymers or require a processing temperature too high for a polymer substrate to sustain.

The sol-gel process based on hydrolysis and condensation of metal or semi-metal alkoxides provides a means to prepare thin ceramic films at low temperature. By this approach, a solution of metal or semi-metal alkoxides is hydrolyzed and condensed in the presence of an acid or base catalyst. The resulting sol is spread on a given substrate, dried at room temperature, and further thermally cured into hard ceramic coatings. Since the condensation is accompanied by release of a large amount of water and alcohol, sol-gel films often crack during the drying and curing processes. It is rather difficult to prepare crack-free coatings thicker than a few hundred angstroms, and sintering at a high temperature is often required for these sol-gel coatings to develop sufficient mechanical properties.

Since the sol-gel process of metal alkoxides is conducted in a solvent, organic materials can be easily incorporated, and this technology has led to the advent of numerous inorganic-organic hybrid materials. Due to the flexibility of the organic component, these hybrid materials can form suitably thick crack-free transparent films. Although the curing temperature is limited by the decomposition temperature of the organic components, these films can have sufficient mechanical properties. Using metal alkoxides and organic modified silanes but by different approaches, Schmidt et al.⁴⁻¹⁰ and Wilkes et. al.¹¹⁻¹⁷ have independently developed inorganic-organic hybrid coatings that exhibit excellent abrasion resistance (see [Chapter 1](#) for details). The Schmidt method is based on the vulcanization of 3-glycidoxypropyltrimethoxysilane (3-GPTMS) or 3-methacryloxypropyltrimethoxysilane (3-MPTMS) modified nanometer metal oxide particles by either ring-opening polymerization of the epoxy groups or the free radical polymerization of the vinyl groups. The Wilkes method, however, is based on the hydrolysis and condensation of

abrasion resistant coatings, is comprehensively reviewed. Many other topics are only briefly discussed based on information from reviews, textbooks, and some original publications. Using the f-DETA/TMOS system as an example, [Chapter 2](#) systematically describes the preparation of abrasion resistant coatings and the basic characterization techniques utilized by the author. Major topics covered in this chapter include trialkoxysilylation reactions, coating formulation, surface treatment of substrates, spin- and dip-coating, thickness measurement, and abrasion resistance evaluation. [Chapter 3](#) addresses the influences of formulation and processing variables on the hardness and abrasion resistance of the f-DETA/TMOS coatings. [Chapter 4](#) describes the mechanism of the primer 3-aminopropyltriethoxysilane to enhance the adhesion of sol-gel hybrid coatings to polycarbonate substrates. [Chapters 5](#) and [6](#) mainly address the influences of pH and the equivalent ratio of water to alkoxy silane on the relative condensation reactivity of $-\text{Si}(\text{OEt})_3$ and $\text{Si}(\text{OMe})_4$ as well as the morphology of the resulting coatings. [Chapter 7](#) explores a wide range of trialkoxysilylated compounds based on linkages of siloxane, urea, urethane and epoxy. In addition to a one-step approach, a two-step approach and a moisture-curing approach are also introduced. In [Chapter 8](#), attempts are also made to prepare sphereosilicate containing abrasion resistant coatings. The dissertation ends with recommendations for further work in [Chapter 9](#).

CHAPTER 1. INTRODUCTION

1.1. THE SOL-GEL PROCESS

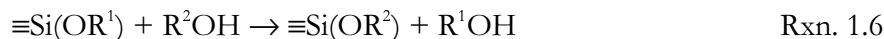
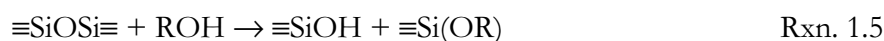
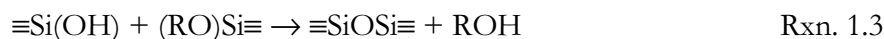
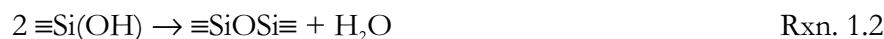
The sol-gel process is a ceramic preparation method based on hydrolysis and condensation of metal or semi-metal alkoxides, halides, nitrates, and other salts. The method has been developed and widely used by ceramists to prepare special chemically uniform complex ceramic powders, coatings and films, foams and monolithic objects, which are difficult to obtain by other methods. The same hydrolysis and condensation reactions are also utilized to prepare cyclic, linear and three-dimensional network polysiloxanes. For example, moisture vulcanization of polysiloxane rubbers is based on the hydrolysis and condensation of silanol/alkoxysilane groups in the polysiloxane recipe. The sol-gel process is very complicated in both chemical kinetics and processing. However, after nearly half a century of continuous developments, abundant knowledge has been accumulated in the sol-gel area and numerous related technologies have been created for various industrial applications. The sol-gel process has been reviewed in a number of papers and books. Among them, *Sol-Gel Science: Physics and Chemistry of Sol-Gel Processing*¹⁸, authored by Brinker and Scherer, is one of the most comprehensive and influential works. Since it is not only unnecessary but also impossible to cover the entire sol-gel area, this chapter will only provide some fundamental knowledge that will help the reader to understand the structures and properties of the inorganic-organic hybrid materials discussed in this dissertation.

1.1.1. Sol-Gel Reactions

The sol-gel process involves hydrolysis of a metal or semi-metal salt and condensation of the resulting hydrolysates. Considering silanes are the critical components for the abrasion

resistant coatings developed in this work, the discussion will focus on sol-gel reactions of tetraalkoxysilanes. Other metal salt systems undergo similar reactions, but may exhibit completely different chemical kinetics. For example, when a metal alkoxide co-hydrolyzes with an alkoxysilane, the metal alkoxide is often much more reactive than the alkoxysilane. To prevent early precipitation of metal oxide, the metal alkoxide is sometimes partially deactivated by reacting with acetylacetonone or other related chelating reagents.

The sol-gel process of alkoxysilanes, for example, tetramethoxysilane (TMOS) and tetraethoxysilane (TEOS), begins with the hydrolysis of silicon alkoxide, which gives silanols and alcohol according to Rxn 1.1



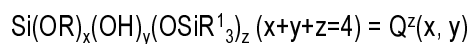
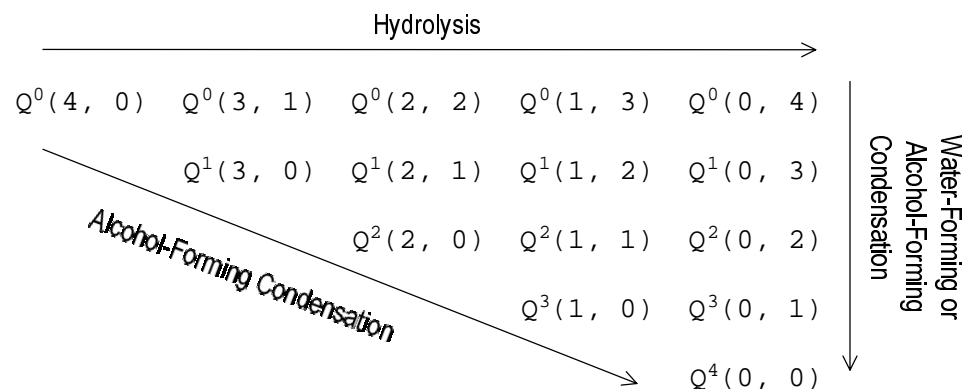
The generated silanols immediately begin to self-condense to form siloxanes and the by-product water and this reaction is referred to as *water-forming condensation* (Rxn 1.2). The term *oxolation* is used for similar reactions in metal alkoxide systems. The silanols also react with alkoxysilanes to give siloxanes and alcohol and this reaction is referred to as *alcohol-forming condensation* (Rxn 1.3). Similar reactions in metal systems are termed *alcoxolation*. The reverse reactions of the hydrolysis, water-forming condensation, and alcohol-forming condensation are called (*re*)*esterification* (Rxn 1.4), *hydrolysis of siloxanes* (Rxn 1.5) and *alcoholysis of siloxanes* (Rxn 1.6), respectively. If the sol-gel process is conducted in an alcoholic medium, the exchange of alcohol between the alkoxysilane and the solvent is also important and this exchange reaction is usually termed *transesterification*. Finally, silanols, as Bronsted acids, can react with bases to produce silanolates (Rxn 1.7). For example, tetrahydroxysilane or orthosilicic acid reacts with sodium hydroxide to form sodium silicates. The hydrolysis and condensation reactions are the

most important reactions in the sol-gel process. Other reactions also influence the kinetics of the sol-gel process and their relative importance depends on the concentration of the reactants, pH, temperature and pressure.

Alkoxysilane molecules involved in a sol-gel process can include one to four alkoxy substituents, these alkoxysilane groups undergo gradual hydrolysis and condensation, thus leading to many monomeric or polymeric molecules. The structure of these molecules can be mainly defined by the substituents of the silicon atoms and the siloxane network linking these silicon atoms. During the sol-gel process, common substituents for a silicon atom include alkyl (R), alkoxy (OR), hydroxy (OH), and silyloxy ($-\text{OSi}\equiv$, Si-O-Si oxo bridge bond) groups. In silicone chemistry, the letters M, D, T and Q are widely used to symbolize silicon atoms carrying three to zero alkyl substituents, respectively. Silicon species with different numbers of alkyl and silyloxy substituents can be easily distinguished by both solution and solid state ^{29}Si NMR spectroscopy. Hydroxy and alkoxy substituents cause smaller changes to the chemical shift of the central silicon atom, so silanols and alkoxysilanes similar in structure can only be distinguished by high resolution solution FT-NMR spectroscopy. The number of silyloxy substituents reflects the way the silicon atom is linked to the rest of the molecule, while other groups are just “dangling” groups, which are structurally less important. Therefore, the average number of silyloxy substituents can reflect the extent of condensation for silicon species (M, D, T, or Q) in the system. In ^{29}Si NMR spectroscopy, silicon species with *different numbers of alkyl and silyloxy substituents* are specified by the Eggelhardt notation¹⁹. In this notation, the number (0-4) of silyloxy substituents is indicated by a superscript to the right side of the symbol (e.g. T or Q) for the silicon atom. For example, Q^z represents any silicon atoms that have a formula $\text{Si}(\text{OR})_x(\text{OH})_y(\text{OSi}\equiv)_z$ ($x+y+z=4$). The Eggelhardt notation can be conveniently used to describe the backbone of a siloxane molecule. However, when dealing with the kinetics of sol-gel reactions, where the influence of alkoxy and hydroxy groups is important, the numbers of these groups are also specified^{20,21}. In this dissertation, the notations $\text{Q}^z(x, y)$ and $\text{T}^z(x, y)$ are designated for silicon species that have a general formula $\text{Si}(\text{OR})_x(\text{OH})_y(\text{OSi}\equiv)_z$ ($x+y+z=4$) and $\text{RSi}(\text{OR})_x(\text{OH})_y(\text{OSi}\equiv)_z$ ($x+y+z=3$). For example, the symbols $\text{Q}^0(4, 0)$, $\text{Q}^0(0, 4)$ and $\text{Q}^4(0, 0)$

represent tetraalkoxysilane, orthosilicic acid and a *completely condensed Q*, respectively. Similarly, $T^0(3, 0)$, $T^0(0, 3)$ and $T^3(0, 0)$ represent alkyltrialkoxysilane, alkylsilanetriol, and a *completely condensed T*, respectively.

Using the $Q^z(x, y)$ notation, the sol-gel process of a tetraalkoxysilane can be illustrated in Fig. 1.1. In this figure, moving horizontally from the left to the right corresponds to the hydrolysis of the left alkoxysilane, and moving diagonally from left top to the right bottom corresponds to the alcohol-forming condensation of the upper left alkoxysilane. However, moving vertically from the top to the bottom can correspond to either the water-forming condensation of the upper silanol or the alcohol-forming condensation of the upper silanol. The ultimate condensation product should be quartz, which contains $Q^4(0, 0)$ exclusively, However, normal sol-gel processes of tetraalkoxysilanes are far from complete, and the final products often include a distribution of these fifteen $Q^z(x, y)$ species. The sol-gel process of alkyltrialkoxysilanes (T) can be similarly illustrated using the ten $T^z(x, y)$ species.



R = alkyl groups

R^1 = any alkoxy, hydroxy or silyloxy group

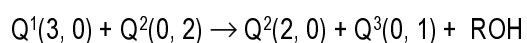
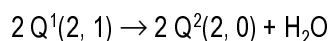
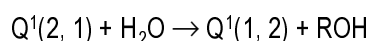


Fig. 1.1. Silicon derivatives formed during the sol-gel process of a tetraalkoxysilane. Modified according to the literature²⁰⁻²²

1.1.2. Mechanisms of Sol-Gel Reactions

The sol-gel process can be promoted by acids, bases, and some metal salts. Acids and bases are commonly used as catalysts in sol-gel processes, while metal salt catalysts, such as dibutyltin dioctate and titanium (IV) salts, are frequently used for room temperature moisture vulcanization of silanol terminated polysiloxanes²³. Silanol condensation can also be promoted thermally and this is the basis for thermal curing of sol-gel derived materials.

Sol-gel reactions, including hydrolysis, condensation, transesterification and reesterification, are essentially nucleophilic replacement of one or more substituents at the central metal or semi-metal atom by nucleophiles such as water (hydroxide ions), alcohols (alkoxide ions), silanols (silanolate ions) and alkoxy silanes. Due to the similarities, the nucleophilic replacement mechanisms of the corresponding carbon compounds were immediately utilized to explain some experimental facts found in sol-gel reactions. The nucleophilic replacement of a carbon compound can often be explained by a mechanism between two limiting cases²⁴, the S_N1 mechanism and the S_N2 mechanism. By the S_N1 mechanism, the substrate first dissociates into a carbocation intermediate (R^+) and a leaving group in a rate-determining step, then in a second step, the carbocation quickly combines with the nucleophile. The overall reaction is only first-order with regard to the substrate. However, in the S_N2 mechanism, the attack of the nucleophile and elimination of the leaving group occurs concertedly in a rate-determining step through a triangular bipyramid transition state (TS). The overall reaction is first-order with regard to the substrate and nucleophile. In most cases, the addition of the nucleophile and elimination of the nucleophile are neither sequential nor synchronous, i.e., the substrate has partially dissociated before the addition of the nucleophile. The extent of dissociation is dependent on the polarity and dielectric constant of the solvent, and the overall reaction maintains first order with regard to the substrate and nucleophile.

For the sol-gel process of metal or semi-metal alkoxides, however, the empty d-orbitals of the central metal or semi-metal atom can also participate in chemical bonding, and hence enable an expansion of the coordinate number from four to five or six. Therefore, the addition of a nucleophile often results in a metastable penta- or hexa-coordinate silicon intermediate, which

decomposes subsequently to the final products. Aluminum alkoxides are an exception because the aluminum atom forms only three covalent bonds with alkoxy groups, and hence it can accept a nucleophile by expanding its coordination number from three to four using its empty p-orbital. The presence of such a metastable intermediate not only increases the reaction rate by reducing the activation energy, but also changes the nucleophilic displacement mechanism to a nucleophilic addition/elimination mechanism (referred to as S_N2^{**} or S_N2^* in reference ¹⁸). The overall reaction rate is also first-order with respect to the substrate and nucleophile by the addition/ elimination mechanism.

Most transition metal ions often can form stable penta- or hexa-coordinate compounds by hybridizing their (n-1)d orbitals with their *ns* and *np* orbitals. The silicon atom, however, must use its *3d*-orbitals to hybridize with its *3s* and *3p* orbitals to promote such a high coordination number. Since this hybridization is energetically less favorable, silicon typically forms tetra-coordinate compounds. Penta- or hexa-coordinate silicon compounds can only be found in fluorosilicates (i.e. K_2SiF_6) and ring-strained compounds. However, the involvement of *3d*-orbitals in sol-gel reactions has been supported by the fact that silicon halides and alkoxides hydrolyze much faster than the corresponding carbon compounds. The especially strong catalytic effect of fluorides for sol-gel reactions of tetraalkoxysilanes^{24,25} is also ascribed to the involvement of a penta- or hexa-coordinate silicon intermediate.

Both the S_N2 -type mechanism (either concerted or non-concerted) and the addition/elimination mechanism can explain most experimental facts. It is difficult to tell which is the real mechanism unless the intermediates (penta- or hexa-coordinate silicon) are confirmed or captured. No well-documented examples of unimolecular reactions have been reported to support any kind of S_N1 mechanism (siliconium intermediate), although this possibility cannot be completely excluded¹⁸. Generally, the acid catalyzed reactions are more likely to occur by a S_N2 mechanism; while the base catalyzed reactions are more likely to occur by an addition /elimination mechanism (Sections 1.1.2.1 and 1.1.2.2).

Both the nucleophilic substitution mechanisms (including S_N1 and S_N2) or the nucleophilic addition/elimination mechanisms have been historically used to explain acid- or base-catalyzed sol-gel reactions including hydrolysis, condensation, reesterification and

transesterification. These mechanisms have been reviewed comprehensively by Brinker and Scherer in Chapter 3, *Sol-Gel Science*¹⁸. The following discussion is only limited to well-accepted mechanisms for the hydrolysis and condensation of alkoxysilane.

1.1.2.1. Hydrolysis

A few in depth kinetic studies have been conducted for acid/base catalyzed hydrolysis of alkoxysilanes²⁶⁻³². Listed below are some experimental facts about the rate laws, stereochemistry, steric effects, inductive effects, and solvent effects for these reactions.

- 1) **Rate laws:** acid catalyzed hydrolysis usually shows third-order reaction kinetics (first order in the silane, water, and acid catalyst)^{26,27}, while the base catalyzed hydrolysis is only first order in the silane and the base^{26,28}.
- 2) **Stereochemistry:** in many cases, the hydrolysis is accompanied by inversion of the silicon configuration, especially silanes with good leaving groups like $-X$ (halide) and $-OCOR$ ²⁸. However, configuration retention has also been observed in sterically hindered systems or systems involving poor leaving groups such as $-OR$ and $-OH$ ^{29,30}.
- 3) **Steric effects:** Both acid- and base-catalyzed hydrolyses can be hindered by bulky substituents of the silane³¹.
- 4) **Inductive effects:** inductive effects are usually less important than steric effects. However, they are quite manifest for organic modified silanes $R_xSi(OR)_{4-x}$ ³². By acid catalysis, the hydrolysis rate of $R_xSi(OR)_{4-x}$ increases significantly as the number of alkyl substituents (x) increases; however, the opposite tendency holds for based catalyzed hydrolysis.
- 5) **Solvent effects:** acid-catalyzed hydrolysis has no obvious solvent effects, but relatively large solvent effects are observed in base-catalyzed hydrolysis. In base-catalyzed hydrolysis of TEOS, the hydrolysis rate in dioxane is much slower than the rate in ethanol, which in turn is slower than in methanol²⁶.

The acid-catalyzed hydrolysis is believed to occur through a S_N2 substitution²⁸. By this mechanism, the alkoxysilane is first protonated by the acid in a quick near equilibrium reaction. The water molecule attacks the protonated silane from the rear of the protonated alkoxy group,

and forms a triangular bipyramid *TS* (Fig. 1.2). In the *TS*, both the water and protonated alcohol molecules occupy the axial positions while the other three groups take the equatorial positions. The water molecule acquires a partial positive charge from the protonated alkoxy. The *TS* decomposes subsequently to a protonated silanol by eliminating an alcohol molecule, and the process is accompanied by inversion of the silicon tetrahedron. The protonated silanol later transfers the proton to water, alkoxy silanes, alcohols, or other silanols. The rate-determining step in this mechanism is the attack of the water molecule at the protonated alkoxy silane. Based on this mechanism, the overall reaction is first-order with regard to the concentrations of acid, water and silane, respectively.

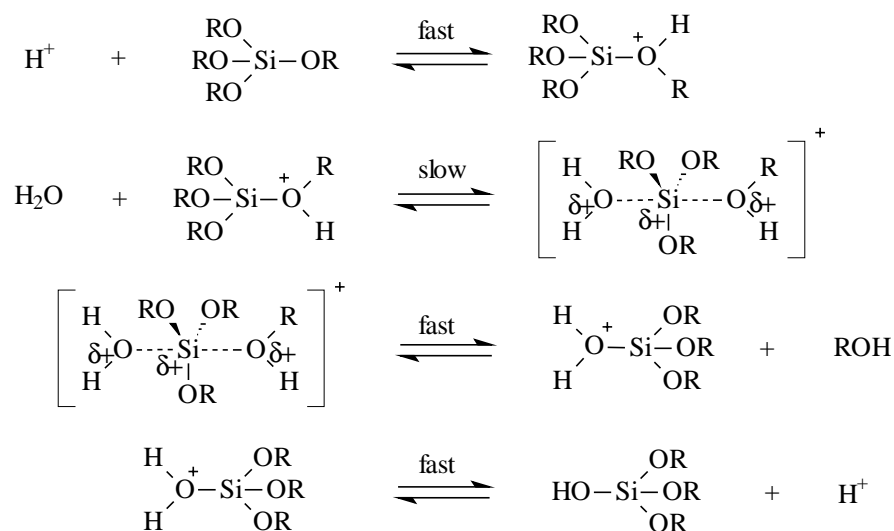


Fig. 1.2. The S_N2-type reaction mechanism for acid-catalyzed hydrolysis. Modified according to Pohl et al.²⁸

According to this mechanism, the acid-catalyzed hydrolysis should have a slight negative inductive effect due to the partial positive charge in the transition state. In other words, electron-donating groups such as alkyl groups are expected to increase the hydrolysis rate. The major function of the acid is to protonate the alkoxy group and make it a good leaving group, so strong Lewis acids may also be good acid catalysts according to this mechanism. Bulk substituents can apparently prevent the nucleophile from approaching the central silicon atom, thus reducing the

hydrolysis rate. The rate law, stereochemistry, inductive effects and solvents effects derived from this mechanism can successfully explain the experimental facts stated earlier in this section.

The retention of the silicon configuration in some cases has been explained by a nucleophilic addition/elimination mechanism that involves the flank-side attack of the water molecule to a neutral alkoxy silane³³. In this mechanism, the water molecule occupies an axial position in the *intermediate*, and later transfers a proton to the leaving alkoxy group that takes up an equatorial bond (bonds in the triangular plane), leading to a retention of the silicon configuration.

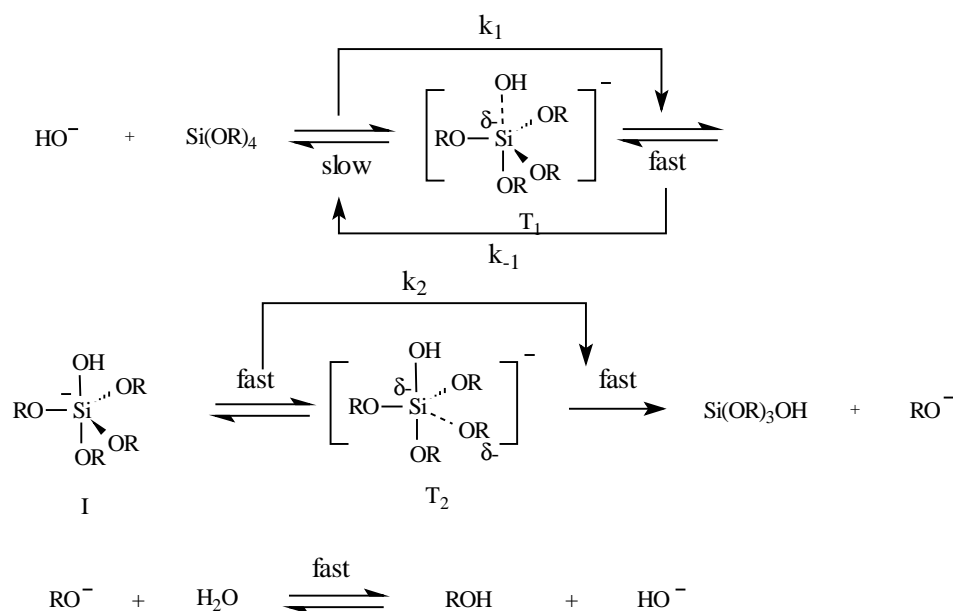


Fig. 1.3. The two transition state mechanism for the base-catalyzed hydrolysis. Modified according to Pohl et al.²⁸

The base catalyzed hydrolysis has been explained by both the S_N2 mechanism³⁴ and the nucleophilic addition/elimination mechanism²⁸. However, the latter mechanism is more widely accepted. According to this mechanism (Fig. 1.3), the hydroxide ion from the base attacks the silane through a first TS to form a penta-coordinate silicon metastable intermediate. The intermediate decomposes subsequently through a second TS to a silanol and an alkoxide ion, which later acquires a proton from water and regenerates the hydroxide ion. Since the water

concentration is far greater than the base concentration, the hydrolysis rate is only first order in the silane and the hydroxide ion according to the steady state approximation.

In this mechanism, the central silicon atom in both TSs and intermediate possesses a negative charge, so a strong positive inductive effect is expected, i.e. electron-withdrawing substituents are expected to increase the hydrolysis rate. In addition, the promotion of hydrolysis rate by polar solvents should also be observed if this mechanism is correct. The rate law, inductive effects, and solvent effects suggested by this mechanism are in accord with the experimental results mentioned earlier for the base catalyzed hydrolysis.

1.1.2.2. Condensation

The condensation of alkoxy silanes includes two parallel reactions: the water-forming condensation and alcohol-forming condensation. Both can be catalyzed by acids, bases, and some metal salts. Dibutyl dioclate and TAZOR catalysts (DuPont) based on titanium salts are effective catalysts for room temperature moisture vulcanization of silanol/ alkoxy silane containing polysiloxanes³⁵, but they are rarely used in the sol-gel process.

The condensation of silanols/ alkoxy silanes has not been well studied because the reaction is much more complicated than the hydrolysis of alkoxy silanes. Only a few stable silanols, such as diphenylsilanediol, 3-aminopropylsilanetriol, are thermally stable at room temperature and may be used as starting materials for such studies. Most kinetic studies had to be based on the collective behaviors (e.g. the gelation time, viscosity) observed during sol-gel reactions of alkoxy silanes. The following are a few experimental facts about the rate law, inductive effect, and steric effects about some acid/base catalyzed condensation of silanols/alkoxy silanes:

- 1) **Rate laws:** Pohl and Osterholtz²⁸ have studied the dimerization of several alkylsilanetriols. They found that in acid catalysis, the dimerization rate was proportional to the proton concentration and the silanetriol concentration squared, while in base catalysis, it was proportional to the base concentration and the silane concentration squared.
- 2) **Inductive effects:** the inductive effect in condensation is similar to that of hydrolysis. By acid catalysis, ethylsilanetriol condenses faster than orthosilicic acid in a ²⁹Si NMR study of

a mixture of ethyltriethoxysilane and TEOS³⁶. It has been also found that pH at which the condensation occurred at a minimal rate increased in the order of $\text{RSi}(\text{OH})_3 < \text{R}_2\text{Si}(\text{OH})_2 < \text{R}_3\text{SiOH}$ ²⁸. These experimental results suggest that electron-donating substituents can increase the reactivity of silane in an acid catalyzed condensation, but decrease that in a base catalyzed condensation.

- 3) **Steric effects:** the condensation also exhibits an obvious steric effect. Voronkov et al have found that the condensation rate of triorganosilanols decreases as both the length /branch of the chain of the alkyl substituents and the number of aromatic substituent increase³¹. Although inductive effects are clearly important, Voronkov et al also stated that in the acid-catalyzed condensation of dialkylsilanediol, steric effects predominated over inductive effects³¹. This conclusion was further extended to that the inductive effects resulting from longer-chain alkyl substituents were unimportant for functional silanes that carry the same number of alkyl groups³¹.

Various reaction mechanisms have been proposed to explain these experimental data. The $\text{S}_{\text{N}}2$ mechanism has been frequently used to explain the acid-catalyzed condensation²⁸. By this mechanism, the condensation begins with the rapid protonation of silanol groups (vs alkoxy silane groups in hydrolysis). Then another silanol molecule attacks the protonated silanol to form a triangular bipyramid silicon TS, which subsequently releases a water molecule and forms a siloxane bond. If the attacking silanol group is replaced by an alkoxy silane group, then the reaction becomes an alcohol-forming condensation. However, due to the increased steric hindrance (-R vs -H), this reaction is expected to be more difficult.

Figure 1.4 shows the $\text{S}_{\text{N}}2$ -type mechanism for the acid catalyzed dimerization of silanetriol. In the TS, the silicon atom possesses a partial positive charge, and hence electron-donating substituents should increase the condensation rate. Assuming the reaction of a silanol with the protonated silanol (k_2) is the rate-determining step, the condensation rate law can be derived as:

$$-\text{d}[\text{silanetriol}]/\text{dt} = k_1 k_2 / k_{-1} [\text{silanetriol}]^2 [\text{H}^+] \quad \text{Eqn. 1.1}$$

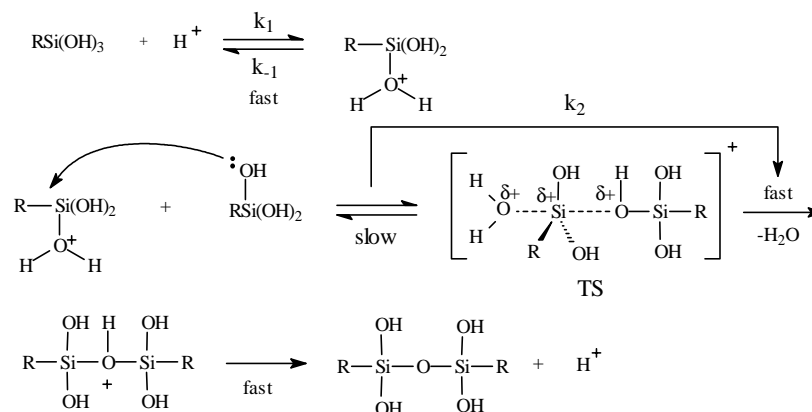


Fig. 1.4. The one transition state mechanism for the acid-catalyzed condensation for silanetriol. Modified according to Pohl et al.²⁸

The base-catalyzed condensation probably proceeds via a nucleophilic addition/elimination mechanism. By this mechanism, the reaction begins with the deprotonation of silanol. Then the resulting silanolate ion reacts with a neutral silanol by forming a negatively charged penta- or hexa-coordinated intermediate³⁷⁻⁴¹, which decomposes subsequently to siloxane and regenerates the hydroxide ions, leading to a water-forming condensation. The hexa-coordinate silicon intermediate has also been proposed to explain the large negative activation volume for the base catalyzed condensation obtained from the dependence of condensation rate on pressure³⁸.

Figure 1.5 shows the addition/elimination mechanism proposed by Swain et al. using the base-catalyzed condensation of silanetriol as an example³⁹. The reaction rate derived from this mechanism is first order to the base but second order to the silanol²⁸. The mechanism can accommodate the alcohol-forming condensation by allowing the silanolate ion to attack neutral alkoxy silane. Because of the full negative charge in the TSs and intermediate, the reaction is expected to exhibit strong positive inductive effects, so electron-donating substituents should strongly promote the rate of the base-catalyzed condensation.

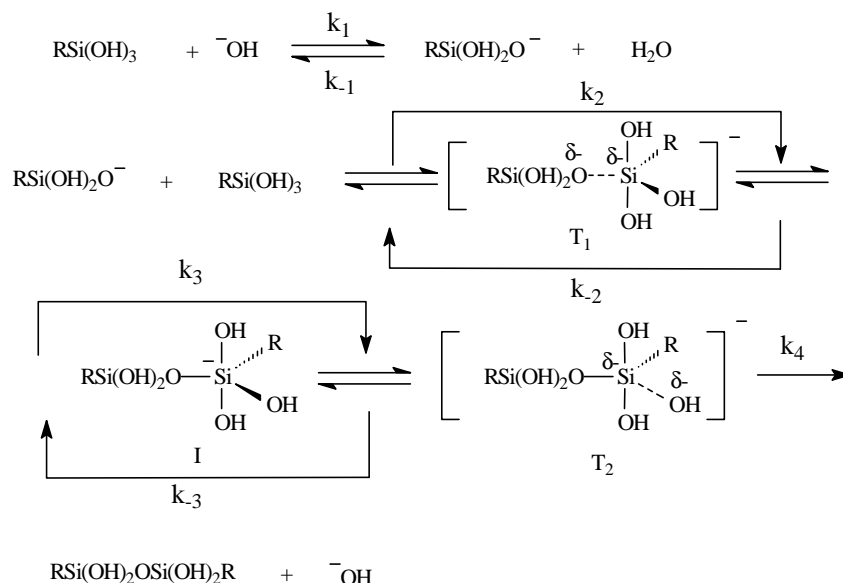


Fig. 1.5. The two transition state mechanism for the base-catalyzed condensation of silanetriol. Modified according to Swain et al.³⁹

In both acid and base catalyses, the rate of alcohol-forming condensation is proportional to the concentration of silanol, alkoxy silane, and the catalyst concentration (third-order overall kinetics). Equation 1.2 provides the rate law for the acid catalyzed condensation, which consists of the contribution of water-forming condensation and alcohol-forming condensation.

$$d[(\text{SiO})\text{Si}]/dt = k_{\text{cw}}[\text{SiOH}]^2[\text{H}^+] + k_{\text{ca}}[\text{SiOH}][\text{SiOR}][\text{H}^+] \quad \text{Eqn. 1.2}$$

k_{cw} is the rate constant of the water-forming condensation, k_{ca} is the rate constant of the alcohol-forming condensation. The rate law for base-catalysis condensation can be obtained by substituting $[\text{OH}^-]$ for $[\text{H}^+]$. Since the silanol concentration increases with the water concentration in a sol-gel process, it is expected that the water-forming condensation predominates in a water-abundant condition, while in a water-deficient condition, the alcohol-forming condensation prevails.

The electron-withdrawing ability of major substituents in a sol-gel process increases in the order $\text{OR} < \text{OH} < \text{OSi}\equiv$ ⁴². If the inductive effect is the primary factor governing the sol-gel process, silanols or alkoxy silanes with more silyloxy substituents (i.e. Q^2 or Q^3) should be more easy to deprotonate but more difficult to protonate. On the other hand, for silanols or

alkoxysilanes having less silyloxy groups, the oxygen atoms should be more nucleophilic, while the central silicon atoms should be less electrophilic. Consequently, condensation between silanols or alkoxysilanes with less silyloxy substituents (i.e. Q^0 - Q^0) prevails in acid catalysis, while in base catalysis, the most favorable condensation should be between silanols or alkoxysilanes with more silyloxy substituents (i.e. Q^3 - Q^3).

However, except for the inductive effect, sol-gel reactions are also subject to the influences of steric hindrance. The steric hindrance of the substituent increases in the order $\text{OH} < \text{OR} \ll \text{OSi}\equiv$, so the reactivity of Si-OH/Si-OR is expected to decrease with the increase of the number of silyloxy groups of the silicon central atom. Hence, the monomeric species (without any silyloxy group) should be more reactive than the polymeric species if only the steric effect is considered. In acid catalysis, the steric effect is in accord with the inductive effect, so the most favorable condensation occurs between monomeric species. For this reason, during the sol-gel process of tetraalkoxysilane, the system quickly consumes its monomeric species and the later condensation occurs mainly between the clusters (cluster-cluster reaction). In basic catalysis, however, the steric effect counteracts the inductive effect. Although silanols with more silyloxy substituents are more sterically hindered, they are easier to deprotonate to silanolate active species, which is indispensable for base catalyzed condensation. Therefore, the most favorable condensation in base catalysis, in reality, is often between the least sterically hindered monomeric species and the sterically more hindered, but more abundant, silanolate species (monomer-cluster reaction).

Reactions between neighboring groups, which lead to closed-loop condensations, are also very important in the sol-gel process. Under similar conditions, neighboring silanol/alkoxysilane groups in the same molecule or cluster often have more chances to collide with each other, hence, they often react faster than groups from two different molecules or clusters.

The pH of the medium is the critical factor that determines whether the reaction occurs by acid-catalysis or base-catalysis. The acid catalyzed sol-gel reactions of TMOS have been studied by Assink et al. by ^1H and ^{29}Si NMR^{21,22,43}. In an acidic solution (1.64×10^{-3} M HCl), the hydrolysis was, as expected, much faster than related condensation reactions. The rate constants for hydrolysis, water-forming condensation and alcohol-forming condensation were ca. 0.2,

0.006 and 0.001 mol⁻¹min⁻¹, respectively. Similar studies have also been carried out by Pouxviel for TEOS⁴⁴. The hydrolysis and condensations of this compound were significantly lower than those of TMOS because of the steric hindrance of the relatively large ethoxy groups.

Assuming equal reactivities of silanol groups and alkoxy silane groups, Assink et al. have simulated the early sol-gel process of TMOS²⁰. The calculated results based on the rate constants mentioned above were compared with ²⁹Si NMR results²⁰. The hydrolysis and condensation reactions of monomeric species were in accord with the prediction. However, the concentrations of Q¹ were underestimated while the concentrations of Q² were overestimated. The disagreements between the modeling and the experimental data indicated that steric effects, inductive effects and cage effects have significant influences over the reactivity of functional groups. Therefore, the equal reactivity assumption, which is rather successful in organic polymerization, does not hold true in the sol-gel process.

1.1.2.3. Alkoxy silane/Silanol Condensations by Metal Salt Catalysts

Inorganic or organic metal salts such as dibutyl dioctate and titanium tetrabutoxide have been applied to promote silanol condensation. These catalysts have been widely used to vulcanize one-part or two-part polysiloxane products³⁵. Silanols in these recipes are either from silanol terminated polysiloxanes or from the hydrolysis products formed by reaction of the alkoxy silane in the system with moisture in air.

During the reaction, the metal salt catalyst reacts with silanol to form M-O-Si bonds (M=metal), which constitute the catalytic center of silanol condensation. A few mechanisms and active species have been proposed to explain the catalytic effect of dibutyltin dioctate for silanol/alkoxy silane condensation. These mechanisms involve complexes containing Sn-O-Si reactive bonds²³. The condensation occurs as free silanol groups attack the silicon atom of the reactive species by replacing the tin complex (Van der Weij)⁴⁵ or one of the alkoxy substituents (Severnyi et al.)⁴⁶. According to Severnyi et al. and Van der Weij, the role of atmospheric moisture is to modify the tin carboxylate and convert it into an active tin hydroxide that can react with the alkoxy silane to produce an organotin silanolate.

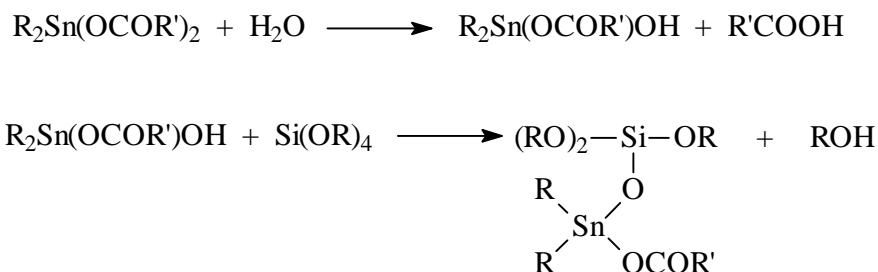


Fig. 1.6. The activation of organotin dicarboxylate in moisture vulcanization

Titanium catalysts are frequently used to formulate one-part silicone resins using hydroxy terminated polydimethylsiloxane. It is well known that titanium alkoxides can be decomposed by almost any compound containing active hydrogen, such as water and alcohol. Although it is not clear what is the active form of the catalyst and which is the critical step, the mechanism of moisture vulcanization has been proposed to be as follows²³:

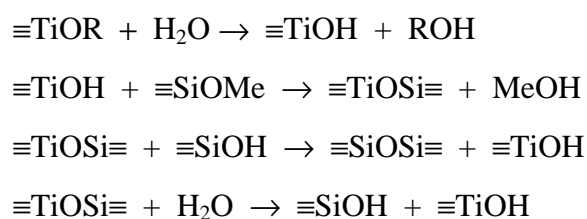


Fig. 1.7. The mechanism of silanol/alkoxysilane condensation in the presence of titanium catalyst.

In this dissertation, titanium butoxide is used as the catalyst for moisture cured one-part sol-gel coatings that include organic modified silanes and pre-hydrolyzed TMOS. Except for the two metal salts mentioned above, metal oxide colloids such as alumina and zirconia also showed some catalytic effects on silanol/alkoxysilane condensation (see [Chapter 7](#)).

1.1.3. Relevant Concepts of Fractal Analysis and Their Application in the Sol-Gel Process

The structures of clusters or particles generated by the sol-gel process are typically highly irregular or disordered. These clusters and particles can often be described mathematically as

fractals, which are characterized by self-similarity (more accurately defined by both dilation invariance and translation variance)⁴⁷. The self-similarity means the invariance of the structure (including statistically invariance of structure) under different levels of resolution, i.e. similar structure features, are exhibited under different magnifications.

The fractal concept can be explained using a lattice representation. Suppose 3-dimensional space is divided equidistantly along the x, y, z axes, an object can be divided into mass sites (occupied sites), surface sites (occupied sites with adjacent empty sites) and pore sites (empty sites in the convex hull of the occupied sites)⁴⁷. The numbers of the three types of sites (M_{mass} , M_{surf} , or M_{pore}) within a radius R from a fixed site of each type scales with R according to the following equations.

$$M_{\text{mass}}(R) \propto R^{D_{\text{mass}}} \quad \text{Eqn. 1.3}$$

$$M_{\text{surf}}(R) \propto R^{D_{\text{surf}}} \quad \text{Eqn. 1.4}$$

$$M_{\text{pore}}(R) \propto R^{D_{\text{pore}}} \quad \text{Eqn. 1.5}$$

where D_{mass} , D_{surf} and D_{pore} are fractal dimensions for the related mass fractal, surface fractal and pore fractal. If mass and surface scale alike, the object is called a *mass fractal* ($D_{\text{surf}}=D_{\text{mass}}$); if the pore space and surface scale alike ($D_{\text{pore}}=D_{\text{surf}}$), it is called a *pore fractal*; if only the surface is fractal (i.e. $D_{\text{pore}}=D_{\text{surf}}=3$), the system is called a *surface fractal*, or a *boundary fractal*. Note a pore fractal can be viewed as a reverse mass fractal. If the occupied sites and unoccupied sites are interchanged, the pore fractal becomes a mass fractal. Physically, the fractal dimension D reflects a material's space filling or space expanding ability.

Small angle scattering of x-rays, neutrons and light are the most important experimental techniques for measuring the fractal dimension of fractal objects such as macromolecular clusters. These experiments measure the dependence of the scattered radiation intensity $I(\theta)$ on the radial scattering angle (θ). The scattering profiles are often recorded as the scattering intensity or the Rayleigh factor as a function of the scattering vector (s) defined as:

$$s = \frac{2}{\lambda} \sin\left(\frac{\theta}{2}\right) \quad \text{Eqn. 1.6}$$

where λ is the wavelength of the incident radiation in the medium, and θ is the radial scattering angle. s correlates to a length scale (d) in real space according to $d = 1/s$.

The scattering intensity of a mass fractal and a surface fractal corresponds to the Fourier transformation of the structure of fractal objects squared. The scattering intensities of an ideal mass fractal and an ideal surface fractal show a power-law dependence on the scattering vector, s , according to the following equations⁴⁸:

$$I_{\text{mass}}(s) \propto s^{-D_{\text{mass}}} \quad \text{Eqn. 1.7}$$

$$I_{\text{surf}}(s) \propto s^{-(6-D_{\text{surf}})} \quad \text{Eqn. 1.8}$$

However, a real object is only a fractal over a particular length scale. The inner cutoff of material fractals (d_{min}) is ultimately limited by the interatomic distances (ξ), while the outer cutoff (d_{max}) is limited by the size of the object (often described by the radius of gyration R_g). For a real fractal object, the scaling laws indicated by Eqns. 1.7 and 1.8 only hold true within $d_{\text{max}}^{-1} < s < d_{\text{min}}^{-1}$. Several levels of scaling behavior may also exist over various length scales in an object.

The SAXS profile for uncorrelated systems (e.g. dilute systems containing randomly dispersed macromolecules) is illustrated by Fig. 1.8. According to Schaefer and Keefer⁴⁹, the profile can be divided into the Limiting, the Guinier, the Porod, and the Bragg regions depending on the radius of gyration of the clusters (R_g) and the average interatomic /interchain distance (\mathbf{a}).

The intensity of scattered waves in the Limiting region ($s \gg R_g^{-1}$) reflects the concentration and weight average molecular weight of the clusters. The Guinier region ($sR_g < 1/10$) lies in the low scattering angle region, within which the intensity of scattering $I(s)$ varies exponentially with s according to the Guinier's law:

$$I(s) \sim \text{Exp}(-4\pi^2 s^2 R_g^2 / 3). \quad \text{Eqn. 1.9}$$

If Eqn. 1.9 is applicable, the radius of gyration can be calculated from the slope of the scattering profile plotted as $\log I(s)$ vs s^2 in the Guinier region.

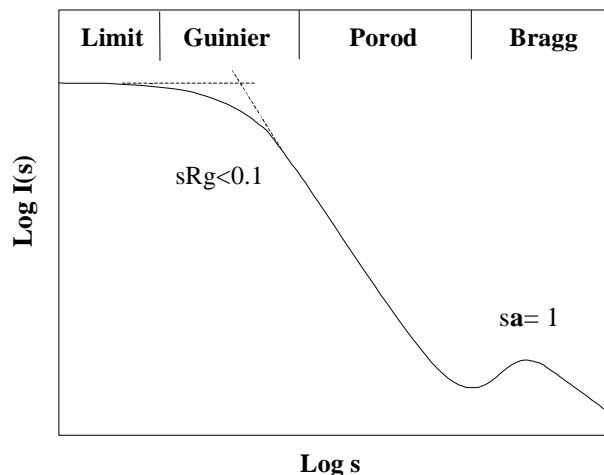


Fig. 1.8. A schematic $\text{Log } I(s)$ vs $\text{Log } s$ profile for small angle x-ray scattering for a dilute macromolecular solution⁴⁹.

At higher scattering angles where $sa \sim 1$ is the Bragg region. In amorphous systems, diffuse peaks may be observed for each correlating interatomic or interchain distance (\mathbf{a}), while in systems containing crystalline materials, sharp peaks may be observed for different lattice inter-planar distances. This is the region studied by wide angle x-ray diffraction.

Between the Guinier and the Bragg regions ($R_g^{-1} < s < \mathbf{a}^{-1}$) is the power law region, where the scattering intensity decays exponentially as s increases (scaling region), i.e. $I(s) \sim s^P$. Where P is a negative constant independent of R_g and \mathbf{a} , but reflects the fractal dimensions of the objects by⁵⁰:

$$P = D_{\text{surf}} - 2 D_{\text{mass}} \quad \text{Eqn. 1.10}$$

By plotting $\ln(I(s))$ as a function of $\ln(s)$ (Porod plot), the constant P can be readily obtained as the slope of the linear region. D_{mass} is the mass fractal dimension ($0 \leq D_{\text{mass}} \leq 3$), and D_{surf} is the surface fractal dimension ($2 \leq D_{\text{surf}} \leq 3$). For uniform three-dimensional objects, which have sharp interfaces with their surrounding medium, $D_{\text{mass}} = 3$, $D_{\text{surf}} = 2$ and P reduces to -4 (Porod's law). For mass fractal, $D_{\text{mass}} = D_{\text{surf}}$, and $P = -D_{\text{surf}}$, so the mass fractal dimension can be directly obtained from the slope ($-3 \leq P \leq 0$). For surface fractal objects, $D_{\text{mass}} = 3$ and $P = D_{\text{surf}} - 6$, so the Porod slope for surface fractal objects is greater than -4 but less than -3 ($-4 \leq P \leq -3$). [Table 1.1](#)

shows mass fractal dimensions of various objects. In some literature, the Porod region only stands for the region where Porod's law applies ($P=-4$), while other regions are referred to as the power law regions.

Table 1.1. Porod slopes for various structures according to Schaefer and Keefer⁵¹

Objects	Porod Slope	Fractal Type
Linear ideal polymer (random walk/Gaussian chain)	-2	Mass Fractal Slope = $-D_{\text{mass}}$
Linear swollen polymer (self-avoiding walk)	-5/3	
Randomly branched polymer	-16/7	
Swollen branched polymer	-2	
Diffusion-limited aggregate	-2.5	
Multiparticle diffusion-limited aggregate	-1.8	
Percolation (single cluster)	-2.5	Surface Fractal Slope = $D_{\text{surf}} - 6$
Fractal rough surface	-3 to -4	
Smooth surface	-4	

The above results are only for pinhole collimated irradiation. For slit-collimated irradiation, the Porod slope after considering the smearing effect of the slit leads to⁵²:

$$P_{\text{slit}} = P_{\text{pinhole}} + 1 \quad \text{Eqn. 1.11.}$$

Inorganic-organic hybrid materials may display multiple levels of structural features on length scales ranging from angstroms to millimeters. However, instruments based on a single type of radiation source only have a limited detection range. For example, SAXS typically only shows structural features in the range of several angstroms to several hundred angstroms. Fortunately, the problem can be solved by combining absolute intensity measurements from small-angle light scattering (SALS), ultra-low angle x-ray scattering and conventional SAXS or small angle neutron scattering (SANS)⁵³.

For correlated systems of interacting scattering clusters or particles, the scattering intensity reflects both the geometry and the packing or distribution of the dispersed substance. For N randomly oriented and centrosymmetric clusters or particles, the scattered intensity can be expressed as:

$$I(s) \sim N \cdot P(s) \cdot S(s) \quad \text{Eqn. 1.12}$$

where $P(s)$ is the form factor of the particle which contains information on size, shape, and internal structure. $S(s)$ is the structure factor reflecting the packing order of the clusters (e.g. correlation distance, ξ) in the assembly. For uncorrelated systems, $S(s)=1$, and $I(s)$ simply describes isolated clusters.

The separation of these two contributions is an extremely difficult task and has seldom been solved completely. The problem can be illustrated using the resulting scattering curve and the form and structure factors related to an interacting micelle system (Fig. 1.9). In this system, the Guinier range disappears from the intensity curve. The correlation peak is still visible but is displaced with respect to its position in $S(s)$ at $s=1/\xi$. Therefore, *it is not possible to derive these characteristic distances directly from the scattering intensity plot*. However, since $S(s)$ gradually approaches 1 at high s , it is still possible to calculate the fractal dimension from the slope of a Porod intensity plot. In this work, the correlation distance between clusters or particles is approximately given as the reciprocal of the s value corresponding to the maximum intensity of a peak in the SAXS profile.

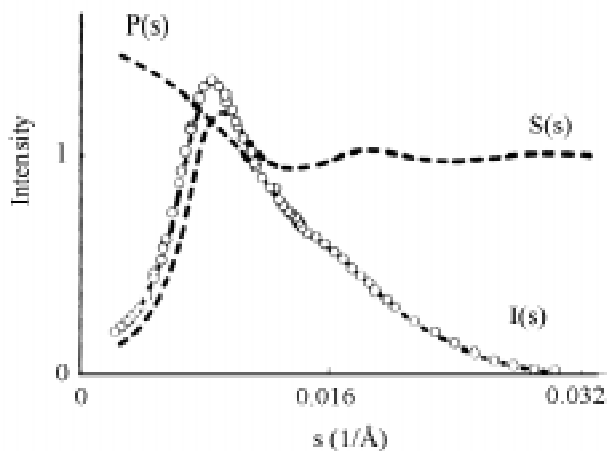


Fig. 1.9. The experimental scattering curve $I(s)$ resulting from the product of the form factor $P(s)$ and the structure factor $S(s)$ for a system of interacting charged micelles⁵⁴

1.1.4. Gelation

Due to continuous condensation, a silicic acid solution, obtained by sol-gel reactions of tetraalkoxysilane or the acidification of soluble metal silicates, often slowly thickens (increases in viscosity) and finally forms a gel externally like organic gels. At the gelation point, there are usually sudden changes in many physical properties, for example, viscosity and the storage modulus. The time of gelation, t_{gel} , is sometimes defined as the time corresponding to an infinite steady state viscosity η . Practically, t_{gel} is defined as the time when the viscosity reaches a certain large value or when the gel becomes so rigid that the probe (e. g. rotating spindle) tears the gel in a rheology test. The reciprocal of the gelation time is frequently used to describe the condensation rate for tetraalkoxysilanes in a sol-gel process. In principle, the overall condensation rate can be described by the statistical average of all condensation reaction rates; however, this quantity cannot be easily measured. The dependence of gelation time on temperature^{55,56} generally complies with the well-known Arrhenius equation:

$$\text{Log}\left(\frac{1}{t_{\text{gel}}}\right) = A - \frac{E}{RT} \quad \text{Eqn. 1.13}$$

where t_{gel} is gelation time, R is the ideal gas constant, A is the pre-exponential constant, T is absolute temperature, and E is the superficial activation energy. The activation energy depends on the catalyst and alkoxy group, and its typical value is around 10-20 Kcal/mol^{55,56}.

With other factors being fixed, a decrease in the size of the alkoxy groups^{57,58} generally decreases t_{gel} . Similarly, an increase in the equivalent ratio of water to alkoxide (\mathbf{r})^{59,60} and concentration of alkoxide^{59,61} also decreases t_{gel} . Of course, a change in the concentration of one component may also be accompanied by relatively large changes in concentrations of other components. For example, while fixing the solvent to silicate ratio, t_{gel} initially decreases as \mathbf{r} increases. However, after \mathbf{r} passes a critical value, the dilution of the system caused by the addition of water begins to reduce the hydrolysis and condensation rates, thus increasing the gelation time⁶².

Gelation corresponds to the transition of finite clusters (sol) to an infinite cluster spanning over the whole container (gel). In silicic acid solution, orthosilicic acid monomers first

condense to dimers, trimers and tetramers, etc, which further condense in such a way to maximize the number of Si-O-Si bonds and minimize the number of terminal hydroxy groups (via internal condensation)³⁴. By this route, short chains cyclize to rings, which in turn combine into polyhedral structures⁶³. Those polyhedrals further condense to larger particles leaving some OH groups on the outside. Depending on the pH of the solution, these particles can either interconnect to chains and then crosslink to a gel⁶⁴ or grow in size at the expense of small particles by an *Ostward ripening mechanism* to form a metastable silica suspension.

The gelation process has been explained by classical theory⁶⁵, percolation models⁶⁶, and kinetic methods (including Smoluchowski equations^{67,68} and computer simulation⁶⁹). This dissertation will not attempt to describe these theories. However, the structures predicted by computation simulations will be briefly introduced since they clearly illustrate the structure of silica clusters developed under different reaction conditions—an aspect that will be addressed in [Chapter 6](#).

1.1.5. Structural Evolution Prior to Gelation

Numerous studies including rheological measurements have indicated that the structures of sols or gels of silica are highly dependent on the reaction conditions, especially pH of the solution and equivalent ratio (r) of water to silane. For example, Sakka et al.⁷⁰⁻⁷² and Kamiya et al.⁷³ have found silicate systems developed by acid catalysis and base catalysis behave surprisingly different in their viscosity-concentration-molecular weight relationships. Noticeably, silica sols developed using a strong acid catalyst ($r=0.5-1$) are flexible, chainlike and spinnable; while those developed using a base catalyst are highly branched and nonspinnable. Spinnability is defined as the ability to draw fibers from the solution. In this section, the structure of silica clusters generated under different reaction conditions is discussed.

1.1.5.1. Computer Simulation of Cluster Growth

Kinetic growth processes such as the sol-gel process often result in self-similar fractal clusters. According to Meakin⁷⁴, the formation of those fractals can be computer-simulated using a *lattice model* by selecting a set of three key elements describing the growth process:

- 1) **The reactants:** the reactants can be either monomers or clusters, and the coordination number of the reactants will affect the choice of lattice.
- 2) **The trajectories:** reactive monomers or clusters undergo a random walk in a Brownian trajectory before they collide with each other. In a ballistic trajectory, however, reactive species travel a long distance towards each other without colliding with other species. The former case is closer to liquid phase reactions, while the latter is more similar to gas phase reactions.
- 3) **The relative rates of reaction and transport:** monomers and clusters are allowed to react during their first collision in a diffusion-controlled mode. In contrast, many collisions are required to form a bond during a collision in the reaction-limited mode. The number of collisions and the probability of reaction during an encounter depends on the local structure rather than the overall structure of the cluster.

Figure 1.10 shows the structures and fractal dimensions of computer-simulated clusters developed under the stated reaction conditions. The labels Eden, Vold, Witten-Sander, etc. represent the computer models from which the cluster structures are obtained. The clusters derived by the ballistic models will not be discussed since they do not reflect the situation of liquid phase reactions. In the sol-gel process of tetraalkoxysilanes, cluster growth may proceed predominantly between monomers and clusters or between clusters and clusters. The monomer-cluster growth model requires a continuous supply of monomers that condense preferentially with clusters rather than with themselves. Apparently, solution or melt crystal growth is an example of monomer-cluster growth although this process occurs in a highly ordered manner. The monomer-cluster growth model has two limiting cases: reaction limited monomer-cluster aggregation (RLMCA) and diffusion limited monomer-cluster aggregation (DLMCA). The

DLMCA model gives a low fractal dimension because of the random walk nature of Brownian diffusion and the irreversible reaction at the first collision with the growing cluster. The reaction limited model is characterized by a barrier to bond formation (i.e. activation energy). The Eden model, which leads to a compact smooth cluster ($D_{\text{mass}} = 3$), is a RLMCA model. In this model, all lattice sites are assumed accessible and filled with equal probability. A “poisoned” Eden model⁷⁵ has also been proposed to accommodate some lattice sites that are prohibited from occupation. During the sol-gel process of alkoxy silanes, some sites are prohibited from occupation because of unreacted alkoxy silane groups or incorporation of organosilanes such as methyltrimethoxysilane. Depending on the number of poisoned sites and their distribution, the poisoned Eden growth can generate structures that vary from uniformly pore fractals to surface fractals to mass fractals. Generally, the clusters formed by DLMCA (Witten-Sander, $D_{\text{mass}}=2.50$) has a lower fractal dimension than those formed by RLMCA (Eden, $D_{\text{mass}}=3.00$).







	REACTION-LIMITED	BALLISTIC	DIFFUSION-LIMITED
MONOMER-CLUSTER	EDEN  $D = 3.00$	VOID  $D = 3.00$	WITTEN-SANDER  $D = 2.50$
CLUSTER-CLUSTER	RLCA  $D = 2.00$	SUTHERLAND  $D = 1.80$	DLCA  $D = 1.80$

Fig. 1.10. Simulated structures resulting from various kinetic growth models. Fractal dimensions are listed for 3-D clusters although only their 2-D analogs are displayed. Each cluster contains 1000 primary particles.⁷⁴

The cluster-cluster aggregation model is applicable to sol-gel systems that have no continuous supply of monomers and no predominant condensation between monomers and high

molecular species. This model also includes the two similar limiting cases: reaction limited cluster-cluster aggregation (RLCA) and diffusion limited cluster-cluster aggregation (DLCA). Similar to the case of monomer-cluster aggregation, the DLCA model forms more extended clusters ($D_{\text{mass}}=1.80$) than the RLCA model, which yields clusters with a D_{mass} of 2.00.

1.1.5.2. The pH-Dependence of Sol-Gel Reactions¹⁸

The pH-dependence of sol-gel reactions of tetraalkoxysilanes and the resulting cluster structures is schematically described by Fig. 1.11 using an arbitrary r value and reaction rate constants^{34,42}.

By the reaction mechanism, the hydrolysis of the silane (curve H in Fig. 1.11) can be divided into two pH regions: $\text{pH} < 7$ and $\text{pH} > 7$. At $\text{pH} < 7$, the hydrolysis occurs via acid-catalysis and the reaction rate is proportional to the hydrogen ion concentration. For $\text{pH} > 7$, the hydrolysis occurs via base-catalysis and the reaction rate is proportional to the hydroxide ion concentration. The overall hydrolysis rate reaches a minimum at ca. $\text{pH} 7$, where the contributions from both mechanisms are equally small.

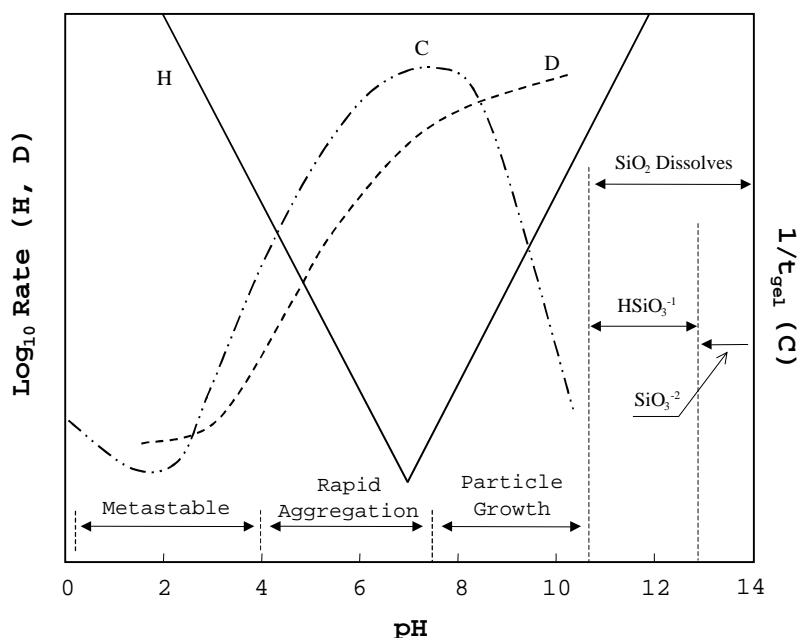


Fig. 1.11. Schematic representation of the influences of pH on the rates of hydrolysis (H), condensation (C) and dissolution (D)^{34, 42}.

The condensation rate (curve C in Fig. 1.11) depends on the relative ease of protonation and deprotonation of the silanol or alkoxy silane groups, which is reflected by the point of zero charge (PZC) of the colloidal particle surfaces. The PZC for silica is around pH 1-3. At this pH, the silica surface is expected to be equally protonated and deprotonated, thus the PZC is roughly the boundary between acid catalyzed and base catalyzed condensations. In the range of pH 0-6, the dissolution rate of siloxanes (curve D in Fig. 1.11) is relatively low (especially at pH 0-4) and thus the overall condensation rate depends mainly on the condensation rate. The condensation in the range of pH 0-2 is predominately acid catalyzed and the reaction rate decreases steadily as pH increases. In the range of pH 2-7, the condensation is believed to be overwhelmingly base-catalysis and the condensation rate increases steadily with pH. At pH 7-14, the condensation is still base-catalyzed, however, due to the increasing importance of dissolution of siloxane bonds, the overall condensation rate decreases sharply. At pH 12-14, the dissolution reactions become so dominant that most silicon species convert to low molecular weight metasilicates or silicates.

pH in a nonaqueous solution is not well-defined. The pH-dependence of gelation time changes slightly from catalyst to catalyst, but similar tendencies are followed⁷⁶. Cihlar recently studied the hydrolysis and condensation of TEOS⁷⁷ and ETS40 (a hydrolysate of TEOS)⁷⁷ using a number of acid or base catalysts. pH measurement was properly calibrated to accommodate the solvent effect on the acidity. The results indicated that for the selected catalysts, the rate of hydrolysis typically depended on pH of the solution but not on the chemical structure of the catalyst. The minimum rate of hydrolysis was at pH 7.0, while the minimum rate of condensation (given as the reciprocal of the gelation time) was at ca. pH 2.0.

1.1.5.3. The pH-Dependence of Cluster Structures¹⁸

The structures of clusters formed during the sol-gel process of a silicon alkoxide depend on pH and r in the system. Figure 1.12 roughly illustrates the cluster/particle structural evolution at different pHs during the sol-gel process of aqueous silica.

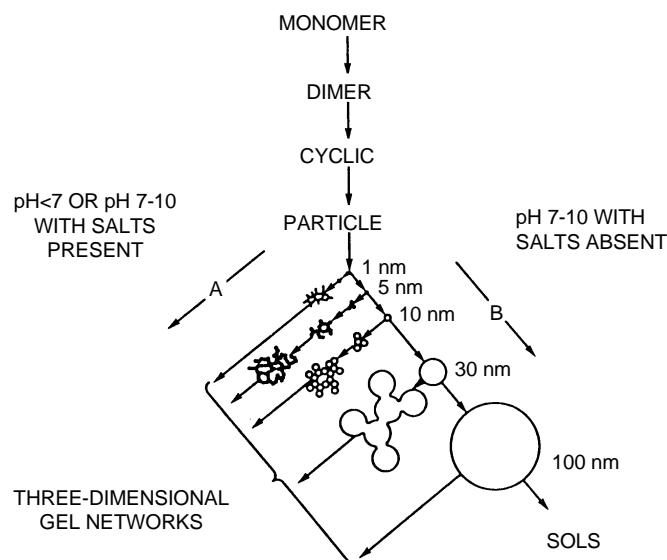


Fig. 1.12. Polymerization behavior of aqueous silica. Redrawn according to Iler, R. K. *The colloid chemistry of silica and silicates*⁷⁸

Below pH 2, both hydrolysis and condensation occur by acid-catalysis and the hydrolysis is much faster than the condensation (Fig. 1.11). For $r > 2$, the hydrolysis of TMOS is expected to finish at an early stage of the process ($t/t_{\text{gel}} < 0.01$). At pH 1, a TMOS system can be actually depleted of monomers (Q^0) at $t/t_{\text{gel}} > 0.01$, yet this system has a much lower concentration of Q^4 than a similar system developed under a neutral condition⁷⁹. Since the system is depleted of monomers (Q^0) quickly, later condensation (still far from gelation) occurs mainly between polymeric silanols (Q^1 or Q^2) via a RLCA route, leading to weakly-branched structures ($D_{\text{mass}} \sim 2$). Because of the low solubility of siloxane (siloxane bond hydrolysis), this temporary, nonequilibrium structure is unable to rearrange and hence is kinetically stabilized.

Under water-deficient hydrolysis conditions ($r < 2$), the actual average functionality of the silicon species is reduced (no ether-forming condensation occurs) because of the incomplete hydrolysis and condensation. Consequently, more weakly branched structures are formed, leading to the increased dependence of the viscosity on the concentration and molecular weight of the clusters. The unreacted alkoxy silane groups in those structures can be condensed by

adding sufficient amounts of water in a later step. The final gel structure developed by such a two-step approach often differs from that of a similar system developed by a one-step approach.

The weakly branched structures in acid-catalyzed condensation may be related to the relatively high reactivity of less condensed silicon species (due to inductive effects). Because of this, monomer-monomer condensation is faster than monomer-cluster condensation, which is in turn faster than cluster-cluster condensation. Consequently, monomers are consumed quickly and the later reactions occur mainly between clusters (RLCA). Trace amounts of fluoride or hydrofluoric acid significantly can promote the formation of a negative charged penta- or hexa-coordinate silicon intermediate. Even though pH is less than 2, the presence of fluoride or hydrofluoric acid can lead to a reaction pathway similar to the base-catalyzed mechanism, and the final gel structure is similar to those obtained at $\text{pH} > 2$ (RLMCA), at which range the base catalyzed reaction is predominant.

Above pH 7.5, both hydrolysis and condensation occur by the base-catalyzed mechanism (Fig. 1.11). However, since outer silanol groups of the clusters are partially dissociated, cluster-cluster aggregation is limited because of the electrostatic repulsion between the clusters. Because of a slow hydrolysis rate of tetraalkoxysilane and a higher dissolution rate of siloxane bonds, the system has a continuous supply of monomers. Therefore, condensation occurs mainly through an RLMCA route. In a TEOS derived silicates, ^{29}Si NMR showed a trend of maximization of Q^0 and Q^4 at the expense of Q^2 and Q^3 in this pH range¹⁸. By increasing the solubility of silica, the increase in pH, temperature or pressure is expected to promote the growth of silica particles. Many stable monodisperse silica sols have been prepared for industrial purposes at this pH range.

The condensation still occurs via RLMCA at $r < 2$, but unreacted alkoxy silane groups are more likely to be incorporated in the growing clusters. Under this condition, the cluster growth can be described by a poisoned Eden model, which can accommodate alkoxy silane groups that do not undergo any condensations. Mass or surface fractals or uniformly porous objects may result depending on the number and distribution of poisoned sites. A second step can be used to hydrolyze the unreacted alkoxy silane groups, and again the resulting gel often has a different structure from that obtained via a single-step hydrolysis.

The unique monomer-cluster condensation model in base-catalyzed condensation may be related to 1) the stronger acidity of silanols containing more silyloxy substituents and 2) lower steric hindrance and a relatively high concentration of monomers. The small size of monomers also allows them to fill in the small gap within a cluster so that clusters of high fractal dimension or particles (surface fractals) are formed.

In the range of pH 2-7, the hydrolysis proceeds by acid catalysis while the condensation occurs by base catalysis (Fig. 1.11). As pH increases, the hydrolysis rate decreases while the condensation rate and dissolution rate of siloxanes increase. The condensation is likely to occur by the monomer-cluster condensation, which leads to structures ranging from mass fractals to surface fractals to porous uniform clusters, depending on the number and distribution of unhydrolyzed sites. The poisoned Eden model and the Eden model may be used to describe gel structures derived at $r \ll 2$ and $r \gg 2$, respectively. At pH 2-4, the hydrolysis rate is rather fast and both the condensation rate and the dissolution rate of silica are relatively low, hence the process is condensation-limited. As no significant electrostatic repulsion exists between particles, aggregation occurs along with the growth of particles. However, the particle size is often limited (2-4 nm) because of a lack of monomer supply. As pH value increases in the range of pH 5-7, the dissolution rate of siloxane bonds increases and the monomer generated can lead to further particle growth (*Ostwald ripening*). Since the particles or clusters are not sufficiently charged under these circumstances, they usually undergo rapid aggregation (Fig. 1.11).

Two-step approach may be used to prepare sols of different fractal dimensions. Tetraalkoxysilane has been hydrolyzed by an acid catalysis step and a subsequent base catalysis step⁸⁰⁻⁸⁵. The initial acid catalysis is expected to promote structurally extended clusters, while the latter base catalysis leads to a higher extent of condensation. Since the monomer has been mostly converted to Q^1 , Q^2 or Q^3 during the earlier acid catalysis, the following condensation under the base catalysis should occur by an RLCA manner if the *Ostwald ripening* can be neglected. In fact, gels produced by a two-step approach are rather different in both morphology and properties from those prepared by a single-step method. Figure 1.13 shows Porod slopes and corresponding fractal dimensions for a set of silicate solutions that were prepared by a one- or two-step approach. The 2-step acid catalyzed condensation usually gave a lower fractal

dimension than the 2-step base catalyzed condensation, which in turn gave a lower fractal dimension than a 1-step base catalyzed condensation⁸⁶.

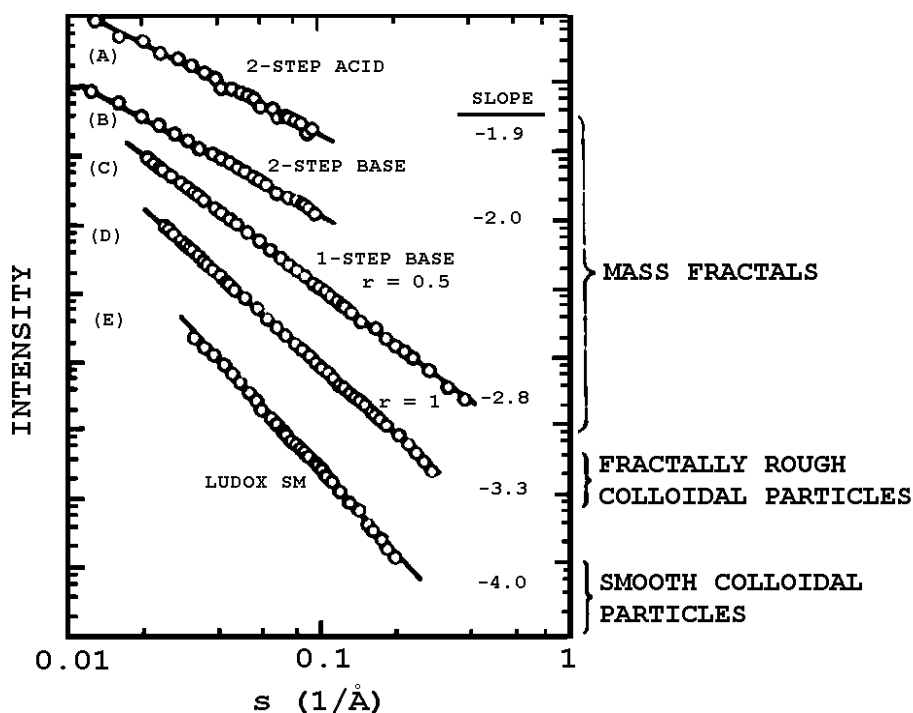


Fig. 1.13. Porod plots of silicate solutions prepared by: (A) two-step acid-catalyzed TEOS system; (B) two-step acid and base-catalyzed TEOS system; (C) one-step base-catalyzed TEOS system ($r=1$); (D) one-step base-catalyzed TEOS system ($r=2$); (E) aqueous silicate system Ludox.⁸⁶

1.1.6. Structural Evolution after Gelation¹⁸

After gelation, gels often undergo “aging” and drying before finally being sintered. These processes are usually accompanied by noticeable volume shrinkage and structure reconstruction. Aging and drying are also two important steps during the preparation of inorganic-organic hybrid materials (Section 1.2), in either monoliths or films. However, these materials are only cured at a temperature lower than the decomposition temperature of organic compounds. The curing process differs from the sintering in that the former is mainly caused by the condensation of

residual silanol groups, while the latter is mainly due to the mass transport of trace amounts of melts.

1.1.6.1. Aging of Gels

During the aging period, gels undergo *syneresis*, *coarsening* or *phase transformation*. These processes can significantly influence the gel structure, which affects the following drying and curing (or sintering) processes.

When a gel ages in a closed container, the gel network shrinks spontaneously by expelling the solvent and condensation by-products. This phenomenon is called *syneresis*. The driving force for the process is usually the same condensation that leads to gelation. However, for particulate gels whose gelation is due to the collapse of the electric double layer that stabilizes the sols, the syneresis can be driven by van der Waals forces since those systems are already highly condensed. The shrinkage causes partial interpenetration of clusters or particles, and the degree of interpenetration depends on the fractal dimension of the clusters or particles.

The syneresis can be divided into *macrosyneresis* and *microsyneresis*. By macrosyneresis, the solvent or condensation by-products are expelled out of the entire gel network, and a separate liquid phase and a separate gel can be observed. Microsyneresis is a micro-phase separation inside the gel that causes fluctuations in distribution of the gel material and solvents. During such process, the solvent and condensation by-products are gradually separated from the gel material and form pores or capillaries inside the gel. Microsyneresis often causes turbidity of the gel due to light scattering caused by phase separation. The porosity in dried organic gels is attributed to microsyneresis. However, its relative importance in the formation of porosity is unclear in inorganic gels since porosity in these gels may also result from cluster structure.

Coarsening or ripening is a process characterized by dissolution and reprecipitation due to the solubility differences between surfaces of different radii of curvature. Before gelation, the coarsening process mainly causes the growth of colloidal particles at the expenses of small particles. After gelation, colloidal particles can be in close contact, so coarsening or ripening leads to not only the growth of particles, but also the fusion of particles by transporting gel

material to any necks between particles (Fig. 1.14). The necks have negative radii and hence relatively low solubility, so reprecipitation often occurs at these places. The growth of necks adds to the strength and stiffness of the network. Generally, the rate of coarsening is influenced by factors affecting the gel solubility, which include temperature, pressure, pH, and the type of solvent.

Phase transformation (i.e. crystallization or transition of crystalline phase) may occur when an metal oxide gel undergoes aging. This does not occur in silica based gels and will not be discussed here.

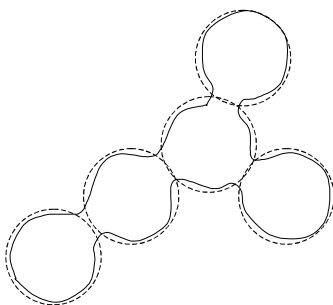


Fig. 1.14. Dissolution and reprecipitation cause the growth of necks between particles, increasing the strength and stiffness of the gel¹⁸.

Microsyneresis, coarsening and phase transformation increase the strength and stiffness of the gel network, thus they often reduce the shrinkage and cracking possibility and lead to a high porosity.

1.1.6.2. Drying of Gels

Syneresis during aging only causes limited shrinkage. Extensive shrinkage occurs in the drying process as huge amounts of solvent and condensation by-products evaporate from the gel. Depending on the drying rate, the drying of gels can be divided into three stages (Figs. 1.15 and 1.16): the constant rate period (CRP), the first falling rate period (FRP1), and the second falling rate period (FRP2)^{87,88}. The three-stage drying process was also used by Brinker et al. to describe the dip-coating process of inorganic sols^{89,90}. To help understand the drying process of

the inorganic-organic hybrid materials, a brief description of these three drying periods is provided.

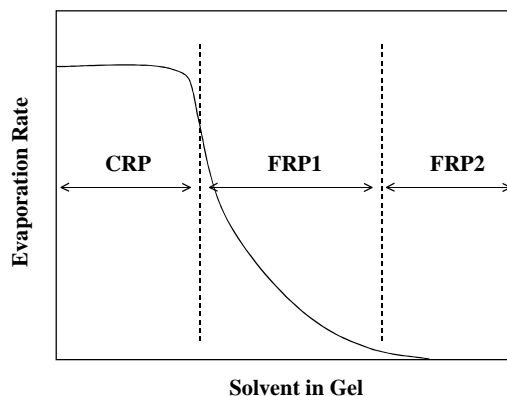


Fig. 1.15. Illustration showing three stages of solvent evaporation from gel⁹¹

During the constant rate period, the total evaporation rate remains roughly the same as the evaporation rate of the bulk solvent at the same temperature. Syneresis may be faster than solvent evaporation at the beginning, and this results in accumulation of free liquid in the container. As the rate of evaporation loss becomes greater than the rate of liquid expulsion due to syneresis, the liquid-vapor interface is about to enter the gel network. Assuming there is no interaction between the liquid and the gel network, further evaporation will expose the network. However, the capillary forces and osmotic forces cause the compliant network to shrink and the liquid to flow from the interior to the surface to replace what has evaporated, opposing the exposure of the network. Therefore, the evaporation rate of the solvent is roughly maintained the same during this period. Because of solvent evaporation, the gel surface temperature drops below the environmental temperature.

As the drying continues, the network becomes increasingly strong and stiff owing to the formation of new chemical bonds, the close contact of colloidal particles, and the decrease in porosity. Once the gel network becomes strong enough to resist the capillary forces and the osmotic forces, the shrinkage rate drops rapidly (further shrinkage is very limited) and not enough liquid can diffuse to the surface to replace the liquid that is lost by evaporation. Therefore, the liquid-vapor interface begins to enter the body of the gel, and this is called the

critical point (referred to as the leatherhard point in clay technology). At this point, the radius of the liquid/vapor meniscus becomes equal to the radius of the pore, so the capillary force reaches its maximum value.

After the critical point, the rate of evaporation rate drops rapidly and the surface temperature increases slightly. This is a stage called the first falling rate period (FRP1). During this stage, further evaporation drives the meniscus into the body, and the surface may become more transparent. However, the liquid in the pores near the surface remains connected to the liquid body although vapor or air pores exists in this region. In other words, there are contiguous pathways along which the inner liquid can flow to the surface under the influence of capillary forces. Most vaporization is still occurring at the exterior surface and the surface remains below ambient temperature. The rate of evaporation is, of course, sensitive to the ambient temperature and the vapor pressure.

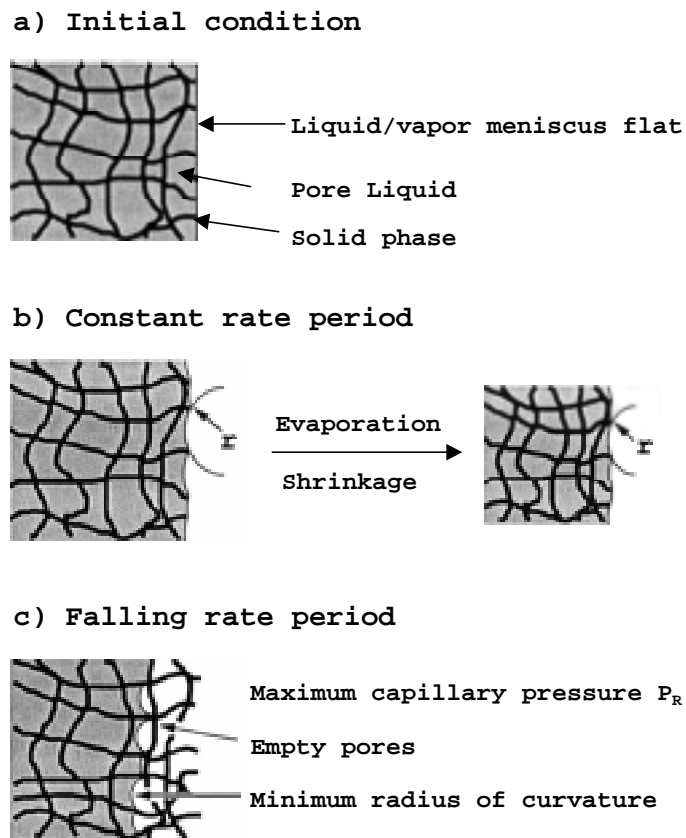


Fig. 1.16. Illustration showing the liquid/vapor interfaces during different drying stages¹⁸

As the meniscus recedes into the body, the gradient of capillary force drops and so does the flux of liquid to the surface. Eventually, it becomes so slow that the liquid near the gel surface exists in pockets isolated from the body liquid. Therefore, the liquid no longer flows to the surface and the diffusion of vapor becomes the only way for liquid to escape from the gel. The liquid in pockets only represents a small fraction of the liquid, so its contribution to the evaporation is negligible. This is the so-called second falling rate period (FRP2). In this period, evaporation occurs inside the body, the surface temperature reaches the ambient temperature, and the rate of evaporation becomes less sensitive to the ambient temperature and humidity.

The shrinkage of the gel network is highly dependent on the ability of the cluster to interpenetrate each other. Mandelbrot⁹² showed that when two rigid structures of diameter R are placed independently of each other in the same region of space, the number of intersections (overlaps or entanglements), $M_{1,2}$, is expressed as:

$$M_{1,2} \propto R^{D_{\text{mass},1} + D_{\text{mass},2} - d} \quad \text{Eqn. 1.14}$$

where $D_{\text{mass},1}$ and $D_{\text{mass},2}$ are the respective fractal dimensions and d is the dimension of the embedding space. For three dimensional space, $d = 3$. If $D_{\text{mass},1} = D_{\text{mass},2} < 1.5$, then the overlaps or entanglements $M_{1,2}$ approaches zero as R increases infinitely, so the structures are mutually transparent. However, If $D_{\text{mass},1} = D_{\text{mass},2} > 1.5$, the probability of overlap or entanglement increases infinitely with R , so the structures are mutually opaque.

Since acid catalysis usually leads to clusters of a low fractal dimension ($D_{\text{mass}} = 1.8-2.0$), the spanning and isolated clusters in the gel can interpenetrate to a high degree, leaving little porosity. On the other hand, base catalysis usually forms clusters or particles of a relatively high fractal dimension ($D_{\text{mass}} = 2.0-3$, mass or surface fractals), and these clusters or particles are far less interpenetrable, thus the resulting gel has relatively high porosity. Similarly, gels aged under conditions of high silica solubility tend to form less interpenetrable particles (high fractal dimension), hence resulting in high porosity in the final gel (Fig. 1.17).

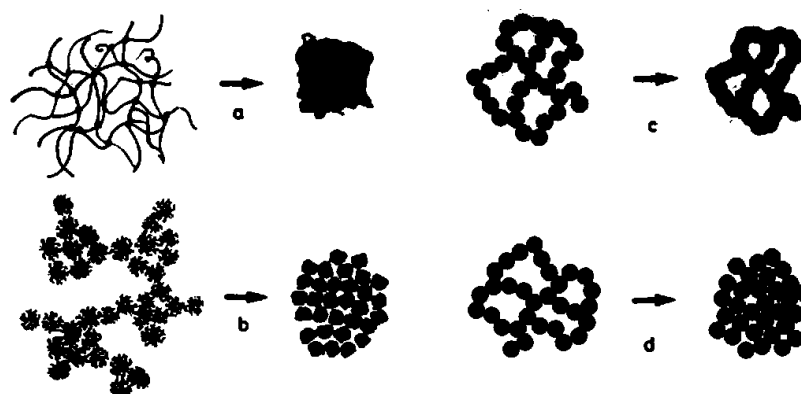


Fig. 1.17. Schematic representations for drying of a gel obtained by acid catalysis (a) and base catalysis (b), and aging of a particulate silica gel under conditions of high (c) or low (d) solubility.⁹³

Although osmotic pressure is significant for some gels that have strong interaction between the solid gel and the liquid, the capillary forces are believed to be the most important forces that cause shrinkage of the gel network and transport of the liquid from the gel interior to the surface. Created by the meniscuses as the liquid-vapor interface enters the pores on the surface of the gel, the capillary force (P) is governed by Eqn. 1.15 and reaches its maximum when the radii of the liquid meniscus reaches the radii of the pores at the critical point. Fracture is most likely to occur at the critical point during the whole drying process.

$$p_v = p_0 \exp\left(-\frac{PV_m}{RT}\right) \quad \text{Eqn. 1.15}$$

where V_m is the molar volume of the liquid, p_0 and p_v are the vapor pressures of the smooth liquid and the meniscus, respectively. R is the ideal gas constant and T is absolute temperature.

Mathematical models have been established by Scherer⁹⁴⁻¹⁰¹ to predict the stress distribution within a gel according to the geometry of the gel object, permeability of the network (D), viscosity of the liquid (η_L), viscosity of the network (H_G), evaporation rate (V_E), and the surface tension of the pore liquid (p_0). For the constant rate period (CRP), assuming the gel exhibits Newtonian viscosity, an analytical solution has been obtained for the stress distribution in a gel film (Fig. 1.18) drying from both sides:

$$\sigma_x = \frac{H_G V_E}{L} \left[\frac{\alpha \cosh(\alpha \cosh(\alpha z/L))}{\sinh(\alpha)} - 1 \right] \quad \text{Eqn. 1.16}$$

$$\text{where } \alpha = \sqrt{\frac{L^2 \eta_L}{DH_G}} \quad \text{Eqn. 1.17}$$

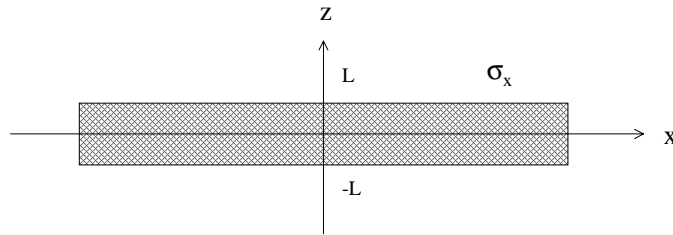


Fig. 1.18. A film gel undergoing a drying process from both surfaces.

The theory indicates that the outer layers of the film are under tension while the inner layers are under compression, and that the surface stress concentration can be reduced by increasing the permeability of the gel and surface tension. An obvious method to increase the permeability is to enlarge the pore size. The stress at the surface (at the critical point) is proportional to the film thickness if the film is not very thick ($\alpha \leq 1$). In case of very thick films ($\alpha \gg 1$), the surface stress becomes independent of the film thickness.

Fracture of the gel during the drying process may be avoided by increasing the pore size and aging time. The former reduces the cracking possibility by increasing the permeability of the gel; while the latter does that by increasing the gel strength as well as the pore sizes. Chemical additives including surfactants and so-called 'drying control chemical additives' (DCCA) are found helpful in reducing cracking. For example, formamide¹⁰²⁻¹⁰⁵, oxalic acid¹⁰⁶, glycerol¹⁰⁷ have been used to reduce cracking and to process relatively large monolithic gels, which are often called xerogels. The presence of these chemicals is expected to influence the cluster formation and later the syneresis. *Supercritical drying*^{108,109} is another way of reducing or eliminating the surface stress concentration and preparing large gel objects. By this method, the cracking problem is avoided by eliminating the capillary forces since the distinction between the liquid and vapor phases no longer exists in the supercritical state. The gels prepared by this

method are often called aerogels since they are very porous and extremely low in density, refractive index and thermal conductivity. Aerogels maintain most of the structural features of the original gel and are usually transparent.

1.1.7. Advantage and disadvantages of the sol-gel process

The sol-gel process provides a versatile method for ceramic processing. It can be used to prepare powders, fibers, films or coatings, porous or monolithic objects. Since the metal alkoxide starting materials can be prepared in extremely high purity and the formation of metal oxides is not diffusion-controlled as in normal ceramic sintering, ceramics produced by this way are very pure and chemically uniform. In addition, these oxide particles are often only a few nanometers in diameter, while usual ceramic powders have a particle diameter of a few microns. Consequently, ceramic preforms derived from the sol-gel process can be sintered at a temperature several hundred degrees lower than the normal sintering temperature. The solution processing nature of the sol-gel approach also allows organic or biochemical compounds to be incorporated without decomposition or losing their biochemical reactivity, so various inorganic-organic hybrid materials including biochemical sensors can be prepared. The organic components in these hybrids can be calcinated at high temperature to prepare porous materials with well-controlled pore sizes.

The sol-gel process, however, also suffers from several disadvantages. Firstly, the metal alkoxide raw materials are quite expensive compared with the clays, oxides or carbonates used for traditional ceramics. However, this causes no major problem if the ceramic is only used for a coating application. Secondly, the sol-gel process is usually accompanied by a huge release of solvent and condensation by-products, thus it is not easy to closely control the dimension of the final objects. Thirdly, the huge release of solvent and condensation products often causes cracking of ceramic preforms during drying and curing processes, although drying controlling chemical agents and supercritical fluid extraction may be used to overcome this problem.

1.2. INORGANIC-ORGANIC HYBRID MATERIALS

Inorganic-organic hybrid materials include any materials that are composed of both inorganic and organic components. Traditionally, inorganic-organic composites refer to glass or carbon reinforced or inorganic oxide filled resins, which are prepared by mechanical mixing. The separation of inorganic and organic components in these materials occurs at the micrometer level (10^{-4} - 10^{-6} m). Hybridization at the nanometer level (10^{-7} - 10^{-9} m) can be accomplished by several methods. These methods include: 1) embedding nanometer inorganic materials into organic polymers or resin (PMMA/silica^{110,111}), 2) impregnation of organic monomers into inorganic micro porous gels followed by polymerization (PMMA/silica¹¹²), and 3) hydrolysis and condensation of metal or semi-metal alkoxides along with silane coupling reagent and other organic modified silanes. Since phase separation typically occurs at a length scale of less than 1/20 of the wavelength of visible light, these materials are usually transparent. At the molecular level (10^{-9} - 10^{-10} m), however, the division between inorganic and organic materials becomes hazy, so the term *inorganic-organic hybrid material* is not so frequently used. For example, polydimethylsiloxanes (PDMS) and polyphosphazenes have both inorganic backbones and organic side groups, yet these materials are often classified as inorganic polymers rather than inorganic-organic hybrid materials. Many polyelectrolytes are comprised of organic backbones and metal ions but are also not categorized as hybrid materials. The term *inorganic-organic hybrid material* is specially used to refer to microphase-separated hybrid materials in this dissertation. These materials are generally divided into the following four types according to their preparation method.

1.2.1. Embedment of Nanometer Particles into Polymer Matrices

Inorganic-organic composites can be formed by polymerizing suspensions of nanometer particles of ceramics in organic monomers. These ceramic particles may be prepared by surface treatment of nanometer particles or by sol-gel reactions of metal alkoxides in the presence of a surfactant.

Schmidt et al.^{4-6,113} have prepared stabilized silica or metal oxide sols that include surface vinyl or epoxy groups and these particles were polymerized into an organic polymer matrix. The functionalized inorganic sols were prepared by modifying existing sols with silane coupling reagents such as 3-MPTMS and 3-GPTMS, or by sol-gel reactions of silicon or metal alkoxides in the presence of these silane coupling reagents. Chemical additives like carboxylic acids or acetylacetone were often utilized to reduce the reactivity of the more reactive metal alkoxides so that early precipitation of metal oxides did not occur. Partial hydrolysis of silane coupling reagents prior to addition of the metal alkoxide was also used to prevent formation of metal oxide precipitates. Schmidt et al. referred to their new hybrid materials as ORMOSILs (**organic modified silane**) and ORMOCERs (**organic modified ceramics**). These hybrid materials have been developed in the form of hard contact lens materials, UV-curing optical materials, low surface energy coatings, and scratch resistance coatings⁷⁻⁹.

By a similar approach, Philipse et al.¹¹⁴ and Sunkara et al.¹¹⁵ have prepared inorganic-organic hybrids using free radical polymerization of methyl methacrylate containing 3-MPTES treated Ludox silica colloids. Novak et al.¹¹⁶ have also prepared polymerizable silica sols by hydrolyzing TMOS in the presence of 2-hydroxyethyl methacrylate (HEMA). The hydrolysis was only partial so that a few reaction sites were reesterfied or transesterfied by HEMA. Later the vinyl group could be polymerized via a free radical polymerization. A silica/HEMA/PEMA (poly(ethyl methacrylate)) system has been also studied by Bourgeat-Lami et al.¹¹⁷

1.2.2. Co-Hydrolysis and Condensation Methods

Inorganic-organic hybrid materials can be readily prepared by sol-gel reactions of metal or semi-metal alkoxides in the presence of triethoxysilylated polymers/organic compounds. This approach is represented by the work of Wilkes and coworkers^{118,119}, and the resulting materials are often referred to as CERMERS (combination of **ceramic** and **polymer**). Polymers that have been incorporated in the CERAMERS include polydimethylsiloxane, poly(propylene glycol), polyimide, poly(tetramethylene oxide) and typical oxides incorporated included silica, alumina, titania and zirconia¹¹⁹. These polymers were often terminated with hydroxy or amine groups and

then functionalized with 3-isocyanatopropyltriethoxysilane (3-ICPTES). Compounds containing triethoxysilyl endgroups were also added as endcappers in stepwise polymerizations to functionalize polymers like polyimides. By changing the composition of the inorganic component, the material properties can be modified continuously from that of the polymeric component to that of the inorganic component. Small organic compounds were also similarly functionalized and used to prepare inorganic-organic hybrid coatings. These hybrid coatings will be reviewed in more detail when discussing abrasion resistant coatings^{11,17}.

Non-functionalized organic compounds may also be incorporated into many metal alkoxide sol-gel systems. In these cases, these systems usually involve no chemical bonding between the inorganic and organic components, and the organic species is only physically trapped into the inorganic network. Intimate contact of the organic component with the network is possible if both components are compatible.

1.2.3. Impregnation of Polymers into Porous Ceramics

Porous ceramics may be impregnated with organic monomers and then cured to inorganic-organic hybrid materials. Silica gels have been the most widely studied materials in this class. Organic monomers of various types have been impregnated into SiO₂ gels and polymerized into transparent nanocomposites¹¹², and PMMA including 33% of silica was reported to have a Vickers hardness of 220 kg/mm¹²⁰. In these materials, a continuous inorganic network should be expected.

1.2.4. In-Site Formation of Metal Oxides in Polymer Networks

In-situ hydrolysis of metal or semi-metal alkoxides in a polymer matrix is another way for preparing inorganic-organic hybrid materials. Jiang and Mark¹²¹ have prepared silica toughened siloxane elastomers by swelling polydimethylsiloxane (PDMS) networks with TEOS. Silica particles were formed in situ by sol-gel reactions of TEOS. Several acid and base catalysts have been utilized to find the best condition for promoting the desired particulate silica morphology. Acid catalysis produced brittle materials (possibly due to unzipping of the PDMS

chains) while base catalysis produced stronger or toughened materials. Silveira¹²² also investigated the sol-gel reactions of TEOS in a solution of PMMA in THF using acid catalysis and phase separation phenomena were studied using light scattering and scanning electron microscopy.

1.3. ABRASION RESISTANT COATINGS

1.3.1. Wear Phenomena

Surface interaction occurs whenever two objects become in contact with each other so that forces of action and reaction are brought into play. As the two contacting objects move with respect to each other, between the interface of the two objects occur a number of phenomena including temperature increase, friction forces, electrostatic charge generation, removal of materials from either object or transfer of materials from one object to the other, chemical reactions, and adhesion. Among them, *friction*, *wear*, and *adhesion* belong to mechanical interactions and are subjects of a science called *tribology*. Friction arises from the tangential forces across the interface that resist the relative motion of the two contacting objects, and it relates to the overall energy consumption during a surface interaction. Wear phenomena, however, are related to the removal of materials from the surface of either contacting body or transfer of materials from one contacting body to the other as a result of contact interaction. Adhesion is the ability of the contacting bodies to withstand tensile forces after being pressed together due to electrostatic forces, van der Waals forces, hydrogen bonding or chemical bonding. This effect seldom occurs to a marked extent, however, it is the basis of modern friction theory. The adhesion theory has gradually replaced the roughness theory and become the accepted explanation for friction¹²³.

Unlike the Young's modulus and hardness, etc., which are fundamental properties of a material, surface interaction properties depend on not only a number of fundamental properties

of the material, but also the surface topography, the environment, and the relative velocity of the two contacting objects. While other factors also affect the surface interaction properties, here the major concerns are the influences of fundamental properties of materials on wear phenomena. Knowledge of the relationships between surface interaction properties and major intrinsic properties of a material can provide valuable guidance to the design and preparation of both wear resistant and lubrication materials.

The fundamental properties of a material that significantly influence its surface interaction properties can be divided into bulk properties, surface properties, and thermal properties¹²³. The most important bulk properties are yield strength, hardness, the Young's modulus, shear modulus, and fracture toughness. Surface properties include chemical reactivity, surface energy, and interfacial energy of the two contacting objects. The chemical reactivity is the tendency for a surface to acquire a surface film of different chemical composition from that of the substrate (metal oxides, sulfides), or to absorb molecules from the environment (water, air). The surface energy reflects the work that must be done to create a fresh surface, while closely related is the interfacial energy that determines the compatibility of two contacting objects. The contact of two compatible objects can result in amalgamation or mixing at the interface, thus leading to high adhesive wear. Thermal properties are also very important when sliding takes place at a high speed so that a marked increase in surface temperature occurs. For polymer materials, the glass transition temperature and melting point are important parameters affecting surface interaction properties.

Many close or intimate relationships exist between these fundamental properties. For example, materials with strong chemical bonds are often more resistant to deformation. Diamond, alumina, zirconia have extremely strong chemical bonding, so they are extremely hard and widely used as abrasives. Graphite, however, only has weak van der Waals forces between each close-packed graphite atomic layers, so they are very soft and can be used to make a solid lubricant. Generally, the yield strength is 25% of the Young's modulus for pure fully work hardened metals¹²⁴, and 35% for some metal alloys¹²⁵. Also the penetration hardness is approximately equal to three times the yield strength for many pure metals, alloys and nonmetals and this has been demonstrated both theoretically and experimentally¹²⁶. For pure metals, the

surface energy scales with the square root of the hardness¹²³. The Young's modulus also generally increases with the melting point of the metal and it correlates with the thermal coefficient of expansion by¹²⁷:

$$E\alpha^2 = \text{constant} = 15 \text{ N/m}^2\text{°C}^2 \quad \text{Eqn. 1.18}$$

E is the Young's modulus and α is the thermal coefficient of expansion.

Mechanistically, wear can be generally classified into several categories including *adhesion wear*, *abrasive wear*, *surface fatigue wear* and *corrosive wear*. In real situations, wear phenomena are often caused by a combination of these wear mechanisms rather than a single mechanism. Compared with many inorganic materials, polymers usually have poor surface strength and are less resistant to abrasive wear. This problem is especially serious for optical polymers since minor indentations or scratches of these materials during daily cleaning can cause a rapid reduction in transparency. [Figure 1.19](#) shows the classifications of wear and their possible causes and effects for tribological interactions of polymers. Due to the significant influences of abrasive wear to optical polymers, the following discussion will be confined to the influences of fundamental properties on the abrasive wear rate. However, while abrasion wear may be the major cause for transparency reduction of optical polymers, the influences of other mechanisms should not be neglected. For example, crack formation and film delamination of many abrasion resistant coatings during a Taber abrasion test may be caused by fatigue wear.

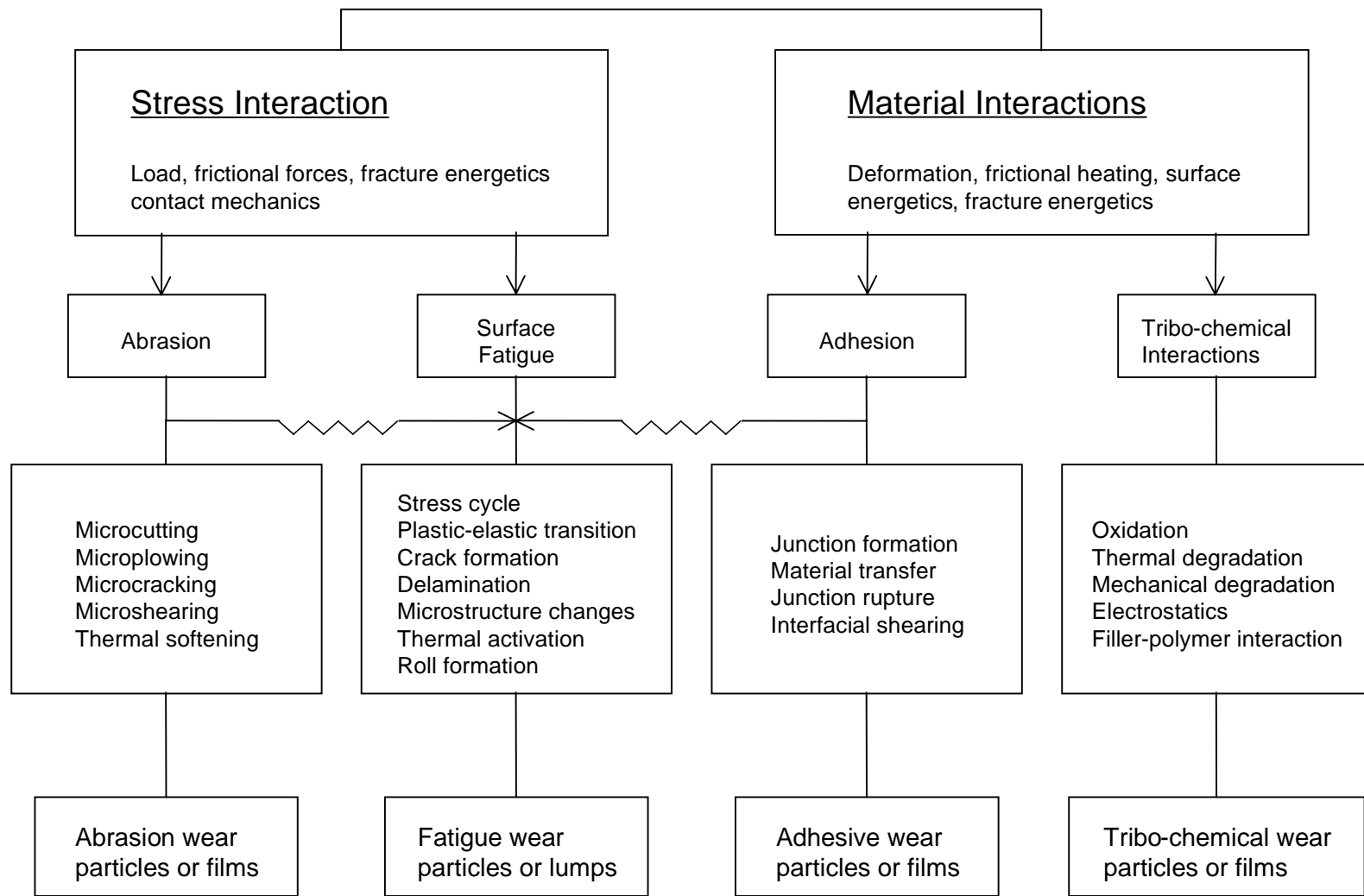


Fig. 1.19. Tribological interactions of polymers. Redrawn according to Lee¹²⁸

When two contacting objects are in relative motion, abrasion wear occurs via displacement of materials from either object due to the presence of hard protuberances or the presence of hard particles between the surfaces. These particles can be either contaminants from the environment or fragments from either object. Polymer materials are rather soft compared with ceramics and metals, hence their surface can be easily damaged by abrasion. Depending on intrinsic properties of the material and the exterior condition, abrasive wear can be caused by microplowing, microcutting, and microcracking mechanisms (Fig. 1.20). These mechanisms occur to various degrees for brittle polymers, ductile polymers and elastomers¹²⁹. For brittle polymers, the wear volume (V_w) is inversely proportional to hardness (H) by¹³⁰:

$$V_w = k_1 L d \tan \theta / \pi H \quad \text{Eqn. 1.19}$$

where $\tan \theta$ is the mean slope of the asperities, L is the load and d is the displacement, k_1 is a proportional constant related with the properties of the abrasives and polymer substrate.

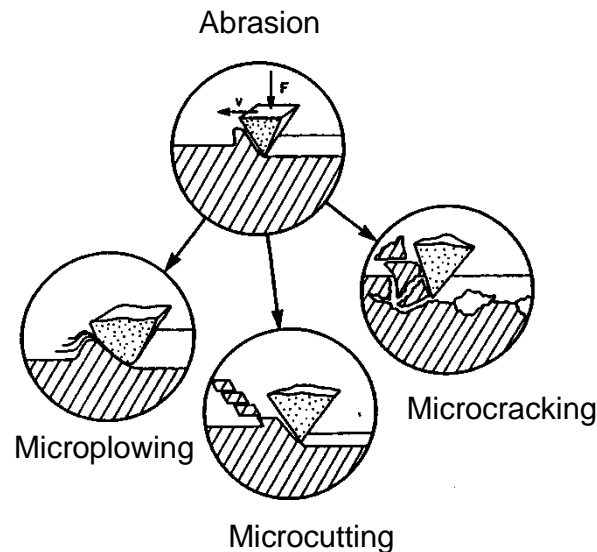


Fig. 1.20. The mechanisms for abrasive wear ¹²⁹

Ratner¹³¹ has proposed a three-stage abrasion wear process that includes: 1) deformation of the substrate at the contact area, 2) relative motion opposed by a friction force, and 3) rupture of the material at the junction area. The extents of action in these three stages are strongly dependent on the hardness of the substrate (H), the coefficient of friction between the two

contacting substrates (μ), and the rupture work of the material (A), respectively. The rupture work (A) is usually described by the area under a stress-strain curve, so it is expected to scale with the product of breaking stress (σ) and elongation at break of the material (ϵ). The wear volume (V_w) removed in such a process is expressed as:

$$V_w = k_2 \cdot \mu \cdot d / H \cdot \sigma \cdot \epsilon \quad \text{Eqn. 1.20}$$

where k_2 is a proportionality constant, $\sigma \cdot \epsilon$ is a measure of rupture work or toughness. The importance of this equation lies in the inverse proportionality of wear rate to *the hardness as well as the toughness of the substrate*. Many other equations have also been deduced to describe the wear volume for various substrates and situations¹³²⁻¹³⁶.

The same polymer can suffer from different types of wear depending on the shape of the abrasive, the cutting rate and the bulk temperature. This can be exemplified by the deformation behavior of MFR80 polycarbonate (Dow Chemical Co.) during scratch tests^{137,138}. [Figure 1.21](#) shows the deformation map of the material in room temperature tests. The normal load and cone angle of the test are stated as the coordinate and abscissa, respectively. The results indicate that the material suffers from ductile plowing and plastic deformation at a relatively large cone angle but brittle machining at a high load and a small cone angle. With a cone angle $>150^\circ$ and a load less than 0.8 N, the deformation is fully elastic. Increasing the bulk temperature leads to the expected suppression of brittle fracture. Strangely, a decrease in scratch rate from 2.6 mm/s to 0.0026 mm/s results in a decrease in the area of the ductile plowing region. It is believed that at a high scratch velocity, the energy dissipation leads to local adiabatic heating of the material and hence a rise in local temperature, which results in the suppression of brittle failure. Similar analyses have also been conducted by the same authors for polytetrafluoroethylene, polyethylene and polymethacrylate^{139,140}.

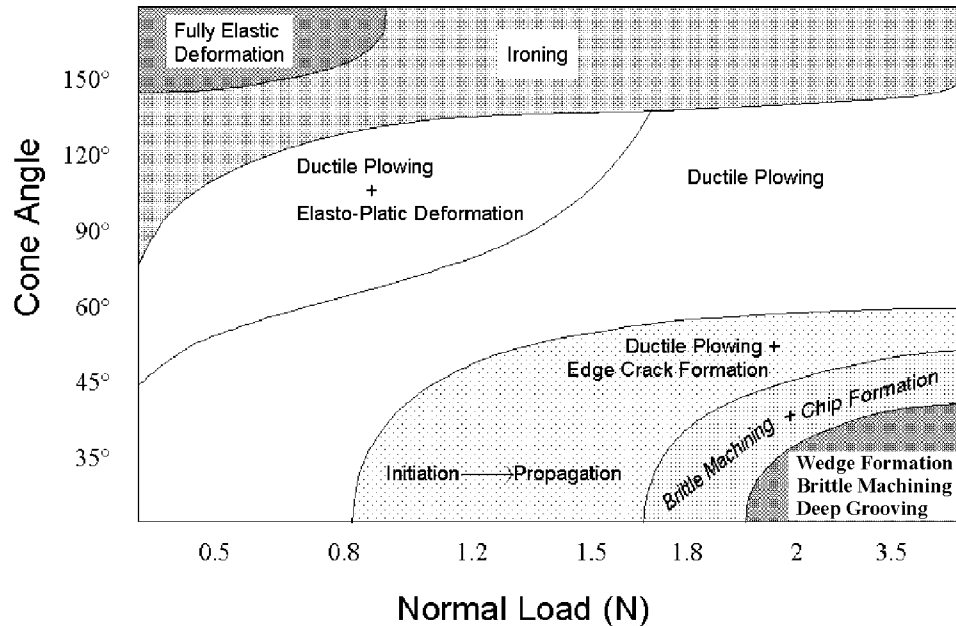


Fig. 1.21. A deformation map of MRF80 polycarbonate. The tests were carried out at room temperature at a scratch velocity of 2.6 mm/s. (Redrawn according to References ^{137,138})

1.3.2. Approaches for Controlling Polymer Wear

Polymer wear can be controlled by lowering surface energy or increasing the hardness and toughness. In general, a lower surface energy and a high hardness help to lower adhesive wear, while a high hardness and a high toughness help to minimize abrasion wear and fatigue wear. According to Lee¹²⁸, the wear resistance of polymers may be improved by: 1) controlling or designing bulk properties, e.g. molecular weight, molecular weight distribution, entanglement density, microstructure, liquid crystalline structure, etc.; 2) modifying the surface (e.g. by plasma, photopolymerization, silicone, etc.); and 3) particulate or fibrous reinforcement. By surface modification, a layer of a tough and rigid material is formed on the surface of the polymer object so that the inner weak material does not directly contact the abrasive. This method is effective for protecting polymers used for decoration, glazing, glasses etc., which only suffer from mild surface interaction when in contact with other objects. The other two approaches increase abrasion resistance of the material by improving their intrinsic properties.

For example, CR39 resins, optical polymers prepared by free radical polymerization of diallyl diglycol polycarbonate, offer better abrasion resistance than linear optical polymers like PMMA and PC. The improved abrasion resistance of CR39 resins can be attributed to their high crosslink density¹⁴¹. Compared to surface modification, the development of new polymers usually involves high expense, a long investment cycle and great risks, and has limited potential in improving wear resistance. In cases of bearings and transporting pipes where wear is of prime importance, polymers with high abrasion resistance should be chosen. Under extreme situations, metal or ceramic parts may be used instead of polymers.

1.3.3. Abrasion Resistant Coatings

1.3.3.1. Coatings by Plasma Treatment/Polymerization

Plasma treatment/polymerization of monomers can create a dense film on polymer surfaces, which can potentially prevent the substrate material from wear¹²⁸. The plasma treatment has the advantages of: 1) applicable for both batch and continuous processes, 2) low capital investment, 3) suitability for many systems and 4) controllability of experimental conditions. However, the method also suffers from two major drawbacks: (A) the inability to produce films on many substrates and (B) the tendency to form thick films. Plasma is a highly ionized state of gas that includes ground or excited states of atoms and molecules, ions and electrons. Plasma treatment of polymer surfaces can lead to dissociation of bonds and ionization of atoms, hence resulting in a highly crosslinked surface, which is usually more wear resistant than the non- or weakly crosslinked surface. For example, tetrafluoroethylene and hexafluoroethane have been grafted onto wool or polypropylene fibers to reduce the friction coefficient¹⁴². Plasma polymerization of organic monomers such as styrene has also been used to form abrasion resistant coatings on substrates; however, this process is completely different from free radical polymerization. Plasma polymerization usually leads to heavily crosslinked systems that cannot be attained by normal free radical polymerization. Ceramic films may also be prepared on polymer surfaces by the plasma method. For example, hexamethylcyclotrisilazane

can be pyrolytically converted into a material which has a high content of amorphous siliconoxynitride which is quite wear and corrosion resistant¹⁴³.

1.3.3.2. Inorganic-Organic Hybrid Coatings

Silicones, silsesquioxanes, and some inorganic-organic hybrid materials have been proven to be good abrasion resistant coatings. These materials are commonly developed by the sol-gel process, and can be spread on polymer surfaces as sols and thermally or photochemically cured into hard coatings to protect the inner polymers from wear.

Silica modified polymethylsilsesquioxanes have been claimed as good abrasion resistant coatings for glazing plastics by H. A. Clark in the 1970s^{144,145}. Their application on bisphenol-A polycarbonate (bis-A PC) and poly(methyl methacrylate) (PMMA) was evaluated by Vincent et al¹⁴⁶. These hard coatings were prepared by hydrolyzing methyltrimethoxysilane in the presence of colloidal silica (Ludox), so the resulting materials should be poly(methylsilsesquioxane) bonded silica resins. The catalyst was acetic acid, and the coating formula had a shelf life of about four days. The resins could be spread on PMMA and bis-A PC substrates and thermally cured into an extremely hard, clear protective coating. [Table 1.2](#) lists the Taber test results of these coatings on bis-A PC and PMMA substrates. It was stated that the coating had good adhesion on these two substrates and excellent adhesion could be obtained after it was thermally cured. The curing temperatures for coatings on PMMA and bis-A PC were 80°C and 130°C, respectively. Small amounts of alkali acetates were good catalysts for the thermal curing process. The coatings also provided the polymer substrates with resistance to many chemicals including organic solvent, oils, acids or bases, etc.

Table 1.2. Abrasion resistant coatings based on methylsilsesquioxane and silica¹⁴⁶. Test method: Taber Abraser, 500 cycles, 500-gram load with CS10F wheels.

Substrate	MeSiO _{3/2} :SiO ₂	Delta % Haze
Plate Glass	0/100	0.5
Uncoated PMMA	50/50	20
Coated PMMA	50/50	2.5
Uncoated Bis-A PC	50/50	40
Coated Bis-A PC	50/50	1.7
PMMA	100/0	4.2
PMMA	90/10	3.0
PMMA	80/20	1.4
PMMA	70/30	0.6
PMMA	60/40	1.5
PMMA	50/50	0.6

Inorganic-organic hybrid abrasion resistant coatings have been pioneered by the work of Schmidt et al. in Germany (ORMOSILs and ORMOCERs)⁴⁻¹⁰ and Wilkes et al. in the United States (CERAMERS)¹¹⁻¹⁷. These hybrid materials were developed using sol-gel reactions, but different approaches were utilized. By controlling phase-separation between inorganic and organic components at the nanometer scale, these materials have high transparency in the visible light range and therefore are suitable optical coatings for transparent plastics.

The earliest ORMOSIL was prepared by Philipp and Schmidt by co-hydrolyzing glycidoxypropyltrimethoxysilane (3-GPTMS) with TEOS or titanium tetra(2-propoxide) (TiOiPr)¹⁴⁷. Both final gels were brittle, so 3-methacryloxypropyltrimethoxysilane (3-MPTMS) was added and the vinyl group was later thermally cured by a free radical initiator. These materials were claimed to have good flexibility, oxygen permeability and might be used in hard contact lens applications.

Schmidt et al. later formulated another abrasion resistant coating using aluminum tri(2-propoxide), 3-GPTMS and propyltriethoxysilane^{7,148}. By this approach, aluminum tri(2-

butoxide) (preparation of boehmite sols) was pre-hydrolyzed and then mixed with 3-GPTMS and n-propyltriethoxysilane in the molar ratio of 2:5:3¹⁴⁹. The mixture was spread on a PC substrate and cured at 90-130°C using methylimidazole as a catalyst to produce a clear coating, which showed good adhesion to the substrate. The vulcanization reaction is believed to be ring-opening polymerization of the epoxy groups in the system catalyzed by methylimidazole. Boehmite alone is also believed to be a catalyst for the polymerization.

Table 1.3. Scratch and Abrasion Tests of different coatings (composition in mol%: metal oxide 20, epoxysilane: 50; SiO₂: 30)⁷

Test	Coatings and Polymers				
	CR 39 (Uncoated)	PMMA (Uncoated)	Coating 1 M=Zr	Coating 2 M=Ti	Coating 3 M=Al
1) (Load in g)	1-2	<1	10	20-30	50
2) (Haze in %) 200 rev	12-13	20	-	1.5	
3) (haze in %)	4a	-	-	1.2a	-
	15b	-	-	6b	-

Minimum Vickers diamond indent load in grams required to detect a scratch optically by microscopy.

Percentage of scattered light after Taber abrasion compared to a nonabraded surface.

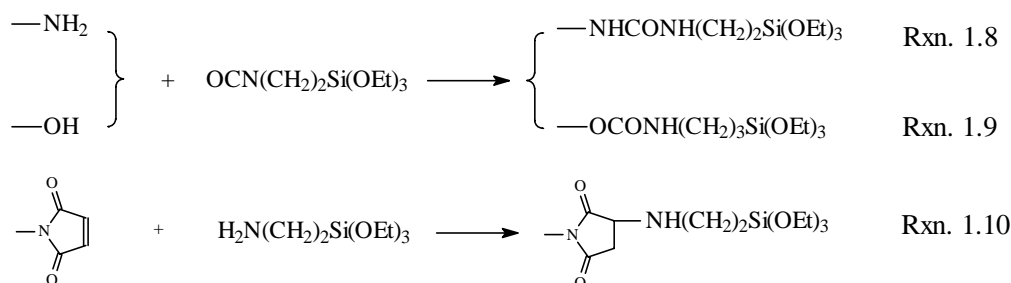
Special abrasive test simulating cleaning under dust-contaminated conditions: a: diamond powder, b: boron nitride powder.

Hybrid materials based on vulcanization of 3-GPTMS stabilized zirconia, titania along with silica were also developed and tested for scratch and abrasion resistance. Table 1.3 lists the scratch and abrasion test results for some coatings on CR39 PC and PMMA substrates. Among them, the boehmite based ORMOCER exhibited the best scratch and abrasion resistance.

The CERAMER abrasion resistant coatings have been developed using hydrolysis and condensation of triethoxysilylated *small organic compounds* along with metal or semi-metal alkoxides. The earliest CERAMER abrasion resistant coatings were reported by Wang and Wilkes using sol-gel reactions of f-DETA^{11,13,150}, the reaction product of one mole of DETA with 3 moles of 3-ICPTES. Zirconia or titania sols were also incorporated to increase the

refractive index of the coating¹⁵¹. Adhesion between the coatings and PC substrates was found quite satisfactory by the use of a Tape test (ASTM standard D3359-87).

Tamami, Betrabet and Wilkes have also introduced other triethoxysilylated organic compounds¹⁵²⁻¹⁵⁴. The organic compounds included 4,4'-aminophenyl disulfone, tri(2-aminophenyl)phosphine oxide, triethylenetetraamine, polyethyleneimines, and melamine (Table 1.4). Tri(2-aminophenyl)phosphine oxide was prepared by nitration of triphenylphosphine oxide followed by reduction of the nitro groups to amino groups using hydrazine as a reducing reagent. All the amines were triethoxysilylated by reacting with 3-ICPTES (Rxn. 1.8).

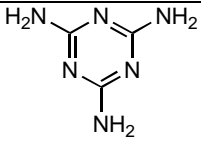
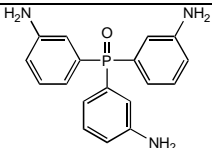
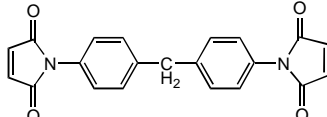
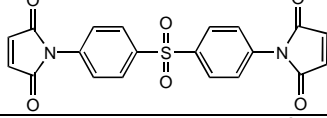
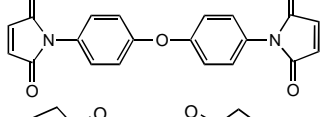
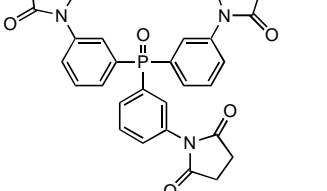


These functionalized materials were later hydrolyzed by reacting with an aqueous hydrochloric acid solution in appropriate solvents like tetrahydrofuran (THF), dimethylformamide (DMF), or 2-propanol so that the reaction occurred homogeneously. The sulfone and phosphine oxide amines were also functionalized by reacting with maleic anhydride and the resulting maleimide was later triethoxysilylated with 3-aminopropyltriethoxysilane by a Michael addition reaction (Rxn. 1.10). Similarly these materials were pre-hydrolyzed with a dilute aqueous hydrochloric acid solution, then applied on aluminum or bis-A PC substrates and thermally cured at 130-170°C. All these coatings demonstrated good wear abrasion resistance on the substrates mentioned above. ²⁹Si NMR spectroscopy indicated that a high curing temperature could lead to a higher extent of curing and better abrasion resistance^{155,156}. Zirconium 2-proxide was also incorporated into the f-DETA system, however, no obvious improvement to the abrasion resistance was observed¹⁵⁴.

The spectrum of organic modified silanes was further widened by Wen and Wilkes¹⁴⁻¹⁶ by including diols and triols such as glycerol, glycol, 1,4-butanediol, 1,6-hexanediol, resorcinol

and polyamines including 3,3'-iminobispropylamine (Table 1.5). Existing systems studied included DETA and polyethyleneimine. All these materials were functionalized with a slight excess of 3-ICPTES (Rxn. 1.9). The functionalized materials, along with TMOS or TEOS, were again diluted with 2-propanol, or THF or DMF and pre-hydrolyzed with a dilute hydrochloric acid solution. The resulting sols were applied on substrates and thermally cured into good to excellent abrasion resistant coatings on either bis-A PC or CR39. A marked increase of abrasion resistance was revealed by incorporating TMOS into functionalized DETA, IMPA, and polyols, and the highest concentration of TMOS that could be reached without cracking the coating during the curing process was about ca. 60%. The incorporation of TMOS reduced the adhesion of the coating to the bis-A PC and CR39 substrate, however, treatment of these substrates with a 3-aminopropyltriethoxysilane (3-APS) primer or oxygen plasma could significantly increase the adhesion. The enhanced adhesion is believed to be due to the hydrogen bonding between the amino group in 3-APS with the carbonate group in the PC substrate. A molecular dynamic (MD) simulation supported the hydrogen-bonding hypothesis. The influence of coating hardness on the abrasion resistance was also studied. For the aliphatic polyol based systems, the wear resistance increased with the coating hardness, but no obvious correlation was revealed between coatings with different types of organic components. Aluminum alkoxides, zirconium alkoxides, and titanium alkoxides were incorporated into the f-DETA system^{17,157}, and the f-DETA50Zr50 system, which contains 50 wt% of f-DETA and 50 wt% of zirconium butoxide, exhibited better abrasion resistance. This coating also maintained its abrasion resistance and adhesion to the bis-A PC substrate after treating in boiling deionized water for one hour (hot-wet condition). Wen, Jordens, and Wilkes¹⁷ have also demonstrated the potential for a UV absorber to be incorporated into the sol-gel coatings so that abrasion resistant and UV resistant coatings might be prepared.

Table 1.4. Inorganic-organic hybrid coatings and their abrasion resistance reported in reference ¹⁵²⁻¹⁵⁴. Test Method: Taber abraser, 200 cycles, 250 g load, CS-10 wheels.

Organic Compounds	Silane Coupling Reagents	Cure Conditions	Abrasion Resistance*
$\text{H}_2\text{NCH}_2\text{CH}_2\text{NHCH}_2\text{CH}_2\text{NH}_2$	3-ICPTES	146°C/3 hrs.	98.5%
		100°C/3 hrs.	96 %
		80°C/3 hrs.	95 %
Polyethyleneimine 600-1800		135°C/3 hrs.	96 %
		132°C/12 hrs.	94-97.5%
		135°C/3 hrs.	96%
	3-APS	135°C/3 hrs.	~97%
		135°C/3 hrs.	~96%
		135°C/3 hrs.	92%
		135°C/3 hrs.	96%

* Defined by transmittance

Table 1.5. Typical coatings which have percent transmittance beyond 90% in Taber test with CS-10 abrasers and 500 cycles/500 g¹⁴

Organic Compounds	Acronyms	Coupling Reagents	Silanes	Typical* Formulation
Diethylenetriamine	DETA	3-ICPTES	TMOS	f-DETA50TMOS50
Glycerol	GLYL	3-ICPTES	TMOS	f-GLYL60TMOS40
Resorcinol	RSOL	3-ICPTES	TMOS	f-RSOL60TMOS40
Hexanediol	HXOL	3-ICPTES	TMOS	f-HXOL60TMOS40
Bis(3-aminopropyl)imine	BAPI	3-ICPTES	TMOS	f-IMPA60TMOS40
Ethylene glycol	ETYL	3-ICPTES	TMOS	f-ETYL60TMOS40
Poly(ethyleneimine)	PEI	3-ICPTES	TMOS	f-PEI60TMOS40

Formulation are based on the weight percentage of unhydrolyzed silane and functionalized organic compounds

Jordens and Wilkes have applied the coatings derived from f-DETA and TMOS or other metal alkoxides on various metal substrates including aluminum, copper, brass, stainless steel and carbon steel¹⁵⁸⁻¹⁶¹. Except for the carbon steel substrate, the abrasion resistance of all substrates was greatly improved by these coatings. A typical recipe used by Wen and Jordens was made of equal weights of f-DETA and TMOS. The system was in fact provided in a two-part formula: part A consisted of a solution of equal weights of f-DETA and TMOS in 2-propanol (by weight f-DETA:TMOS: ⁱPrOH=1:1:1.14), and part B was a dilute aqueous solution of hydrochloric acid (0.5N). The coating recipe was prepared by slowly adding one part of part B into eighteen parts of rigorously stirred part A. After mixing, the system was allowed to pre-hydrolyze for 5-15 min. at room temperature and the resulting transparent sol was spread on the chosen substrates. Hard abrasion resistant coatings could be formed on the substrates after being thermally cured at a temperature between 130-170°C for ca. 5 hrs. depending on the stability of the coating and substrate.

1.3.4. Summary

The sol-gel process based on the hydrolysis and condensation of metal or semi-metal alkoxides permits the preparation of extremely pure metal oxides. The process can be used to prepare materials in various forms including powders, colloids, films or coatings, porous or monolithic objects. The morphology of sol-gel derived products depends on many factors including the structure of the starting materials, pH, water concentration, solvent, aging and drying. Among them, pH and the ratio of water to alkoxide in sol-gel processes of tetraalkoxysilanes are the key factors influencing the morphology of the final silica gels. At a low pH ($\text{pH} < 1$) in a water-deficient medium, extended polymeric gels (low fractal dimension) are usually obtained. However, at a relative high pH ($\text{pH} = 4-7$), the resulting gels are often more particulate (high fractal dimension). Monodisperse spherical silica particle sols can be prepared at pH 7.5-10, where silica has a relatively high solubility. Multiple step hydrolysis processes may be used to control the morphology of the resulting silica gels.

After gelation, aging, drying and curing processes can also lead to relatively large changes in the gel structure. The gel strength generally increases during the aging process via syneresis and coarsening of the gel. As the solvent and condensation by-products evaporate during the drying period, the gel undergoes extensive shrinkage due to the presence of the condensation reactions, osmotic pressure and capillary forces. The capillary force is believed to be the essential force that causes the huge shrinkage and possible cracking of the gel during the drying process. For this reason, it is difficult to prepare pure inorganic metal oxide films thicker than a few hundred angstroms.

One of the most important advantages of the sol-gel process is its low temperature operation, which allows organic components including proteins to be incorporated without decomposition or denaturation. This special feature has resulted in the advent of a new class of materials called microphase-separated inorganic-organic hybrid materials. The properties of these new materials may be modified to from that of the polymer component to that of the ceramic by changing the structure and composition of the organic and inorganic components. The incorporation of organic component also increases the strength and flexibility of the wet gel,

so thick crack-free films or coatings of moderate strength can be easily prepared at a very low temperature.

During the past fifteen years, various inorganic-organic hybrid materials have been developed as abrasion resistant coatings. For example, Schmidt et al. have developed so called ORMOSIL/ORMOCER coatings by vulcanization of 3-GPTMS or 3-MPTMS modified inorganic nanoparticles. These inorganic particles were prepared by either modification of nanometer metal oxide colloids or hydrolysis of metal alkoxide in the presence of the silanes. Wilkes et al. have also prepared CERAMER coatings by sol-gel reactions of triethoxysilylated organic compounds along with a metal or semi-metal alkoxide and a typical example of such coatings is based on f-DETA and TMOS. Hybrid coatings formed by these methods have been applied on many optical plastics including bis-A PC, CR39 and PMMA and they exhibit good to excellent abrasion resistance. Due to the complexity of the wear phenomena and the differences in the testing methods, it is not possible to compare the performance of these coatings according to the published data. Nevertheless, the application of a thin layer of such hybrid protective coatings has clearly demonstrated to be a very effective approach to enhance the abrasion resistance of the polymer substrates.

To date, CERAMER sol-gel coatings developed from triethoxysilylated organic compounds and tetraalkoxysilanes have shown abrasion resistance close to that of ceramic materials. More important, this approach is still in its infancy stage and hence it still has enormous potential for future development. Even for the most extensively studied f-DETA/TMOS systems, there is still a scarcity of knowledge about the influences of many formulation and processing variables on the gelation time, morphology, and properties of the resulting gels. For these reasons, *this dissertation mainly addresses these fundamental aspects for the f-DETA/TMOS system, which represents many binary systems including both $RSi(OR)_3$ and $Si(OR)_4$. However, some novel trialkoxysilylated organic compounds and new synthetic approaches will also be introduced.*

CHAPTER 2. PREPARATION AND CHARACTERIZATION OF ABRASION RESISTANT COATINGS

2.1. INTRODUCTION

Abrasion resistant coatings to be addressed in this dissertation were developed by sol-gel reactions of a metal or semi-metal alkoxide and a trialkoxysilylated organic compound less than 2000 g/mole in molecular weight. Among them, the system based on the triethoxysilylated diethylenetriamine or f-DETA was the most extensively studied. The sol-gel reactions of this system were carried out either by a *one-step approach*, a *two-step approach*, or a *moisture vulcanization* approach (Fig. 2.1). Whichever processing method was used, the overall process for preparing such sol-gel hybrid coatings generally involved the following six fundamental steps:

- (1) trialkoxysilylation of an organic compound;
- (2) formulation of abrasion resistant coating recipe;
- (3) surface treatment of the selected substrates;
- (4) spreading of the coating recipe onto the surface-treated substrates;
- (5) drying and curing of the wet sol layer into an abrasion resistant coatings;
- (6) characterization of the final coating.

Among these six steps, step (1) depended mainly on the functional groups in an organic compound, while steps (2) and (5) might be affected by the acidity/basicity and solubility of the functional organic compounds and the selection of the processing method. Steps (3), (4), and (6) were mainly related to the substrate treatment, coating formation, and quality control, which were common to most sol-gel derived coatings.

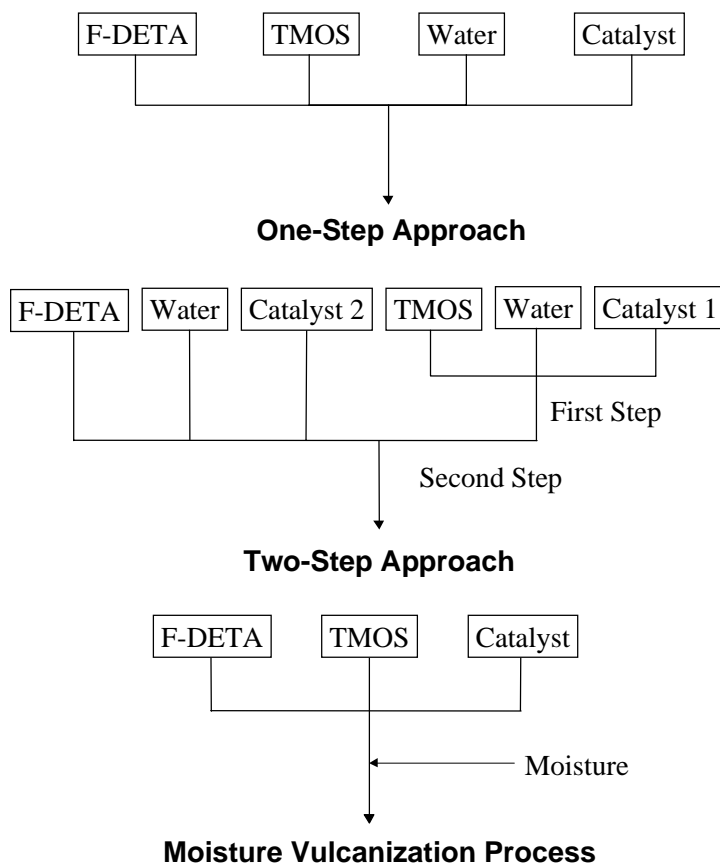


Fig. 2.1. The one-step approach, two-step approach and moisture vulcanization approach used for preparation of f-DETA/TMOS sol-gel coatings.

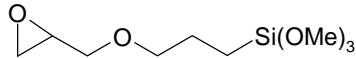
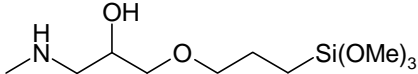
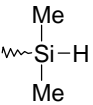
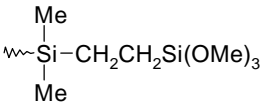
Table 2.1 lists chemical reactions utilized to attach trialkoxysilyl groups to organic compounds containing the specified functional group. Reaction 1 was used to functionalize diethylenetriamine (DETA), bis(3-aminopropyl)imine (BAPI), and 1,3-bis(3-aminopropyl)-tetramethyldisiloxane. Many linear aliphatic diamines were also triethoxysilylated by this reaction, however, the resulting compounds turned out to be crystalline materials insoluble in hot alcohol or even N,N-dimethylformamide (DMF) (at $<100^{\circ}\text{C}$) and hence were not appropriate for preparing sol-gel derived coatings. Reaction 2 was used to functionalize triethanolamine (TEA) and N,N,N',N'-tetra(2-hydroxypropyl)ethylenediamine (THPEDA). Reaction 3 is the same as Reaction 1 except that the position of amine and 3-isocyanato groups in the silane and organic compound are exchanged. Isophorone diisocyanate was triethoxysilylated by this reaction and

the resulting compound was a colorless crystalline material soluble in isopropanol at ca. 50°C. The counterpart of 1,6-diisocyanatohexane, however, turned out to be a crystalline material that did not dissolve in hot isopropanol and DMF (<ca. 100°C). Ethylenediamine was functionalized by reacting with 3-glycidoxypropyltrimethoxysilane (3-GPTMS) by Reaction 4. The resulting compound was a colorless solution in methanol, and it polymerized and even gelled when the solvent evaporated. Reactions 5 and 6 were applied to introduce triethoxysilyl groups to various siloxane compounds such as tetrakis(dimethylsilyl) silicate and vinyl dimethylsilyl cubic octasilicate, and the resulting compounds were generally colorless oily liquids.

The formulation of abrasion resistant coatings depended on the choice of processing method (Fig. 2.1). In a one-step approach, the water component was directly added to a mixture of a trialkoxysilylated compound and a metal alkoxide. In a two-step approach, however, the metal alkoxide was pre-hydrolyzed by a portion of the water component before the addition of trialkoxysilylated compound and the rest of the water component. Alternatively, commercial colloidal metal oxides were directly used to replace the metal alkoxide, and by this route, the pre-hydrolysis step could be omitted. Coatings by both the one- and two-step approaches were dried at room temperature and then thermally cured at ca. 125 for bisphenol-A polycarbonate and ca. 170°C for metal substrates. By a moisture vulcanization approach, the coating recipe was usually a mixture of a trialkoxysilylated organic compound, a pre-hydrolyzed metal alkoxide, and a titanium alkoxide catalyst. The water component for hydrolysis and condensation of this recipe was obtained from moisture in air when the system was cured at ambient conditions. For this reason, the moisture-cured system usually must be cured at room temperature in a humid environment (80% humidity) for 2-4 weeks.

Since Chapters 3, 5-7 of this dissertation will mainly discuss the f-DETA/TMOS coatings developed by the one-step approach (Fig. 2.2), the following sections will systematically describe the experimental details of the six fundamental steps of this process. In fact, sol-gel coatings derived from trialkoxysilylated organic compounds mentioned above were rather similar in coating formulation and characterization, so many of the techniques/processes utilized for the f-DETA/TMOS system were also adequate for the other systems mentioned above. The details of those systems will be presented in Chapters 7 and 8.

Table 2.1. Some chemical reactions that were utilized in this research to attach –Si(OR)₃ groups to organic compounds

No.	Group A (Organic Compounds)	Group B (Silanes)	Products	Examples of Organic Compounds
1	-NH ₂	OCN-(CH ₂) ₃ Si(OEt) ₃	-NHCONH(CH ₂) ₃ Si(OEt) ₃	Diethylenetriamine
2	-OH		-OCONH(CH ₂) ₃ Si(OEt) ₃	Triethanolamine
3	-NCO	H ₂ N-(CH ₂) ₃ Si(OEt) ₃	-NHCONH(CH ₂) ₃ Si(OEt) ₃	Isophorone diisocyanate
4	-NH ₂			Ethylenediamine
5	-CH=CH ₂	H-Si(OEt) ₃	-CH ₂ CH ₂ Si(OEt) ₃	Vinyldimethylsilyl cubic octasilicate
6		CH ₂ =CH-Si(OMe) ₃		(H(CH ₃) ₂ SiO) ₄ Si

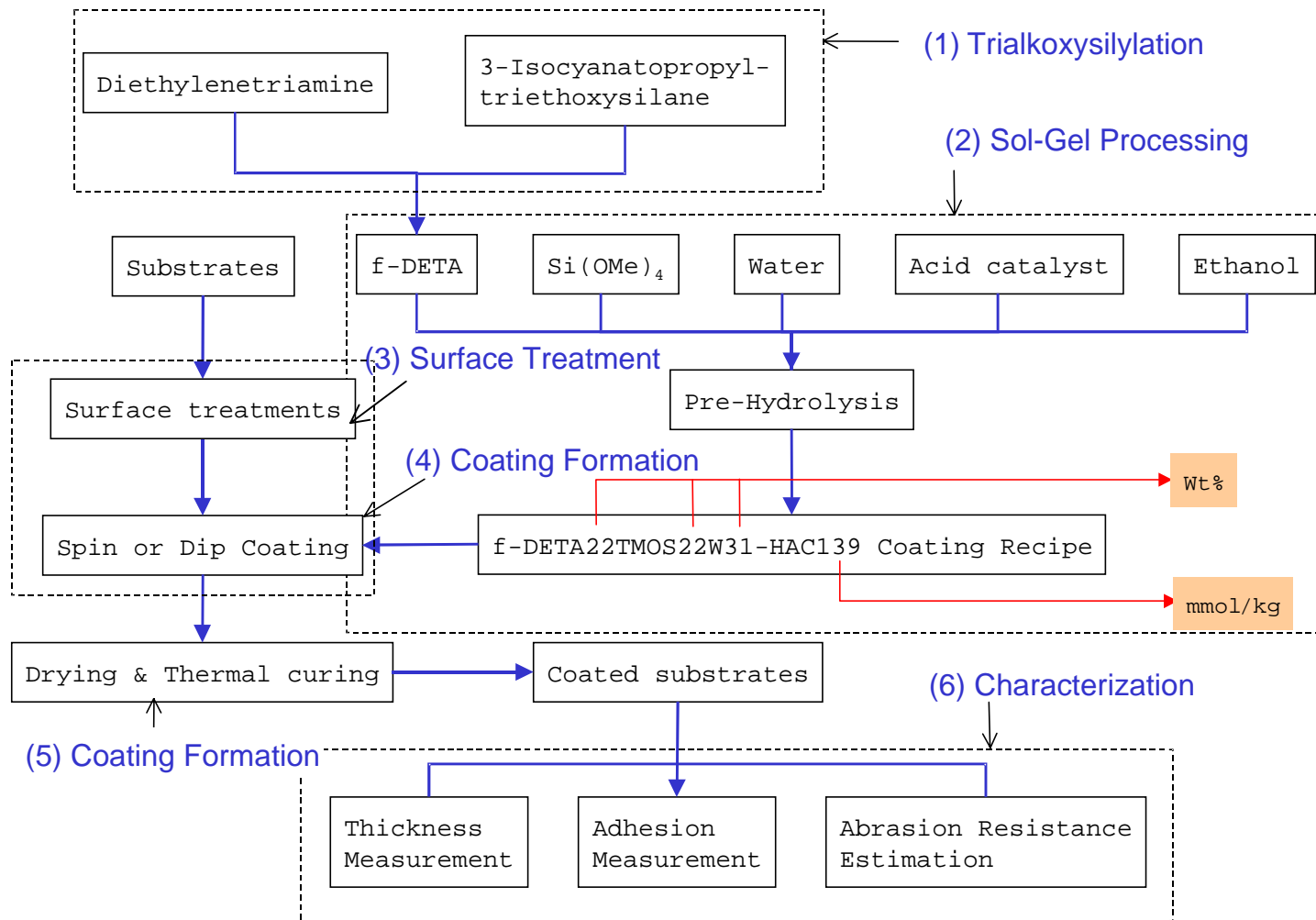


Fig. 2.2. A flowchart showing the six fundamental steps of the one-step approach for preparation of the f-DETA/TMOS sol-gel inorganic-organic hybrid coatings.

2.2. TRIETHOXYSYLYLATION OF DIETHYLENETRIAMINE

The triethoxysilylation of DETA or preparation of f-DETA was the first step to prepare a f-DETA/TMOS abrasion resistant coatings (Fig. 2.2). This step simply involved the reaction of one mole of DETA with three moles of 3-isocyanatopropyltriethoxysilane (3-ICPTES) (Fig. 2.3). However, the choice of the alcohol solvent might have an influence on the reactivity of the final product since the triethoxysilyl groups in the system can react with the alcohol solvent by transesterification. When f-DETA was first introduced by Wang and Wilkes in 1991¹², the reaction was carried out in 2-propanol. Their synthetic procedure was later adopted by Betrabet¹⁵⁵, Wen¹⁴, Jordens¹⁵⁹ with almost no modification. F-DETA used at the early stages of this work was also prepared by this method and the following is the procedure for preparing this compound.

A 250 ml flask was charged with 5.00 g of DETA (99% Aldrich) and 20 g of 2-propanol. To this DETA solution were slowly added 39.3 g (ca. 5% in excess) of 3-ICPTES (95%, Gelest). During the addition of 3-ICPTES, the solution was rigorously stirred and cooled by an ice bath to avoid possible side reactions. After all the 3-ICPTES had been added, the mixture was stirred at room temperature for another 12 hours and a 70 wt% solution of f-DETA in 2-propanol was obtained. The f-DETA solution was stored in a closed container and used *within a week after preparation*.

Recent ¹³C solid state NMR studies (discussed in Chapter 5) indicated that if the starting f-DETA that was stored in 2-propanol for more than 3-4 weeks, the resulting coating had a substantially higher concentration of 2-propoxy groups than similar coatings derived from freshly prepared f-DETA. It was reasoned that, during storage, some triethoxysilane groups in f-DETA had slowly reacted with the solvent 2-propanol and became 2-propoxysilane groups (transesterification). 2-propoxysilane groups are less reactive towards hydrolysis and condensation, and thus are more likely to remain in the final gel. For this reason, the 2-propanol solvent was replaced by ethanol to avoid structural changes of functional groups associated with transesterification. In ethanol, the f-DETA monomer was expected to maintain consistent

reactivity if stored in a closed container. The following provides the details for the modified triethoxysilylation procedure.

A 250 ml flask was charged with 5.00 g of DETA (99% Aldrich) and 20 g ethanol. Then 40 g (ca. 7% in excess) of 3-ICPTES (95%, Gelest) were slowly added to the DETA solution as the mixture in the flask was rigorously stirred and cooled by an ice bath. After all the 3-ICPTES had been added, the mixture was stirred for 12 hours and a 70% solution of f-DETA in ethanol was obtained. Similarly, this product was stored in a closed container.

Ethanol is more reactive towards isocyanato groups than 2-propanol and hence it may compete with the secondary amine group in DETA for 3-ICPTES. However, FTIR indicated that the process only led to a trace amount of urethane ($\text{EtOCONH}(\text{CH}_2)_3\text{Si}(\text{OEt})_3$), indicating that the reactivity of ethanol towards the isocyanato group is, as expected, much lower than that of the secondary amine group.

2.3. FORMULATION OF F-DETA/TMOS COATING RECIPES

2.3.1. General Approaches for Coating Formulation

After preparation of f-DETA, the next step was to formulate f-DETA/TMOS coating recipes. Excluding the catalyst (usually only a small amount), a f-DETA/TMOS coating recipe typically included four components: f-DETA, TMOS, water and an alcohol (either 2-propanol or ethanol). In this quaternary system, f-DETA and TMOS are partially miscible with water, while any other two components are infinitely miscible. Therefore, during coating formulation, extra alcohol solvent was added so that the resulting recipe had a suitable balance between the "solids" concentration, water concentration, and spreadability on bis-A PC substrates. To maintain a sufficient "solids" concentration in a coating recipe, the combined concentration of f-DETA and TMOS was controlled to 40-60 wt%. After hydrolysis, the recipe would have a solids concentration of about 20-40 wt% since large amounts of methanol and ethanol were generated.

The water concentration was modified in the range of 5-40 wt%. Generally, a lower water concentration led to a lower extent of condensation and hence poor abrasion resistance of the final coating. However, if it was higher than 40 wt%, the recipe would not spread on bis-A PC substrates and consequently smooth coatings could not be formed.

The hydrolysis and condensation were mainly catalyzed by acid catalysts including hydrochloric acid, phosphoric acid and acetic acid, which will be abbreviated in coating nomenclature as HCL, HPO, and HAC, respectively. As sol-gel reactions are generally considered to undergo specific acid catalysis or specific base catalysis^{28,162}, the overall reaction rate is mainly dependent on pH. However, the starting material f-DETA often included an uncertain small amount of free amines, which could be from an excess amount of either f-DETA or 3-ICPTES. Consequently, some acid catalyst would be consumed and accurate control of pH was in fact not practical. If an excess amount of a weak or intermediately strong acid is used as the catalyst, parts of the acid react with the residual amine to form an ammonium salt, which forms a buffer system with the remaining acid, leading to stabilization of pH. With hydrochloric acid, phosphoric acid ($pK_a1=1.3$, $pK_a2=7.21$), and acetic acid ($pK_a=4.76$) as the catalyst, which are different in acidity strength, the pH of the coating recipe was controlled reproducibly to a value within the range of 0-5.

A number of f-DETA/TMOS coating recipes was formulated by adding various amounts of water and TMOS to a fixed amount of a 47 wt% f-DETA solution in 2-propanol. These formulae fell on the f-DETA47ⁱPrOH53-TMOS-water section in the f-DETA-TMOS-water-ⁱPrOH quaternary phase diagram (Fig. 2.4), where f-DETA47ⁱPrOH53 represents a 47 wt% solution of f-DETA in 2-propanol. In this tertiary system (reshaped to an equilateral triangle in Fig. 2.5), the two independent formulation variables can be represented by the TMOS concentration and the equivalent ratio (r) of water to alkoxy silane. A third formulation variable was introduced by changing the pH of the system. Changing the alcohol concentration leads to deviation of composition from this f-DETA47ⁱPrOH53-TMOS-water section. However, a slight change in the solvent concentration generally does not lead to significant changes in the performance of the final coating, so most experiments discussed in this dissertation are based on compositions on the f-DETA47ⁱPrOH53-TMOS-water system.

By the weight ratio of f-DETA to TMOS, the compositions in Fig. 2.5 can be divided into a f-DETA50TMOS50 series (A, B, C, D, E), a f-DETA56TMOS44 series (E), a f-DETA65TMOS35 series (F, M), and a f-DETA100 series (G, H, I, J, K, L), which correspond to a gradual change in the TMOS concentration. In the series f-DETA50TMOS50 and f-DETA100, compositions A, B, C, D, E and compositions G, H, I, J, K, L correspond to a change of r from 0.55, 1.1, 2.2, 3.3, to 4.4 and 0.47, 0.93, 1.86, 3.72, 7.44, and 14.9, respectively. As r increases, both the f-DETA50TMOS50 and f-DETA100 series change from a homogeneous system to a heterogeneous system. Experiments showed that with an r value of 3.3 or 4.4 (Compositions A and B), the f-DETA50TMOS50 recipe was heterogeneous. However, in the presence of an acid catalyst, the system quickly became homogeneous as the alkoxy silane groups were hydrolyzed to hydrophilic silanol groups. With different catalysts, the compositions shown in Fig. 2.5 were used to form abrasion resistant coatings on bisphenol-A, aluminum or brass substrates. The influences of pH, r , and the TMOS concentration on the optical properties, morphology, hardness and abrasion resistance of the final coating will be systematically addressed in Chapters 3 and 6.

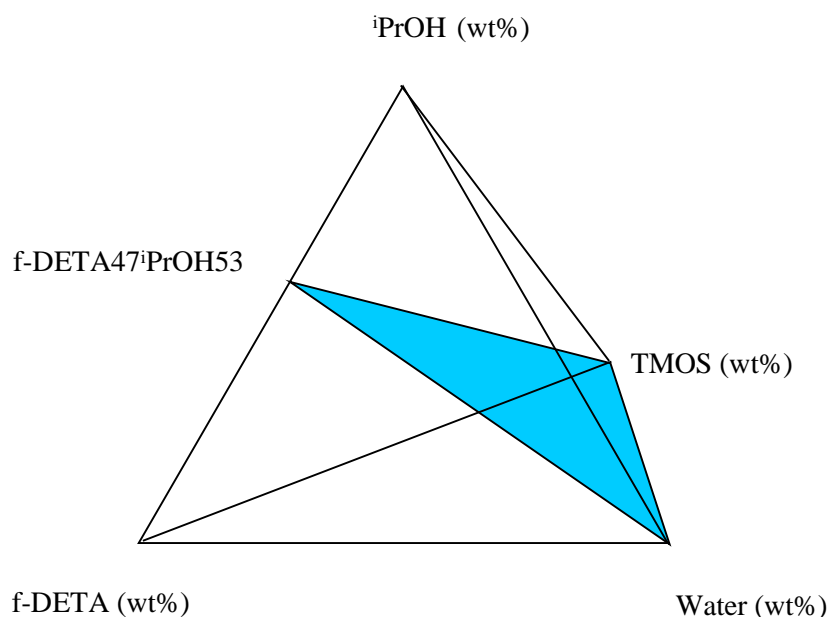


Fig. 2.4. The f-DETA-TMOS-water-ⁱPrOH quaternary system showing the sections f-DETA47ⁱPrOH53-TMOS-Water and f-DETA-water-ⁱPrOH.

Since the f-DETA100 series in Fig. 2.5 does not have a constant f-DETA concentration, a f-DETA100' series was prepared by adding various amounts of water to a fixed amount of f-DETA and maintaining the total weight of the recipe unchanged by adjusting the amount of the alcohol solvent. The compositions of both f-DETA100 and f-DETA100' series can be shown on the f-DETA-water-ⁱPrOH section (Fig. 2.6) of the f-DETA-TMOS-water-ⁱPrOH quaternary phase diagram. In both the f-DETA100 and f-DETA100' series, r is gradually changed from 0.47, 0.93, 1.86, 3.72, 7.44, and 14.9. Based on these compositions, the influence of pH and r on the morphology of f-DETA gels was studied and the details will be discussed in Chapter 6.

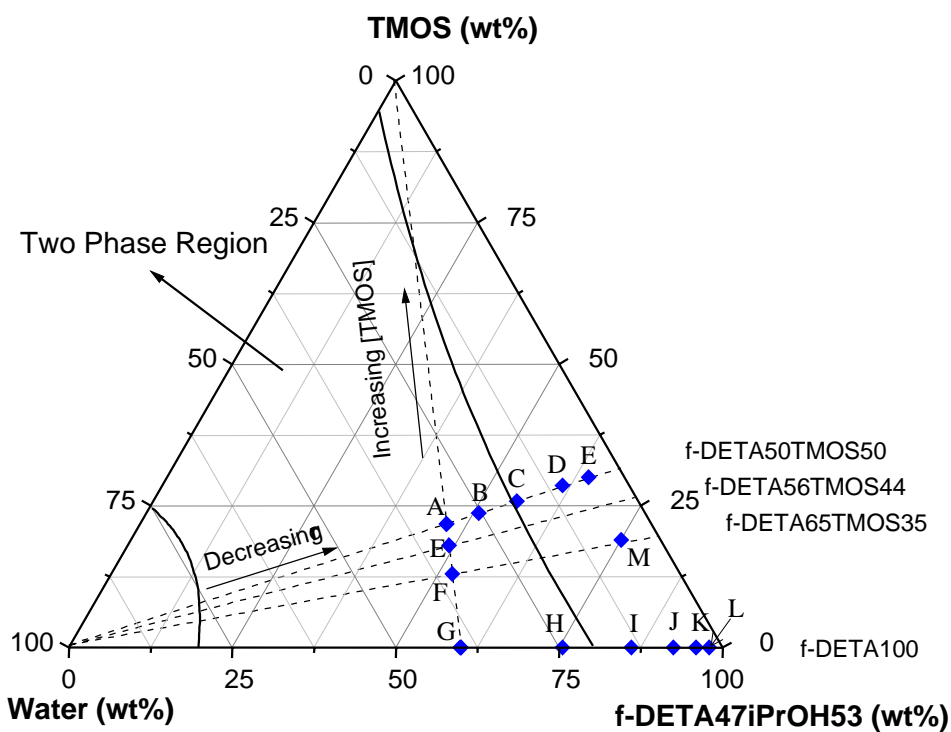


Fig. 2.5. The compositions of f-DETA/TMOS coating recipes studied in this dissertation. Note this section is reshaped to an equilateral triangle and the phase equilibrium lines are only illustrative purposes and are not necessarily precise.

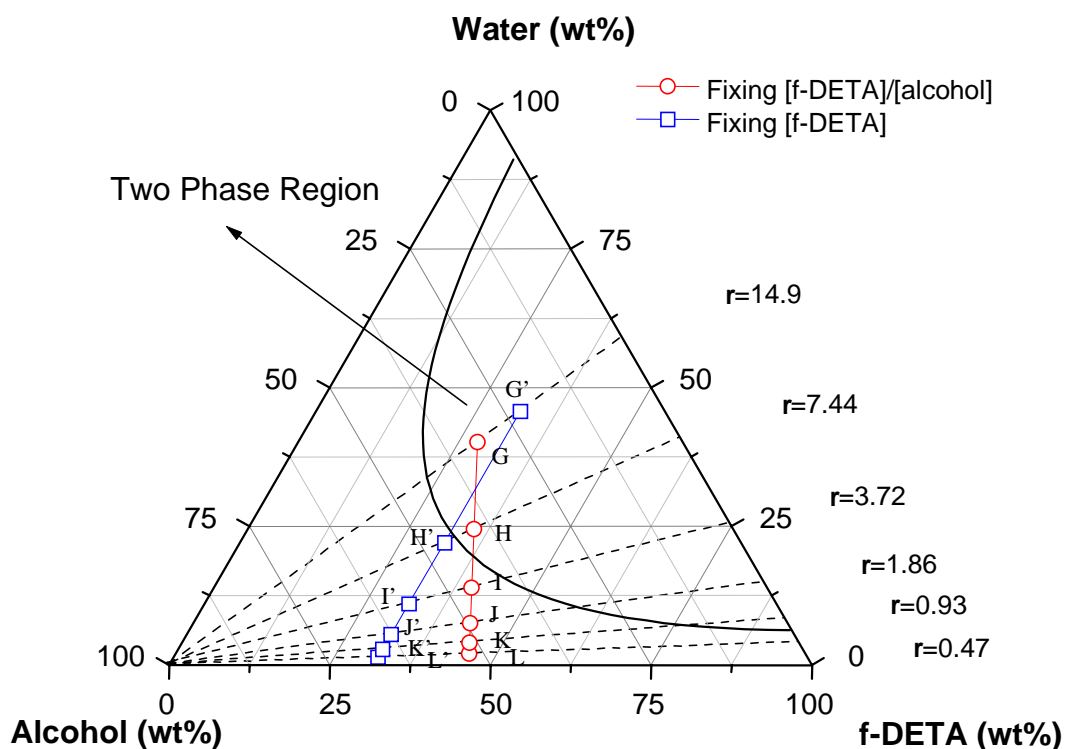


Fig. 2.6. The compositions of f-DETA gels studied in this dissertation. Note phase equilibrium lines are only for illustrative purposes.

2.3.2. Nomenclature

F-DETA/TMOS coating recipes are generally named according to the weight percentage of major components f-DETA, TMOS, water, and the alcohol solvent, and the concentration of the catalyst in millimoles per kilogram of the recipe (excluding the catalyst). In the nomenclature, the catalyst part is separated from the major components by a dash and the alcohol solvent is usually not explicitly stated in the nomenclature. In fact, coating recipes usually only contained trace amounts of the catalyst, so the contribution of the catalyst to the weight of the recipe could be neglected. For example, the recipe f-DETA22TMOS22W31-HAC140 in Fig. 2.2 represents a system containing 22 wt% of f-DETA, 22 wt% of TMOS, 31 wt% of water, 25 wt% of ethanol, and 140 mmol/kg of acetic acid catalyst.

The nomenclature scheme addressed above is quite long, so a shorthand based only on the weight percentage of f-DETA and TMOS with regard to the total weight of these two components is sometimes used. For example, f-DETA50TMOS50 represents a recipe including equal amounts of f-DETA and TMOS. However, due to the uncertainty of this scheme, the synthetic procedures for such coatings are also provided when these recipes are addressed.

Generally, f-DETA/TMOS sol-gel coatings were formulated as a two-part system: part A was a mixture of f-DETA with TMOS in the solvent 2-propanol (or ethanol) and part B was an aqueous solution of an acid catalyst. Coating recipes were formulated by mixing given amounts of part A and part B. After a period of pre-hydrolysis, the resulting transparent sol was spin- or dip-coated on chosen substrates before gelation occurred.

2.3.3. Examples of Coating Recipes

This section describes the preparation of coatings f-DETA31TMOS31W5-HCL27, f-DETA26TMOS26W19-HPO23, and f-DETA22TMOS22W31-HAC140. These three recipes correspond to compositions E, C, and A in [Fig. 2.5](#), respectively.

2.3.3.1. *F-DETA31TMOS31W5-HCL27*

This f-DETA50TMOS50 coating recipe has been used by Wen, Jordens, and Wilkes to prepare abrasion resistant coatings on substrates including bis-A PC, CR39, aluminum, brass, copper, and stainless steel^{14,158,159,161}. To prepare this coating, a silane solution (part A) was prepared by mixing 4 g of f-DETA solution (70 wt% in 2-propanol), 2.8 g of TMOS and 2 g of 2-propanol. Then to this rigorously stirring silane solution was added 0.5 g of 0.5 M aqueous hydrochloric acid (part B). After the mixture had been stirred for 2-3 min. at room temperature, it was spin-coated onto 3-APS treated bis-A PC substrates or degreased brass and aluminum substrates before gelation occurred ($t_{\text{gel}} = 5\text{-}15$ min. at room temperature). The coated substrates usually became nontacky in about three hours in air at ambient conditions.

2.3.3.2. *F-DETA26TMOS26W19-HPO23*

A silane solution (part A) was prepared by mixing 4 g of f-DETA (70 wt% in 2-propanol), 2.8 g of TMOS, and 2 g of 2-propanol. Then 1 g of 0.25 M aqueous phosphoric acid solution (part B) was slowly added to the rigorously stirring silane solution. After 10-15 min. of pre-hydrolysis at room temperature, the resulting sol was spin-coated onto 3-APS treated bis-A PC substrates or degreased brass and aluminum substrates before gelation occurred ($t_{\text{gel}} = 25\text{-}45$ min. at room temperature). The coated substrate became nontacky within 15-30 min. in air at ambient conditions.

2.3.3.3. *F-DETA22TMOS22W31-HAC140*

A silane solution (part A) was prepared by mixing 4 g of f-DETA (70 wt% in ethanol or 2-propanol), 2.8 g of TMOS, 2 g of ethanol (or 2-propanol). An acetic acid solution (part B) was prepared by dissolving 0.1 g of glacial acetic acid in 4 g of water (part B). To prepare the coating recipe, the acetic acid solution was added to the silane solution and the mixture was pre-hydrolyzed for 5-6 hrs. at room temperature, then spin- or dip-coated on 3-APS-treated bis-A PC substrates or degreased aluminum substrates. This recipe had a gelation time of 8-10 hrs. at room temperature. If diluted with 5 g of 50% aqueous ethanol solution (or 2-propanol), the gelation time of this recipe could be extended to about 24 hrs. The dilute recipe had been used for dip coating to obtain very smooth coatings on bis-A PC and aluminum substrates. With this coating recipe, the coated substrate usually became nonstick within 15-30 min. at room temperature.

2.4. SURFACE TREATMENT OF SUBSTRATES

The adhesion between a substrate and a final sol-gel hybrid coating is strongly dependent on physical/chemical conditions of the substrate. An untreated bis-A PC substrate usually had poor adhesion to a f-DETA50TMOS50 coating, but application of a 0.5 wt% 3-APS primer or oxygen plasma treatment of the substrate could effectively promote the bonding between the

interface of these two materials¹⁴. A hydrogen bonding mechanism was proposed to explain the promotion of adhesion by the primer 3-APS¹⁴. The author has also proposed an aminolysis mechanism to explain experimental facts that are difficult to explain by the hydrogen bonding mechanism¹⁶³ and the details of this mechanism will be addressed in [Chapter 4](#).

Experimentally, the primer 3-APS was applied onto bis-A PC substrates by wiping the substrate with a filter paper soaked with a 0.5 wt% APS solution in 2-propanol. A more standard method involved spin-coating a 5% 3-APS solution in 2-propanol (~500 rpm) on bis-A PC substrates. After spreading a layer of 3-APS primer on the substrate, the treated substrate was immediately heated at 125°C for 30 min. The two methods were equally effective, however, the latter method formed coatings of better optical quality.

For metal substrates, a brief degreasing of the substrate with organic solvents such as 2-propanol can ensure sufficient adhesion to a sol-gel derived coating. Sanding of the substrate increases the surface roughness and creates a fresh metal surface, which can increase the adhesion by promoting mechanical-interlocking and enhancing chemical bonding between the substrate and the sol-gel coating, respectively. However, the sanding method also leads to significant changes in the surface feature of the substrate. In this work, the aluminum and brass substrates were only degreased with 2-propanol before being coated with the sol-gel coatings.

2.5. COATING FORMATION

Many coating techniques have been developed to apply coatings on articles of various shape and dimensions. Brush coating, flow coating, and spray coating are easier to apply, but usually have poor control of thickness. Sophisticated commercial dip- or spin-coating apparatuses, however, can provide precise control over the coating thickness. Since the solidification of sol-gel coatings is irreversible, some coating techniques may not provide good quality sol-gel coatings. Even with sophisticated instrumentation, precise process control may be still tricky since the viscosity of the sol-gel recipe increases progressively with the time because of continuous silanol condensation. In this work, simple self-made spin- and dip-coating devices

were utilized to form sol-gel coatings for abrasion resistance evaluation. Here spin- and dip-coating processes and the related equipment are briefly described.

2.5.1. Spin-Coating

A spin coating apparatus usually includes a vertically installed motor, a protecting box, and a horizontal plateau fixed on the vertical shaft of the motor. The substrate can be mounted horizontally on the sample plateau. The spin coating process has been roughly divided by Bornside et al.¹⁶⁴ into five stages: deposition, spin-on, spin-up, spin-off and evaporation, although solvent evaporation often accompanies the spin-up process. During the deposition stage, an excess amount of the coating recipe is dispensed on the upper surface of the substrate. In the following spin-spreading stage, the motor is started and the liquid flows radially outward, driven by the centrifugal force. During this stage, excess liquid flows to the perimeter and leaves as droplets. In the final stage, solvent evaporates and a thin layer of the coating is formed on the substrate.

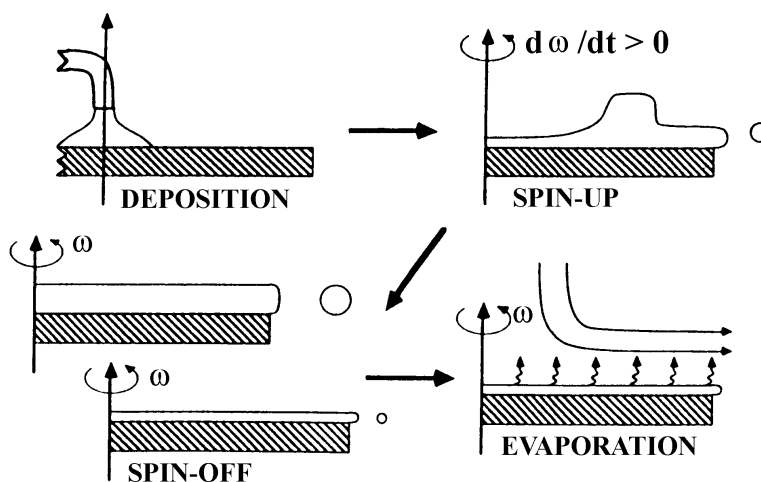


Fig. 2.7. Different stages of the spin coating process. Cited from reference ¹⁶⁴

For Newtonian liquids, which do not exhibit a shear rate dependence on the viscosity, the spin coating process can result in a liquid layer uniform in thickness¹⁶⁵. However, for shear

thinning liquids, the lower shear rate experienced near the center of the substrate causes higher viscosity and hence slightly thicker films there. In order to overcome this problem, some commercial spin coating equipment employs a sophisticated dispensing system that compensates for the thickness difference using a radially moving arm. Assuming the spin-off and evaporation stages are separated, Meyerhofer¹⁶⁶ derived the following equations to predict the final coating thickness and the total elapsed time to achieve this thickness for Newtonian fluids.

$$h_{\text{final}} = \left(1 - \frac{\rho_{A_0}}{\rho_A}\right) \left(\frac{3\eta m}{2\rho_{A_0} \omega^2}\right)^{1/3} \quad \text{Eqn. 2.1}$$

$$t_{\text{final}} = t_{\text{spin-off}} + h_{\text{spin-off}} \rho_A / m \rho_A \quad \text{Eqn. 2.2}$$

where ρ_A is the mass of volatile solvent per unit volume, ρ_{A_0} is its initial value, m is the evaporation rate, η is the viscosity of the fluid, and ω is the angular speed of the substrate.

The spin coating apparatus used for this work consisted of a Dayton 6K573 capacitor start AC motor (3450 RPM at 110V), a Dayton 3PN101C variable auto-transformer, and a steel protecting box. A stainless steel disk was horizontally fixed on the axis of the vertical motor as the coating plateau. The substrate to be protected was mounted on the rotatable plateau and both the plateau and the substrate were enclosed inside the protecting box. Liquid deposition was carried out manually using a pipette. The spin rate was controlled to several hundred RPM by adjusting the auto-transformer. The thickness of coatings prepared this way was adjusted by the viscosity of the coating recipe and the spinning rate of the substrate. The latter was controlled by the voltage of the transformer. With the recipes mentioned in [Section 2.3.3](#), the coating usually had a thickness within 2-8 μm if the voltage of the transformer was adjusted to 30 V. The spin coating process could be used to prepare a relatively large uniform coating using only 2-3 ml of coating recipe or to prepare coatings from recipes that had a pot life as short as 5-10 min. However, this technique was prone to form flow patterns on the coating surface if the recipe was too viscous or too volatile. With a pot life of 15 min. to about 20 hrs., most coating recipes discussed in this dissertation were formed on substrates using the spin coating device described above.

2.5.2. Dip-Coating

The dip coating process is characterized by immersing a substrate in a coating bath and then pulling it out in a controllable way. This process (Fig. 2.8) can be conducted in a batch mode (A-E) as well as a continuous mode (F). The former mode is suitable for rigid substrates; while the latter one is convenient for coating flexible fibers and films. The batch mode consists of five stages including immersion, start up, deposition and drainage, drainage, and evaporation. The continuous mode is similar, however, it has a separate immersion stage and the deposition and drainage stages are overlapped.

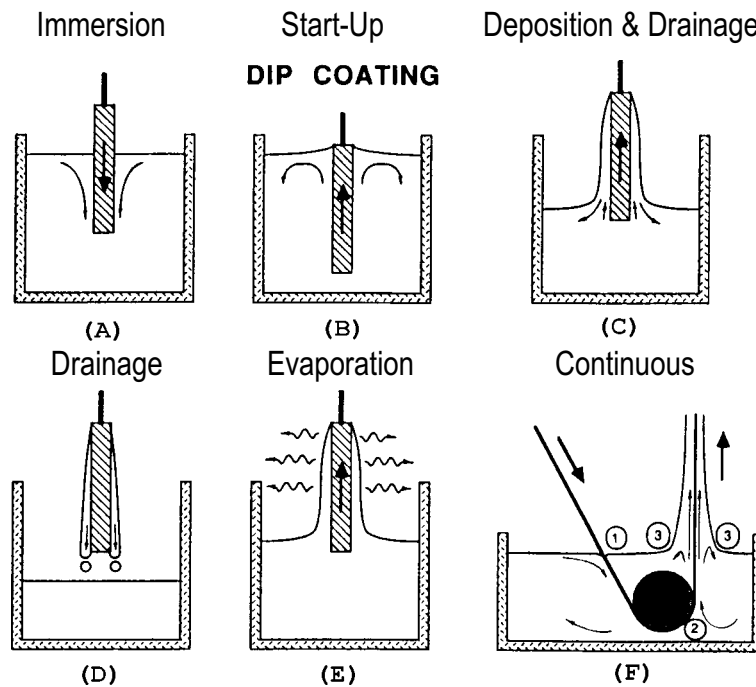


Fig. 2.8. Different stages of the dip coating process¹⁶⁵: (A-E) Batch; (F) Continuous.

For Newtonian liquids, the coating thickness (h) by the dip coating generally depends on the liquid viscosity (η), the pulling speed of the substrate (U), the liquid density (d), and the surface tension (γ_{LV}). In cases when the substrate speed and the liquid viscosity are not high, the coating thickness may be predicted from Eqn. 2.3¹⁶⁷.

$$h = \frac{0.94(\eta U)^{2/3}}{\gamma_{LV}^{1/6}(\rho g)^{1/2}} \quad \text{Eqn. 2.3}$$

For deposition of sol-gel film, the dependence of the viscosity on the shear rate and solvent evaporation has significant influences over the coating thickness. The solvent evaporation in turn depends on the partial pressure of the solvent in the coating chamber and this may be controlled in the commercial coating apparatus. Convection inside the coating chamber is also a factor influencing the coating thickness. Brinker and Ashley¹⁸ investigated the relationship between the film thickness and withdrawal speed for a variety of silicate sols with precursor structures ranged from rather weakly branched “polymers” to highly condensed particles. The coating thickness was found roughly proportional to the expected 2/3 power of the withdrawing speed of the substrate.

A simple dip coating equipment contains a coating sink and a pulling system to control the pulling rate of the substrate. The coating sink employed in this work was 1 cm wide, 10-15 cm long and 15-20 cm tall. The sink size was so designed that large dimension substrates might be coated using a relatively small amount of fluid. The substrate was usually pulled manually from the coating bath. The recipe f-DETA22TMOS22W31-HAC140 was dip-coated on bis-A PC and aluminum substrates. For this purpose, The recipe f-DETA22TMOS22W31-HAC140 was pre-hydrolyzed for 6 hrs., then diluted with a 50 wt% 2-propanol aqueous solution to 2/3 of the original concentration. Coatings prepared by this method were 3-6 μm thick after curing.

The dip coating process is very appropriate for coating a large number of substrates. However, the method requires a relatively long pot life of the coating recipe. Most coating recipes developed in this work were not suitable for dip coating because of the limited pot lives. The requirement of a large amount of coating fluid also limited the use of this technique. For example, to use the coating sink mentioned above to coat a 3.5 \times 3.5 inch² substrate, 100 ml of coating was required for dip-coating, while for spin coating, only 2-3 ml was required. However, the dip coating process usually provided very smooth coating surfaces.

2.6. THERMAL CURING

Thermal curing of the coating was controlled by a temperature-time profile. The selection of curing temperature depended on the balance of the thermal stability of the sol-gel coating and the substrate. For polymeric substrates, the curing temperature should be ca. 20°C below the glass transition temperature of the polymeric substrate to maintain the dimensional stability. For metallic substrates, however, the curing temperature depended on the thermal stability of the sol-gel coating. The f-DETA/TMOS coating usually turned slightly brownish after several hrs. of curing at 180°C in air, so the highest curing temperature of this coating formula was limited to 175-180°C. The highest curing temperature and the related curing time were the most important variables during this stage. Their influences on the hardness and abrasion resistance of the final gel will be discussed in [Chapter 3](#).

2.7. CHARACTERIZATION OF THE COATING

2.7.1. Measurement of Coating Thickness

The coating must have a proper thickness (usually 2-6 μm) to provide sufficient abrasion resistance, so a method for coating thickness measurement is required. The coating thickness was estimated using a well-calibrated scanning electron microscope. In order to have a sectional view of the coating, a small piece of the substrate was mounted with the section (sputtered with gold to acquire electronic conductance) facing the incident electron beam.

[Figure 2.8](#) shows coating fragments on the section of a coated bis-A PC substrate. The coating fragments observed by SEM were formed when the substrate was cut to a certain size (ca. 0.5×0.5 cm^2). The SEM image indicates that the thickness of this coating is about 3 microns. Generally, the thickness of the coatings prepared by spin- or dip-coating processes mentioned

earlier was in the range of 2-10 microns. The thickness varied with the solid concentration and pre-hydrolysis time of the coating recipe.

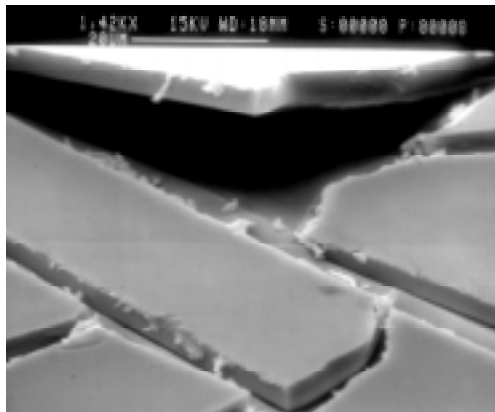


Fig. 2.9. The estimation of coating thickness by scanning electron microscopy

The refractive index and thickness of a coating may be measured concurrently via a Metricon 2010 instrument. The instrument includes a 633 nm laser, a high refractive index prism ($n=1.80$ or higher), and a photodetector (Fig. 2.10). During the measurement, the test film is pressed against the prism by a coupling head so that the film is brought into close contact with the base of the prism. A laser beam is incident on the interface between the prism and the film from the prism side and is reflected into photodetector. During the measurement, the intensity of the reflected beam (I) is recorded as a function of incident angle (θ). A sharp change in the intensity of the reflected beam can be detected at the critical angle for total internal reflectance, from which the refractive index can be calculated. In this operation, the instrument functions as a normal Abbe refractometer. For a bilayer of different refractive indices (e.g. a coating on a thin substrate), the light reflected from the interface between the prism and the coating can interfere with the light reflected from interface between the coating and the substrate. Hence, an interference pattern may be recorded. The refractive index and coating thickness can be calculated concurrently according to the θ values corresponding to the intensity minima, where the two reflected beams cause destructive interference. The method is generally effective if: 1) the coating is about 0.48-15 μm (depending on the refractive index of the film, the substrate and the prism) and 2) the coupling between the prism and the coating is strong.

Inorganic-organic hybrid coatings based on f-DETA and TMOS usually had a refractive index in the range of 1.55-1.50, which was very close to that of bis-A PC substrate (1.58). The refractive index and thickness had not been measured successfully for a f-DETA/TMOS coating on the polycarbonate substrates (1/16 inch thick) because of the small gap in refractive index between the coating and the substrate and poor coupling between the coating and the prism. The thick bis-A PC substrate often prevented a close coupling between the prism and the coating. With aluminum foil as a substrate, however, both refractive index and coating thickness were measured concurrently. Free sol-gel films were also used for refractive index measurement and in this case, only the refraction index could be obtained.

Figure 2.11 shows interference patterns recorded for two pieces of aluminum foil spin- and brush-coated with an f-DETA22TMOS22W31-HAC140 recipe, respectively. In the case of brush coating, the coating had a rather smooth surface and hence good coupling with the prism, so many minima are detected. Calculation based on these minima yielded a refractive index of 1.506 and a coating thickness of 5.2 μm . Their standard deviations for these two parameters were also be provided by the calculation although the results are not stated here. Since only two minima were detected for the spin-coated sample owing to the relatively poor smoothness of the coating and hence poor coupling, calculation only gave a refractive index of 1.506 and a coating thickness of 2.7 μm .

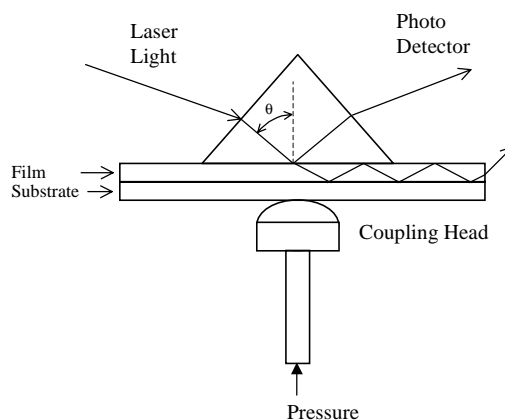


Fig. 2.10. Principal components in a Metricon 2021 instrument.

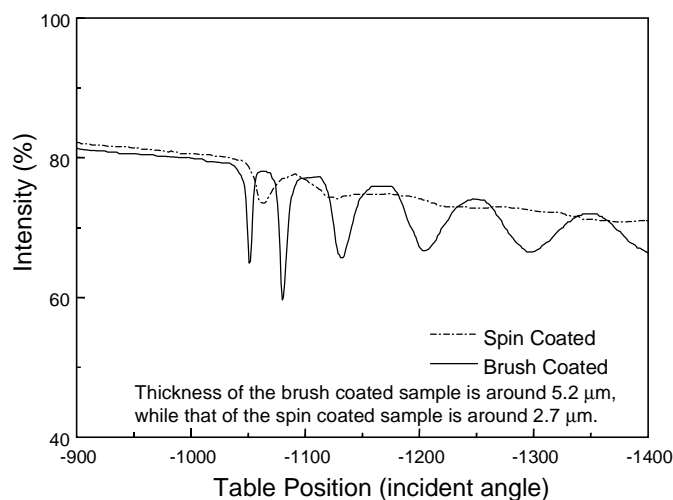


Fig. 2.11. Measurement of refractive index and thickness of a f-DETA22TMOS 22W31-HAC140 coating ($n \approx 1.506$) on aluminum foil.

2.7.2. Evaluation of Adhesion

Adhesion between the coating and the substrate is of great importance to the success of a protective coating. Without sufficient adhesion, a coating of excellent properties in terms of resistance to weather, chemicals, scratches, or impact would be meaningless to the substrate. Therefore, it is necessary to establish a method for adhesion evaluation. In this work, the cross-cut test described by ASTM standard D 3359-87 was used to estimate the adhesion between sol-gel hybrid coatings and bis-A PC substrates.

In this test, two perpendicular sets of equidistant parallel cuts $\frac{3}{4}$ inch (20 mm) in length and 1 mm apart (note sol-gel coatings in this work was 3-10 μm thick) were made using a sharp razor blade on cured defect free sol-gel coatings. As required, all the cuts must be made in one steady motion using a sufficient pressure to cut to the substrate, and any detached flakes or ribbons of coatings were removed by a soft brush and tissue. The tape test was carried out using a 1-inch (25 mm) wide Scotch[®] semitransparent pressure-sensitive tape. Two complete laps of tape were removed and discarded. An additional length was removed at a steady rate and a 3-inch (75 mm) long piece was cut. The center of this tape was placed on the grid and smoothed

into place by a finger. To ensure good contact with the film, an eraser on the end of a pencil was used to rub the tape firmly. Within 90 ± 30 seconds of application, the tape was removed by seizing the free end and rapidly pulling it off as close to an angle of 180° as possible. Then the grid area was checked for removal of coating from the substrate using the illuminated magnifier and the adhesion was rated according to the following scale illustrated in Table 2.2. The test was then repeated in two other locations on each test panel and the number of tests, their means and range were reported.

Table 2.2. Classification of Adhesion Test Results

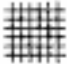
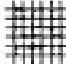
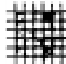
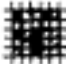
Surface of Cross-Cut	None					Greater than 65%
Classification	5B	4B	3B	2B	1B	0B
5B: perfect adhesion 4B-3B: acceptable adhesion 2B-0B: adhesion needs improvement.						

Table 2.3 lists adhesion test results between 3-APS treated bis-A PC substrates and f-DETA/TMOS sol-gel coatings (Section 2.3). These coatings generally exhibited an adhesion rating of 3B-4B on the tested substrate by cross-cut test (ASTM standard D 3359-87)

Table 2.3. Adhesion of f-DETA/TMOS coatings on bis-A PC substrates

Coating formulae	f-DETA31TMOS31 W5-HCL27	f-DETA26TMOS26 W19-HPO23	f-DETA22TMOS22 W31-HAC140
Primer	0.5 wt% 3-APS	0.5 wt% 3-APS	0.5 wt% 3-APS
Curing condition	125°C/ 4 hrs.	125°C/ 4 hrs.	125°C/ 4 hrs.
Adhesion Rating*	4.0 B	4.0 B	3 B
Number of Tests	3	3	3
Range of Adhesion	4 B	4 B	3-4 B

* ASTM Standard D 3359-87

2.7.3. Evaluation of Abrasion Resistance

Abrasion resistance of a substrate or coating is rated by the changes of weight, optical properties or surface features incurred by a well-controlled surface interaction. These surface interactions are usually accomplished via steel wool abrasion, Taber abrasion (ASTM D 1044 or ISO 3537), sand impingement (ASTM 673 or DIN 52348 E), scratch testing, and pencil hardness testing (ASTM D 3363). However, experimental results based on different methods may be incompatible because the mechanism of surface damage varies with the testing methods.

In this work, abrasion resistance of sol-gel coatings was evaluated according to the transmittance or surface damage caused by a specified Taber test. The following sections briefly introduce the ASTM standards for Taber test and haze measurement of optical polymers, then focus on the experimental methods employed for transmittance measurement and microscopic analysis.

2.7.3.1. Standard Taber Abrasion Test

The Taber Abraser from Taber Industries is one of the industry standards used in the wear and durability testing of ceramics, plastics, textiles, metals, leathers, rubbers, painted, lacquered and electroplated surfaces. Specifications for this test have been stipulated by standards organizations such as ASTM, ISO and DIN¹⁶⁸. ASTM standard D 4060-95 describes the abrasion resistance test of organic coatings by the Taber Abraser. This test requires the organic coating to be applied at uniform thickness on a smooth rigid plane. The sample can be either a disk 4 inch (100-mm) in diameter or a plate 4 inch (100-mm) square and with a ¼-inch (6.3 mm) hole centrally located on each panel. After curing, the surface is abraded by rotating the panel under a pair of loaded abrasive wheels. The abrasion resistance is calculated as loss in weight in a specified number of abrasion cycles, as loss in weight per unit cycle, or as number of abrasion cycles required to remove a unit amount of coating thickness. The recommended abrasive wheels are CS10 (mild) or CS17 (harsh) resilient calibrase wheels. However, CS10F (very mild) resilient calibrase wheels are also widely used. These abrasion wheels are 0.5 inch (1.27 cm) thick and contain rubber bonded alumina particles. Due to age hardening of the rubber

bonding material, the wheels should not be used after the manufacturer's suggested expiration date. To maintain a similar surface condition for each test, the abrasion wheels need to be resurfaced with an S-11 abrasive disk for 50 cycles before testing.

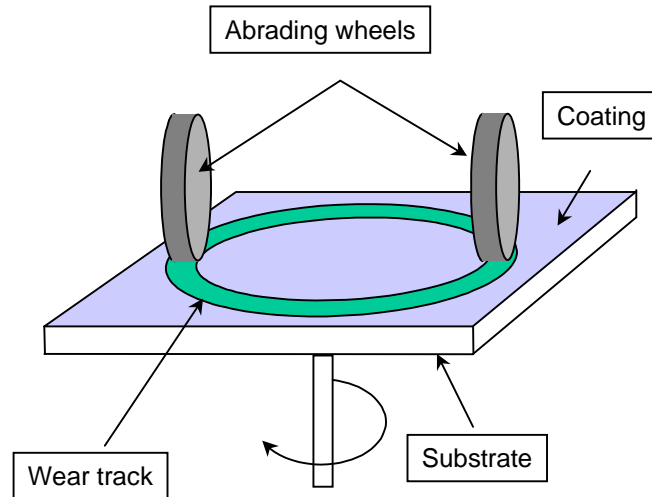


Fig. 2.12. Illustration of the Taber abrasion test.

2.7.3.2. Standard Optical Test for Abrasion Resistance of Transparent Plastics

The abrasion resistance of transparent plastics or optically transparent coatings on these plastics can be measured by changes of haze and transmittance incurred by a specified abrasion test on the surface. ASTM standard D 1044-94 describes a standard test method that judges the abrasion damage by the percentage of transmitted light (percent haze) which, in passing through a Taber track described by ASTM D 4060-95, deviates from the incident beam by a *specified angle*. CS10F Calibrase wheels are recommended for the Taber test.

The percent of haze is calculated by the ratio of diffuse transmittance to the total transmittance (Eqn 2.4). According to the ASTM standard, the light diffused from the surface of a Taber track only deviates from the incident beam by a narrow angle, while light diffused internally by a specimen deviates from the incident beam by a wide angle (Fig. 2.13). ASTM Standard D 4060-95 requires that only the light flux deviating more than 0.044 rad (2.5°) on the average be considered in the assessment of abrasive damage and that the hazemeter used for such

measurement of haze meet the requirements described by ASTM standard D 1003. Normal hazemeters have a larger field angle (a large aperture), which allows light deviating more than the specified angle to enter the detector. Consequently, these instruments often yield a lower haze reading than a standard hazemeter for the same sample.

$$\text{Haze} = \frac{\text{Intensity Of Diffuse Transmittance}}{\text{Intensity Of Total Transmittance}} \times 100\% \quad \text{Eqn. 2.4}$$

Statistical analyses based on a round of experiments, involving six materials tested by six laboratories, are also reported in ASTM Standard D 1044 regarding repeatability and reproducibility of the described test method. The results showed that experiments based on the same operator, the same equipment and under the same test condition are quite repeatable; whereas experiments based on different operators, different equipment and different test conditions exhibit some deviations.

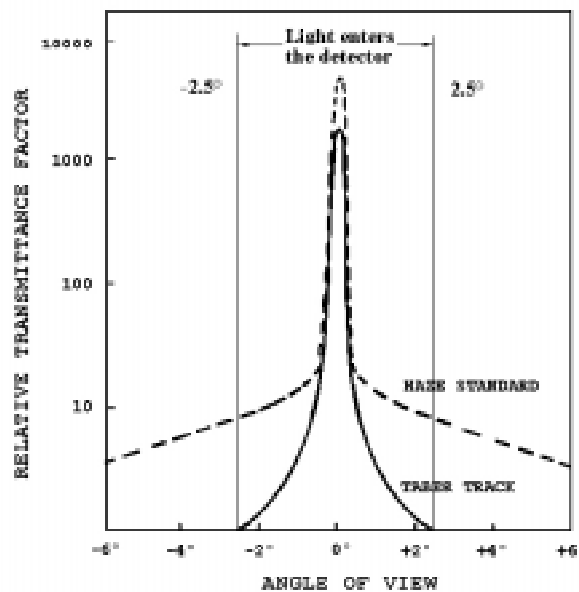


Fig. 2.13. Light scattering from the surface of Taber abrasion tracks (quoted from ASTM Standard 1044-94)

2.7.3.3. Evaluation of Abrasion Resistance in this Work

The abrasion resistance of sol-gel derived coatings was rated according to the transmittance of the Taber track incurred by a specified Taber test. The testing procedures complied with those utilized by Betrabet¹⁵⁴ and Wen¹⁴, but deviated from the ASTM standards in selection of abrading wheels and optical instrument. These modifications were utilized to make use of existing equipment as well as to help to differentiate the abrasion resistance between various sol-gel derived coatings. The following paragraphs provide the experimental details for the Taber test and transmittance measurement utilized in this work.

The Taber abrasion test generally involved a pair of CS10 wheels rather than the CS10F wheels (milder than CS10) recommended by ASTM standard D1044-95 although the latter wheels were also used in some cases for comparison. It was hoped that the use of “harsher” CS10 wheels would help to amplify the difference of abrasion resistance between various sol-gel derived coatings. Unless otherwise specified, a typical Taber test usually involved a 500-gram load per wheel and 500 cycles of abrasion. The spacing between the two abrasion wheels was 1 inch (2.54 cm). The sample size was generally 3.5×3.5 inch² (8.9×8.9 cm²) for bis-A PC substrates, and 3×3 inch² (7.6×7.6 cm²) for metal substrates.

The transmittance measurement was conducted on a Shimadzu-9000 photometer, which does not comply with the requirements of ASTM standard D 1003. The distance from the sample to the detector was about 5.1 cm in this instrument. The test utilized a 420 nm light beam (0.4×10 mm² in size) to scan across the Taber track rather than to use incandescent light to illuminate the Taber track like in ordinary hazemeters. As the light beam scanned radially across the wear track, the absorbance of the sample was recorded as a function of scanning distance. The absorbance of wear track was calculated as the absorbance difference between the Taber wear track and the unabraded regions on both sides of the track (Fig. 2.14). Conversion between transmittance and absorbance was carried out using Eqn 2.5.

$$\text{Transmittance} = 10^{-\text{Absorbance}} \times 100\% \quad \text{Eqn. 2.5}$$

In principle, a Shimadzu-9000 photometer can detect a minimum absorbance of 0.001, which corresponds to a transmittance of 99.8%. However, due to the background noise from the

coating and the substrate, the absorbance measurement often has quite large uncertainties if the transmittance is within 99-100 %. To differentiate the abrasion resistance for a sample series, the Taber test should involve a sufficiently large number of abrasion cycles so that the coating samples lose at least 2% transmittance during the test. After the test, the Taber track must be inspected to see if the abrasion damage is mostly limited to the coating. In case of significant substrate damage, the transmittance value of the Taber track does not correspond to the real abrasion resistance of the coating.

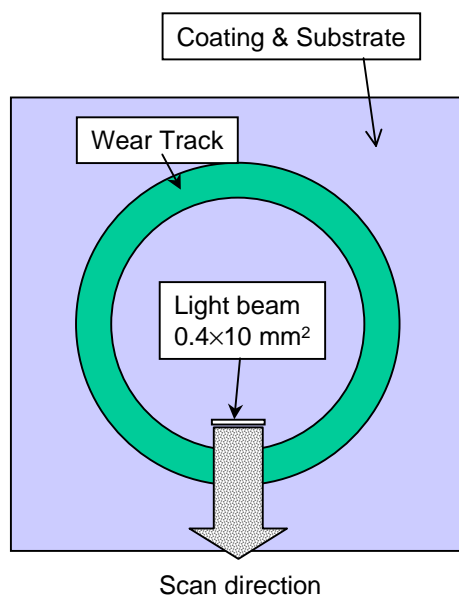


Fig. 2.14. Absorbance or transmittance measurement of a Taber wear track.

Figure 2.15 shows absorbance curves obtained by scanning a 420 nm (purple) or a 633 nm (red) light beam across a Taber track on a bis-A PC substrate with a f-DETA100 coating. The Taber track was caused by 500 cycles of abrasion using a pair of CS-10 wheels, each with a 500-gram load. The beams size for the absorbance measurement was $0.2 \times 1 \text{ mm}^2$. The result indicates that the absorbance of the red light beam by the wear track was only about 90% of the absorbance of the purple light. Note the “absorbance” measured here was actually caused by the scattering of light by defects on the Taber track. If the Rayleigh’s law held in this circumstance, the intensity of scattered light would be inversely proportional to the fourth power of the wavelength (λ). Therefore, under the same conditions, red light should be scattered to a lower

degree than purple light and hence have a lower “absorbance”, which is in accord with the experiment. To have better sensitivity, the 420-nm light was generally utilized to evaluate the abrasion resistance of sol-gel derived coatings.

The influence of the beam size on the absorbance measurement was also studied. Figure 2.16 shows absorbance curves obtained by scanning a light beam (420-nm in wavelength) of four different sizes across the Taber track described in Fig. 2.15. The four beam sizes included $0.2 \times 1 \text{ mm}^2$, $0.4 \times 0.4 \text{ mm}^2$, $0.4 \times 10 \text{ mm}^2$ and $0.4 \times 16 \text{ mm}^2$. According to these curves, a smaller beam size tended to read the absorbance value for each scratch, whereas a larger beam yielded an average reading for each beam-size region along the scanning path. Since the abrasion resistance is rated by the average haze or transmittance rather than individual scratch of the Taber Track, a beam size of $0.4 \times 10 \text{ mm}^2$ was generally selected for transmittance measurement.

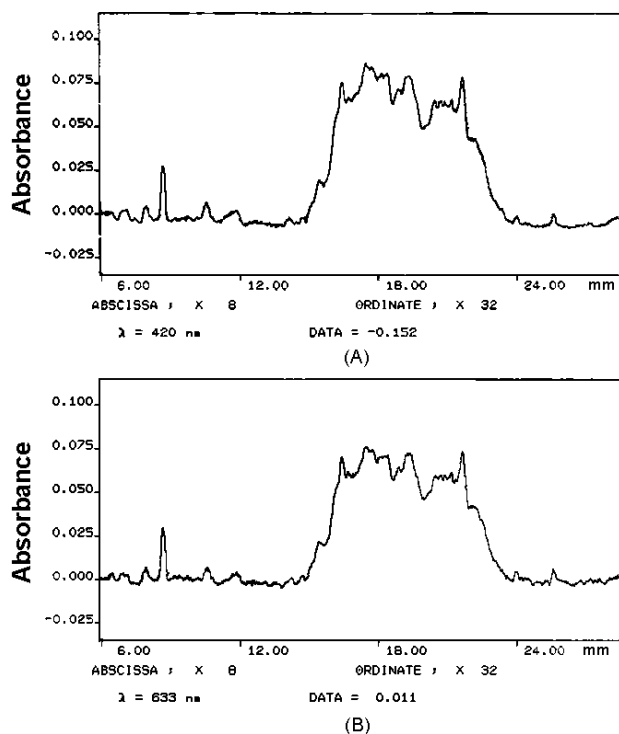


Fig. 2.15. Absorbance curves obtained by scanning of a 420 nm and a 633 nm light beam of $0.2 \times 1 \text{ mm}^2$ in size across a Taber track on bis-A PC substrate with a f-DETA100 coating. The Taber track was created by 500 cycles of abrasion using a pair of CS-10 wheels and a 500-gram load per wheel.

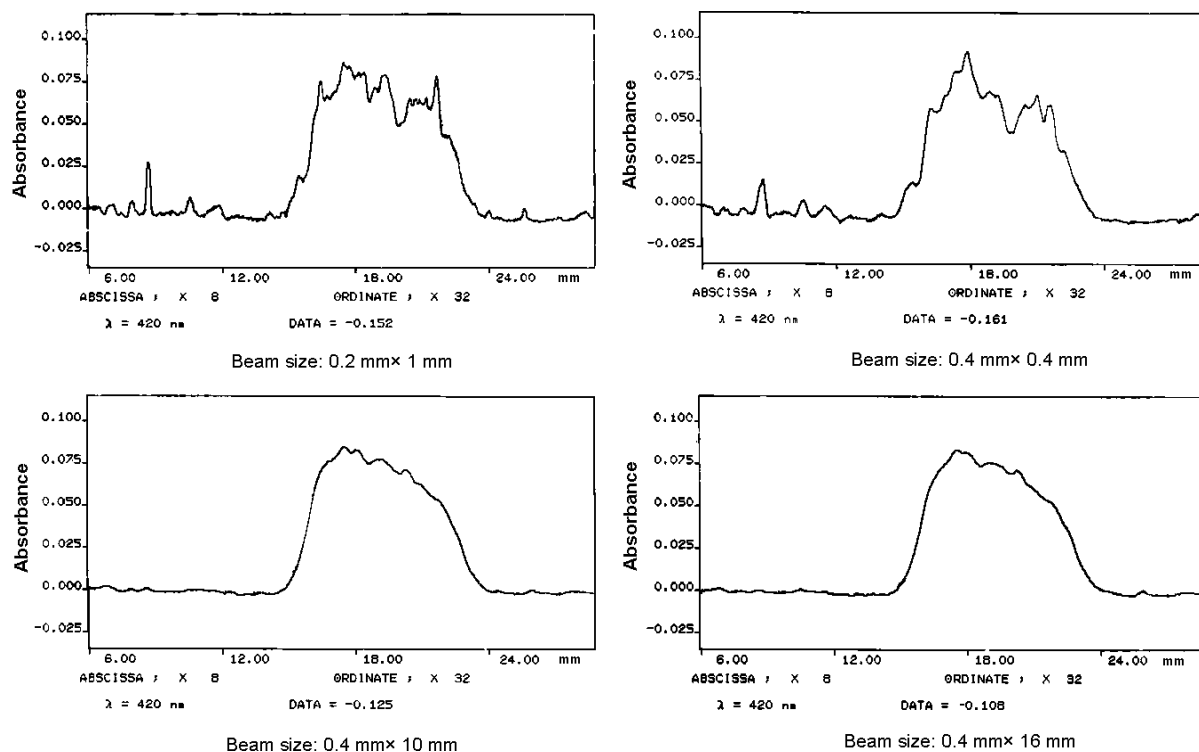


Fig. 2.16. Absorbance curves obtained by scanning 420 nm light beams of $0.2 \times 1 \text{ mm}^2$, $0.4 \times 0.4 \text{ mm}^2$, $0.4 \times 10 \text{ mm}^2$, and $0.4 \times 16 \text{ mm}^2$ in sizes across the Taber track mentioned in Fig. 2.15.

2.7.3.4. Microscopy Methods for Evaluation of Abrasion Resistance

The optical test method discussed above is established on the relationship between the haze or transmittance and the extent of surface damage of a Taber track. Both optical microscopy and scanning electron microscopy allow direct observation of the damage incurred by a specified Taber test and hence can be utilized to compare the abrasion resistance for a set of substrates or coatings. Statistical analysis of the specks and scratches on a Taber track, in principle, may enable quantitative evaluation of abrasion resistance. Optical microscopy (both transmission and reflection images) and scanning electron microscopy (secondary electron images) were used in this work. The advantages and disadvantages of these methods for abrasion resistance evaluation were compared using f-DETA/TMOS or f-DETA/Silica coatings as examples.

2.7.3.4.1. Optical Microscopy

When a light beam is incident on a Taber track, specks and scratches on the substrates cause light scattering. Except a few large specks or wide and deep scratches, the majority of defects on a Taber track only cause slight deflection of light, so most transmitted or scattered rays can pass through the light path of a transmission microscope without obstruction. Therefore, under this imaging mode, minor defects on Taber tracks behave somehow like phase objects, which show phase contrast but no amplitude contrast. Under an ideal optical situation (no spherical deviation, chromatic deviation and stigmatism), such phase objects should exhibit no contrast in an *in focus* image. However, under slightly defocus condition, these phase objects can be revealed and the image contrast is proportional to the defocus value. Large specks or scratches on Taber tracks cause large deflection of light, which may be blocked from imaging, and hence those defects can show obvious amplitude contrast and can be revealed under an *in focus* condition. For this reason, transmission optical microscopy is generally more sensitive to large specks or deeper and wider scratches.

Figure 2.19 shows the transmission optical micrographs of the Taber tracks on an uncoated bis-A PC substrate after 50 (A), 150 (B), 300 (C), and 500 (D) cycles of abrasion. These Taber tests involved a pair of CS10 wheels, each with a 500-gram load. According to these micrographs, the surface damage within the earlier 150 cycles of abrasion was mainly due to the formation of scratches by a micro-plowing or micro-cutting mechanism (Fig. 2.18). However, after ca. 300 cycles of abrasion, new scratches were formed mainly by removal of old scratches, and hence the wear should be partly caused by a micro-fatigue mechanism (Fig. 2.18).

Figure 2.20 shows the transmission optical micrographs for the Taber tracks on a bis-A PC substrate with a f-DETA26TMOS26W19-HPO24 coating after 50 (A), 150 (B), 300 (C), and 500 (D) cycles of abrasion. The Taber tests were carried out under the same condition as in the case of Fig. 2.19. Similarly, these micrographs reveal that the density of scratches on the wear track increases with the number of abrasion cycles. Compared to the uncoated bis-A PC substrate, this coated substrate suffered from far less surface damage after the same number of abrasion cycles, indicating the abrasion resistance of the substrate was bolstered by the sol-gel

coating. Unlike the uncoated PC substrate, the wear of the sol-gel coating was mainly caused by a micro-cracking mechanism rather than a micro-plowing or micro-cutting (Fig. 2.18).

In general, the transmittance of the substrate usually decreased exponentially as the number of abrasion cycles increased because later scratches were increasingly caused by removal of old scratches. This tendency is shown in Fig. 2.17 using a set of bis-A PC substrates that were either uncoated or coated with f-DETA/TMOS coatings.

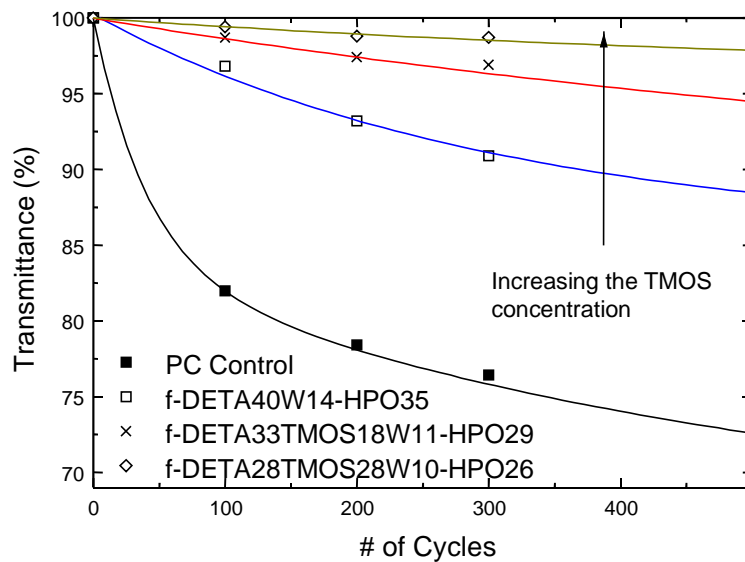


Fig. 2.17. The transmittance of Taber tracks as a function of the number of abrasion cycles. The substrates for these tests were bis-A PC. Abrasion tests involved CS10 wheels and a 500-gram load per wheel.

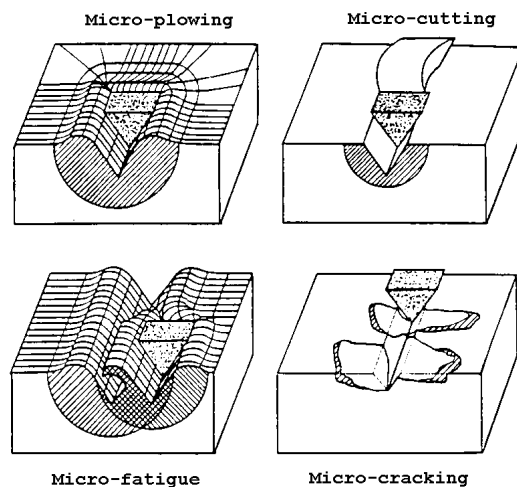


Fig. 2.18. Mechanisms for material removal¹⁶⁹.

To evaluate the abrasion resistance of coatings on metal substrates, reflection microscopy was used since the metal substrates are not optically transparent. The sol-gel coatings described here were usually transparent, and hence the surface feature of metal substrates often interfered with the observation of the Taber tracks. However, the removal of the surface feature of the metal substrate during a wear test could also indirectly reflect the abrasion resistance of a coating and two experiments discussed in [Chapter 3](#) are based on this technique. The interference of surface features of the substrate was successfully minimized by sputtering a gold layer on the wear track under study. By doing this, the smooth undamaged area became a mirror, which reflected incident light back to form bright images. Whereas defects such as scratches caused diffuse scattering of the incident light, so most of reflected light was blocked by the entrance port of the objective lens and hence dark images were formed for these defects. Experiments indicated that sputtering a gold layer on the Taber track could significantly enhance the image contrast of the Taber track. Transparent polymer substrates were also sputtered with a layer of gold and studied by reflection microscopy. Using this method, minor scratches could be clearly observed on a Taber track that showed a transmittance of up to 99%.

[Figure 2.21](#) provides a direct comparison of Taber tracks caused by CS10 and CS10F wheels on bis-A PC substrates with a f-DETA22TMOS22W31-HAC140 coating. The abrasion tests involved a 500-gram load and 500 (micrographs A and B) or 1000 (micrographs C and D)

cycles of abrasion. After these tests, all substrates maintained a transmittance of ca. 98%. Under reflection optical microscopy, however, a great number of minor scratches on the wear track was imaged. With the same abrasion wheels, the Taber tracks caused by 1000 cycles of abrasion, as expected, showed a higher density of scratches than the tracks caused by only 500 cycles of abrasion. In addition, these micrographs also indicate that the CS10 wheels were prone to cause deeper and wider scratches on the coating than the CS10F wheels. Clearly, this agreed with the claim of the manufacturer about the two types of wheels.

2.7.3.4.2. Scanning Electron Microscopy

Compared to optical microscopy, scanning electron microscopy (SEM) has the advantages of high spatial resolution and large depth of field, so it is widely utilized for morphology and fracture surface analysis. Here reflection optical micrographs and secondary electron micrographs of the same Taber tracks are compared.

[Figure 2.22](#) shows reflection optical micrographs and secondary electron micrographs of Taber tracks on an uncoated bis-A PC substrate and a bis-A substrate with a f-DETA58Ludox42 coating. The recipe f-DETA58Ludox42 was made of 58% of f-DETA and 42% of Ludox colloidal silica (see in [Chapter 7](#) for details). The abrasion tests utilized CS10 wheels and a 500-gram load per wheel. The uncoated substrate was abraded for 20 cycles while the coated substrate was abraded for 500 cycles. The SEM micrographs generally exhibit much lower image contrast for scratches than the reflection optical micrographs, especially for shallow scratches. According to these results, it is concluded that reflection optical microscopy should be a better tool for Taber track analysis of highly abrasion resistant coatings.

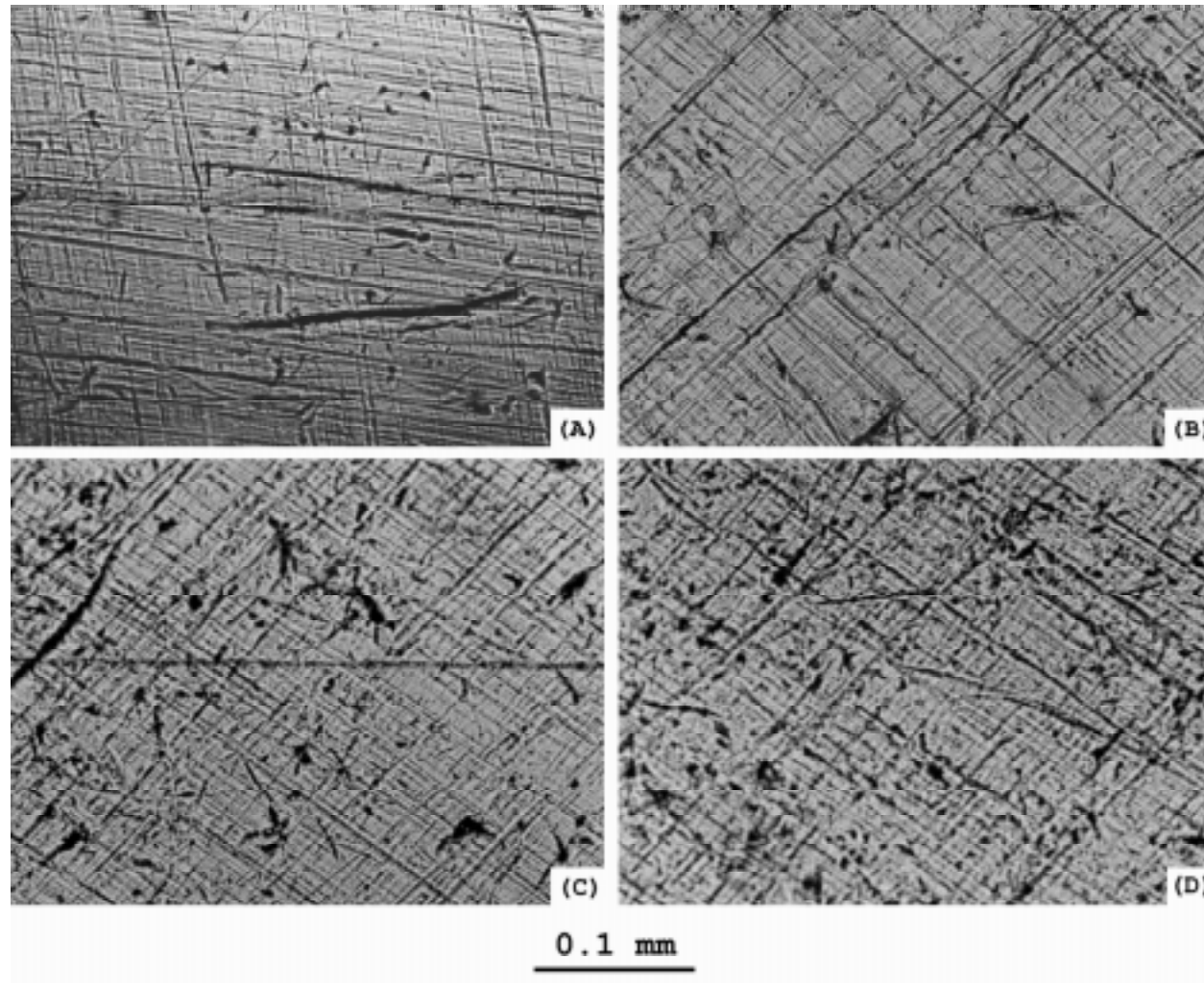


Fig. 2.19. Transmission optical micrographs of the Taber tracks on an uncoated bis-A PC substrate after 50 (A), 150 (B), 300 (C) and 500 (D) cycles of abrasion. CS10 wheels and 500-gram loads were used in the tests.

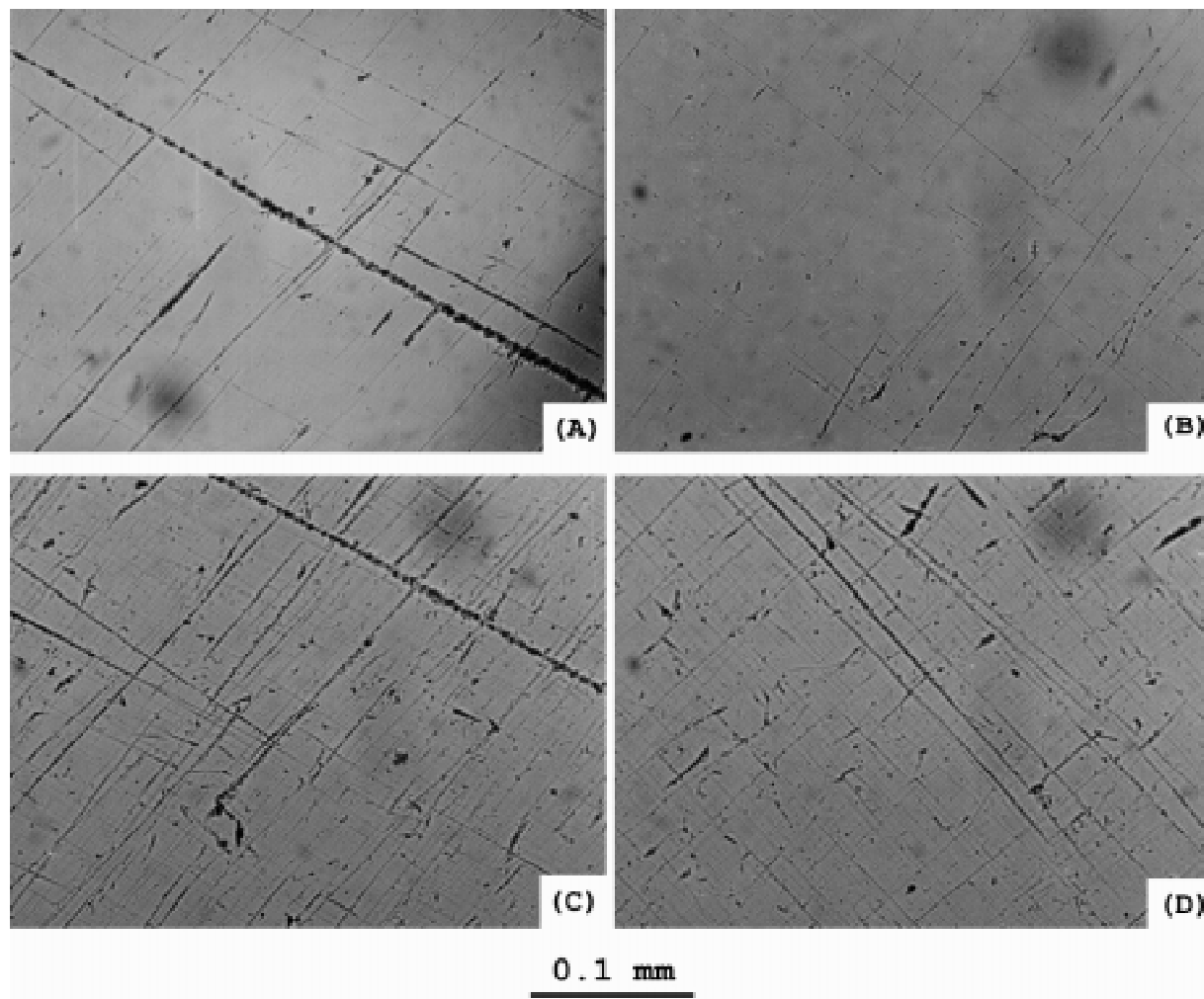


Fig. 2.20. Transmission optical micrographs for the Taber tracks on a bis-A PC substrate with a f-DETA26TMOS26W19-HPO24 coating after 50 (A), 150 (B), 300 (C), and 500 (D) cycles of abrasion. CS10 wheels and 500-gram loads were used in the tests.

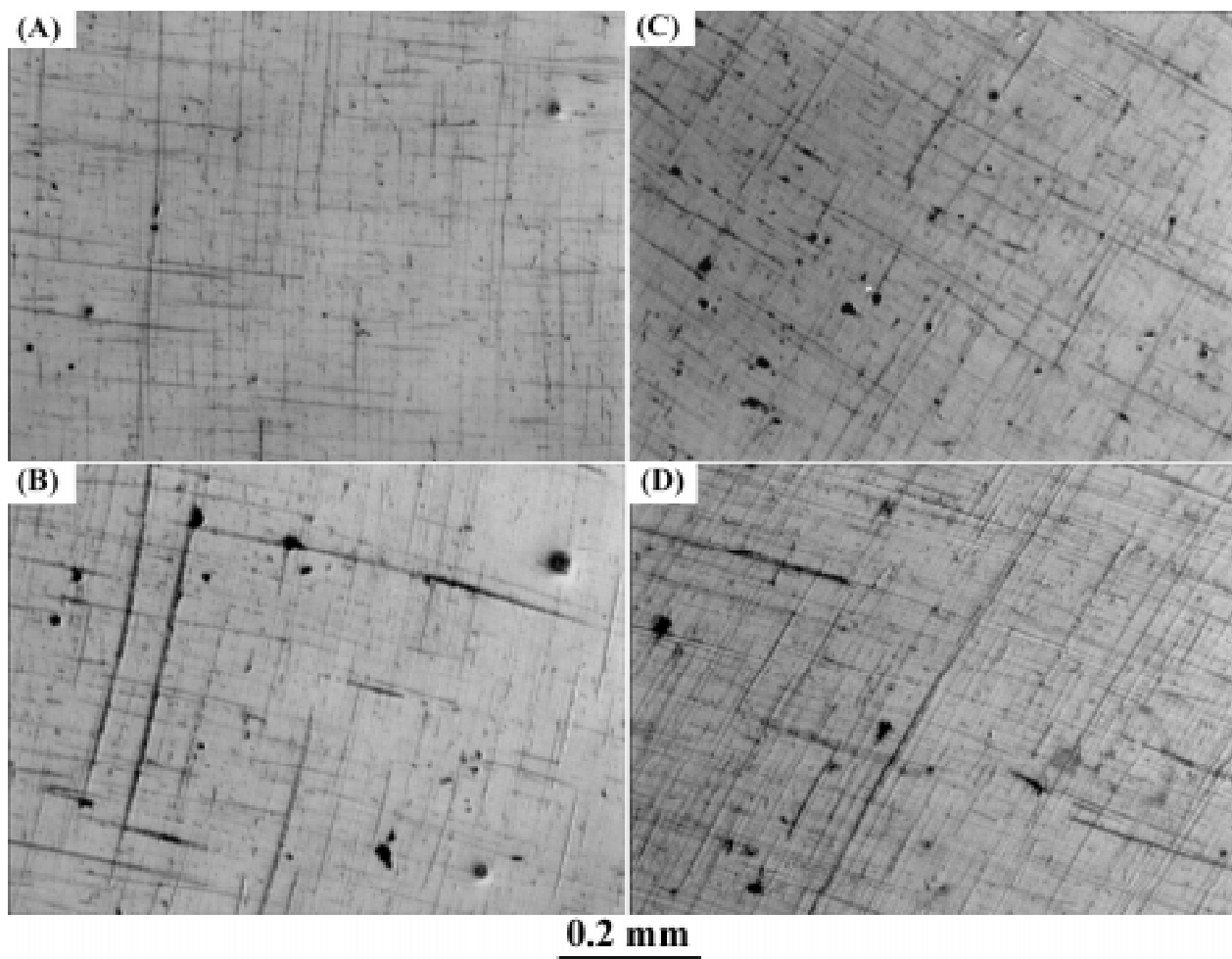


Fig. 2.21. Reflection optical micrographs of Taber tracks on bis-A PC substrates with f-DETA22TMOS22W31-HAC140 coatings. Test conditions were (A) CS10F wheels, 500 cycles; (B) CS10 wheels, 500 cycles; (C) CS10F wheels, 1000 cycles; and (D) CS10 wheels, 1000 cycles. All tests had a 500-gram load on each abrasion wheel.

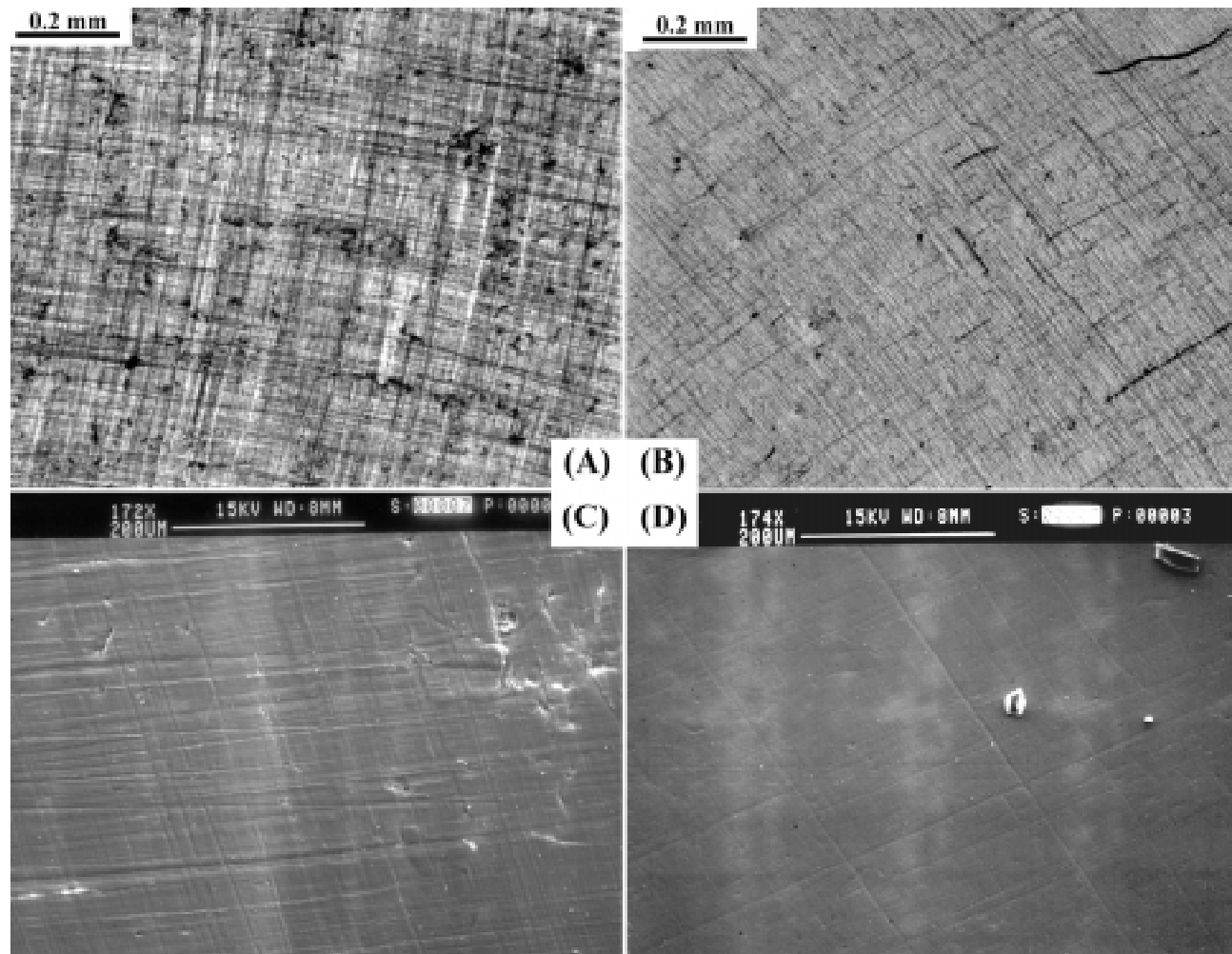


Fig. 2.22. Reflection optical micrographs and secondary electron micrographs of Taber tracks on bis-A PC substrates: (A) and (C): uncoated, 20 cycles of abrasion; (B) and (D), with f-DETA58Ludox42 coating, 500 cycles of abrasion. CS10 wheels and 500 g loads were used in the tests.

CHAPTER 3. ABRASION RESISTANT COATINGS DERIVED FROM TRIETHOXYSILYLATED DIETHYLENETRIAMINE AND TETRAMETHOXYSILANE

3.1. INTRODUCTION

During the past few years many inorganic-organic hybrid materials have been developed as protective coatings to improve the abrasion resistance of optical polymers like bisphenol-A polycarbonate (bis-A PC) and poly(methyl methacrylate) (PMMA)^{5,7,11-14,16,17,144,145}. These hybrid materials were generally prepared by hydrolysis and condensation of trialkoxysilylated organic compounds and metal or semi-metal alkoxides. The earliest and most extensively studied trialkoxysilylated compound has been f-DETA, the reaction product of one mole of diethylenetriamine (DETA) with three moles of 3-isocyanatopropyltriethoxysilane (3-ICPTES).

F-DETA was originally introduced in 1991 by Wang and Wilkes to develop abrasion resistant coatings¹¹⁻¹³. Later, it was found that the hardness and abrasion resistance of the f-DETA coating could be increased by incorporation of tetramethoxysilane (TMOS)¹⁴. The f-DETA/TMOS sol-gel coating was applied on a number of substrates including bis-A PC, CR39, aluminum, brass, copper, stainless steel and common carbon steel^{158,159,161}. Good abrasion resistant coatings were obtained on all these substrates with the exception of common carbon steel. Although sol-gel coatings based on f-DETA and TMOS have demonstrated very good abrasion resistance, the f-DETA/TMOS system is still far from fully developed. For example, prior to the author's work, the sol-gel coatings were generally hydrolyzed and condensed in a strong acid medium with a deficient amount of water. Under this condition, the recipe only had a gelation time of 5-15 min., which makes it inconvenient for many coating operations.

This chapter attempts to address the influence of the formulation and processing variables on the gelation time, hardness and abrasion resistance of the coatings. By systematically

modifying pH, the concentration of TMOS and water, curing time, curing temperature, the author hopes to find recipes that not only have a longer gelation time but also lead to better abrasion resistance.

3.2. EXPERIMENTAL

3.2.1. Materials and Surface Treatments

Diethylenetriamine (DETA, 98%), 3-aminopropyltriethoxysilane (3-APS, 99%), tetramethoxysilane (TMOS, 99+%), and 3-isocyanatopropyltriethoxysilane (3-ICPTES, 95%) were purchased from Aldrich Chemical Company and used without further purification. DETA was triethoxysilated in a 2-propanol solvent using 3-ICPTES according to Wen¹⁴ and the f-DETA product prepared by this method was a 70 wt% solution in 2-propanol. To minimize transesterification between the ethoxysilane group and 2-propanol, this material was used within a week after preparation.

Bis-A PC sheets 3.5"×3.5" in² in size (Lexan[®], GE) were purchased from the Atlantic Plastics Company. APEC HT9353[®] polycarbonate sheets 4"×6" in² were kindly provided by the Bayer Corporation. It is a copolycarbonate including 35 % of bisphenol TMC (Fig. 3.1) and 65 % of bisphenol-A, and has a glass transition temperature of ca. 184°C. Both the bis-A PC and APEC PC substrates were treated with 0.5 wt% 3-APS to improve their adhesion to the sol-gel coatings. Brass substrates 3"×3" in² were obtained from the McMaster Carr Company. Aluminum substrates 4"×6" in² were purchased from the Q-Panel Company. The metal substrates were simply treated by degreasing with 2-propanol.

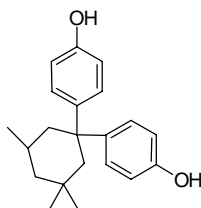


Fig. 3.1. Molecular structure of bisphenol TMC (1,1-bis(4-hydroxyphenyl)-3,3,5-trimethylcyclohexane)

3.2.2. Formulation of Coating Recipe

As introduced earlier in [Chapter 2](#), f-DETA/TMOS coating recipes were formulated using f-DETA, TMOS, water, an acid catalyst and a 2-propanol solvent. The acid catalyst was hydrochloric acid, phosphoric acid, or acetic acid, which will be represented in the coating nomenclature as HCL, HPO and HAC, respectively. The nomenclature of the coating recipes is based on the coating components and their concentrations. The concentration of each component, excluding the acid catalyst, is stated as its weight percentage with regard to the total weight of f-DETA, TMOS, water and the solvent, while the catalyst concentration is stated as millimoles per kilogram (mmol/kg) of the recipe excluding the catalyst. In the nomenclature, the catalyst part is separated from the major components by a dash and the solvent content is usually not explicitly stated. For example, recipe f-DETA30TMOS30W5-HCL27 contains 30 wt% f-DETA, 30 wt% TMOS, 5 wt% water and 35 wt% 2-propanol and the concentration of hydrochloric acid concentration is 27 mmol/kg. Since this nomenclature scheme does not explicitly reflect the stoichiometry between the water and the alkoxy silane components, the equivalent ratio (r) of water to alkoxy silane is also provided when addressing the influence of water on the abrasion resistance of the final coating.

[Table 3.1](#) lists six typical f-DETA/TMOS coating recipes, along with their r ratios, pHs and gelation times. Since the sol-gel reactions are generally considered to undergo specific acid catalysis or specific base catalysis^{28,162}, the reaction rates should be mainly dependent on pH of the system. However, the starting material f-DETA often included an uncertain small amount of free amines, which could be from an excess amount of either f-DETA or 3-ICPTES.

Consequently, some acid catalyst would be consumed and accurate control of pH would be in fact impractical. For this reason, pH was controlled using acids of different acidity strength. In the presence of an excess amount of a weak or intermediately strong acid, parts of the acid reacted with the residual amine to form an ammonium salt, which constituted a buffer system with the remaining acid, thus leading to stabilization of pH. By using hydrochloric acid, phosphoric acid, and acetic acid, pH of the coating recipe was reproducibly controlled to the range listed in Table 3.1. Experiments indicated that sol-gel reactions of f-DETA/TMOS coatings within pH 0-5 provided transparent sols that could form smooth sol-gel coatings. A further increase in pH usually led to a silica precipitate or a sol inappropriate for making smooth transparent coatings. Table 3.1 indicates that the gelation time of the f-DETA/TMOS system decreases progressively as pH increases in the range of pH 0-5. This is in contrast to the unitary TMOS or TEOS system, which usually exhibits a maximum gelation time at ca. pH 2¹⁸.

Table 3.1. F-DETA/TMOS coating recipes and their gelation times and pH.

Formulation	r Ratio	Gelation Time	pH Value*
f-DETA30TMOS30W5-HCL27	0.55	3-5 min.	0.4-0.5
f-DETA22TMOS22W31-HCL20	4.4	7 min.	1.7-1.9
f-DETA26TMOS26W19-HPO23	2.2	20-30 min.	2.6-2.7
f-DETA22TMOS22W31-HPO20	4.4	30-45 min.	2.5-2.4
f-DETA22TMOS22W31-HAC140	4.4	6-8 hrs.	4.2-4.0
f-DETA22TMOS22W31-HAC20	4.4	~12 hrs.	5.2-5.1

* Measured by a pH glass electrode

3.2.3. Preparation of Abrasion Resistant Coatings

The coating recipes were pre-hydrolyzed for some time, and spin-coated on the desired substrates before gelation occurred. The curing temperature was chosen according to the balance between the dimensional stability of the substrate and the thermal stability of the sol-gel coating. For the plastic substrates, the glass transition temperature established the upper limit of the curing temperature. The real curing temperature was 15-25°C lower than this temperature to

avoid possible thermally induced warping of the substrate. Coatings applied to the bis-A PC substrate (T_g =ca. 150°C) were dried at room temperature and cured typically at 60°C for 30-60 min., and then at 125-130°C for about 4 hrs. For APEC HT9353[®] PC (T_g =184°C), the curing temperature could be increased to about 170°C without causing warping of the substrates. With metal substrates, the curing temperature of the coating was mainly limited by the thermal stability of the sol-gel coatings. Regardless of the catalyst, f-DETA/TMOS sol-gel coatings often became brownish in color after being cured in air at 175°C for several hours. The coated metallic substrates reported here were cured at 170°C for 4 hrs.

3.2.4. Characterization

The refractive index values were measured using a Metricon Instrument, while the UV/Vis spectra were acquired on a Hitachi U-2000 spectrometer. “Free” sol-gel films of 0.05-0.2 mm thick were used for the measurement of refractive index and the data were based on the average of five measurements at four different sample locations. The films samples were prepared by casting the pre-hydrolyzed recipes into polystyrene dishes, and then the sol samples in the polystyrene dishes were dried at room temperature in a ventilation hood for 24 hrs. The resulting transparent sol-gel films were delaminated from the dishes, and thermally cured at conditions described later.

Abrasion tests were conducted using a Taber Abrader in a manner similar to the specifications of ASTM D4060. For transparent polymeric substrates, the abrasion resistance of a coating was rated according to the transmittance of the wear track after a *principal Taber test* involving 500 abrasion cycles using a pair of CS-10 resilient wheels, each with a 500-gram load. In some cases, the abrasion test was also carried out to 250, 500, 1000 cycles of abrasion to study the influence of the abrasion cycles on the abrasion resistance of a coating. For opaque metallic substrates, the surface damage caused by a specified Taber test (often *the principal test*) was used to compare the abrasion resistance for a set of coating samples.

The transmittance was measured on a Shimadzu CS-9000 UV/Vis photometer. In this test, a 420 nm light beam (0.1×10 mm² in size) was used to scan across the wear track, and the

intensity of the transmitted beam was recorded as a plot of the absorbance vs. the position of the light beam. From the absorbance curve, the transmittance of the wear track was calculated from the absorbance difference between the Taber track and unabraded areas. The rating of abrasion resistance was given as the average of transmittance measured at six to eight different locations from two samples. Good abrasion resistant coatings generally should retain a transmittance of 96% after the *principal Taber test*.

For metallic substrates, the surface damage of a coating caused by a specified Taber test track was analyzed by an Olympus optical microscope. Alternatively, the removal speed of the surface feature by a Taber test was also used to gauge the protection of the metal substrate by the sol-gel coatings.

Isothermal thermogravimetry (TG) was conducted on a Seiko TG/DTA instrument with an air flow of 20 cm³/min. TG samples were prepared by pre-hydrolyzing the coating recipes in the same manner as in case of the related coating preparation. The resulting gel was desolvented, dried at room temperature in polystyrene dishes for three days, and then ground into powders for TG experiments. Utilizing the weight loss curve, a suitable curing temperature-time profile could be determined for curing a given coating.

Vickers microhardness was measured on a LECO DM-400 hardness tester using a load of 10 g and a loading time of 10 seconds. The testing samples were prepared by applying a layer of pre-hydrolyzed coating recipes on glass slides, following by drying at room temperature for 24 hrs. and then thermally curing at conditions requested by experiments. Before applying the coating, the surfaces of glass slides were activated by boiling in a 10 wt% KOH solution for 10 minutes, followed by cleaning with deionized water. Glass slides were used as the coating substrate to minimize the yielding effect of the substrate. It is realized this substrate differs from a metallic or polymeric system but it provides a consistent substrate to study the influence of processing /formulation variables on the hardness. The thickness of such coatings was 25-50 microns, while the penetration depth of the indenter was around 3 microns. Therefore, the influence of the substrate should be reduced to a considerably low level. All hardness data were obtained based on the average of ten measurements.

3.3. RESULTS AND DISCUSSION

3.3.1. Optical Properties

Coatings derived from f-DETA and TMOS were highly transparent. A dip-coated f-DETA22TMOS22W31-HAC140 coating of 3-5 μm thick on a bis-A PC substrate, after cured at 125°C for 4 hrs., only led to an extra haze of 0.2-0.4 %. F-DETA/TMOS coatings were also colorless. No absorbance bands could be found in their UV/Vis spectra in the range of wavelength from 250 nm (ultraviolet) to 1100 nm (infrared). Figure 3.2 shows the UV/Vis spectra of f-DETA50TMOS50 and f-DETA48silica52 films cured at 125°C for 4 hrs. The f-DETA/silica film was prepared by adding Ludox[®] silica gel into a pre-hydrolyzed f-DETA. With a thickness of ~ 0.2 mm, both films maintained a transmittance of $\sim 90\%$ in the visible light range. Further experiments indicated that f-DETA/TMOS sol-gel coatings could still maintained colorless after they were heated at less than 150°C in air for ca. 4 hours. However, exposure of f-DETA/TMOS coatings at 170°C in air for more than 4 hours could lead to obvious yellowing of the coating.

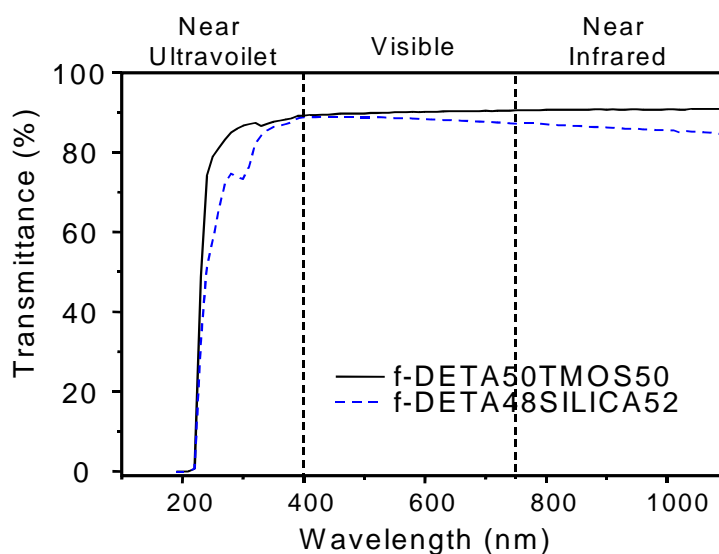


Fig. 3.2. UV/Vis spectra of free sol-gel films based on gels f-DETA/TMOS and f-DETA/Ludox silica

The refractive index at 632.8 nm for a cured f-DETA/TMOS coating was generally around 1.50-1.54. It increased with the extent of curing, but decreased as the TMOS concentration increases (Fig. 3.3). Due to its dependence on the extent of curing, the refractive index may be used to determine the extent of curing for a given coating system.

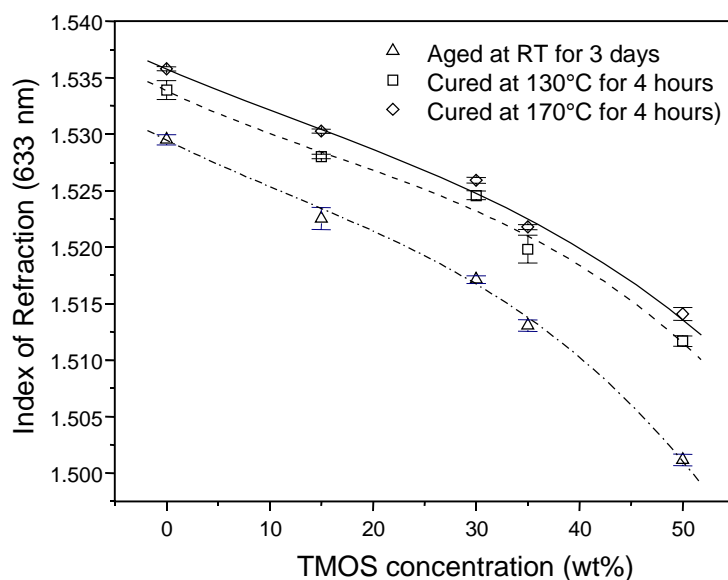


Fig. 3.3. Refractive index of the f-DETA/TMOS coatings obtained using an acetic acid catalyst and cured under different conditions

3.3.2. Thermal Curing of the Coatings

The thermal curing of sol-gel coatings was controlled by a temperature-time profile that described the temperature change during the curing process. To avoid coating cracking, pre-curing steps at low temperatures (60-100°C) were often necessary in the temperature profile. Figure 3.4 shows the weight changes of a f-DETA22TMOS22W31-HAC140 gel under three different isothermal processes. During the TG experiment, the weight of the gel decreased in an exponential way in the isothermal processes. After 6 hrs., the coating material lost 5.9%, 8.3% and 9.8% of its weight at 80°C, 130°C and 170°C, respectively. Most of the weight losses

occurred during the initial two hours and further curing at the same temperature did not lead to significant weight losses.

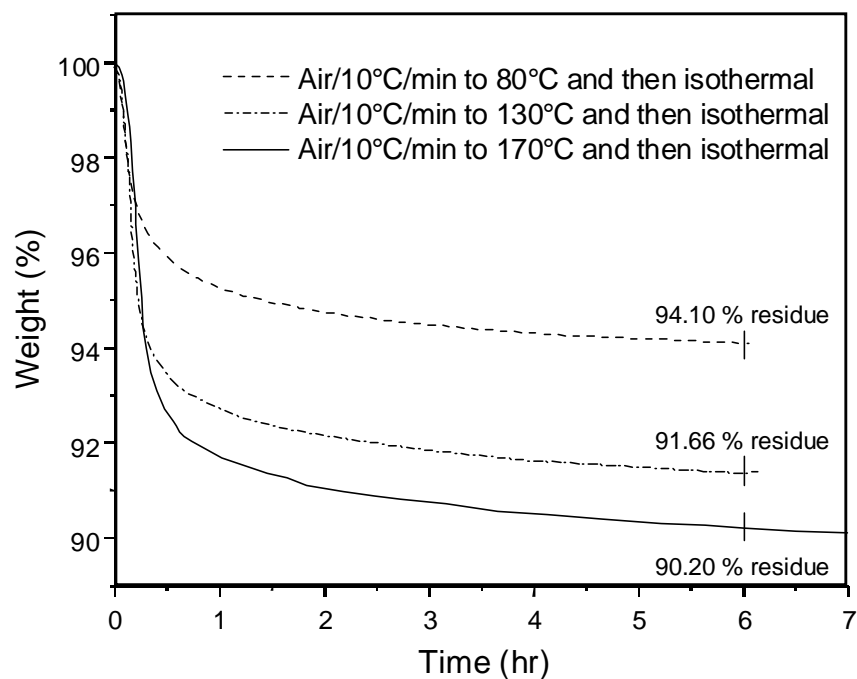


Fig. 3.4. Isothermal TG scans for gel f-DETA22TMOS22W31-HAC140 at various temperatures.

Figure 3.5 shows the weight changes for four f-DETA/TMOS gels under a temperature profile that included four 2-hour isotherms at 80, 125, 150 and 175°C. Between these isotherms, the temperature was increased at a rate of 10°C/min. These four tested gels are f-DETA31TMOS31W5-HCL27, f-DETA22TMOS22W31-HCL20, f-DETA22TMOS22W31-HPO20, and f-DETA22TMOS22W31-HAC140, which will be mentioned simply by their catalyst part of the nomenclature. During the TG experiments, all the samples showed exponential decays in their weight in each isotherm. Compared with the other gels, the water-deficient HCL27 gel lost weight at a relatively slow rate at 80°C, but approached the other water-abundant gels at 150°C and 175°C. This behavior is believed to be related to the relatively low silanol concentration in the HCL27 gel. In general, gels with a low silanol concentration condense more by an alcohol-forming condensation route. However, the alcohol-forming condensation reaction has a higher

activation energy and hence proceeds at a slower rate than the water-forming condensation reaction. Therefore, the HCL27 gel lost less weight than the water-sufficient gels at 80°C and 125°C. However, since all the samples had the same amount of alkoxy silane groups, the eventual weight losses for the four samples became similar at a 150°C and 175°C at which the alcohol forming condensation occurred at a much faster rate.

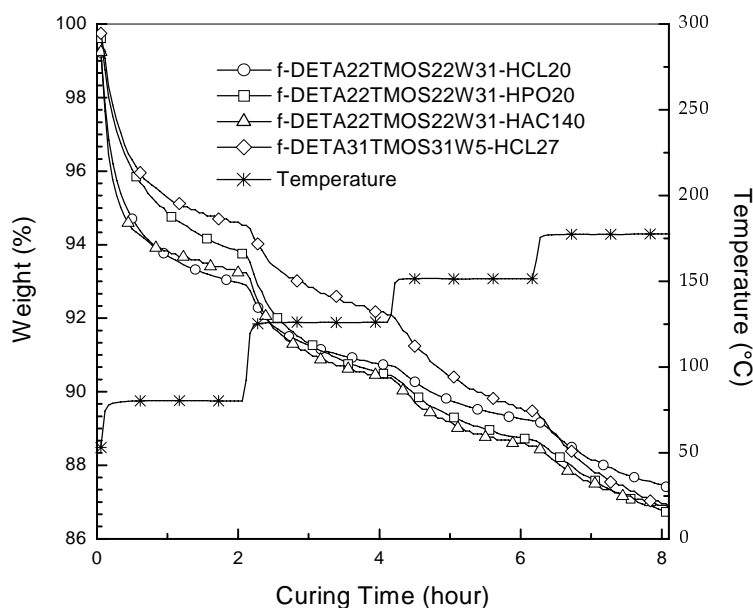


Fig. 3.5. Isothermal gravimetric diagrams of f-DETA/TMOS gels formulated using different acid catalysts and water concentrations.

Figure 3.6 shows the TG/DTA profiles for gel HAC140 under the illustrated temperature profile. The temperature profile includes a hold at 80°C for 2 hrs., followed by a ramp at 10°C/min. to 800°C and then another hold at 800 °C for 10 min. During the experiment, gel HAC140 displayed an onset of some weight loss between 80-130°C, which further increased between 140-350°C. Oxidation and combustion of organic compounds occurred at about 430°C. After 700 °C, the sample was mostly oxidized to silica, and a constant weight was reached at 50.2% of the original weight.

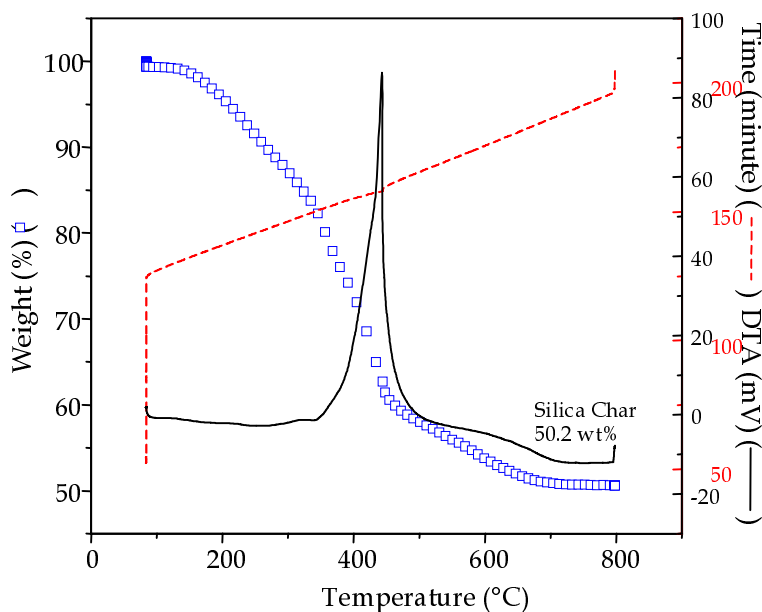


Fig. 3.6. The thermal gravimetric profile of gel f-DETA22TMOS22W31-HAC140 obtained at a temperature ramp of 10°C/min.

The extent of curing could be estimated by the yield of silica char *assuming* f-DETA/TMOS gels were quantitatively converted to silica at 800°C after 10 minutes of heating. The sample weight typically displayed an exponential decay during these isotherm processes due to elimination of the hydrolysis and condensation by-products. During an isothermal process, the sample weight could be closely simulated by an extended exponential decay function given as.

$$W = W_{\infty} - (W_0 - W_{\infty}) \text{Exp}[-((t - t_0) / \tau)^{\beta}] \quad \text{Eqn. 3.1}$$

here W_0 is the weight at time t_0 , W_{∞} is the limiting weight that may be obtained if the holding time at the temperature is sufficiently long, τ is the decay constant and β is a dimensionless coefficient. The value of τ reflects the rate of condensation; while the value of β reflects the closeness of the weight profile to a first-order exponential decay. For β less than unity, Eqn. 3.1 can be viewed as a stretched exponential, while for $\beta=1$, Eqn. 3.1 corresponds to a normal first order exponential decay function.

Table 3.2 lists the parameters W_{∞} , τ , β , and estimated extent of condensation during each isothermal period for the four gels shown in Fig. 3.5. The extent of curing was calculated

according to the yield of silica char. During the calculation, it was assumed that all the silicon species were oxidized and converted to silica. A system with only f-DETA and TMOS (i.e. a recipe without any solvent, water and catalyst) was considered to have an extent of condensation of 0%. Whereas the same system with complete conversion of all the RSi(OEt)_3 groups and TMOS to $\text{RSiO}_{3/2}$ and SiO_2 , respectively, was thought to be 100% condensed. After being cured at 80°C, 125°C, 150°C and 175°C for 2 hrs., respectively, these gels showed quite similar weight losses, although they were derived from recipes that differed in either pH or water concentration. Under this temperature profile, the β values for these gels were around 0.5 at 80°C and 125°C and approached unity at 150°C and 175°C.

Table 3.2. Curve-fitting parameters and extent of curing for four f-DETA/TMOS gels

Curing Temp.	Parameters	HCL27 ^a	HCL20 ^b	HPO20 ^c	HAC140 ^d
80°C	W_∞ (%)	94	92	92	93
	τ (min.)	20	8.6	24	2.6
	β	0.66	0.45	0.44	0.44
	Ext. of Curing ^e	78%	90%	91%	81%
125°C	W_∞ (%)	91	90	89	90
	τ (min.)	76	66	59	57
	β	0.58	0.56	0.46	0.64
	Ext. of Curing ^e	81%	92%	94%	85%
150°C	W_∞ (%)	89	89	88	88
	τ (min.)	71	64	71	62
	β	0.90	0.92	0.84	0.83
	Ext. of Curing ^e	84%	94%	95%	88%
175°C	W_∞ (%)	86	86	86	86
	τ (min.)	81	91	84	81
	β	0.88	0.87	1.11	0.89
	Ext. of Curing ^e	88%	97%	98%	90%

a. HCL27=f-DETA31TMOS31W5-HCL27

b. HCL20= f-DETA22TMOS22W31-HCL20

c. HPO20=f-DETA22TMOS22W31-HPO20

d. HAC140=f-DETA22TMOS22W31-HAC140

e. Estimated by extrapolating the curing time to infinite according to Eqn. 3.1

For practical applications, it is often required that a coating be cured within a certain time (<5 hrs.). For curing sol-gel coatings, an adequate temperature profile could be designed according to the TG profile of the uncured coating material. In cases when the weight loss follows a first-order exponential weight decay, the weight loss after a period of two decay constants can reach 86% of the total weight that the sample can lose if the holding time at this temperature is sufficiently long. For a stretched exponential decay ($\beta < 1$), the weight loss during this period can be even higher. Therefore, without causing a significant reduction in the extent of curing, the adequate holding time at each isotherm of a curing temperature profile should be 2-3 decay constants. According to this principle and the decay constants in [Table 3.2](#), a reasonable holding time at 80°C might be 30-40 min., while at other higher temperatures, 2-4 hrs. of curing would probably be sufficient.

3.3.3. Influences of Formulation and Processing Variables on the Hardness and Abrasion Behavior

For a given type of material, the abrasive wear rate is usually inversely proportional to its hardness¹⁷⁰. The proportionality constant is related to the chemistry and morphology of the contacting materials, so care must be taken in correlating the abrasion resistance of a material to its hardness. Early results have confirmed that the abrasion resistance of the coating could be increased by incorporation of TMOS¹⁴. Here the influences of TMOS, the curing temperature and curing time on the hardness of the coating are addressed.

[Figure 3.7](#) shows the increases of microhardness of the f-DETA22TMOS22W31-HAC140 coating with the curing time and curing temperature. With a curing temperature of 80°C, the hardness of coating HAC140 only increased from 45 to 54 kgf/mm² as the curing time was increased from 6 to 24 hrs. While at 135°C, the hardness increased from 80 to 105 kgf/mm² as the curing time was similarly increased. Therefore, after a certain period of curing (~4 hrs.), increasing curing time without increasing curing temperature only resulted in very limited hardness increase.

[Figure 3.8](#) illustrates that the hardness of f-DETA/TMOS coatings also significantly increases with the concentration of TMOS). After curing at 135°C for 12 hrs., coatings with the

weight ratio of TMOS/(f-DETA+TMOS) of 0%, 35% and 50% exhibited a Vickers hardness of 46, 68 and 92 kgf/mm², respectively. The concentration of TMOS in the recipe was limited to about 60 wt% (excluding the solvent, water and catalyst). Beyond this concentration, the resulting coatings often cracked during the drying and curing processes because of the lower flexibility and high shrinkage. For this reason, microhardness data for coatings with TMOS concentration above 60 wt% could not be obtained.

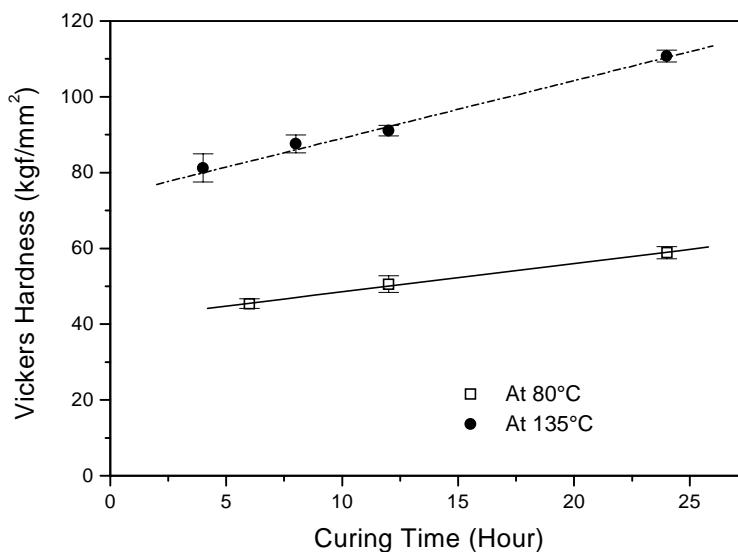


Fig. 3.7. Vickers microhardness of f-DETA22TMOS22W31-HAC139 coatings cured at different conditions. The substrate is glass.

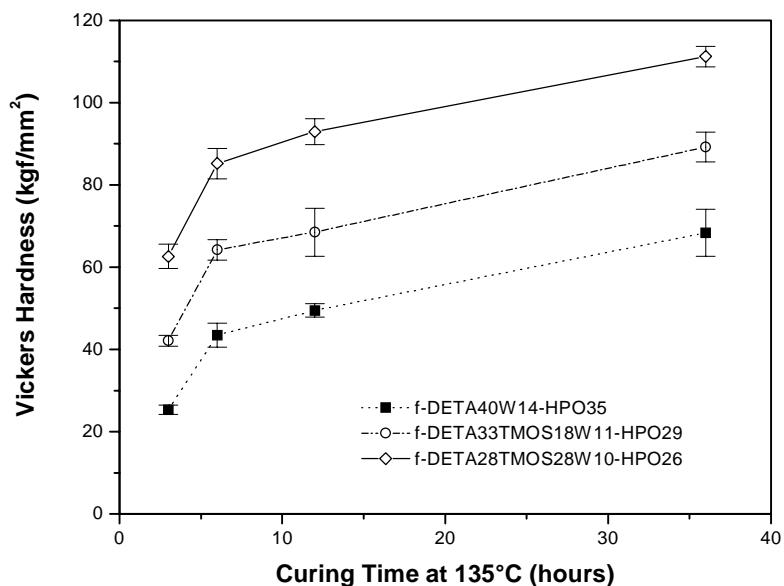


Fig. 3.8. Dependence of Vickers hardness on the concentration of TMOS. The substrate is glass.

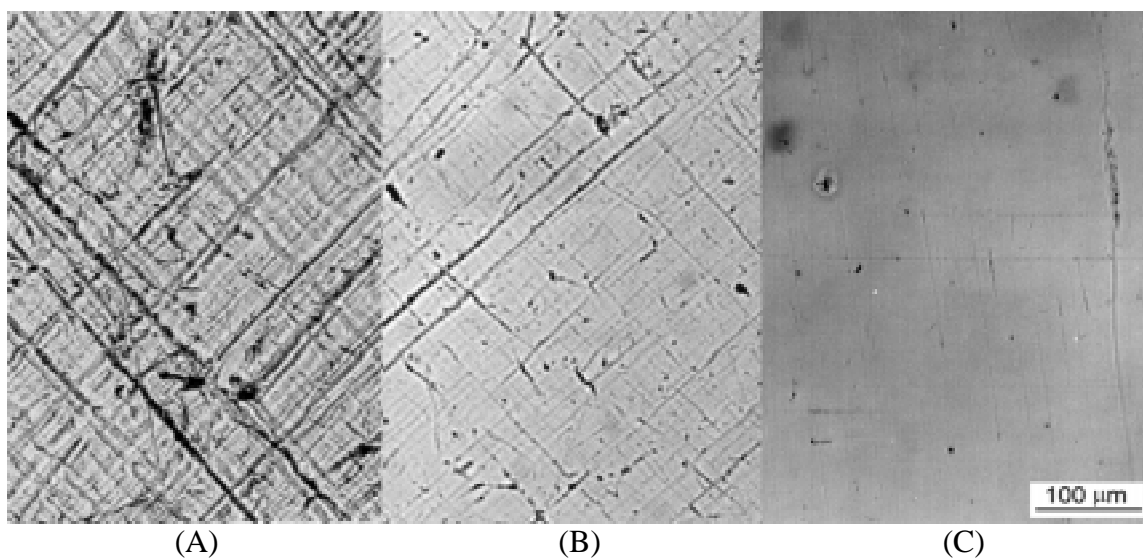


Fig. 3.9. Transmission optical micrographs for wear tracks on bis-A PC substrates: (A) uncoated after 150 cycles; (B) coated with f-DETA28TMOS28W10-HPO27 after 500 cycles; (C) coated with f-DETA22TMOS22W31-HAC139 after 500 cycles.

The performance of a coating in an abrasion test depends on the film thickness. To compare the intrinsic abrasion resistance of various coatings, the films should be thick enough so that the abrasion does not penetrate the coating and damage the substrate. For most coatings reported in this study, the thickness of the sol-gel coatings was found to be ca. 3-5 μm by scanning electron microscopy. Generally, if an f-DETA/TMOS coating (3-5 μm thick) could maintain a 94% of transmittance after a *principal Taber test* (CS10 wheels/500 g load, 500 cycles), then wear of the surface would be mostly limited to the coating layer, although a few scratches might cut through the coating. Adhesion of the coating to the substrate is another major exterior factor affecting the performance of a coating. In cases of weak adhesion, the coating could be scraped off easily from the substrate during the abrasion test, and hence exposing the inner substrate to direct abrasion.

Figures 3.9 A-C show the transmission optical micrographs of Taber tracks on an uncoated bis-A PC substrate (A) and coatings f-DETA28TMOS28W10-HPO27 (B) and f-DETA22 TMOS22W31-HAC140 (C) on the same bis-A PC substrates. The Taber test involved a pair of CS10 wheels, a 500-gram load per wheel. The uncoated bis-A PC substrate was abraded for 150 cycles, whereas the coated bis-A PC substrates were abraded for 500 cycles. The results indicated that the f-DETA22TMOS22W31-HAC140 coating was far less scratched than the f-DETA28TMOS28W10-HPO27 coating, which was in turn far less scratched than the uncoated substrate, although the uncoated substrate was only abraded for 150 cycles. Note the transmission optical micrographs were taken at a slight defocus imaging condition, under which only relatively deep and thick scratches can be observed.

The abrasion resistance of a given coating depends strongly on the extent of curing, which in turn depends on the silanol group concentration in the uncured gels. The curing process involves homo-condensation of silanol groups and hetero-condensation between the silanol groups and alkoxy silane groups. Therefore, increasing the extent of hydrolysis should promote thermal curing and hence improve the abrasion resistance of the coating.

Raising the water concentration in the recipe (represented by r) is a method of increasing the extent of hydrolysis. Using f-DETA/TMOS coated bis-A PC substrates, the dependence of the abrasion resistance on r was studied. The abrasion resistance was graded by the transmittance

of the wear track caused by the *principal Taber test* described earlier. In these tests, both phosphoric acid and acetic acid were used as catalysts, respectively. The coating formulae using a phosphoric acid catalyst were pre-hydrolyzed for 30 min., while those using an acetic acid catalyst were pre-hydrolyzed for 6 hrs. All these coatings were cured at 60°C for 30 min. and then 130°C for 4 hrs. With phosphoric acid as the catalyst, an increase of r from 0.5 to 4.4 led to an improvement of the abrasion resistance of the resulting coatings from a transmittance of ca. 90% to ca. 98% (Fig. 3.10). For recipes using an acetic acid catalyst, the increase of the coating abrasion resistance with r was more noticeable. In this case, as r increased from 1.1 to 4.4, the resulting coating showed an increase of transmittance from 86% to above 98%. Therefore, at a given curing temperature and curing time, a high water concentration indeed helps to increase the concentration of silanol groups and extent of curing.

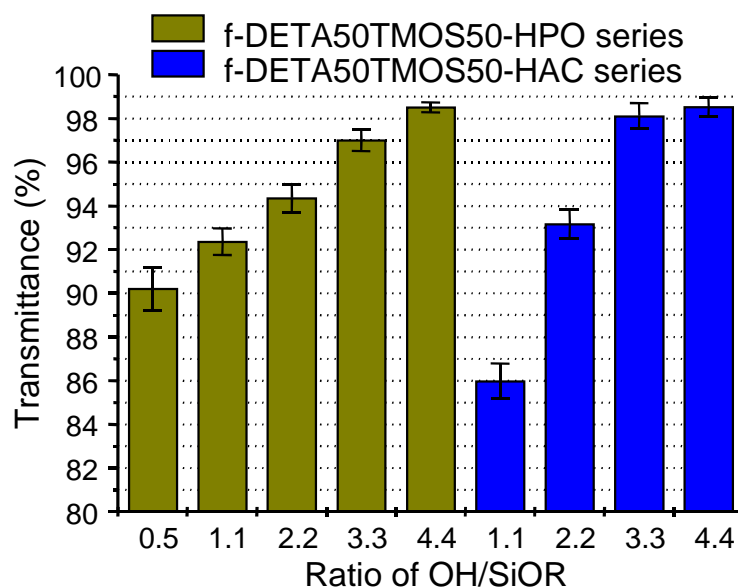


Fig. 3.10. The transmittance of the wear track after 500 cycles of abrasion for 1:1 f-DETA/TMOS coatings on bis-A PC with different ratio of OH/OR. Curing conditions: 130°C for 4 hrs.

For a given catalyst and formulation, lengthening the hydrolysis time is another way of increasing the extent of hydrolysis although too long a hydrolysis time will lead to gelation. The influence of the hydrolysis time on the abrasion resistance of the resulting coating was studied using a phosphoric acid system and two acetic acid systems containing equal weights of f-DETA

and TMOS. For phosphoric acid system, the value of r was 2.2, while for the acetic acid system, it was either 2.2 or 4.4. The recipes were allowed to pre-hydrolyze for different times before being applied on bis-A PC substrates. After curing at 130°C for 4 hrs., the coated substrates were abraded using the *principal Taber test* mentioned earlier. The abrasion resistance of the three series of coatings is illustrated in Fig. 3.11. In the case of phosphoric acid catalyst, the coatings prepared by hydrolyzing for 30 min. and 60 min. were similar in their abrasion resistance, and both showed a transmittance of ca. 95%. On the contrary, the abrasion resistance of the acetic acid system was rather sensitive to the pre-hydrolysis time. With an r of 2.2, the coatings prepared by pre-hydrolyzing for 5 hrs., 8 hrs. and 10 hrs. showed an abrasion resistance of 85%, 92%, and 93%, respectively. With this recipe, a pre-hydrolysis time of 8 hrs. was required so that the resultant coatings could offer appreciable abrasion resistance (~92% transmittance). A similar trend was also observed for the recipes with an r of 4.4. The coatings showed an improvement of abrasion resistance from ca. 96% to 98.5% as the pre-hydrolysis time was extended from 3.5 hrs. to 7.5 hrs. On the average, as r was increased from 2.2 to 4.4, the acetic acid coating system exhibited an overall increase of 6-10% in the abrasion resistance. Practically, when acetic acid was used as the catalyst, the r ratio was often set to ca. 4 and the hydrolysis time was 5-6 hrs.

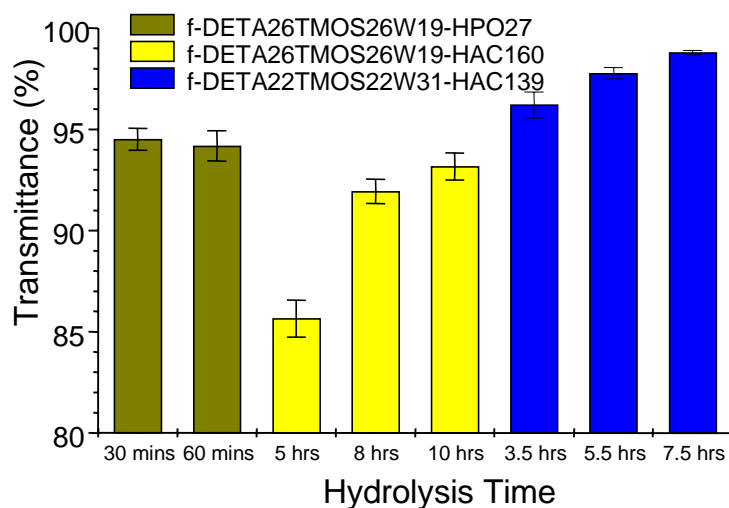


Fig. 3.11. The transmittance through the wear track after 500 cycles for f-DETA26 TMOS26W19 coatings on bis-A PC using HPO or HAC catalysts. Curing conditions: 130°C for 4 hrs.

Increasing curing temperature can also promote the water-forming condensation and alcohol-forming condensation, thus increasing the extent of curing. However, as mentioned earlier, the curing temperature was limited by the thermal stability of the plastic substrate and sol-gel coatings. For bis-A PC substrates, the upper curing temperature was 135°C. Figure 3.12 shows the abrasion resistance of f-DETA22TMOS22W31-HAC140 coatings that were cured at either 80°C or 130°C. These coatings were based on bis-A PC substrates and were subjected to the *principal Taber test* mentioned earlier. According to Figure 3.12, after curing at 130°C for more than one hour, the coatings maintained an abrasion resistance of more than 98%. The coatings cured at 80°C were also very good although not as good as the ones cured at 130°C. After curing at 80°C for more than four hours, the coatings had an abrasion resistance of ca. 96%. Experiments also indicated that if this coating was cured at 80°C for less than 4 hrs., then small domains of the coating on the wear track were partly or even completely removed during the abrasion test, although most parts maintained rather good transmittance. It was possible that under this condition the adhesion between the sol-gel coatings to the substrate had not developed to its full level.

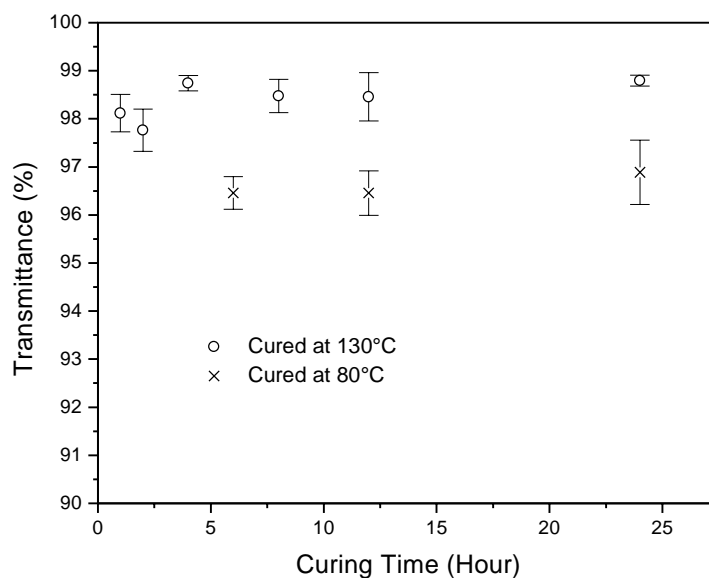


Fig. 3.12. Transmittance of the wear track after 500 cycles for f-DETA22TMOS22W31-HAC140 coatings on bis-A PC substrates.

The f-DETA/TMOS coatings were also applied on APEC HT9353[®] polycarbonate. The coating on this substrate could be cured as high as 175°C without causing warping of the substrate. (Recall that APEC HT9353[®] polycarbonate has a glass transition temperature of 184°C.) Table 3.3 lists the weight percentage of f-DETA and TMOS of several coating recipes (solvent and water excluded), their curing conditions and abrasion resistances (by transmittance after a *principal Taber test*). According to these results, the recipe containing 50% f-DETA and 50% TMOS50 (f-DETA22TMOS22W31-HAC140) showed excellent abrasion resistance (a transmittance of ca. 98.5%) after curing at 125-150°C for 4 hrs. A further increase in the curing temperature to 180°C often led to cracking and delamination of this coating.

Table 3.3. Abrasion resistance of f-DETA/TMOS coatings (APEC-HT9353[®] substrate) cured at difference conditions. The abrasion test was conducted using the basic Taber test (CS-10 wheels, 500 g/500 cycles).

Coating Recipe	Curing Conditions	Transmittance (%)
Uncoated	----	84.3 ± 0.6*
Pure f-DETA	180°C/ 4 hrs.	95.0 ± 0.8
65% f-DETA, 35% TMOS	180°C/ 4 hrs.	97.4 ± 0.3
56% f-DETA, 44% TMOS	170°C/ 4 hrs.	98.2 ± 0.2
56% f-DETA, 44% TMOS	150°C/ 4 hrs.	98.2 ± 0.2
56% f-DETA, 44% TMOS	125°C/ 4 hrs.	97.7 ± 0.3
50% f-DETA, 50% TMOS	180°C/ 4 hrs.	cracks during curing
50% f-DETA, 50% TMOS	150°C/ 4 hrs.	98.4 ± 0.2
50% f-DETA, 50% TMOS	125°C/ 4 hrs.	98.5 ± 0.5

The uncoated APEC-HT9353[®] polycarbonate was abraded with CS-10 wheels for 25 cycles.

With a slightly lower the concentration of TMOS, the coating recipe including 56% f-DETA and 44% TMOS is expected to be more flexible and hence could survive a curing process at 170°C for 4 hrs. According to Table 3.3, this coating exhibited excellent abrasion resistance (a transmittance of 98 %) after curing at 125°C, 150°C or 170°C for 4 hrs. Coatings prepared using 56% f-DETA and 44% TMOS on APEC PC substrates were also subjected to extensive abrasion tests that involved a pair of CS10 wheels and a 500-gram load per wheel, but the abrasion cycle

was extended to 1000 cycles. During these tests, the transmittance of the resulting wear track was measured after 250, 500 and 1000 cycles of abrasion. Figure 3.13 shows the optical transmittance of the wear tracks on these substrates. The coatings cured at 150°C and 170°C generally showed better abrasion resistance than the coating cured at 125°C after 250 and 500 cycles of abrasion, *but the latter show better results after 1000 cycles of abrasion*. Optical microscopy indicated that the major cause for the coatings cured at 150°C and 170°C to lose transparency after 1000 cycles of abrasion was the delamination of the coatings from the substrate, rather than just the usual scratching of the coating. This phenomenon could be attributed to the higher hardness but lower toughness of the coatings cured at a temperature at 170°C. For this reason, the balance between the hardness and toughness should also be considered when developing a good abrasion resistant coatings.

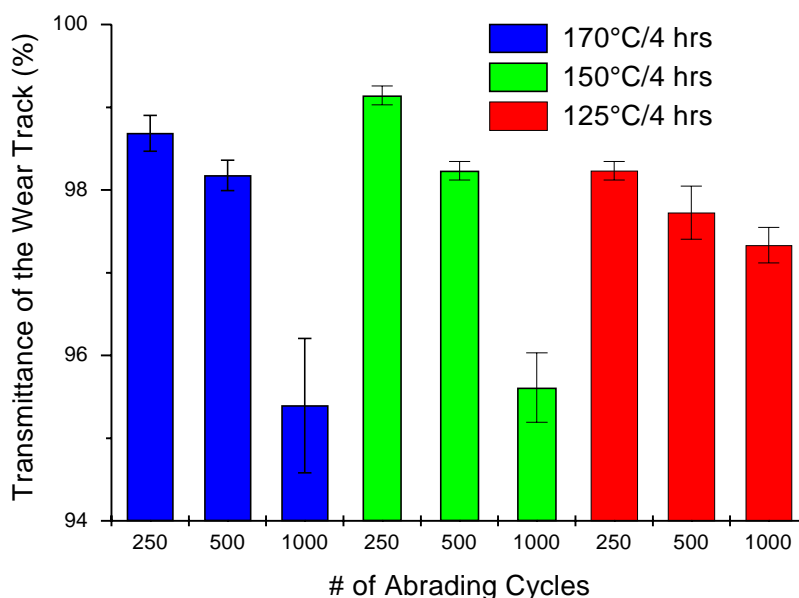


Fig. 3.13. Optical transmittance of APEC-HT9353[®] polycarbonate coated with f-DETA56TMOS44 sol-gel coatings following the Taber abrasion test. The Taber test was conducted using CS-10 resilient abrasion wheels and a 500-gram load on each wheel.

3.3.4. Abrasion Resistant Coatings on Metal Substrates

The f-DETA/TMOS coatings formulated using a hydrochloric acid catalyst were also applied to metal substrates like copper, brass, aluminum and stainless steel and this resulted in considerable success in improving the abrasion resistance of those substrates^{158,159,161}.

Reflection optical microscopy was used to compare the abrasion resistance of uncoated and coated aluminum and brass substrates. Again, the coated substrates were subjected to the *principal Taber test*; the uncoated ones were abraded with the same wheels and loads but less abrasion cycles were used.

Figure 3.14 shows optical micrographs for the surfaces of four aluminum substrates. Micrograph 3.14 (A) shows original fringe-like features on an uncoated aluminum substrate formed during manufacturing. Micrograph 3.14 (B) shows the typical “X” type scratch patterns left by the Taber test on an uncoated aluminum substrate. These two pictures show that the surface fringes on the substrate could be removed by only 25 cycles of abrasion, thus exhibiting the extremely poor abrasion resistance of aluminum. Micrographs 3.14 (C) and 3.14 (D) reveal the wear tracks on aluminum substrates that were coated with f-DETA26TMOS26W19-HPO23 (HPO23) and f-DETA22TMOS22W31-HAC140 (HAC140), respectively. After the abrasion test, these two substrates principally display the original surface fringe patterns, and the “X” type scratch pattern can only be barely seen. Clearly, the coating successfully protected the weak aluminum substrate from wear. As indicated by the density of “X” type scratches, the HAC140 coating (Micrograph 3.14 (D)) clearly had an edge over the HPO23 coating in abrasion resistance.

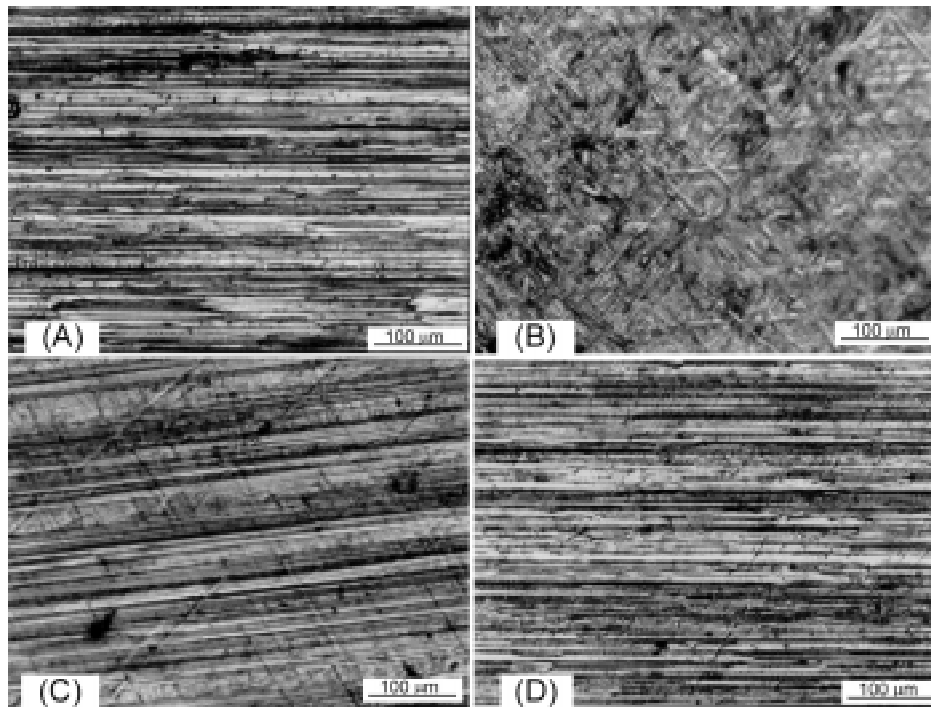


Fig. 3.14. Reflection optical micrographs of aluminum substrates: (A) uncoated and unabraded; (B) uncoated and abraded for 25 cycles; (C) coated with recipe f-DETA26 TMOS26W19-HPO23 and abraded for 500 cycles; (D) coated with recipe f-DETA22 TMOS22W31-HAC140 abraded for 500 cycles. The Taber tests involve CS-10 wheels, each with a 500-gram load.

Figure 3.15 shows the reflectance optical micrographs for three brass substrates. Micrograph 3.15 (A) shows the original surface features of an uncoated brass surface caused by manufacturing. Micrograph 3.15 (B) reveals the “X” type Taber scratches on an uncoated brass substrate that was abraded for 50 cycles. Micrograph 3.15 (C) shows the Taber wear track for the same brass substrate coated with the HPO23 coating. In this example, brass is much a harder substrate than aluminum, however, after only 50 cycles of abrasion, its surface features from manufacturing (Micrograph 3.15 (A)) were also replaced by dense deep “X” type scratches (Micrograph 3.15 (B)). If the substrate was protected by the HPO23 coating, then only a few shallow scratches can be observed even after 500 cycles of abrasion (Fig. 3.15 C), indicating the coating was also effective for brass substrates. In fact, it is the coating properties rather than the

substrate that determine the abrasion resistance of the system as long as wear is limited to the coating layer

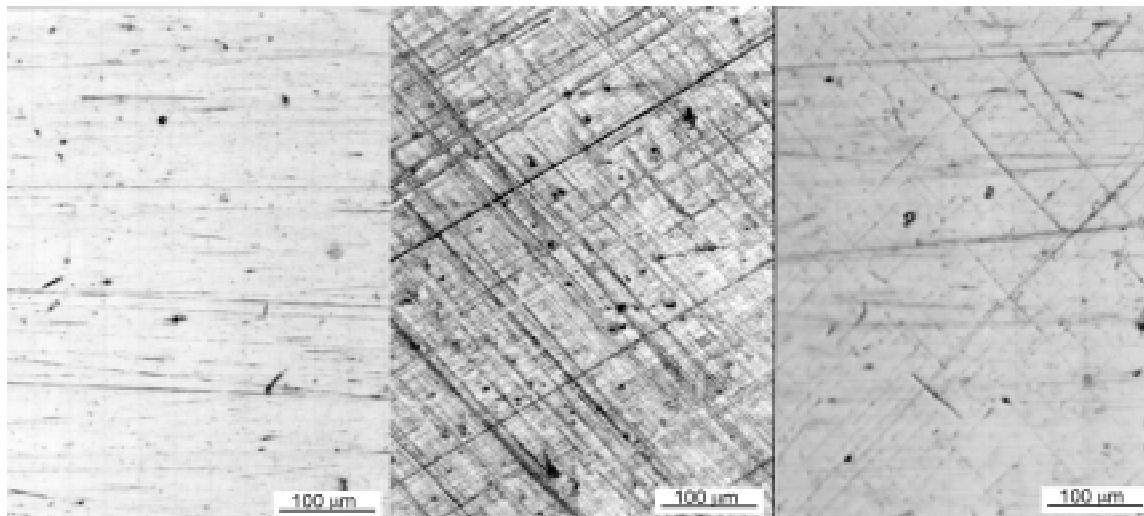


Fig. 3.15. Reflectance optical micrographs of (A) uncoated brass surface (unabraded); (B) uncoated brass surfaces after 50 cycles of abrasion; (C) aluminum substrate coated with f-DETA26TMOS26W19-HPO23 after 500 cycles of abrasion. The Taber tests involve CS-10 wheels, each with a 500-gram load.

3.4. CONCLUSIONS

The inorganic-organic hybrid materials derived from sol-gel reactions of f-DETA and TMOS provided optically transparent coatings. These materials could be applied to many substrates including bis-A PC, APEC HT9353[®] PC, aluminum and brass and thermally cured to form hard abrasion resistant coatings on these substrates.

Formulated with f-DETA, TMOS, water and 2-propanol, the gelation time of the coating recipe could be controlled from several min. to over 12 hrs. using an acid catalyst of proper acidity strength. The thermal curing processes of these coatings were studied by TG/DTA and suitable curing temperature profiles were established according to the TG/DTA results.

The abrasion resistance and microhardness of the sol-gel coating depended on many factors including the TMOS concentration, water concentration, curing time, curing temperature, and the hydrolysis time. The abrasion resistance and hardness of the coating increased apparently with the curing temperature and the concentration of TMOS in certain limits. The curing temperature depended on the stability of the coating and substrate. Generally, a high curing temperature could increase the hardness but it could also lower the toughness, hence, the resulting coating might be more sensitive to long term abrasion. Because of this, coatings cured at 125°C could be less abrasion resistant than the same coatings cured at 170° in a 250 cycle Taber test, but better than the latter in a 1000 cycle Taber test. The TMOS concentration was also limited by an upper value, which was dependent on curing temperature, and above which the resulting coating might crack during the drying and curing processes. Increasing the water concentration also led to noticeable increase in abrasion resistance. While a certain minimum curing time might be needed for a given coating to have good abrasion resistance, it was found that lengthening this curing time usually only led to limited increases in the hardness and abrasion resistance. For a weak acid catalyst, the abrasion resistance of a coating also increased with the pre-hydrolysis time of the recipe. With acetic acid as the catalyst, a f-DETA/TMOS formula with an r of 4.4 and a pre-hydrolysis time of 5-6 hrs. could form extremely good abrasion resistant coatings.

CHAPTER 4. THE MECHANISM FOR 3-APS TO STRENGTHEN THE INTERFACE BETWEEN POLYCARBONATE AND SOL-GEL HYBRID COATINGS[†]

4.1. INTRODUCTION

Silane coupling reagents¹⁷¹ are frequently used to strengthen the bonding of glass fibers to polymeric matrices for composite materials and to promote the adhesion of adhesives and sealants to glass substrates. While it is quite clear that silane coupling reagents interact with glass substrates or silsesquioxane/silica materials through siloxane bonding formed by condensation of silanol groups^{171,172}, the interaction of silane coupling reagents with polymer surfaces is much more complicated. It is believed to be dependent on the functional group of the silane coupling reagent, the topography of the surface, the nature of the polymer matrix and the processing method¹⁷³. Models based on chemical bonding, interdiffusion and interpenetrating network (IPN) formation in the interphase region have helped to explain many phenomena in thermoset composites like glass fiber (GF)/amino silane/epoxy¹⁷⁴, GF/vinyltriethoxysilane/PMMA¹⁷⁵, GF/3-methacryloxypropyltriethoxysilane/polystyrene¹⁷⁶ and GF/3-aminopropyltriethoxysilane (3-APS)/polyethylene¹⁷⁷ (composites are referred to here as a fiber/coupling agent/polymer matrix system). However, the extent of chemical bonding is not known in thermoplastic matrices although appreciable improvements in the flexural strength of composites containing silane treated fibers have been observed^{172,173}. It has been assumed that compatibility (solubility) of silane with the polymer matrix in thermoplastic composites is more important to the adhesion for thermoplastic matrices, but chemical reactions between the species could add additional strength¹⁷³.

[†] Published in J. Inorg. Organomet. Polym. **1998** 8(1) 33

During the past few years, it was found that 3-APS could greatly enhance the adhesion of hybrid organic-inorganic silsesquioxane/silica based sol-gel coatings to bisphenol-A polycarbonate (bis-A PC) and CR-39[®] polycarbonate substrates^{14,17}. The latter substrate is prepared by radical polymerization of diallyl diglycol carbonate. The hybrid sol-gel coating was applied to increase the abrasion resistance of the substrate. During the surface treatment, both polymer substrates were degreased with 2-propanol, then coated with a thin layer of 3-APS primer solution in 2-propanol. To obtain satisfactory adhesion, bis-A PC substrates could be treated with a 0.5 wt% 3-APS solution, for CR-39[®], however, a 3-APS concentration of 5 wt% or above was required. When the solvent evaporates, a portion of the 3-APS could partially hydrolyze and condense to form a white powdery layer on the substrate, especially in a humid atmosphere. The powdery material should be wiped off before applying the sol-gel coating. In the case of bis-A PC, the curing temperature of the applied sol-gel coatings was below the glass transition temperature of the substrate so that the substrate could maintain its dimensions. For the CR-39[®] substrate, however, the curing temperature could be higher than the glass transition temperature (T_g for CR-39[®] is ca. 70°C) since the substrate is crosslinked. Under this crosslinked condition, the interdiffusion of 3-APS into the substrates is expected to be somewhat more hindered.

Wen et al. have suggested that 3-APS may interact with a polycarbonate substrate through hydrogen bonding between the amine protons in 3-APS and the carbonyl groups in the substrate¹⁴. Computer simulation based on a molecular dynamics (MD) method indicated that the energy due to hydrogen bonding is substantially sufficient to tentatively explain the marked adhesion increase. However, the hydrogen bonding model still failed to explain: 1) why the coating could sustain a hot-wet condition (in boiling water) without delamination due to competing hydrogen bonding from water; and 2) why the CR-39[®] substrate should be treated with a primer containing >5 wt% 3-APS to obtain good adhesion, while for bis-A PC substrate, only 0.5 wt% APS in the primer was sufficient.

A chemical bonding mechanism based on aminolysis of the carbonate groups by 3-APS is proposed in this chapter. According to this mechanism, the outermost polycarbonate layer is

slightly penetrated by 3-APS when the substrate is treated with a 3-APS solution. Then, in this layer, the amine groups from 3-APS react with the carbonate groups in the polymer substrate as schematically illustrated in Fig. 4.1. During the reaction, polycarbonate chains undergo a lower degree of chain scission at the carbonate linkages and triethoxysilyl groups become chemically bonded to the substrate through urethane linkages. Finally, under the influence of any moisture present, reacted or unreacted APS molecules are partially hydrolyzed and condensed to form a thin layer of 3-APS gel, which later may react with a sol-gel coating through silanol condensation. By this mechanism, the sol-gel coating is covalently bonded to the substrate, and hence enhanced adhesion and appreciable moisture resistance are obtained. The degree of aminolysis or chemical bonding of 3-APS with the substrate increases with the extent of 3-APS penetration into the substrate. Since CR-39[®] resin is crosslinked and hence less swellable, a more concentrated 3-APS solution may be required to keep the substrate at the same level of aminolysis.

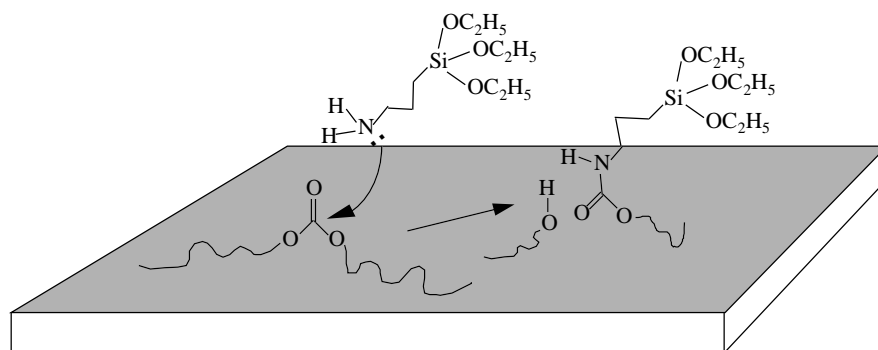


Fig. 4.1. Proposed chemical bonding of 3-APS to a polycarbonate substrate

The 3-APS primer and the aminolysis mechanism may potentially be extended to poly(methyl methacrylate) (PMMA) substrate, which is also an excellent glazing material. Similar to bis-A PC, this polymer can be treated with a sol-gel coating to increase abrasion resistance. On this occasion, however, 3-APS reacts with ester groups in the substrate and becomes attached to the substrate through amide groups. In this research, specific model solution

experiments as well as substrate surface analyses were conducted on some or all three polymers including bis-A PC, CR-39[®] and PMMA to confirm the proposed aminolysis mechanism.

4.2. EXPERIMENTAL AND CHARACTERIZATION PROCEDURES

Bis-A PC sheets (1.6 mm thick, Lexan[®]) were manufactured by the General Electric Company. 3-APS (99%, Aldrich) was purchased from Aldrich Chemical Company and used without further purification. CR-39[®] polycarbonate sheets (1.6 mm thick) were obtained from PPG Industries, Inc. PMMA samples were prepared by a bulk free radical polymerization of methyl methacrylate (Aldrich, 98%) in sheet form (3 mm thick) at 80°C using benzoyl peroxide as an initiator.

A mixed solution of bis-A PC and 3-APS in chloroform was used as a model system to study the interactions at the interface of these two substrate materials. GPC, ¹H NMR and ¹³C NMR experiments were conducted for the mixture and the pure materials, and the chemical cleavage was confirmed by a decrease in molecular weight and appearance of new endgroups or changes in chemical shifts for specific atoms in 3-APS.

GPC was conducted on a Waters 490 Instrument with a set of 500Å, 10³Å, 10⁴Å and 10⁵Å ultrastyrigel columns at 30°C. Chloroform was used as the mobile phase and the flow rate was set to 1 ml/min. A bis-A PC sample for GPC was prepared by dissolving 20-30 mg of the polymer into 10 ml of HPLC grade chloroform. A mixture sample of the polymer and 3-APS was prepared by dissolving 20 mg of bis-A PC and 20 mg of 3-APS into 10 ml of HPLC grade chloroform. The mixture sample was aged for 24 hrs. before the GPC experiment. Both GPC samples were filtered using a 0.2 µm filter before being injected into the GPC column.

¹H NMR and ¹³C NMR spectra were acquired on a Varian 400 spectrometer and both experiments were carried out with 5 mm NMR tubes. Peaks were identified using the Aldrich NMR library¹⁷⁸ and NMR simulation programs from ACD labs¹⁷⁹. 3-APS and bis-A PC samples for ¹H NMR were prepared by dissolving 10-20 mg of the material in ca. 1 ml of deuterated

chloroform. ^{13}C NMR samples were similarly prepared except that the quantities of the samples were increased to 50-80 mg. A mixture of bis-A PC with 3-APS was prepared for ^1H NMR by dissolving 20 mg of each material in ca. 1 ml of deuterated chloroform. For ^{13}C NMR, 60-80 mg of each material was used instead to prepare the mixture. The ^1H NMR and ^{13}C NMR spectra of the mixtures were acquired after the samples had been aged for 24 and 72 hrs., respectively.

Reflectance infrared spectroscopy was used to study the interaction of the bis-A PC substrate with 3-APS. FT-IR spectra were acquired on a Nicolet 50XB spectrometer with a Harrick reflectance attachment. The reaction of the carbonate group in bis-A PC with the amine group in 3-APS and the resulting cleavage of the carbonate chains should be indicated by the appearance of a urethane group absorption. To prepare an IR specimen with a moderate penetration depth of 3-APS into the substrate, a bis-A PC sample ($\sim 1 \times 1 \times 0.16 \text{ cm}^3$ in size) was slowly boiled ($\sim 82^\circ\text{C}$) in 10 ml of a 0.5% 3-APS solution in 2-propanol until the solvent evaporated, and then heated in an air circulating oven at ca. 150°C for 30 min. The IR specimen was also used later for XPS analysis.

A 5400 Perkin-Elmer XPS instrument was used to study the bis-A PC, PMMA, CR-39[®] and glass substrates which were treated with 3-APS solution in 2-propanol. By comparing the binding energies of the N 1s electrons obtained by XPS, it is possible to find out the chemical form of the nitrogen at the surfaces of the three substrates, and then to determine if aminolysis had occurred. All polymer samples for XPS were cut into ca. $1 \times 1 \times 0.16 \text{ cm}^3$ size before treating with 3-APS. Three bis-A PC specimens were prepared using different surface treatments. The first specimen (bis-A PC #1) was heated in 10 ml of a 0.5% APS solution in 2-propanol at 80°C for 1 hour, then dried at 100°C in a nitrogen atmosphere. The second specimen (bis-A PC #2) was soaked in 10 ml of a 0.5% APS solution in 2-propanol for 18 hrs. at room temperature and then dried under vacuum. The third specimen (bis-A PC #3) was the one used for IR analysis as mentioned earlier. PMMA and CR-39[®] samples were also heated at 80°C in 10 ml of a 5 wt% 3-APS solution in 2-propanol for 4 hrs. and then dried at 80°C for 3 hrs. A free amine reference was prepared by treating a small piece of glass with 0.5 % 3-APS solution in 2-propanol and allowing it to dry in air at ambient conditions.

4.3. RESULTS AND DISCUSSION

4.3.1. Solution NMR Experiments

In a solution containing both bis-A PC and 3-APS, if the reaction suggested in Fig. 4.1 indeed occurs, the average molecular weight of the polymer should be drastically reduced and extra groups like phenol or urethane groups should be detectable.

Figure 4.2 shows GPC scans for the pure bis-A PC polymer and a mixture of the polymer with 3-APS. The GPC scan for the mixture was acquired after the solution was aged at room temperature for 24 hrs. The results indicated that the molecular weight of the polymer was reduced significantly due to the cleavage of the backbone.

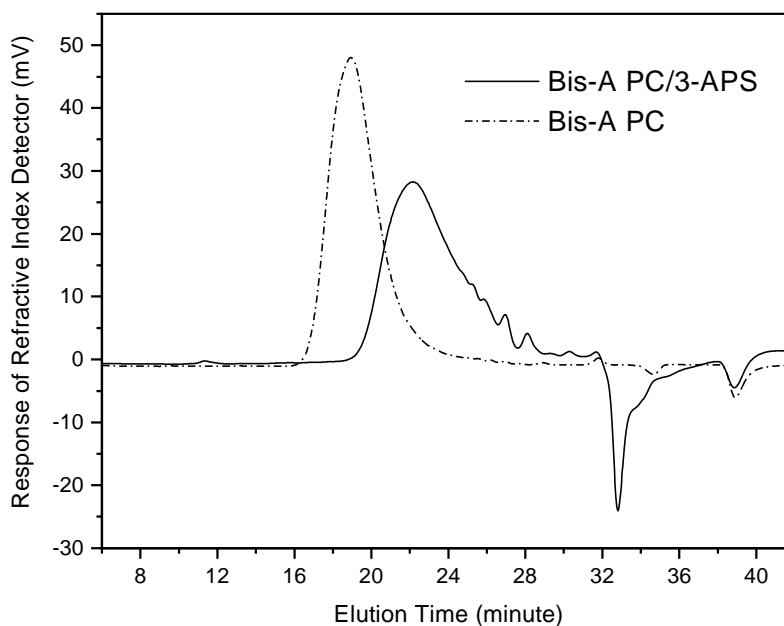


Fig. 4.2. GPC scans for a bis-A PC sample and a mixture of the polymer with 3-APS. The weight ratio of the polymer to 3-APS in the mixture is 1:1, and the solvent is chloroform

Figure 4.3 shows the ^1H NMR spectra for the bis-A PC alone (A), the polymer/3-APS mixture (B) and only for 3-APS (C). Except the amide and phenol protons, all protons in the spectra are labeled according to the carbon atoms to which they are linked in Fig. 4.4. The spectrum for the polymer/3-APS was acquired after the solution was aged at room temperature for 24 hrs. By comparing spectrum A, B, and C, it can be easily concluded that some amine groups had reacted with the carbonate groups since amide protons H25 and propyl protons H26, H27 can be observed. The presence of protons H15 and H16 also indicates new phenol endgroups were formed during the reaction. Protons H18 from phenol groups normally resonate at δ 5.5, which is also the region for amide protons according to the Aldrich NMR library and ACD NMR simulation. However, since hydrogen atoms in the OH groups are usually more difficult to detect due to a stronger hydrogen bonding interaction, especially at a low concentration, the peak at δ 5.5 was assigned to amide hydrogen atoms.

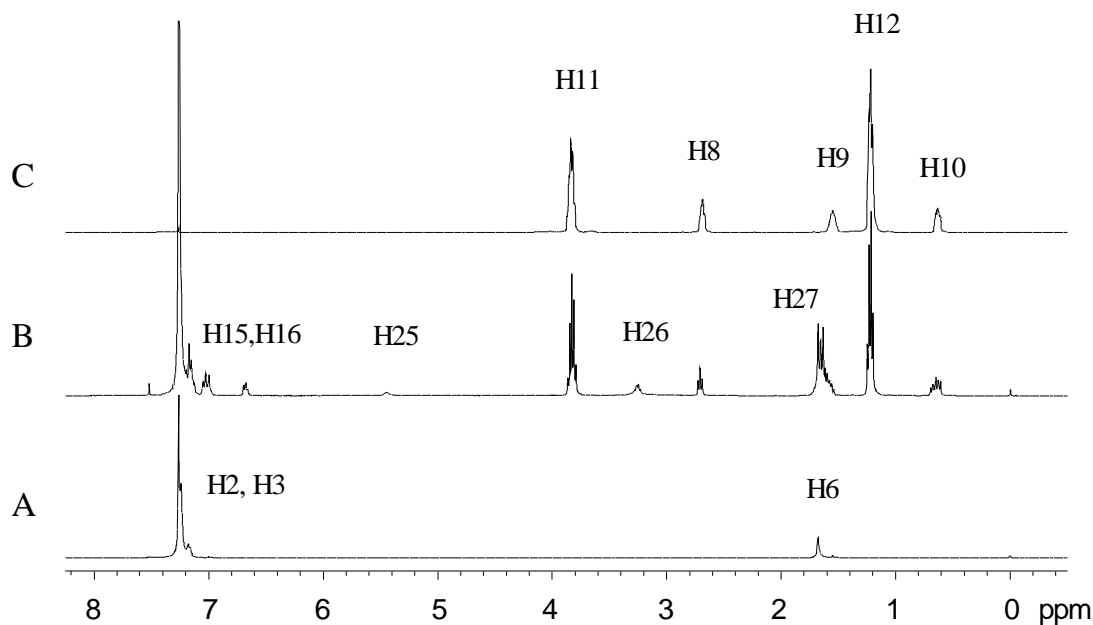


Fig. 4.3. ^1H NMR spectra for the bis-A PC (A), a mixture of the polymer with 3-APS (B) and 3-APS alone (C). The weight ratio of the polymer to 3-APS in the mixture is 1:1, and the solvent is deuterated chloroform

Proton NMR results were further supported by ^{13}C NMR spectra (Fig. 4.5). The assignment of the carbons in the spectra refers to the corresponding carbons in Fig. 4.4. The spectrum for the bis-A PC/3-APS sample was collected after the solution was aged at room temperature for three days. According to NMR simulation, the side peaks 21 and 22 in Fig. 4.5 can be assigned to the carbon atoms at phenyl groups which are linked to 3-APS molecules through a urethane bond (Fig. 4.4). By comparing the chemical shifts of C26, C27 and C28 with standard chemical shifts for corresponding carbons in 3-APS found in the Aldrich NMR library (Table 4.1), it is again concluded that 3-APS had reacted with the bis-A PC.

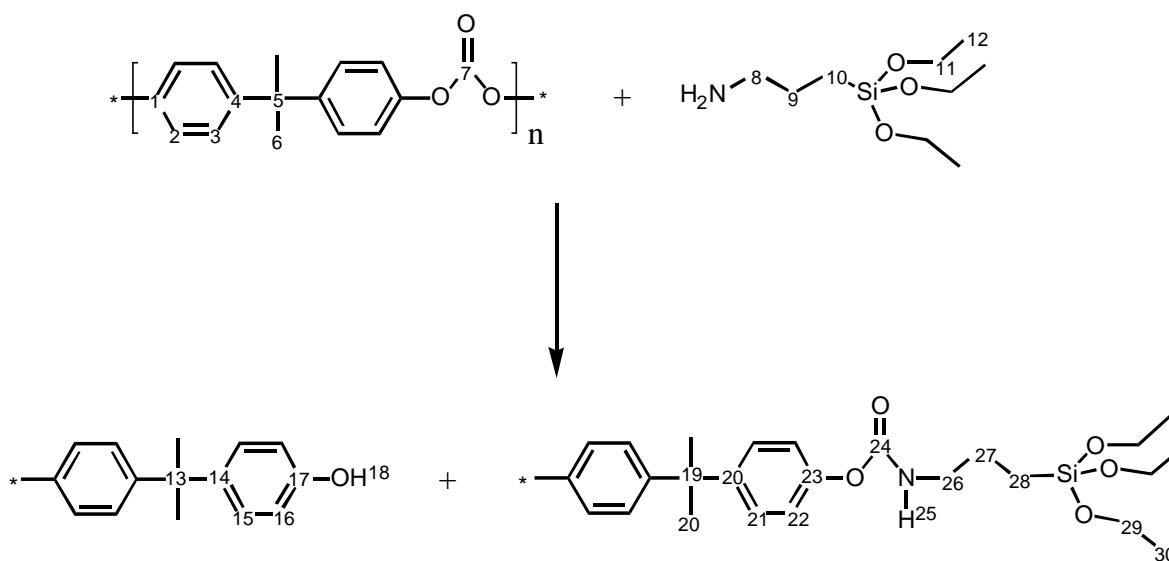


Fig. 4.4. The proposed reaction of 3-APS with bisphenol-A polycarbonate. Important carbon atoms and protons in the reactants and products are labeled for the NMR assignments

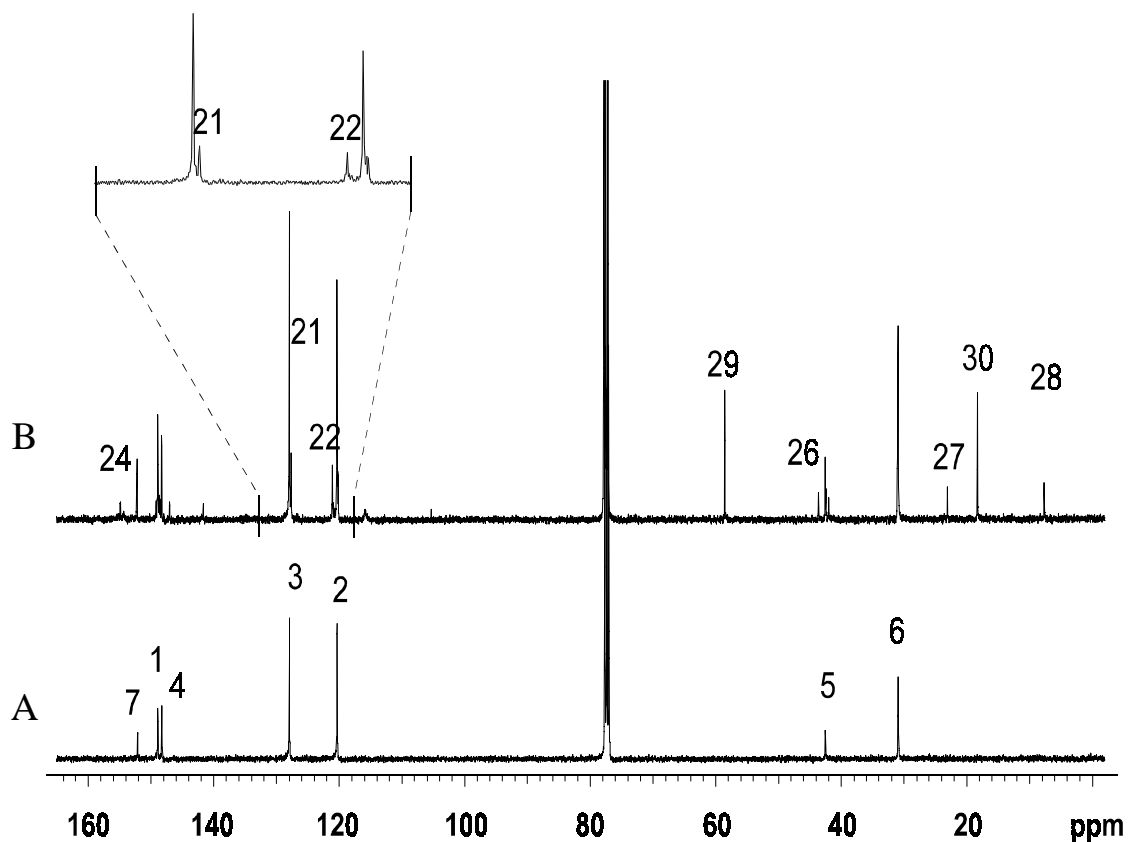


Fig. 4.5. The ^{13}C NMR spectra for a bis-A PC (A) and a mixture of the polymer with 3-APS (B). The weight ratio of the polymer to 3-APS in the mixture is 1:1, and the solvent is deuterated chloroform

Table 4.1. A comparison of chemical shifts for the corresponding carbon atoms in 3-APS and in a mixture of the bis-A PC with 3-APS (in chloroform)

APS (the Aldrich library)		Bis-A PC/3-APS	
# of carbon	δ (ppm)	# of carbon	δ (ppm)
8	45.3	26	43.6
9	27.4	27	23.2
10	7.6	28	7.6
11	18.2	29	18.2
12	58.2	30	58.2

4.3.2. Surface Analyses for Polymers Treated with 3-APS

The concentration of the resultant urethane groups may be detected by attenuated total reflectance IR (ATR). However, the bis-A PC surface was too rigid to form close contact with the ATR crystal prism, so dispersion IR was used instead. In a standard coating process of the polymeric substrate, the surface of bis-A PC was treated with a thin layer of 0.5 wt% 3-APS primer in 2-propanol as stated earlier. Alternatively, the polycarbonate sheets was also soaked in 0.5 wt% 3-APS in 2-propanol for two hours, and then washed with clean 2-propanol before being coated. However, dispersion IR is less sensitive than ATR to the small amount of urethane groups at the surface, so the bis-A PC sample was specially treated so that the polycarbonate surface was swollen to a moderate depth. By this method, a sufficient amount of urethane groups was produced within the swollen layer so that IR detection became possible.

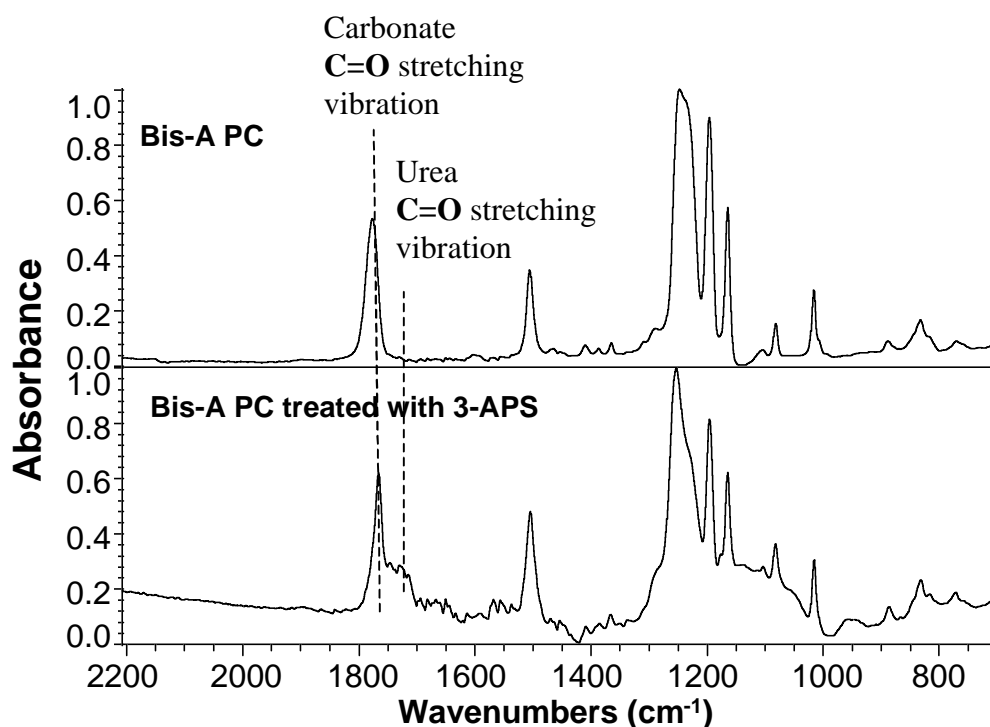


Fig. 4.6. The dispersion FT-IR spectra for a bis-A PC surface with and without treatment by 3-APS

Figure 4.6 shows the dispersion IR spectra for bis-A PC surface with or without treatment of 3-APS. While carbonate carbonyl groups absorb at ca. 1775 cm^{-1} , urethane carbonyl groups should appear at a slightly lower frequency since the nitrogen atom tends to donate its lone electron pair to the carbonyl group, thus weakening the carbon oxygen double bond. In the IR spectrum for the sample treated with 3-APS, the side peak at ca. 1725 cm^{-1} is thereby believed to be due to the presence of urethane bonds.

X-ray photoelectron spectroscopy (XPS) was used to study the surfaces of the three polymeric substrates including PMMA, bis-A PC and CR-39[®] resin. Upon treating with 3-APS, PMMA tends to react with 3-APS by forming amide linkages, while with bis-A PC and CR-39[®], urethane linkages are formed instead. Unlike bis-A PC and CR-39[®], the aminolysis of PMMA occurs in the side chain ester groups rather than in the backbone. To distinguish amide or urethane nitrogen from free amine nitrogen by XPS, a free amine reference was prepared by treatment of a clean glass slide with a 3-APS solution. By adsorbing moisture from the air, 3-APS partially hydrolyzed and condensed with residual silanol groups on the glass surface, and became attached to the substrate.

During the surface treatment of the polymers, it was found that after treating with 5 wt% APS (in 2-propanol) at 75°C for 4 hrs., PMMA was distinctly swollen, bis-A PC moderately, and CR-39[®] remained unswollen. The resistance of CR-39[®] to the 3-APS solution may be due to its crosslinked structure.

Table 4.2 gives the binding energies (B. E.) of the N 1s electrons for the polymer substrates that were treated with 3-APS as described above. The B. E. of the N 1s electrons for the three bis-A PC samples are in the range of 400-400.3 eV, while for PMMA and CR-39[®], they are both 399.6 eV. All these numbers are higher than that for the free amine reference (the glass substrate), which is 399.3 eV. Usually, the B. E. of the N 1s electrons for free amine, amide, urethane and urea nitrogen atoms are around 398-399 eV, $\sim 399.7\text{ eV}$, 400.3 eV, and 399.9 eV, respectively (Table 4.3). Therefore, the nitrogen atoms on the bis-A PC surfaces treated with 3-APS are from urethane groups rather than amine groups. Similarly, the nitrogen atoms on PMMA can be ascribed to amide groups. For the CR-39[®] substrate, however, the B. E. of the N

1s electrons is slightly higher than that of free amine groups on the glass substrate, but significantly lower than that of urethane groups. The peak can be due to two overlapping peaks from free amine groups and urethane groups considering the peak width in a typical XPS instrument is about 1 eV. Since the observed N 1s peak is close to that of a free amine, it is concluded that only a small portion of the amine from 3-APS had reacted and transformed to urethane. Therefore, the aminolysis of CR-39[®] appears to be less efficient than bis-A PC and PMMA under similar condition.

Table 4.2. Binding Energies of N 1s electrons for polymer surfaces treated with 3-APS

Sample	B. E. (eV)
Bis-A PC #1	400.0
Bis-A PC #2	400.3
Bis-A PC #3	400.1
PMMA	399.6
CR39	399.6
3-APS on a glass substrate	399.3

Table 4.3. Binding energies of N 1s electrons for a few nitrogen containing compounds relative to a saturated hydrocarbon (C 1s =285.00 eV)^{180,181}

Compound	B. E. (eV)	Group
Poly(ethyleneimine)	399.07	-CH ₂ -NH-CH ₂ -
Nylon 66	399.81	-CONH-
Nylon 6	399.77	-CONH-
Polyurethane	400.32	-OCONH-
Polyurea	399.89	-NH-CO-NH-
Polyvinylamine HCl salts	401.46	-NH ₃ ⁺
EtNH ₂	398.90	-NH ₂
NH ₄ Cl	401.50	NH ₄ ⁺

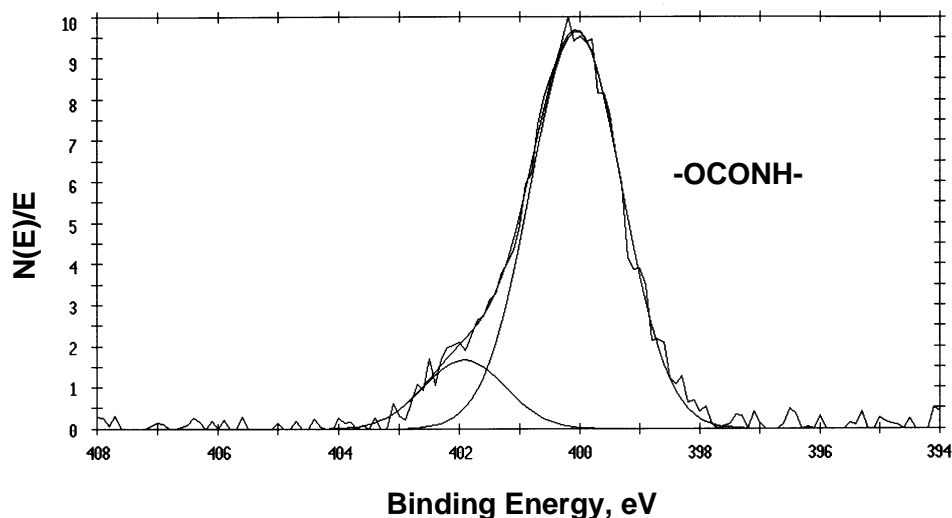


Fig. 4.7. The XPS scan for a bis-A PC sample treated with 3-APS and heated at 145°C for 30 min.

Figure 4.7 shows an XPS scan for N 1s electrons for a bis-A PC sample treated with 3-APS and heated in an air circulating oven at 145°C for 30 min. (bis-A PC #3). Two N 1s peaks were observed at 400 and 402 eV. The strong peak is due to the urethane nitrogen, while the weak one is probably due to oxidation of the amine groups from 3-APS. The oxidation occurred when the sample was heated in air.

4.4. CONCLUSIONS

Solution model studies indicated that 3-APS can cleave polycarbonate chains by aminolysis of the carbonate groups and become chemically attached to the polymer chains. Dispersion IR or XPS analyses also revealed that aminolysis occurs at the surfaces of bis-A PC, CR-39[®] resin and PMMA when in contact with a solution of 3-APS in 2-propanol. The results also showed that under similar condition, CR-39[®] resin is less swellable and the aminolysis at its surface occurs to a lower extent. For that reason, a more concentrated 3-APS solution is required to obtain the same level of aminolysis. In conclusion, treatment of bis-A PC or CR-39[®] with 3-

APS primer allows formation of a thin 3-APS gel layer, which facilitate the covalent bonding of a later alkoxy silane containing sol-gel coating to the modified polycarbonate substrate.

CHAPTER 5. NMR STUDIES OF SOL-GEL COATING MATERIALS BASED ON TRIETHOXYSILYLATED DIETHYLENETRIAMINE AND TETRAMETHOXYSILANE

5.1. INTRODUCTION

The sol-gel process is a well-known ceramic preparation method that involves hydrolysis and condensation of one or more metal or semi-metal alkoxides, halides, and nitrates. During the past few years, abrasion resistant coatings have been developed by the sol-gel process of trialkoxysilylated organic compounds and tetraalkoxysilanes to protect optical plastic substrates such as bisphenol-A polycarbonate, CR39 and PMMA^{11-17,150,151,155-161}. Among them, the most extensively studied coatings were based on f-DETA—the reaction product of diethylenetriamine (DETA) with 3-isocyanatopropyltriethoxysilane (3-ICPTES) and its binary systems with tetraalkoxysilanes and metal alkoxides.

To prepare abrasion resistant coatings for those polymeric substrates, f-DETA was often hydrolyzed and condensed along with tetramethoxysilane (TMOS) and the sol-gel process was typically carried out at pH 0-2 using a hydrochloric acid catalyst or at pH 4-5 using an acetic acid catalyst. Experiments indicated that with the same composition of f-DETA and TMOS, sol-gel reactions at these two pH levels often led to different gel structures and morphologies ([Chapter 6](#)). In this research, ²⁹Si NMR spectroscopy is used to study sol-gel reactions of the f-DETA /TMOS system and to compare the condensation rates of RSi(OEt)₃ and Si(OMe)₄ at these two different pH levels. As the f-DETA/TMOS system often gelled within 10 min. at pH 0-2, it was difficult to acquire a high resolution ²⁹Si NMR spectrum before gelation occurred. For NMR studies at this pH level, [N-(3-triethoxysilyl)-propyl-N'-N'-diethyl]urea (UREA) was introduced as a model compound for f-DETA. However, directly monitoring of the sol-gel process at pH 4-5 for the f-DETA/ TMOS system was quite successful because the gelation time at this pH was

typically 8-10 hrs. A 3-methacryloxypropyltriethoxysilane (3-MPTMS) /TMOS system was also studied to determine whether the observed pH-dependence of RSi(OEt)_3 and Si(OMe)_4 is related to the urea groups in f-DETA and UREA.

The other two issues to be addressed include the hydrolytical stability of the urea groups during the sol-gel process and the completeness of sol-gel reactions after thermal curing. In the presence of an acid or base catalyst, the urea linkages in f-DETA may undergo hydrolysis, leading to form dangling alkyl groups. In addition, sol-gel reactions are often incomplete even after curing at moderately high temperature ($\sim 300^\circ\text{C}$), so some alkoxy groups may remain in the cured gel. Both the hydrolysis of urea and the presence of residual alkoxy groups can lower the density of crosslinks, thus reducing the hardness and abrasion resistance of the gel. Therefore, ^{13}C and ^{29}Si solid state NMR spectroscopies have been utilized to estimate the concentrations of residual alkoxy groups, the extent of the urea hydrolysis, and the condensation extents of T and Q in the cured f-DETA/TMOS gels. The determination of these factors will be useful in establishing and understanding the structure-property relationships for the f-DETA/TMOS gels and related systems.

5.2. EXPERIMENTAL

5.2.1. Chemicals and Coating Preparations

Diethylenetriamine (DETA, 98%), tetramethoxysilane (TMOS, 99+%), and 3-isocyanatopropyltriethoxysilane (3-ICPTES, 95%), diethylamine (DEA, 98%) were purchased from the Aldrich Chemical Company and used without further purification. 3-methacryloxypropyltriethoxysilane (3-MPTES) was purchased from Gelest Inc. F-DETA was prepared by slowly adding 3-ICPTES into a solution of DETA (molar ratio of 3-ICPTES: DETA=3.15) in 2-propanol (or ethanol)¹⁴. The f-DETA prepared by this method was a 70 wt% solution in 2-

propanol (or ethanol). UREA was prepared similarly by slowly adding 3-ICPTES into a solution of diethylamine (molar ratio of 3-ICPTES : DEA=1.05) in 2-propanol.

NMR samples were formulated using f-DETA (or UREA, or 3-MPTES), TMOS, water, 2-propanol (or ethanol), and an acid catalyst. The acid catalyst was hydrochloric acid (HCL), phosphoric acid (HPO) or acetic acid (HAC). Since the sol-gel reactions are generally considered to undergo specific acid catalysis or specific base catalysis^{28,162}, the sol-gel reactions should be nearly independent of the counterions of the acid catalyst. Therefore, the acidity of the NMR sample was adjusted to pH 0-2 and pH 4-5 using a hydrochloric acid and an acetic acid catalyst, respectively. A pH glass electrode was used to estimate the pH.

To prepare samples for solid state NMR experiments, the f-DETA/TMOS recipes were hydrolyzed and the resulting sols were poured into glass dishes, dried at room temperature in a ventilation hood, and cured for 4 hrs. at either 125°C, 130°C or 170°C. The hydrolysis time was generally ca. 5 min. for a hydrochloric acid catalyst, ca. 30-45 min. for a phosphoric acid catalyst, and 5-6 hrs. for an acetic acid catalyst. The cured gels were ground into fine particles before being loaded for NMR experiments.

The nomenclature of a NMR sample (either a sol or a gel) is based on the components and their concentrations in the sample formula. The concentrations of the four major components, including f-DETA (or UREA, or 3-MPTES), TMOS, water and the alcohol solvent, are given as weight percentages with regard to the combined weight of the four major components. Whereas the concentration of the catalyst is given as millimoles per kilogram of the recipe excluding the catalyst. In the nomenclature, the catalyst component is separated from the major components by a dash, and the concentration of the alcohol solvent is often not explicitly indicated. The equivalent ratio of water to alkoxy silane (r) is sometimes stated to reflect the relative amounts of water and alkoxy silane groups. In the f-DETA/TMOS system, water has two hydroxy groups available; f-DETA and TMOS contain nine and four alkoxy silane groups, respectively.

5.2.2. Characterization

Sol-gel reactions of the UREA/TMOS system, 3-MPTES/TMOS system, and f-DETA/TMOS system were studied by solution ^{29}Si NMR spectroscopy using a Varian 400 MHz NMR spectrometer. A small amount of chromium acetylacetonate (0.01 M) was added to the reaction mixture to lower the spin-lattice relaxation time, and the temperature was controlled to 21-22°C during these reactions.

CPMAS ^{13}C and ^{29}Si solid state NMR spectra were acquired using a Bruker MSL 300 MHz instrument with a 7-mm zirconia NMR rotor. The spin rate was 5 kHz for ^{13}C NMR and 3 kHz for ^{29}Si NMR. The ^{13}C NMR spectra were acquired using a proton 90-degree pulse and a relaxation delay of 6 seconds. The same pulse was also used for the ^{29}Si NMR experiments, however, the relaxation time was changed to 10 seconds. For both ^{13}C NMR and ^{29}Si NMR, 500 acquisitions were used for each spectrum.

Quantitative analysis of a sample by CPMAS experiments requires spectra to be acquired at a series of contact times. The contact time series for ^{13}C CPMAS NMR was {0.2, 0.5, 1, 2, 3, 5, 10, 20 ms}; while for ^{29}Si CPMAS NMR, it was {0.5, 1, 2, 3, 4, 8, 16, 32 ms}. Each spectrum was obtained using 500 acquisitions. Peaks in both ^{13}C and ^{29}Si solid state NMR spectra for the f-DETA/TMOS samples were usually relatively wide and they often overlapped each other. The LINEFIT routine in "NUTS", an offline NMR processing program from ACORNNMR Inc., was used to deconvolute overlapped peaks, so the signal intensity for each species could be obtained. By CPMAS experiments, the observed intensity depends on the proton spin-lattice relaxation time in the rotating frame ($T_{1\rho}(\text{H})$), the spin-lattice relaxation time of the observed nucleus in the rotating frame ($T_{1\rho}(\text{C})$ or $T_{1\rho}(\text{Si})$), and the transfer rate of polarization from proton to the observed nucleus ($T_{\text{C-H}}$ or $T_{\text{Si-H}}$). Assuming the system has an infinite proton reservoir, and $T_{1\rho}(\text{H}) \gg T_{1\rho}(\text{C})$ or $T_{1\rho}(\text{Si}) \gg T_{\text{C-H}}$ or $T_{\text{Si-H}}$, the relationship between the magnetization of the observed nucleus $M(t_{\text{cp}})$ and the cross polarization time (t_{cp}) or contact time, using ^{13}C as an example, can be simplified into the following biexponential equation¹⁸².

$$M(t_{cp}) = \frac{M_0}{1 - \frac{T_{C-H}}{T_{1\rho}(H)}} \left[\exp\left(-\frac{t_{cp}}{T_{1\rho}(H)}\right) - \exp\left(-\frac{t_{cp}}{T_{C-H}}\right) \right] \quad \text{Eqn. 5.1}$$

$$\text{For large rf fields, } M_0 = \frac{\nu_H}{\nu_C} M_0^C \quad \text{Eqn. 5.2}$$

M_0^C is the ordinary carbon thermal magnetization under a static magnetic field. By fitting the experimental values of $I(t_{cp})$ to $M(t_{cp})$ and contact time to t_{cp} in Eqn. 5.1, I_0 (corresponding to M_0^C), $T_{1\rho}(H)$, and T_{C-H} can be obtained. The relative concentration of silicon species in a f-DETA/ TMOS gel could be obtained by normalizing I_0 for existing silicon species. The curve fitting was carried out until the results had reached a 95% confidence level using a Levenberg-Marquardt (LM) algorithm in Origin program version 4.1 from Microcal Software, Inc.

Single-pulse Fourier transformed ^{29}Si MAS NMR spectroscopy was carried out using a Bruker MSL 300 MHz spectrometer with a 7 mm zirconia NMR rotor, a pulse angle of 80° , and a relaxation delay of 212 ms. The relaxation delay was chosen according to the spin-lattice relaxation time of Q^4 reported by Glasser et al.¹⁸³.

5.3. RESULTS AND DISCUSSIONS

Alkyltriethoxysilanes and tetraalkoxysilanes, respectively, have three and four Si-OR groups, which can undergo hydrolysis and condensation and yield many monomeric and polymeric species. In these species, a silicon atom may have alkyl, alkoxy, hydroxy and silyloxy (silicon-oxygen-silicon bridges) substituents, and can be represented by a general formula:



In silicone chemistry and ^{29}Si NMR spectroscopy, symbols M, D, T and Q are often used to represent silicon species with 3-0 alkyl substituents, respectively. The number (z) of silyloxy groups is given as a superscript at the right corner of the symbol letter (Engelhardt notation¹⁹). For example, Q^z and T^z represent any silicon atoms described by the general formulae

$\text{Si}(\text{OR})_x(\text{OH})_y(\text{OSi})_z$ ($x+y+z=4$) and $\text{SiR}(\text{OR})_x(\text{OH})_y(\text{OSi})_z$ ($x+y+z=3$), respectively. This dissertation will use the abbreviation $\text{Q}^z(x,y)$ or $\text{T}^z(x,y)$ to represent a silicon atom whenever all of its substituents are known, otherwise the Engelhardt notation such as T^z and Q^z will be used.

In ^{29}Si NMR spectroscopy, the chemical shifts of T and Q are in the range of -40 to -66 ppm and -74 to -110 ppm, respectively¹⁸³. Generally, replacing an alkoxy group by a silyloxy group usually lowers the chemical shift by 8-10 ppm; while replacing an alkoxy group by a hydroxy group increases the chemical shift by ca. 2 ppm. With the same substituents, silicon atoms in cyclic or polyhedral compounds have relatively higher chemical shifts than in unstrained chains or clusters. The chemical shift of silicon also depends on the substituents of its neighbors, so hetero-condensation between T and Q in T/Q binary system can also lead to extra peaks. A large number of silicon species has been detected and identified by high-resolution solution NMR spectroscopy during the sol-gel process of tetramethoxysilane and tetraethoxysilane^{19,63,184,185}. Solid state NMR spectroscopy has lower resolution, but is sufficient to identify silicon species with different numbers of silyloxy substituents. By calculating relative signal intensities for T^z ($0 \leq z \leq 3$) and Q^z ($0 \leq z \leq 4$), the extent of condensation of T and Q can be obtained.

The sol-gel reactions, including hydrolysis of alkoxysilane, water-forming condensation and alcohol-forming condensation, can be catalyzed by both acid and base catalysts. In aqueous systems, the catalysis can be regarded as specific acid catalysis or specific base catalysis^{28,162}. Therefore, the reaction rate depends mainly on the pH of the medium. At the pH corresponding to the transition of the predominant reaction mechanism from acid-catalysis to base-catalysis, the overall reaction rate reaches a minimum. For tetraalkoxysilanes, the minimum hydrolysis rate and the minimum condensation rate occur at ca. pH 7 and at ca. pH 2, respectively. Compared with the tetraalkoxysilane, the alkyltrialkoxysilane has a relatively strong electron-donating alkyl group, so it is expected to be more reactive towards the acid catalyzed reactions, but less reactive towards the base catalyzed reactions. Consequently, its minimum hydrolysis and condensation reaction rates should occur at slightly higher pH values than 7.0 and 2.0, respectively.

Inductive effects in sol-gel reactions of organic modified silanes has been observed in a number of experiments. Schmidt et al.³² have studied the hydrolysis of a series of alkoxysilanes.

They found that in the presence of 1×10^{-3} M hydrochloric acid, the reactivity order of hydrolysis was $\text{Si}(\text{OEt})_4 < \text{TMOS} < \text{MeSi}(\text{OEt})_3 < \text{Me}_2\text{Si}(\text{OEt})_2 < \text{Me}_3\text{SiOEt}$; while in the presence of 2 M ammonia, the reactivity order of hydrolysis was reversed to $\text{Me}_3\text{Si}(\text{OEt}) \sim \text{Me}_2\text{Si}(\text{OEt})_2 < \text{MeSi}(\text{OEt})_3 < \text{Si}(\text{OEt})_4$. Pkarakar et al.³⁶ have studied the condensation of ethylsilanetriol and orthosilicic acid generated by hydrolysis of ethyltriethoxysilane and tetraethoxysilane. Their results suggested that at pH 1.7 and 2.2 the homo-condensation of T was greater than the hetero-condensation between the T silanol and Q silanol, which was in turn greater than the homo-condensation of the Q silanol. Pohl et al.²⁸ have investigated the dimerization of 3-glycidoxypropylsilanetriol at different pH levels. They discovered that the minimum dimerization rate occurred at pH 4.5 rather than ca. pH 2 for silica gel.

Sol-gel reaction rates are also subject to the steric effect of the substituents. In binary systems consisting of T and Q compounds, the alkyl group of the T compound is often a large group and hence sol-gel reaction rates of T may be reduced. In addition, hetero-condensation between T and Q can also further complicate the situation. Therefore, ^{29}Si NMR spectroscopy is used to compare the condensation reactivities of T and Q at pH 0-2 and pH 4-5 in the UREA/TMOS system, 3-MPTES/TMOS system, and f-DETA/TMOS system.

5.3.1. Solution ^{29}Si NMR Analyses

Solution ^{29}Si NMR spectroscopy was used to compare the condensation rates of T and Q at pH 0-2 and pH 4-4.5 for the sol-gel process of systems UREA/TMOS and 3-MPTES/TMOS and to follow the sol-gel process of f-DETA/TMOS coating recipes.

Table 5.1 lists the composition and pH for six samples, along with the reaction times during which NMR spectra were acquired. The reaction time for spectrum acquisition was selected according to the reaction rate of the sample. For samples A and C (acetic acid catalyst), NMR spectra were acquired during the reaction period of 180-210 min., while for samples C and D (hydrochloric acid catalyst), it was acquired during the reaction period of 5-45 min. Sample E served as a model system for recipe f-DETA31TMOS31W5-HCL27 since the real coating recipe had a very short gelation at this pH. For samples E and F, spectra were acquired during the

specified five different periods in Table 5.1. Since the concentration of the observed nucleus changes with reaction time, the observed signal intensity should correspond to the average concentration within the acquisition period. Based on the average concentration during different acquisition periods, the concentration changes of the starting material and major intermediates with reaction time were roughly established.

Table 5.1. Compositions of samples, their pH values and reaction times during which NMR spectra were acquired.

Test #	Sample Name	pH	Reaction times For NMR Experiments (min.)
A	3-MPTES25TMOS25W18-HAC150	~4	180-210
B	3-MPTES31TMOS31W5-HCL27	~0.5	5-45
C	UREA25TMOS25W18-HAC150	~4	180-210
D	UREA31TMOS31W5-HCL27	~0.5	5-45
E	UREA22TMOS22W31-HCL20	~1	5-20, 20-40, 80-100, 140-160
F	f-DETA22TMOS22W31-HAC140	~4.2	30-60, 120-150, 210-240, 300-330

Figure 5.1 shows the stack-plotted NMR spectra for samples A-D in Table 5.1. Samples B and D were formulated using a strong acid (hydrochloric acid). Although both samples had a deficient amount of water, they quickly ran out of monomeric species of T and Q as the reaction started. With a weak acid (acetic acid) catalyst, samples A and C hydrolyzed at a much slower rate, so the reaction was carried out under a water-abundant condition. During the reaction, samples A and C maintained significant amounts of monomeric T and Q, whose structures were identified according to their chemical shifts. No calculations were made to determine the concentration of each T^z or Q^z . However, it is apparent that at pH ~0.5 with the hydrochloric acid catalyst, T and Q species in both the UREA/TMOS and 3-MPTES/TMOS systems had been mostly hydrolyzed and condensed to T^1 and T^2 , Q^1 , Q^2 , and Q^3 after 45 min. of reaction. According to the spectra, T condensed as fast as or even faster than Q at pH~0.5 with the hydrochloric acid catalyst. At pH 4-5 with an acetic acid catalyst, the hydrolysis of both T and Q species was apparently slower. Nevertheless, after 210 min. of reaction, the hydrolyzed Q had converted from Q^0 to Q^1 , Q^2 , Q^3 and even Q^4 . In contrast, although significant amounts of T had hydrolyzed to $T^0(0,3)$ (silanetriol), only a small fraction of them had condensed to T^1 , so the

condensation of T at this pH was much slower than that of Q. The major difference between the UREA system and the 3-MPTES system was that under the water-abundant condition, the latter existed as a biphasic system at the beginning. As hydrolysis proceeded, the organic-rich phase decreased in volume but it never completely disappeared. Precipitation of silica was observed after hydrolyzing for about 2 hrs.

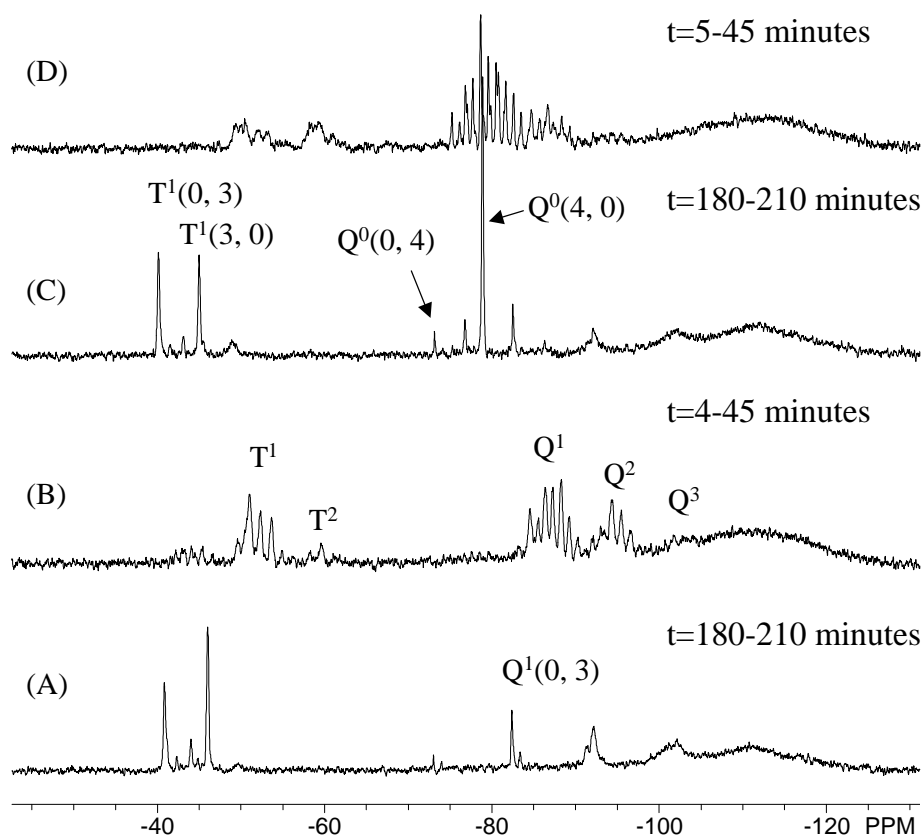


Fig. 5.1. ^{29}Si NMR spectra acquired at the specified hydrolysis time for 3-MPTES25 TMOS25W18-HAC150 (Sample A), 3-MPTES31TMOS31W5-HCL27 (Sample B), UREA25TMOS25W18-HAC150 (Sample C) and UREA31TMOS31W5-HCL27 (Sample D).

The sol-gel process of samples E and F (Table 5.1) was followed by ^{29}Si NMR spectroscopy. Figure 5.2 shows the concentration changes of major T^z and Q^z with reaction time for sample E. During this reaction, the hydrolysis of T finished shortly after the catalyst and

water were added, and the resulting hydrolysates quickly condensed to T^1 (ca. 73%) and T^2 (ca. 27%) in 10 min. Note the concentration of T^z or Q^z in this chapter is the mole fraction with respect to the total moles of T or Q. Further reaction led to an exponential decay in the concentration of T^1 ($t_{1/2} \sim 150$ min.) and a gradual increase in the concentration of T^2 .

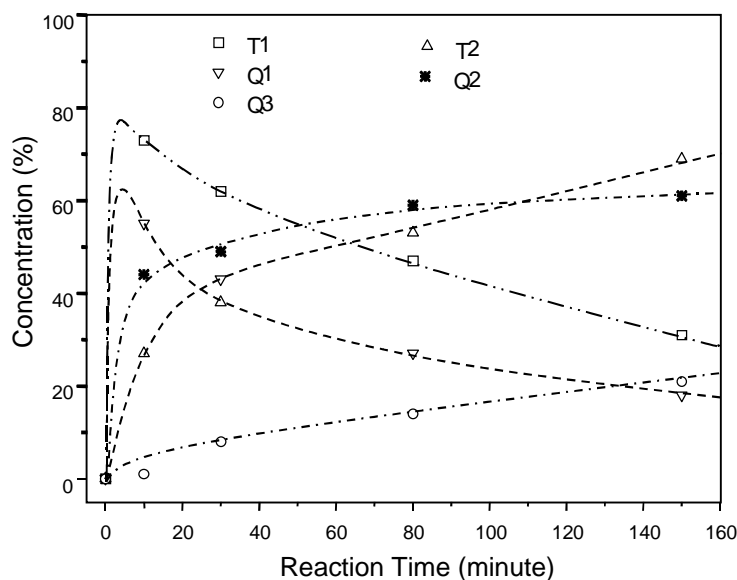


Fig. 5.2. Concentration changes of major T^z and Q^z during sol-gel reactions of UREA22 TMOS22W31-HCL140 (Sample E).

Although a very small amount of TMOS was observed in the spectrum acquired during the initial 20 min. of hydrolysis, the hydrolysis and condensation of TMOS were also very fast. After 10 min. of reaction, the mixture included about 55% of Q^1 , 42% of Q^2 and 2% of Q^3 . Later, the concentrations of Q^2 and Q^3 gradually increased as the concentration of Q^1 decreased exponentially ($t_{1/2} \sim 60-80$ min.). After 150 min. of reaction, T included about 30% T^1 , 63% of T^2 , and a trace amount of T^3 , while Q included 30% of Q^1 , 58% of Q^2 and 21% Q^3 . Since only a small amount of T^3 and Q^3 was formed in the system, gelation did not occur during the NMR experiment. Assuming silanol/alkoxysilane groups are equally reactive and closed-loop condensation does not occur, the critical extents of reaction (p_c) for UREA ($f=3$) and f-DETA ($f=9$), according to Flory and Stockmayer theory, are 67% and 22%, respectively. The equal reactivity approximation does not work well in a sol-gel process, especially in the later sol-gel

process, owing to inductive effects and steric effects. In addition, the sol-gel process involves extensive closed-loop condensation, which makes the Flory and Stockmayer theory inapplicable. However, the gelation time of the f-DETA sample was indeed much shorter than that of the UREA sample. At pH 0-2, the f-DETA sample gelled within 20 min. The gelation time of the UREA was not measured, but it was clearly over 24 hrs.

Figure 5.3 shows the concentration changes of major silicon species of T and Q during the sol-gel reactions of sample F (Table 5.1). One distinct difference between sample E and sample F is that the former ran out of monomeric species rapidly while the latter maintained a significant amount of monomeric species. In sample F, the observed T species included $T^0(3, 0)$ ($-\text{Si}(\text{OEt})_3$), $T^0(2, 1)$, $T^0(1, 2)$, $T^0(0, 3)$ ($-\text{Si}(\text{OH})_3$) and $T^1(0,2)$; while the observed Q species included $Q^0(4, 0)$ (TMOS), $Q^0(3, 1)$, $Q^0(2, 2)$, $Q^0(1, 3)$, $Q^0(0, 4)$ (orthosilicic acid), $Q^1(0,2)$, and $Q^2(0,2)$. These silicon species were identified according to the literature^{186,187}. After 6 hrs. of reaction, the concentration of $T^0(3, 0)$ gradually decreased to ca. 30 %, while the concentration of $T^0(0, 3)$, the major hydrolysis product of T, gradually increased to over 35 %. Only a trace amount of $T^1(0, 2)$ was found after six hours of reaction. Therefore, at pH 4-5, the condensation of T was much slower than the hydrolysis of triethoxysilyl groups. In case of Q, the concentration of TMOS decreased exponentially to about 6 % of the total amount of Q over the 6 hrs. of reaction ($t_{1/2} \sim 85$ min.). The concentration of $Q^0(3, 1)$ and $Q^0(0, 4)$ gradually increased to a maximum of ca. 10 % after 50 min. of reaction, and then decayed in an exponential way over the next 5 hrs. to about 2.5 % ($t_{1/2} \sim 170$ min.). The absence of alkoxy-containing Q^1 and the presence of a high $Q^0(0, 4)$ concentration at the early stage of reaction suggested that the hydrolysis rate of TMOS was significantly faster than the subsequent silanol/alkoxysilane condensation.

The concentration of $Q^1(0, 3)$ reached a maximum concentration of ca. 15% after 150 min. of hydrolysis and condensation, about 100 min. behind the maximum concentration of $Q^0(0, 4)$ and $Q^0(3, 1)$. The concentration of $Q^1(0, 3)$ decreased slowly to ca. 10% after another 150 min. of reaction. During the six hours of reaction, the hydrolyzed Q did not accumulate as $Q^0(0, 4)$ as in the case of T, which accumulated as $T^0(0,3)$, instead they quickly condensed to Q^1 , Q^2 , Q^3 and even Q^4 . In sample E, although the formation of Q^1 and Q^2 occurred very quickly, the concentration of Q^3 was rather low and Q^4 could only barely be seen. The concentration of Q^2 ,

Q^3 and Q^4 could not be estimated directly from their peak areas owing to peak widening, incomplete spin-lattice relaxation of silicon atoms in the colloidal particles, or interference of Q^4 from the glass NMR tube (generally a broad peak from -105 ppm to -115 ppm). However, by subtracting the concentration of Q^0 and Q^1 from the total amount of TMOS in the recipe, the sum of the concentration of these three derivatives was found to be over 70%. Therefore, the overall condensation rate of Q was much higher than that of T.

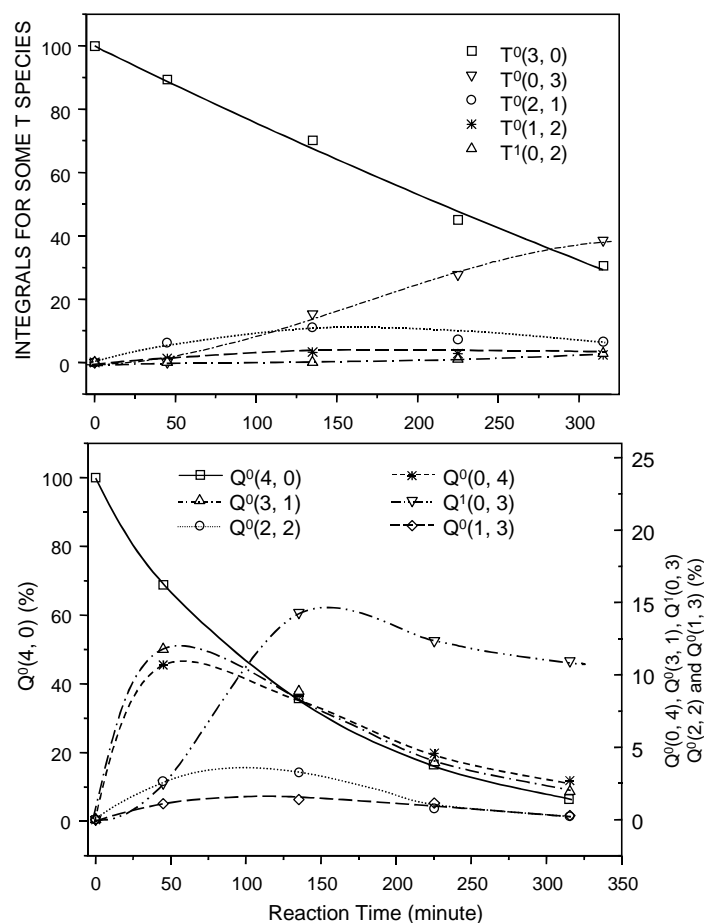


Fig. 5.3. Concentration changes of major T and Q during sol-gel reactions of f-DETA22TOS22W31-HAC140 (Sample F).

In general, the condensation of T and Q at pH 0-2 occurs mainly by the acid-catalyzed mechanism, and T is expected to be more reactive than Q due to inductive effects. Although for f-DETA and 3-MPTES, the condensation rate may be reduced by the steric hindrance of the

bulky alkyl group in these two compounds. However, at pH 0-2, the condensation rate of T was still close to that of Q in reality. As pH increased to about 4-5, the rate of the acid-catalyzed condensation is expected to drop for both T and Q, while the rate of the corresponding base-catalyzed condensation should increase. In fact, the condensation of Q was predominately base catalyzed at pH 4-5 and the overall condensation rate at this pH was much faster than at pH 0-2. In contrast, the base-catalyzed condensation of T at pH 4-5 still remained unimportant although the acid catalyzed condensation rate dropped considerably. Therefore, the overall condensation rate of T at this pH was lower than at pH 0-2.

5.3.2. Solid State ^{13}C NMR Analyses

The f-DETA/TMOS coating recipe includes two alkoxy silane groups: methoxysilane and ethoxysilane. However, since f-DETA was typically prepared and stored in 2-propanol solvent, 2-propoxysilane groups might be formed slowly by transesterification of the ethoxysilane groups with the 2-propanol solvent. In addition, if the sol-gel reaction was carried out in a 2-propanol-containing solvent, these groups might also be formed by transesterification of methoxysilane/ethoxysilane groups and reesterification of silanol groups. Owing to the incompleteness of sol-gel reactions, the cured gel might include small amounts of methoxy (-OMe), ethoxy (-OEt) and 2-propoxy (-OⁱPr) residual groups.

To estimate the concentrations of residual alkoxy silane groups and the extent of urea hydrolysis, the starting material f-DETA was first analyzed. [Figure 5.4](#) shows the ^{13}C NMR spectrum of a newly prepared f-DETA solution in 2-propanol and deuterated chloroform. Peaks in the spectra are assigned to the corresponding carbon atoms in the attached structure. According to quantitative calculation, the total amount of urea groups in the f-DETA raw material was typically about 95% of the total amount of the triethoxysilyl groups. Due to the impurities and the extra amount of 3-ICPTES used to prepare the f-DETA, this ratio was usually less than 100%.

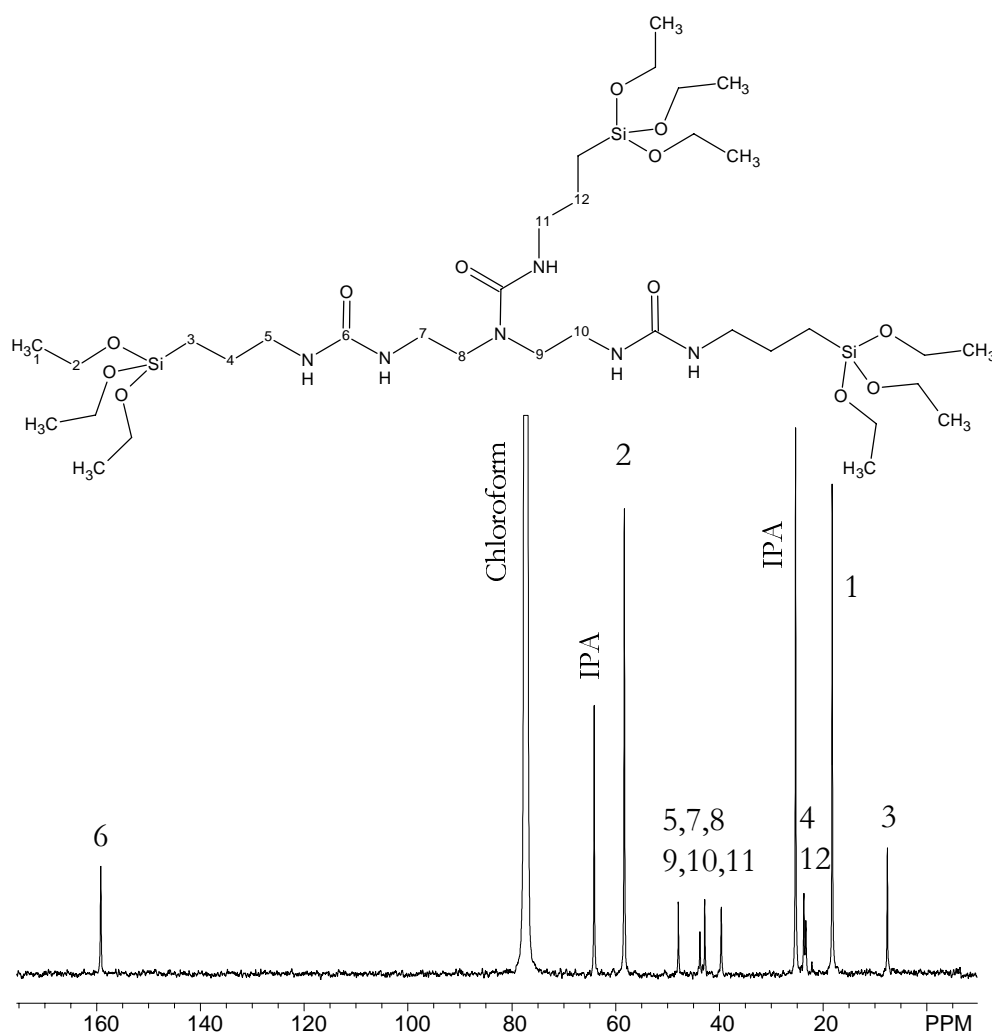


Fig. 5.4. The ^{13}C NMR spectrum for a f-DETA solution in 2-propanol. Peaks are labeled to the related atoms in the attached structure.

The concentration of alkoxy residual groups and the extent of urea hydrolysis were estimated for three gels derived from two typical coating recipes: (1) f-DETA22TMOS22W31-HAC140 and (2) f-DETA31TMOS31W5-HCL27. Two gels, one from each recipe, were derived using a f-DETA that had been stored in 2-propanol for 3-4 weeks (f-DETA^A), and a third gel was derived from the first recipe using a freshly prepared f-DETA (f-DETA^B). All the gels were cured at 125°C for 4 hrs. The three samples will be referred to in the text as HCL27^A, HAC27^A

and HCL140^B, but their full name will be used in graphs and tables. The letters A and B indicated that f-DETA^A and f-DETA^B were used in the recipe, respectively. The ¹³C CPMAS NMR spectra for these three samples (contact time=1 ms) are stack-plotted in Fig. 5.5.

Generally, methoxysilane groups have a peak at ca. 51 ppm, ethoxysilane groups have peaks at ca. 59 ppm (Si-OCH₂CH₃) and ca. 18 ppm (Si-OCH₂CH₃), and 2-propoxysilane groups have peaks at ca. 63 ppm (Si-OCH(CH₃)₂) and ca. 23 ppm (Si-OCH(CH₃)₂). According to the spectrum for pure f-DETA (Fig. 5.4) and characteristic chemical shifts for the above alkoxysilane groups, peaks of the NMR spectra in Fig. 5.5 were assigned to the corresponding atoms in the attached structures. Solid state NMR spectroscopy generally has low resolution, and hence many nuclei of similar chemical shifts are not separated in Fig. 5.5. For example, sharp peaks for C5, C7, C8, C9, C10, and C11 in Fig. 5.4 are replaced by a broad peak at 35-45 ppm in the solid state NMR spectra.

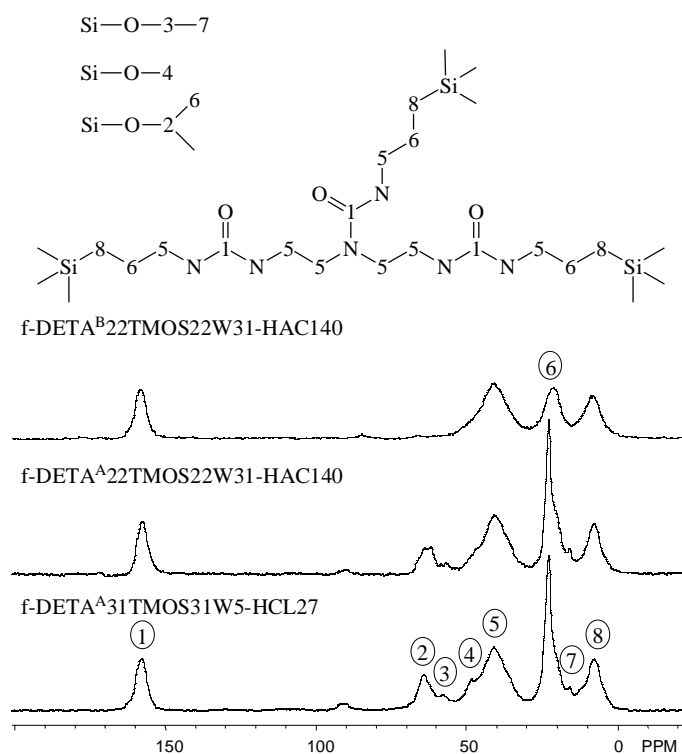


Fig. 5.5. The ¹³C CPMAS NMR spectra (contact time=1 ms) for gels f-DETA^A31TMOS31W5-HCL27 (HCL27^A), f-DETA^A22TMOS22W31-HAC140 (HAC140^A) and f-DETA^B22TMOS22W31-HAC140 (HAC140^B). Peaks are assigned to the related atoms in the attached chemical structures.

According to Fig. 5.5, sample HCL27^A contained all the mentioned alkoxy silane groups and among them the 2-propoxysilyl group was the most abundant. For sample HAC140^A, the -OEt and -OMe groups had quite low concentrations, but the -OⁱPr group still had a relatively large presence. Under the same conditions, but with freshly prepared f-DETA, sample HAC140^B not only had few -OMe and -OEt residual groups but also few -OⁱPr residual groups. By comparing the two gels (fresh f-DETA vs stored f-DETA), *it can be concluded that most Si-OⁱPr groups were formed during the storage of the f-DETA rather than during the sol-gel process.*

For quantitative estimation of the content of the residual alkoxy group and the extent of urea hydrolysis, ¹³C CPMAS spectra were acquired for each sample at a series of contact times and then mathematical treatments described earlier in this chapter were utilized. Figures 5.6 and 5.7 show the stack-plotted CPMAS spectra for the sample HAC140^A and the relationship between integral area of each peak/nucleus and contact time, respectively. However, except peaks 1, 2, and 8, which correspond to a single nucleus (Fig. 5.5), other peaks include contributions from more than one type of nucleus. As an approximation, those overlapped peaks were also fit into Eqn. 5.1 and the corresponding I_0 values were considered to be the roughly the sum of I_0 s for all nuclei. Note this approximation should be only effective if the proton spin-lattice relaxation times ($T_{1\rho}(H)$) and cross-polarization transfer constants (T_{C-H}) for all the nuclei are very similar. Table 5.2 lists the chemical shifts, T_{C-H} s, $T_{1\rho}(H)$ s and I_0 s for the major peaks. Except the carbonyl carbon (peak 1), which has a T_{C-H} of ca. 0.4 ms; other carbon atoms have a value of about 0.1 ms. The $T_{1\rho}(H)$ s, however, are within 4-5 ms for all carbon atoms. Similar results were also obtained for other f-DETA/TMOS samples. Therefore, the application of Eqn 5.1 to overlapped peaks may be a fair approximation.

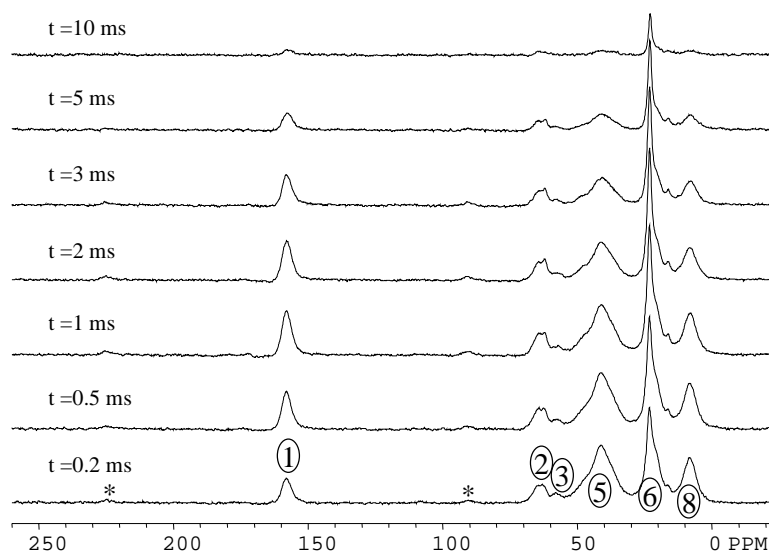


Fig. 5.6. The ^{13}C CPMAS NMR spectra acquired at a series of contact times for gel f-DETA22^ATMOS22W31-HAC140 (HAC140^A). Peak assignments refer to the structure in Fig. 5.5.

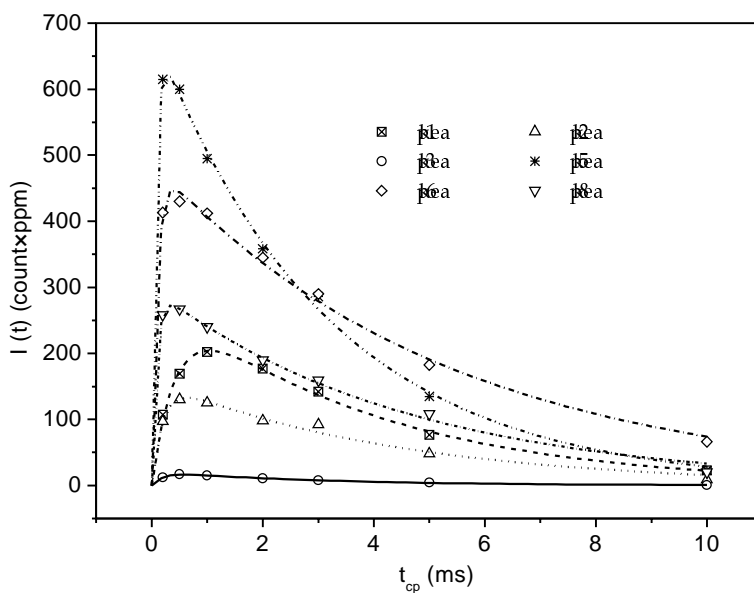


Fig. 5.7. The relationship between the observed NMR signal $I(t)$ and contact time for gel f-DETA22^ATMOS22W31-HAC140 (HAC140^A). Peak numbers refer to the structure in Fig. 5.6.

Table 5.2. Chemical shifts, cross polarization transfer constants, proton spin-lattice relaxation constants and absolute peak intensities of carbon signals in gel f-DETA^{A22} TMOS22W31-HAC140 (HAC140^A)

Peak #	Chemical Shift (ppm)	T _{1ρ} (H) (ms)	T _{C-H} (ms)	I ₀ (count×ppm)
1	159	3.85 ± 0.28	0.41 ± 0.03	267 ± 11
2	63	4.99 ± 1.14	0.11 ± 0.05	154 ± 8
3	58	2.9 ± 0.5	0.2 ± 0.01	20 ± 0.5
5	42-47	5.29 ± 0.30	0.09 ± 0.01	697 ± 18
6	24	5.3 ± 0.3	0.10 ± 0.01	482 ± 11
8	9	4.5 ± 0.3	0.09 ± 0.01	294 ± 7.7

The concentration of the residual 2-propoxy group (R_{O^iPr}) and the extent of urea hydrolysis (R_{urea}) were estimated using Eqns. 5.3 and 5.4. R_{O^iPr} is the mole ratio of the residual -OⁱPr group to the total amount of the Si-OEt group in the recipe, and R_{urea} is the mole ratio of the hydrolyzed urea group to the total amount of -Si(OEt)₃ units in the recipe

$$R_{O^iPr} = \frac{I_6 - I_8}{6I_8} \times 100\% \quad \text{Eqn. 5.3}$$

$$R_{urea} = \frac{I_8 - I_1}{I_8} \times 100\% \quad \text{Eqn. 5.4}$$

where I_1 , I_6 and I_8 are the I_0 values for peaks 1, 6, and 8, respectively. Peak 6 includes contributions from the methylene groups (C6) in f-DETA and the methyl groups (C6) in Si-OⁱPr groups. Because of this, Eqn 5.3 could only give a very rough estimation of the content of the residual 2-propoxysilane group. Principally, the concentration of alkoxy residual groups could also be estimated according to the integral areas for the carbon atom ($\delta \sim 58$ -63 ppm) directly linked to the oxygen atom. However, due to the low concentration of the residual alcoxysilane group, the area of this peak sometimes could not be reliably calculated, especially when the concentration of the -OⁱPr group was low. Therefore, this peak was not utilized in quantitative treatment.

Table 5.3 lists the calculated R_{O^iPr} and R_{urea} for the three f-DETA/TMOS gels mentioned earlier in this section. According to this table, the two gels prepared using f-DETA that had been

stored for 3-4 weeks included about 11-12% 2-propanoxysilyl group; while the gel prepared using freshly prepared f-DETA includes only 2% of this group. These values are apparently in accord with the conclusion obtained by roughly comparing the CPMAS spectra acquired at a contact time of 1 ms. As sample HAC140^B has a low concentration of residual 2-propanoxysilane groups, it may also be concluded that the extent of transesterification of the methoxysilane /ethoxysilane or reesterification of the silanol by 2-propanol was negligible during the sol-gel process. In fact, Peace et al. have indicated that the transesterification usually lags behind the hydrolysis and condensation¹⁸⁸, so sol-gel reactions in the f-DETA/TMOS system could finish before extensive transesterification /reesterification had occurred.

Table 5.3. The ratio of unhydrolyzed Si-OⁱPr and extent of urea hydrolysis for three gels.

#	Recipe	Storage Time of f-DETA (week)	Curing Condition	R _{OⁱPr} (%)	R _{urea} (%)
1	f-DETA ^A 31TMOS31W5-HCL27	3-4	125°/4 hrs.	12	~0
2	f-DETA ^A 22TMOS22W31-HAC140	3-4	125°/4 hrs.	11	4
3	f-DETA ^B 22TMOS22W31-HAC140	<1	125°/4 hrs.	~2	2

The ratio of urea groups to the total amount of -Si(OEt)₃ in the raw f-DETA was accounted.

After considering the ratio of the urea groups to total amount of -Si(OEt)₃ groups in the raw f-DETA, the extent of urea hydrolysis was found to be ~0% for HCL27^A, ~4% for HAC140^A and 2% for HAC140^B. Based on these data, it is concluded that only a negligible amount of urea groups had been hydrolyzed during the sol-gel process.

5.3.3. ²⁹Si Solid State NMR Analyses

²⁹Si CPMAS NMR technology has been used by Betrabet et al. to study the extent of condensation in gels of f-DETA and other triethoxysilylated organic compounds¹⁵⁵. Those gels were developed by hydrolyzing and condensing the related organic modified triethoxysilanes in the presence of a hydrochloric acid catalyst ($r=1$). Their results indicated that f-DETA gel cured at 135°C had a condensation extent of about 64%. This section addresses the influences of pH and water concentration on the extent of condensation of T and Q in cured f-DETA/TMOS gels.

Gels derived from coating recipes f-DETA31TMOS31W5-HCL27 (pH~0.5), f-DETA26TMOS26W19-HPO23 (pH~2), and f-DETA22TMOS22W31-HAC140 (pH~4.2) were investigated by ^{29}Si CPMAS NMR technology. Three gels, one from each coating recipe, were prepared and cured at 130°C for 4 hrs., and a fourth gel was derived from the third recipe and cured at 170°C for 4 hrs. In the following discussion, the four samples will be abbreviated in the text as HCL27, HPO23, and HAC140¹³⁰, and HAC140¹⁷⁰, but their full name will be used in related figures and tables. The superscripts 130 and 170 represent the curing temperature for sample HAC140. Figure 5.8 shows the stack-plotted ^{29}Si CPMAS spectra (contact time=2 ms) for these four gels.

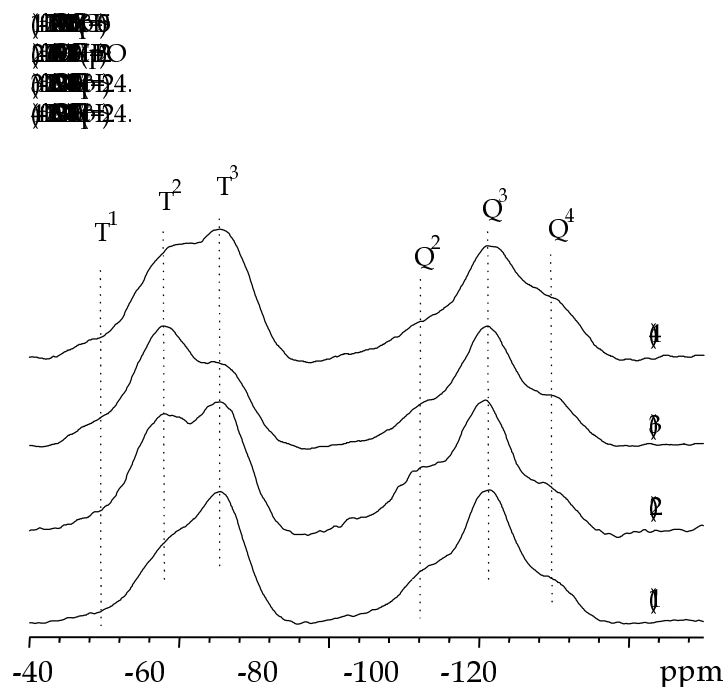


Fig. 5.8. The ^{29}Si CPMAS solid state NMR spectra for several f-DETA/TMOS gels prepared under different conditions.

In these ^{29}Si NMR spectra, T displays a broad peak from -50 to -70 ppm, whereas Q displays a broad peak from -90 to -110 ppm. Both peaks include several overlapping sub-peaks, which correspond to T^0 , T^1 , T^2 and T^3 or Q^0 , Q^1 , Q^2 , Q^3 and Q^4 , respectively. *By a simple comparison, it can be easily concluded that both a lower pH and a high curing temperature*

tended to increase the population of T^3 . However, similar changes in pH and curing temperature seems to have no obvious influence on the distribution of Q. If the relative signal intensities for T and Q are compared, one can find that the T/Q molar ratios (~ 0.8) for these spectra are much lower than the actual T/Q molar ratio in the recipe (1.85). Therefore, Q species in the f-DETA/TMOS gel, especially Q^4 , which has few proton neighbors, were not fully polarized under the applied CPMAS conditions.

Quantitative ^{29}Si CPMAS studies were carried out for the four f-DETA/TMOS samples. Figure 5.9 shows the peak intensity at different contact times and the simulated curves for samples HCL27 and HAC140¹³⁰, respectively. While most silicon species show an apparent decay in peak intensities within contact time from 4 ms to 16 ms, the Q^4 signal, especially in sample HAC140¹³⁰, does not decay until the contact time is longer than 8 ms, indicating an especially large cross polarization constant for the species. In general, the silicon species in sample HAC140¹³⁰, including Q^4 , reach their maximum polarization at a longer contact time than in sample HCL27 due to the lower proton concentration in the former gel. HAC140¹³⁰ and HCL27 gels were developed from a water-abundant condition and a water-sufficient condition, respectively, hence more proton-containing alkoxy groups were eliminated in sample HAC140¹³⁰ by either hydrolysis or alcohol-forming condensation.

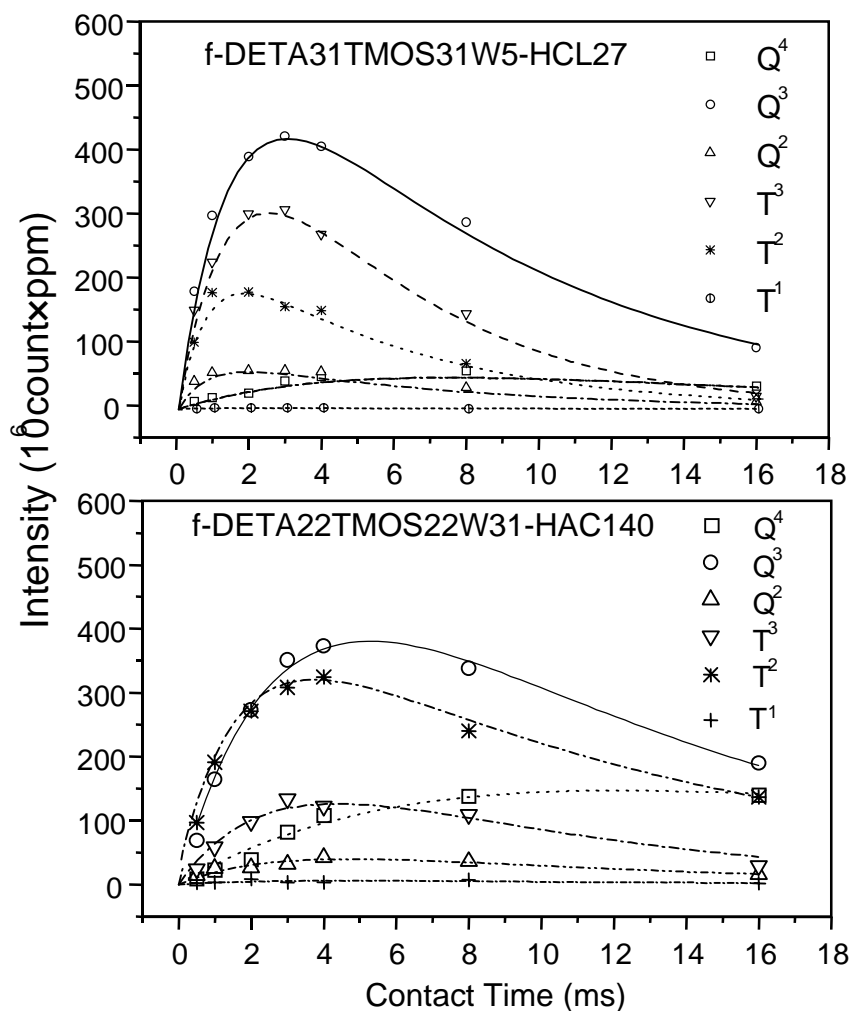


Fig. 5.9. Intensity of each silicon species as a function of contact time in ²⁹Si CPMAS NMR spectra for gels f-DETA22TMOS22W31-HAC140 and f-DETA31TMOS31W5-HCL27.

During the curve-fitting, the signals of less populated silicon species such as T¹ and Q² were too weak, and hence their peak areas could not be accurately calculated. To obtain a convergent or repeatable estimation for T_{Si-H} , $T_{1\rho}(H)$ for these silicon species was fixed to a value obtained from an abundant silicon species. Q⁴ might have a large presence in the sample, however, due to a large T_{Si-H} , its signal did not show an apparent decay until a contact time of 8-16 ms. To fit the Q⁴ intensity curve, spectra at higher contact times were required. However, with 500 acquisitions, the obtained spectra often had extremely poor S/N ratio if the contact time was greater than 16 ms. For a better S/N ratio, the number of acquisitions should be at least

quadrupled in future NMR experiments, which means a significant increase in experimental time. For this reason, quantitative treatments were not carried out for Q⁴.

Table 5.4 lists the CPMAS NMR simulation parameters for gels HCL27 and HAC140¹³⁰. For the sample HCL27, T_{1ρ}(H) for all silicon species is 5-8 ms, while T_{Si-H} for most silicon species other than Q⁴ is in the range of 0.8-1.4 ms. In case of sample HAC140¹³⁰, T_{1ρ}(H) is around 9-12 ms, and T_{Si-H} for silicon species other than Q⁴ is around 3 ms.

Table 5.4. Curve fitting parameters for ²⁹Si CPMAS NMR spectra of gels f-DETA31 TMOS31W5-HCL27 and of f-DETA22TMOS22W31-HAC140

Silicon Species	Chemical Shift (ppm)	T _{1ρ} (H) (ms)	T _{Si-H} (ms)	I ₀ (count×ppm)
f-DETA31TMOS31W5-HCL27 (cured at 130°C for 4 hrs.)				
T ¹	~48	8*	3.0 ± 2.3	11 ± 2.3
T ²	~58	5.3 ± 1.0	0.81 ± 0.15	253 ± 25
T ³	~65	4.6 ± 0.5	1.5 ± 0.2	525 ± 42
Q ²	~94	6.7 ± 1.0	0.79 ± 0.12	77 ± 6
Q ³	~100	7.9 ± 0.6	1.4 ± 0.1	617 ± 28
f-DETA22TMOS22W31-HAC140 (cured at 130°C for 4 hrs.)0				
T ¹	~48	10*	3.0 ± 2.3	11 ± 2.3
T ²	~58	12 ± 1.4	1.7 ± 0.2	433 ± 27
T ³	~65	10*	2.2 ± 0.4	190 ± 17
Q ²	~94	9.1 ± 5.6	2.7 ± 1.6	67 ± 28
Q ³	~100	10 ± 2.3	3.1 ± 0.7	637 ± 99

* The curve fitting is either non-convergent or not unique, so T_{1ρ}(H) was fixed to an acceptable value according to the rest of the calculations.

Since no quantitative data could be obtained for Q⁴, only the distribution of T was calculated. Table 5.5 lists the recipes, curing conditions, and the relative concentration of each T^z in the four f-DETA/TMOS samples. The first three samples reflect the influences of the water concentration and pH on the extent of condensation of T. As pH increases from 0.5 to 4.2, the extent of condensation in T apparently decreases. In spite of its water deficiency, sample HCL27 still has the highest extent of condensation of T, indicating the predominant influence of pH over the condensation rate. Note sample HCL27 might have absorbed some moisture from air when it was dried at room temperature under ambient conditions. The last two samples (Table 5.4) were

based on the same formulation but cured at different temperatures. As expected, the extent of condensation of T in the gel cured at 170°C was higher than in the gel cured at 130°C.

Table 5.5. The distribution of T in gels f-DETA31TMOS31W5-HCL27, f-DETA26TMOS26W19-HPO23 and f-DETA22TMOS22W31-HAC140.

#	Sample Name	pH/r	Curing Conditions	T ¹ (%)*	T ² (%)*	T ³ (%)*	Ext. of Condens.
1	f-DETA22TMOS31W5-HCL27	~0.5/0.55	130°C 4 hrs.	1 ± 0.3	32 ± 4	67 ± 6	88 ± 13
2	f-DETA26TMOS26W19-HPO23	~2/2.2	130°C 4 hrs.	~0	50 ± 5	50 ± 5	83 ± 12
3	f-DETA22TMOS22W31-HAC140	~4.2/4.4	130°C 4 hrs.	2 ± 0.4	68 ± 5	30 ± 3	76 ± 9
4	f-DETA22TMOS22W31-HAC140	~4.2/4.4	170°C 4 hrs.	2 ± 0.07	39 ± 3	59 ± 5	86 ± 10

* Peak deconvolution routine does not given deviations. The deviations given above are calculated according to the curving fitting considering the error transfer in the calculation.

Samples A-F in Table 5.6 were studied by single-pulse Fourier transformed ²⁹Si MAS NMR experiments to estimate the influences of pH and r on the extent of T and Q. Among these samples, sample E was derived from a solution of f-DETA in ethanol, whereas the other samples were prepared using a newly prepared f-DETA solution in 2-propanol.

The spectra for samples A-F are stack-plotted in Fig. 5.10. The single-pulse NMR experiment usually yields more quantitative results, but requires a much longer experimental time. The integral ratio of Q to T (Q/T) for these spectra was found to be within 1.8-2.1, which was quite close to the actual Q/T ratio (1.85) in the formulae. Therefore, the distribution of both T and Q should be approximately reflected by these spectra. According to spectra A-D, *samples prepared in strong acidic media (pH=0-2.5) had a higher extent of condensation of T than samples prepared in weak acidic media (pH=4.2), however, the latter samples typically had a higher extent of condensation of Q.* The curing temperature for samples A-D was 5°C lower than the samples for CPMAS experiments, however, both experiments yielded similar conclusions about the distribution of T. As expected, raising the curing temperature (spectrum E vs F) and water concentration (spectrum A vs B) led to increases in the extent of condensation for both T and Q. A high similarity between spectrum D and spectrum F in Fig. 5.10 indicates that if f-

DETA is freshly prepared, the transesterification do not lead to obvious decrease in the extent of curing, which is in accord with the ^{13}C CPMAS NMR experiments stated earlier.

Table 5.6. The distribution of Q in f-DETA50TMOS50 gels prepared using different acid catalysts and equivalent ratios of water to alkoxysilane (r).

#	Sample Name	pH ^{III} /r	Solvent	Curing Conditions	Q ² (%)	Q ³ (%)	Q ⁴ (%)	Q/T Ratio
A	f-DETA22TMOS31 W5-HCL27	~0.5/0.5	2-Propanol ^I	125°C 4 hrs.	7	85	8	2.0
B	f-DETA22TMOS22 W31-HCL20	1.7/4.4			3	69	28	1.9
C	f-DETA28TMOS28 W10-HPO24	2/1.1			6	79	16	2.1
D	f-DETA22TMOS22 W31-HAC140	4.2/4.4			2	50	47	1.9
E	f-DETA22TMOS22 W31-HAC140	4.2/4.4	Ethanol ^{II}		2	48	50	1.8
F	f-DETA22TMOS22 W31-HAC140	4.2/4.4	2-Propanol ^I	170°C 4 hrs.	2	32	66	1.8

I. f-DETA was stored in 2-propanol for less than a week

II. f-DETA was stored in ethanol.

III. estimated by pH glass electrode.

The distribution of Q in these samples was calculated according to the peak areas for Q², Q³, Q⁴ (Q⁰ and Q¹ did not appear) and the results are listed in Table 5.6. Although the calculated Q/T ratio was very close to the real value, the distribution of T could not be calculated since the T peaks could not be reliably deconvoluted. According to this table, at the same water concentration (sample B vs D and E), the content of Q increases with the pH. As expected, increasing the curing temperature also causes an increase in the extent of curing for Q (sample D vs F). In conclusion, the single-pulse ^{29}Si NMR experiments supported not only the results of the ^{29}Si CPMAS experiments but also the speculations about the pH-dependence of condensation reactivity of T and Q stated earlier in this chapter.

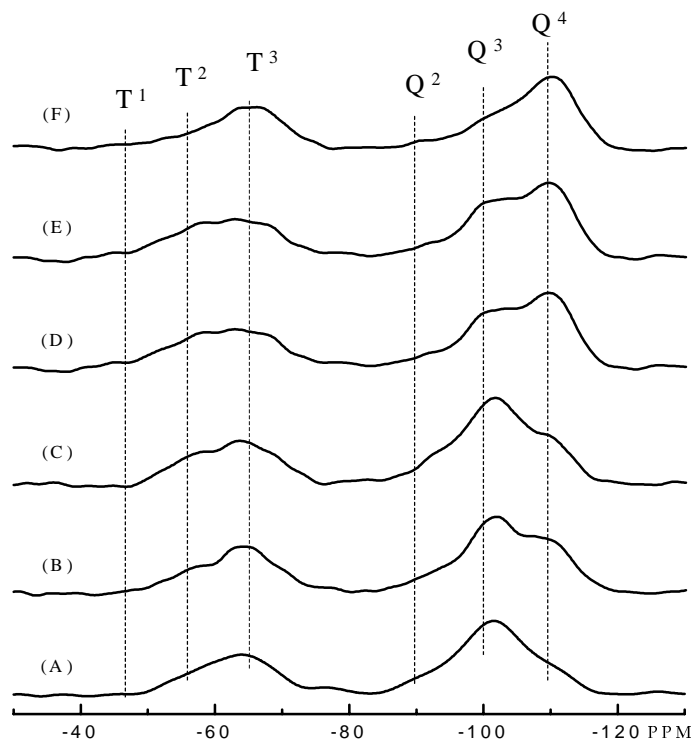


Fig. 5.10. ^{29}Si MAS NMR spectra (Single-Pulse) for f-DETA31TMOS31W5-HCL27 (Sample A), f-DETA22TMOS22W31-HCL20 (Sample B), f-DETA28TMOS28W10-HPO25 (Sample C), f-DETA22TMOS22W31-HAC140 (Sample D), f-DETA22TMOS22W31-HAC140 (Sample E), and f-DETA22TMOS22W31-HAC140 (Sample F).

5.4. CONCLUSIONS

The hydrolysis and condensation of the f-DETA/TMOS system at pH 0-2 and pH 4-5 were studied using ^{29}Si NMR spectroscopy. The results showed triethoxysilane groups (T) in f-DETA condensed as fast as TMOS (Q) at pH 0-2, but lagged far behind the latter at pH 4-5.

Gels derived from various f-DETA/TMOS coating recipes were studied using ^{13}C CPMAS NMR. Generally, $T_{1\rho}(\text{H})$ was found to be about 3-5 ms. $T_{\text{C-H}}$ was around 0.1 ms for most carbon atoms except the carbonyl carbons, whose $T_{\text{C-H}}$ was ca. 0.4 ms. If the gel was

prepared under a water-abundant condition, the contents of residual ethoxy and methoxy groups were rather low. However, these groups could have a relatively large presence if the gel was developed under a water-deficient condition. In cases when the f-DETA was stored in 2-propanol for more than 3-4 weeks, the resulting gel could have a rather high concentration of 2-propoxysilane groups. The 2-propoxysilane groups were mainly formed during storage by transesterification of the ethoxysilane groups with the solvent 2-propanol. These groups are less reactive than methoxysilane and ethoxysilane groups in hydrolysis and condensation reactions and are prone to remain in the final gel. Although the urea groups in f-DETA can be potentially hydrolyzed during the sol-gel reactions, however, experiments indicated that only a very small fraction of these groups was actually hydrolyzed.

^{29}Si solid state NMR spectroscopy was used to estimate the relative compositions of the T^z and Q^z in the cured gels. For the f-DETA/TMOS gels, an increase in the pH in the range of 0-5 increased the extent of condensation of the Q species, but decreased that of the T species. As expected, raising curing temperature and water concentration also led to increases in the extent of condensations for both T and Q.

CHAPTER 6. MORPHOLOGY OF F-DETA/TMOS GELS

6.1. INTRODUCTION

Primary clusters formed during a sol-gel process usually have a highly irregular structure, which is dependent on pH and equivalent ratio (r) of water to metal or semi-metal alkoxide in the system¹⁸. In strong acid media with a small r (ca. 1), silica sols developed from tetraethoxysilane usually consist of extended primary clusters, and may be capable of drawing fibers. Still in acid media but with a high r (ca. 20), sols developed have less extended clusters, and are usually not spinnable. In basic media, sols developed are usually particulate, not spinnable, and tend to form a porous gel¹⁸⁹.

The structure of sol-gel derived clusters can be generally described by mass fractal geometry^{47,92}. The space filling ability of the clusters can be reflected by the mass fractal dimension D_{mass} , which is determined by the power law relationship between the mass (M) of the cluster within any randomly selected region and the radius (R) or a characteristic size of that region:

$$M \propto R^{D_{\text{mass}}} \quad 0 \leq D_{\text{mass}} \leq 3 \quad \text{Eqn. 6.1}$$

according to Eqn. 6.1, extended primary clusters should have a low fractal dimension while condensed clusters should have a high fractal dimension. The fractal dimension of silica primary clusters developed from TEOS in an acid medium usually have a mass fractal dimension of 1.8-2.0, while in a basic medium, the silica primary clusters usually have a mass fractal dimension of 2.8-3.0^{86,190}. Clearly, the mass fractal dimension quantitatively reflects the space filling ability of the silica clusters, i.e. the structural openness of the silica clusters.

The porosity and surface smoothness of a thin film deposited from a sol are related to not only the primary clusters in the sol, but also the subsequent aggregation and drying processes.

According to Brinker et al.^{89,90}, during film formation, the primary clusters in a layer of sol aggregate as solvent evaporates. Subsequently, these aggregated clusters interpenetrate into one another and collapse under the capillary forces exerted during the final stage of drying. The extent of cluster interpenetration depends on the mass fractal dimension of the clusters.

According to Mandelbrot⁹², the mean number of intersections ($M_{1,2}$) for two clusters of radius R and mass fractal dimension of D_{mass} to occupy the same position of three dimensional space is:

$$M_{1,2} \propto R^{2D_{\text{mass}} - 3} \quad \text{Eqn. 6.2}$$

According to Eqn. 6.2, if the clusters have a fractal dimension of less than 1.5, the mean number of intersections between two clusters approaches zero as R indefinitely increases. This means the clusters are mutually “transparent”, and can move through each other freely. On the other hand, if the fractal dimension of the clusters is greater than 1.5, the mean number of intersections increases indefinitely with R . This means the clusters are mutually “opaque”, and overlap of clusters are not possible. In fact, real clusters are finite in size, so clusters should never be completely “transparent” nor completely “opaque”. Based on these analyses, silica sols formed in acidic media usually have a low fractal dimension and are more likely to form smooth and structurally compact films. In contrast, sols formed in basic media usually have a high fractal dimension and are more likely to form rough and porous coatings.

The f-DETA/TMOS sol-gel system is a system consisting of triethoxysilylated diethylenetriamine and tetramethoxysilane, which is essentially a binary system of alkyltriethoxysilane (T) and tetraalkoxysilane (Q). This sol-gel system has been used to develop abrasion resistant coatings for a variety of polymer or metal substrates^{14,159,161}. This chapter provides a general comparison of the pH-dependence of condensation reactivity between T and Q and then discusses the influences of the reactivity order of T and Q on the morphology of the final f-DETA/TMOS gel. Small angle x-ray scattering (SAXS), atomic force microscopy (AFM), and scanning electron microscopy (SEM) are utilized to reveal the influences of pH, r , aging of the gel and evaporation of the solvent on the morphology of the resulting f-DETA/TMOS coatings.

6.2. EXPERIMENTAL

6.2.1. Materials and Surface Treatments

Diethylenetriamine (DETA, 98%), 3-aminopropyltriethoxysilane (3-APS, 99%), tetramethoxysilane (TMOS, 99+%) and 3-isocyanatopropyltriethoxysilane (3-ICPTES, 95%) were purchased from Aldrich Chemical Company and used without further purification. F-DETA was prepared by reaction of DETA with 3-ICPTES (mole ratio 1:3.15) in the solvent 2-propanol or ethanol. The material prepared by this method was a 70 wt% solution in 2-propanol (ⁱPrOH) or ethanol (EtOH).

Coating recipes were formulated using f-DETA, TMOS, water (W), ⁱPrOH or EtOH, and an acid catalyst. The acid catalyst was either hydrochloric acid (HCL) or acetic acid (HAC). The coating recipe is named according to the concentrations of the coating components. The concentration of each major component is given as a weight percentage based on the total weight of the four major components, which include f-DETA, TMOS, water and alcohol solvent. The acid catalyst concentration is given as millimoles per kilogram of the recipe excluding the catalyst (mmol/kg), and it is separated in the nomenclature from the major components by a dash. For example, recipe f-DETA31TMOS31W5ⁱPrOH33-HCL27 indicates the system includes 31 wt% f-DETA, 31 wt% TMOS, 5 wt% water and 33 wt% 2-propanol, and the concentration of the hydrochloric acid catalyst is 27 mmol/kg. However, when discussing the influence of water concentration, the equivalent ratio between water and alkoxysilane (**r**) is often used instead of the weight percentage concentration.

Among the four major components in the f-DETA/TMOS system, water is only partially miscible with f-DETA and TMOS, while any other two components are completely miscible. However, either heterogeneous or homogeneous mixtures might be hydrolyzed to transparent sols in the presence of an acid catalyst. During the coating formulation, pH was measured using a pH glass electrode calibrated using a standard buffer solution (pH=4). Recipes including equal weights of f-DETA and TMOS (f-DETA50TMOS50) usually had a gelation time of from 5-15

min. at pH 0-2, to about 8 hrs. at pH 4-5. These formulae were generally allowed to hydrolyze for a period so that transparent sols were obtained. For SEM and SAXS experiments, gel samples were prepared by casting these sols into polystyrene dishes as films. Films for SEM experiments were about 1-2 mm thick, while for SAXS experiments, they were 0.1-0.5 mm thick. For AFM experiments, smooth coating samples were prepared by spin-coating these sols onto bisphenol-A polycarbonate substrates.

6.2.2. Characterization

Specific surface areas were measured under a static process by means of a Micromeritics ASAP 2010 instrument. The specific surface area was calculated by the BET method and the average pore size was calculated by the method proposed by Barrett, Joyner and Halenda (the BJH method)¹⁹¹.

Scanning electron microscopy was conducted on a Cambridge 200 Stereoscan microscope. The gels were broken into fragments of ca. 1 mm in diameter, dried at 170°C for 4 hrs., and adhered to SEM mounts with graphite double-sided tapes. The sample along with the SEM mount was sputtered with a thin layer of gold to impart the sample surface with electrical conductivity.

Small angle x-ray scattering (SAXS) studies were conducted for gels (in film form) of f-DETA or its mixtures with TMOS. A Philips x-ray generator (model PW1729) was used to provide Cu K_α radiation (1.54Å) and the x-ray was filtered by a nickel filter and collimated by a slit. The experiments were carried out in vacuum and a Kratky-Siemens camera and an M Braun positive-sensitive detector was used. The angular dependence of scattering intensity I(s) was plotted as relative scattering intensity, (I), vs the scattering vector, s, defined by:

$$s = \frac{2}{\lambda} \sin \frac{\theta}{2} \quad \text{Eqn. 6.3}$$

where θ is the radial scattering angle.

Atomic force microscopy (AFM) was conducted by the tapping mode using a Digital Instrument's DI dimensional 3000 instrument and a tapping mode etched silicon probe. A height

image and a phase image were obtained for each sample. In the height images, bright areas usually correspond to protrusions, while for phase images, they correspond to the harder or less adhesive regions.

6.3. RESULTS AND DISCUSSION

6.3.1. The pH-Dependence of Condensation Reactivity for T and Q

The sol-gel process of an f-DETA/TMOS system includes self-condensation T-T and Q-Q as well as cross-condensation T-Q. Here T represents $-\text{Si}(\text{OEt})_3$ groups or its derivatives while Q represents the tetramethoxysilane or its derivatives. The relative reaction rates are expected to influence the distribution of the f-DETA and TMOS (condensation residuals) in the gel.

However, the OH/OR substituents on the same silicon atom usually do not have equal reactivities and the rate constants of condensation may depend on the extent of condensation. Therefore, it is not possible to estimate the sequence distribution of the monomers in the gel by the same statistical method used for linear or slightly crosslinked organic copolymers. To date, little information is available regarding the co-condensation between the T and Q monomers. This section attempts to analyze the pH-dependence of reactivity of T and Q towards self-condensation according to the inductive effect of the substituents of the silicon central atoms.

The condensation for a tetraalkoxysilane has been known qualitatively in the whole pH region. The overall condensation rate is governed by three major reactions: 1) acid catalyzed condensation, 2) base catalyzed condensation, and 3) dissolution of siloxane bonds (reverse reactions of condensation). A minimal condensation rate is usually observed at ca. pH 2, which is close to the isoelectric point (IEP) and the point of zero surface charge (PZC) of silica. The condensation below pH 2 occurs predominantly by acid-catalysis, so the reaction rate decreases as pH increases. Within the range of pH 2-8, base catalyzed condensation becomes predominant and hence, the condensation rate increases steadily with pH. The dissolution rate of siloxane

bonds are generally unimportant within pH 0-4, but increases distinctly at pH>7. Because of this, the overall condensation rate drops sharply at pH>8.

Due to the presence of the electron-donating alkyl group, the silicon atom of T has a slightly higher electron density than that of Q. In the transition state, the silicon atom bears a partial positive charge and a negative charge in the acid catalysis mechanism²⁸ and base catalysis mechanism³⁹, respectively. Therefore, T should be more reactive than Q towards the acid-catalyzed condensation, but less reactive than the latter towards base-catalyzed condensation. These inductive effects have been supported by a few experiments. Pohl et al.²⁸ have studied the pH-dependence of the dimerization rate of 3-aminopropyldimethylsilanol, 3-glycidoxypropylmethylsilanediol, and 3-glycidoxypropylsilanetriol, which have three, two and one alkyl substituents at the central silicon atoms, respectively. The results showed that the minimum dimerization rates of these three compounds occurred at pH 6.5, pH 5.8 and pH 4.5, respectively. Hence, as the number of alkyl substituents increased, the silanol was increasingly prone to undergo the acid-catalyzed dimerization. Pkarakar et al. studied the condensation of ethylsilanetriol and orthosilicic acid formed during hydrolysis of ethyltriethoxysilane and tetraethoxysilane³⁶. They found that at pH 1.7 and pH 2.2, the self-condensation of T was greater than cross-condensation between T and Q, which was in turn greater than the self-condensation of Q. In [Chapter 5](#), the sol-gel processes of the 3-methacryloxypropyltriethoxy-silane (3-MPTES)/TMOS, the [N-(3-triethoxysilyl)propyl-N'N'-diethyl]urea (UREA) /TMOS system, and f-DETA/TMOS system were described. The results showed that at pH 0-2, T in all three systems condenses as fast as or even faster than Q; while at pH 4-5, Q condenses much faster than T. These experiments are obviously in accord with predictions based on inductive effects.

Based on the similarity between T and Q, inductive effects, and experimental evidence, the pH-dependence of condensation reactivity of T and Q are systematically illustrated in [Fig. 6.1](#). T and Q show similar relationships between the condensation reactivity and pH. However, due to the inductive effect, T condenses at a minimum rate at ca. pH 4.5, so the reactivity curve of T is expected to be roughly the reactivity curve of Q but with a shift to the right side by ca. 2.5 pH units. T of ethyltriethoxysilane has little steric hindrance from the ethyl group, so it is expected to condense faster than Q of TMOS within pH 0-2. T of f-DETA, however, contains a

bulk alkyl group, so it may condense slightly slower than Q of TMOS due to the steric hindrance. At pH 4-5, T of ethyltriethoxysilane and f-DETA condenses nearly at its minimal rates. However, at this pH, Q of TMOS condenses predominantly by base-catalysis, and its overall condensation rate is expected to be much faster than its minimum rate at ca. pH 2.0 as well as the condensation of T within pH 4-5.

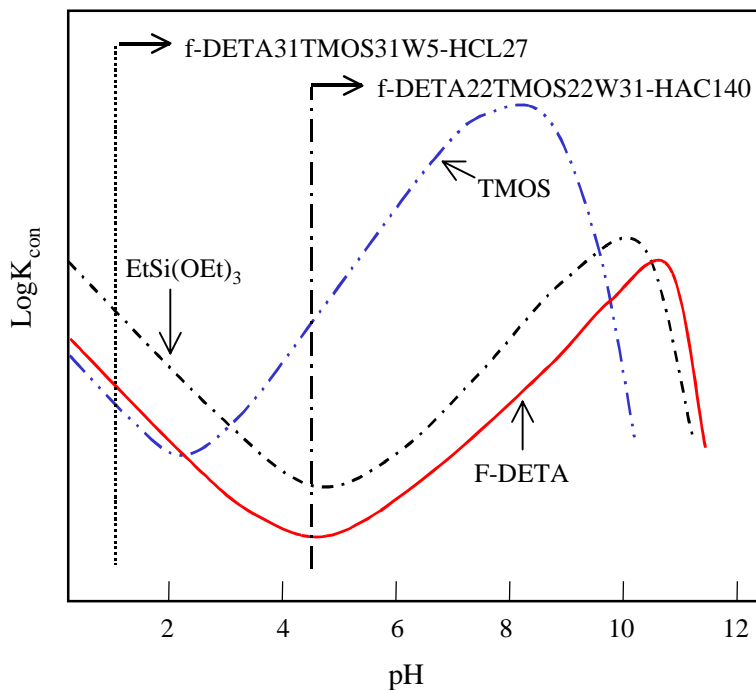


Fig. 6.1. The suggested approximate pH-dependence of the condensation rates for TMOS, EtSi(OEt)₃ and f-DETA.

The major difference between f-DETA and a normal alkyltriethoxysilane is that the former has three triethoxysilyl groups (9 Si-OEt groups) in each molecule while the latter has only one such group. Assuming all silanol/alkoxysilane groups in f-DETA have equal reactivity in the sol-gel process, according to the Flory and Stockmayer theory (ignoring closed-loop condensation), the critical extent of condensation for the system to reach gelation is 22.2% (critical extent of reaction p_c). Even if further condensation of T¹ and T² is ignored, conversion of 66.7% of all T to T¹ will lead to the gelation of the system. Therefore, at the same reaction

conditions, an f-DETA solution usually reaches the point of gelation much earlier than an ethyltriethoxysilane solution containing the same concentration of T.

6.3.2. The Influence of pH on the Morphology

pH and r in the recipe are the two important factors influencing the gel morphology. F-DETA50TMOS50 recipes were formulated by adjusting pH to various levels using several acid catalysts (Table 6.1).

Table 6.1. F-DETA50TMOS50 recipes formulated using different catalysts

#	Catalyst	pH	Comments
1	HCL	0.5-2	Smooth and transparent coating could be prepared by dip coating and spin coating
2	HPO	2.4-2.7	
3	HAC	4.0-4.2	
4	HAC and TMAAC (1:1)	~5	Often forms precipitation of silica
5	TMAOH	~11	

HCL: hydrochloric acid

HPO: phosphoric acid

HAC: acetic acid

TMAAC: tetramethylammonium acetate

TMAOH: tetramethylammonium hydroxide

For the f-DETA50TMOS50 systems, smooth transparent coating films could be formed easily within the range of pH 0-5. However, with a pH>5, the system often formed a white precipitate, which was not suitable for coating applications. The white precipitation is believed to be mainly silica since Q from TMOS condense rather fast in this pH range. Although transparent sols of f-DETA were formed at pH 11, they often did not form smooth transparent coatings. In this chapter, the morphology of films and coatings derived from f-DETA50TMOS50 recipes at different pH in the range of 0-5 is compared.

Small angle X-ray scattering (SAXS) was conducted on four gels derived from f-DETA50TMOS50 recipes. The tested gels are derived from f-DETA22TMOS22W31-HCL20 ($r= 4.4$, pH=1.7), f-DETA31TMOS31W5-HCL27 ($r= 0.55$, pH= 0.5), f-DETA22 TMOS22W31-

HPO20 ($r= 4.4$, $\text{pH}=2.5$), and f-DETA22TMOS22W31-HAC140 ($r= 4.4$, $\text{pH}= 4.2$). The first three recipes were pre-hydrolyzed for 5, 5, and 30 min., respectively, while the last one was pre-hydrolyzed for 6 hrs., then cast in polystyrene dishes and dried slowly over a three-day period at room temperature. In the following discussion, these gels will be mentioned only by the catalyst portion in their recipe nomenclature, for example, HAC140 for f-DETA22TMOS22W31-HAC140.

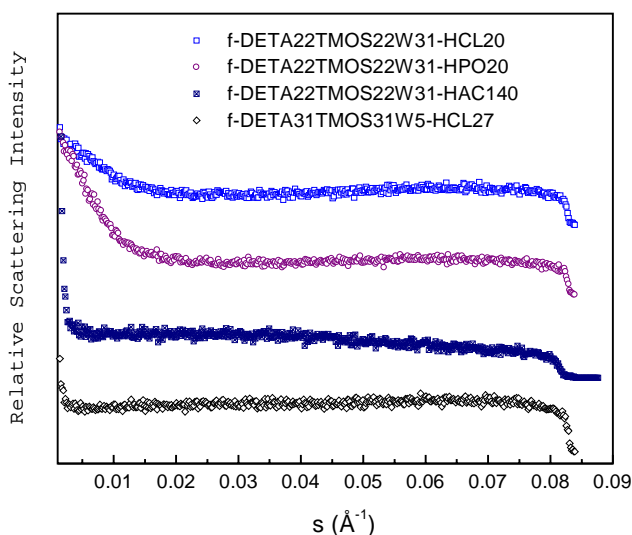


Fig. 6.2. Small angle x-ray scattering profiles (arbitrarily shifted along the y-axis) for 0.2-0.3 mm thick f-DETA/TMOS films derived from different acid catalysts.

Generally, due to shrinkage caused by syneresis (continuous condensation) and capillary forces during aging, drying, and curing processes, the primary clusters developed before gelation become interpenetrated and aggregated. Hence the mass fractal dimensions of the primary clusters cannot be obtained by a SAXS analysis of the gel, but *pores or fluctuation of any components in the nanometer scale* can still be detected. In principle, SAXS can measure the size of structural modulations in electron density within an upper limit of 500 Å. Figure 6.2 shows the SAXS profiles for the four films (0.2-0.3 mm thick) mentioned above. Gels HCL20 and HPO20, which were derived from water-abundant recipes ($r = 4.4$), exhibited obvious scattering in the range of $s = 0-0.01 \text{ \AA}^{-1}$. The scattering is believed to be due to the particulate features (residual

pores) or a very uneven distribution of f-DETA (actually f-DETA remainder) in the films. Gel HCL27 was prepared in a strongly acidic solution with a deficient amount of water ($r=0.5$), and hence more extended clusters are expected to form in the sol. During drying and curing, these clusters can interpenetrate each other and hence the final gel should have a low porosity. The very weak scattering in the SAXS profile indicates that this gel was structurally uniform in the length scale of 10-500 Å (the effective range for SAXS). Gel HAC140 was prepared at pH 4-5 under a water-abundant condition ($r=4.4$), in which case the condensation rate of f-DETA was rather slow and hence open primary clusters are expected to form. Although the condensation of TMOS was relatively fast under this condition, due to the low molecular weight of TMOS, the particle size of silica should be limited. Actually, this gel typically only showed very scattering in the SAXS profile, so it was also structurally uniform in the length scale of ca. 500 Å.

Similar experiments were also carried out for formulae that contain f-DETA but no TMOS. Generally, gels formed using hydrochloric acid showed obvious scattering in the range of $s=10^{-4}$ - $3 \times 10^{-3} \text{ \AA}^{-1}$, although this angular region is close to the limiting resolution of SAXS. Gels formulated with acetic acid catalyst showed rather weak scattering across the whole angular region. Since f-DETA is the only silane-containing component, the observed scattering is believed to be due to the pores existing in the gels, whose sizes and distributions are highly dependent on the fractal dimension of the primary clusters.

Figures 6.3-6.5 show the AFM tapping mode images of gels HCL27 ($r=0.5$), HCL20 ($r=4.4$) and HAC140 ($r=4.4$), respectively. The images (note the differences in the image scale) were obtained from the coatings of these gels on bis-A PC substrates. Figure 6.3 indicates that the continuous matrix of gel HCL27 is rather structurally homogeneous although particles of 0.1-0.2 μm in diameter are present. These large particles, as indicated by the dark domains in phase diagram, should be a *relatively* soft material, while the matrix part should be a *relatively* harder material. These large f-DETA rich domains were formed because of the higher molecular weight of f-DETA and its high condensation rate in strong acid media. Apparently, both the radius of gyration of these particles and their correlation distance had exceeded the resolution limit of the SAXS and hence no correlation length of this magnitude could be detected. Gel HCL20 was different from gel HCL27 only in the water concentration. However, it showed a rather different

structure as indicated in its height and phase images in Fig. 6.4. Unlike gel HCL27, gel HCL20 was mostly composed of hard spherical particles of ca. 50 nm in diameter embedded in a soft continuous matrix. Gel HAC140 was prepared using the same amount of water as was gel HCL20, however, the former was prepared at ca. pH 4.2 using an acetic acid catalyst. Figure 6.5 indicates that gel HAC140 is also particulate in morphology, however, it is made of smaller (ca. 20 nm) and less regular particles. This gel generally only showed weak scattering in its SAXS profile, suggesting the particulate feature only exists on the surface.

The SAXS and AFM results can be rationalized through the pH-dependence of condensation reactivity of f-DETA. With a high condensation rate of f-DETA at pH 0-2, the f-DETA or f-DETA-rich clusters grow rather fast and these clusters tend to collapse by intra-cluster condensation (closed-loop condensation), thus leading to relatively dense and rigid f-DETA or f-DETA-rich particles (a large D_{mass}). These particulate features are somewhat maintained as residual pores or uneven distributed f-DETA components after the drying and curing processes. On the other hand, if the sol-gel reaction is carried out at pH 4-5, the condensation rate of f-DETA or f-DETA-rich clusters are much lower and hence, the resulting clusters have a more extended structure. Although the condensation of TMOS is rather fast under this condition, due to the low molecular weight of TMOS, the growth of particles should be limited before they condense with f-DETA. These extended clusters later can interpenetrate one another when the solvent evaporates, so a more chemically uniform and low porous gel is formed after the gel has been dried and cured.

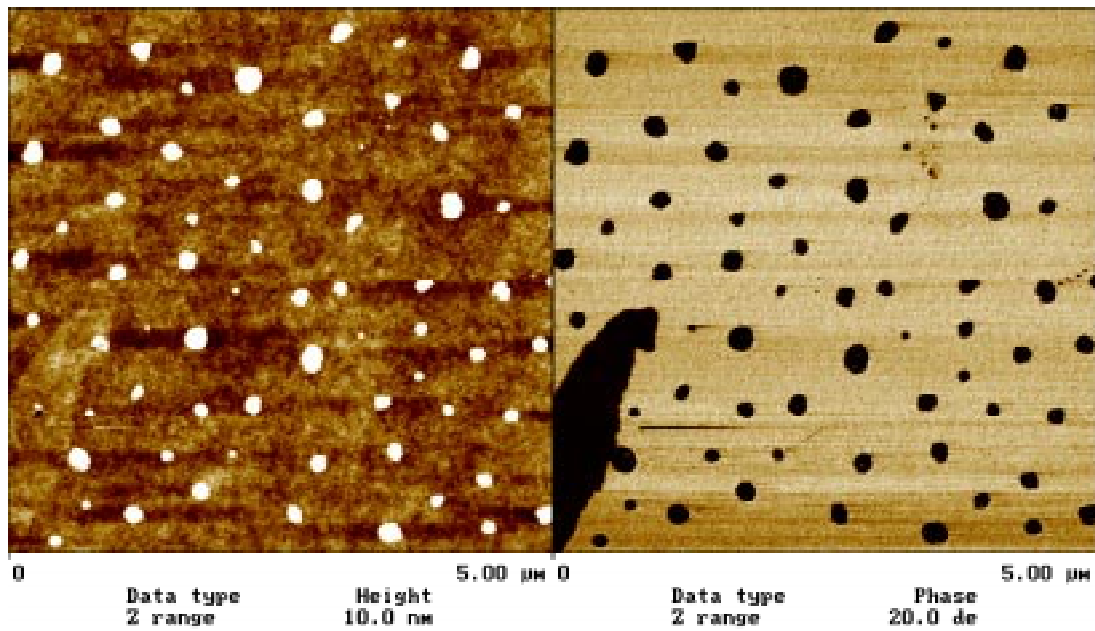


Fig. 6.3. AFM tapping mode images showing surface features of a f-DETA22TMOS22W31-HCL20 coating

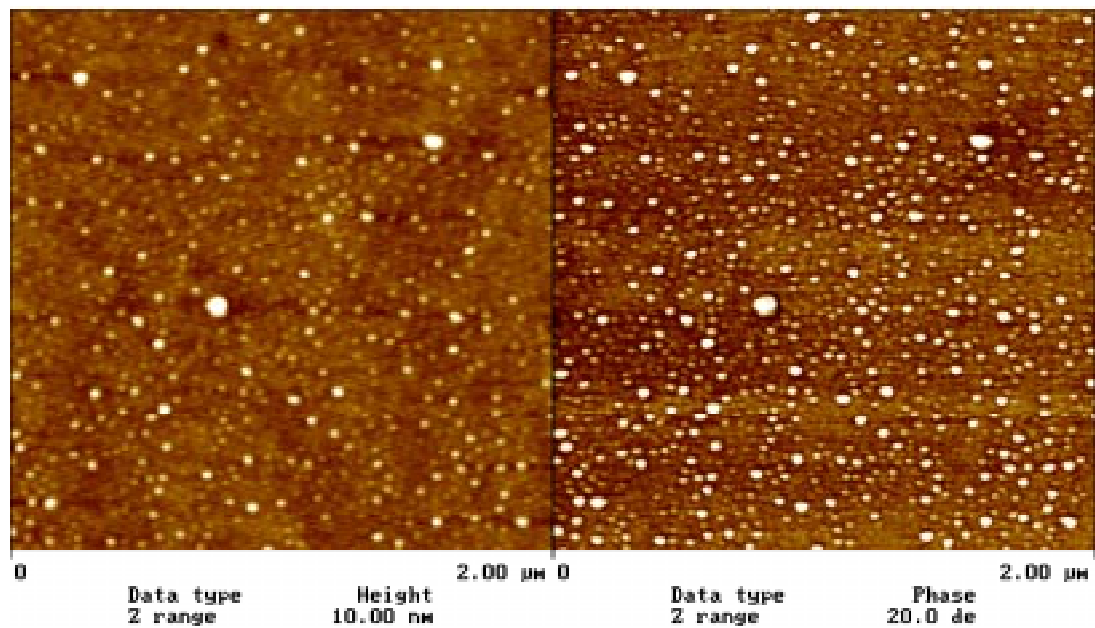


Fig. 6.4. AFM tapping mode images showing surface features of a f-DETA22TMOS22W31-HCL20 coating

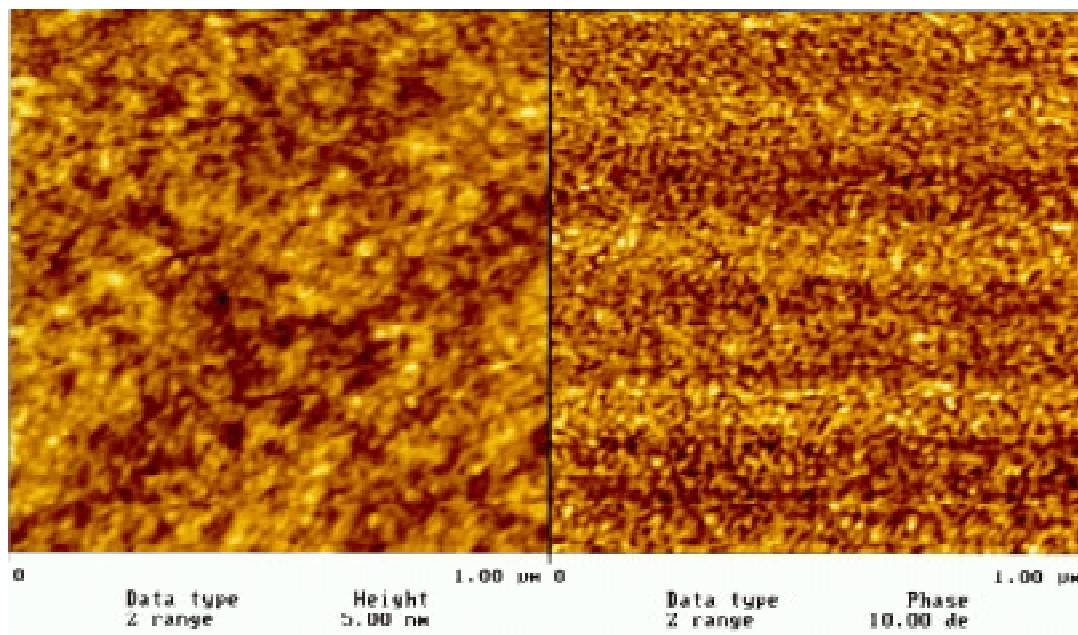


Fig. 6.5. AFM tapping mode images showing surface features of a f-DETA22TMOS22W31-HAC140 coating

6.3.3. The Influence of the Water Concentration on Gel Morphology

The water concentration in a sol-gel system can have a critical influence on the concentration of silanol groups. Generally, a decrease in r reduces the average functionality of the monomer and hence lowers the mass fractal dimension of the resulting clusters. In addition, it may also significantly change the dielectric constant and polarity of the solvent.

Six pure f-DETA gels (46 wt% in 2-propanol) were hydrolyzed and condensed by adding water and hydrochloric acid catalyst. In these recipes, pH was controlled between 0-2 and the amounts of f-DETA and the solvent 2-propanol were fixed. The water concentration was gradually increased so that r in these recipes was 0.46, 0.92, 1.8, 3.6, 7.2 or 14.9, respectively. By this formulation method, the increase of r was accompanied by a slight decrease in the f-DETA concentration. [Figure 6.6](#) shows the SEM micrographs for the fracture surfaces of the resulting six gels. Generally, when r was 0.46 and 0.92, transparent gels were obtained. According to SEM studies, the gel with $r = 0.46$ showed a smooth fracture surface ([Fig. 6.6a](#)).

As r increased to 0.92, the fracture surface topography became slightly rough (Fig. 6.6b), indicating an increase in the particulate feature in the gel. As r increased to 1.8, 3.6 and 7.2, white porous f-DETA particulate gels were formed instead. The particle sizes in these gels are $\sim 0.4 \mu\text{m}$ in Fig. 6.6c, $\sim 2 \mu\text{m}$ in Fig. 6.6d, and $\sim 2 \mu\text{m}$ in Fig. 6.6e, respectively. As r further increased to 14.9, a nearly transparent gel (Fig. 6.6f) was obtained again. This gel distinctly had a more compact structure, however, fine particulate features could still be distinguished by SEM. Under this water-abundant condition, it is conjectured that the silanol groups were stabilized by water, so the growth of clusters and intra-cluster condensation occurred at a slow rate and hence the clusters could remain suspended during the pre-hydrolysis process. Since the particle size was well below the wavelength of visible light, the film obtained was nearly transparent. The stabilization of the system by water could be visualized by the immediate flocculation and precipitation of the transparent sols of f-DETA or f-DETA/TMOS when 2-propanol or ethanol was added to this pre-hydrolyzed system.

Similar experiments were conducted within the range of pH 0-2 in an ethanol medium by adjusting r to 0.46, 0.93, 1.8, 3.6, 7.2 and 14.9. However, the concentration of f-DETA was maintained constant at 18 wt% by controlling the ethanol concentration. As r increased, this series of gels also exhibited the same morphological transition as shown in the gels prepared in 2-propanol (Fig. 6.7). It is believed that as r increases, both the silanol concentration and the polarity of the medium are increased. The former accelerates the cluster growth rate and intra-cluster condensation, while the latter stabilizes the silanol groups and decreases the cluster growth rate and intra-cluster condensation. The former effect is expected to be more important at a small r . However, after r increases to beyond a critical value, the latter effect can significantly offset the influence of the former, thus leading to formation of smaller particles.

Pure f-DETA gels were also prepared using an acetic acid catalyst (pH \sim 4.0) and an value of r changing from 2.2, 4.5, 8.9, 17.8 or 35.6. The series did not include the conditions of $r = 0.46$ and 0.93 since the hydrolysis rates under these conditions were very slow. Highly transparent gels of f-DETA were obtained under all conditions except for $r=2.2$, in which case a translucent gel was obtained. The gels developed at ca. pH 4 with an acetic acid catalyst differed from those developed at pH 0-2 with a hydrochloric acid catalyst. In the latter cases, r values of

1.86, 3.72 and 7.44 corresponded to porous particulate gels. SEM shows that the translucence of the gel with $r = 2.2$ is not caused by the particles, but by the remaining pores, especially pores on the surfaces (Fig. 6.8). For some reason, gradual condensation in the gel (often called microsineresis) appears to have led to the formation of large pores that could not be collapsed by capillary forces (Note this gel was slowly dried at room temperature).

At pH 0-2 using a hydrochloric acid catalyst, the influence of r on the morphology of the f-DETA50TMOS50 gel was also systematically studied. As indicated by AFM and SAXS earlier, the mixture formed a more structurally uniform gel at $r = 0.5$ although some large f-DETA rich particles were noted. However, at $r = 2.0$, an obvious particulate gel was formed as revealed by the SEM image in Fig. 6.9. As r was further increased to 4.4, a highly transparent but still particulate gel was obtained (the HCL20 gel discussed earlier). It is believed that at pH 0-2, the cross-condensation between TMOS with f-DETA blocks parts of those reactive T, so the size of clusters in the f-DETA/TMOS system is usually much smaller than the pure f-DETA system.

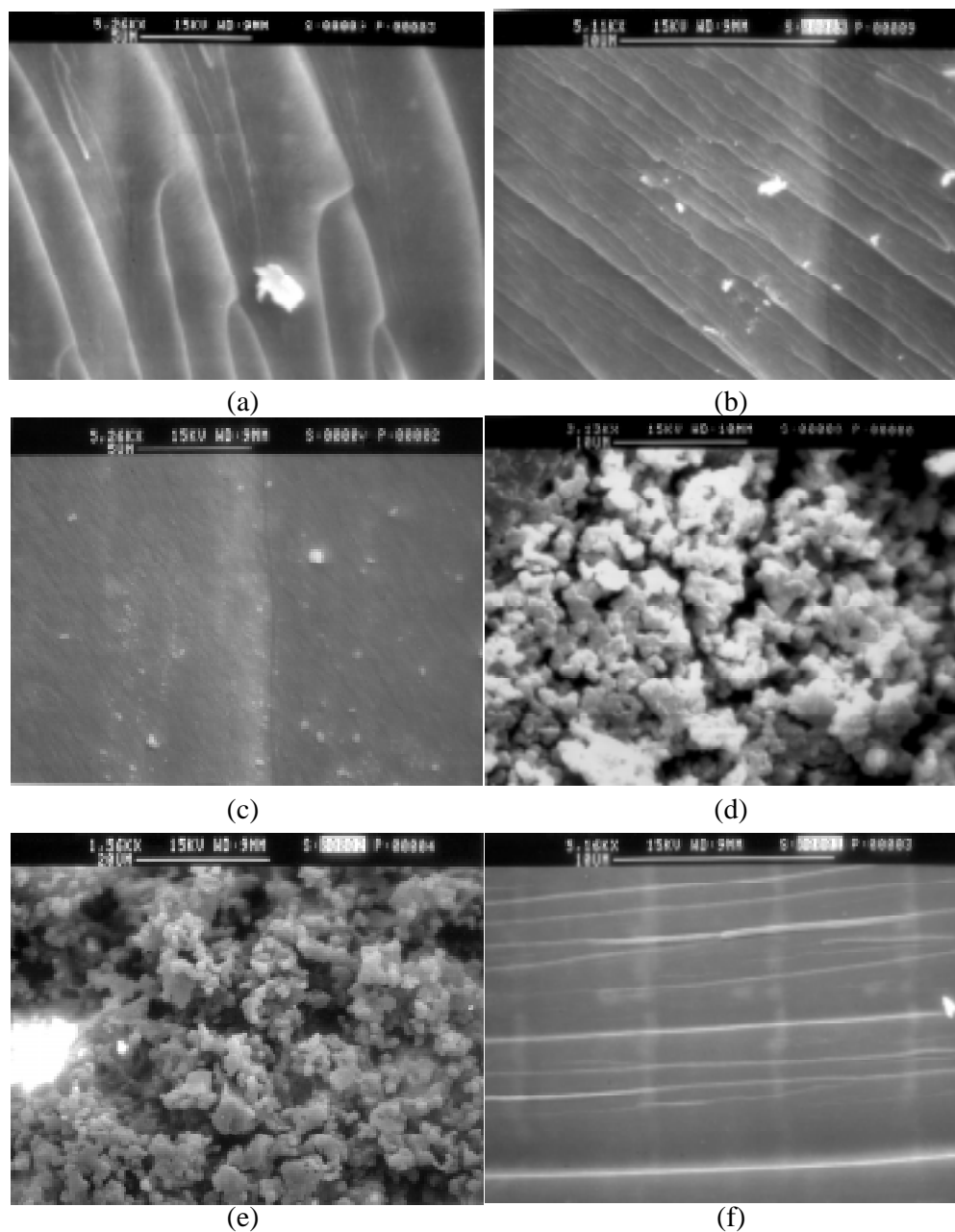


Fig. 6.7. SEM micrographs of f-DETA gels derived in ethanol using HCL catalyst at pH ~0-2. (a) $r = 0.47$, (b) $r=0.93$, (c) $r=1.86$, (d) $r= 3.72$ (e) $r=7.44$, and (f) $r= 14.9$. The f-DETA concentration was fixed at 18 wt% by changing the amount of ethanol.

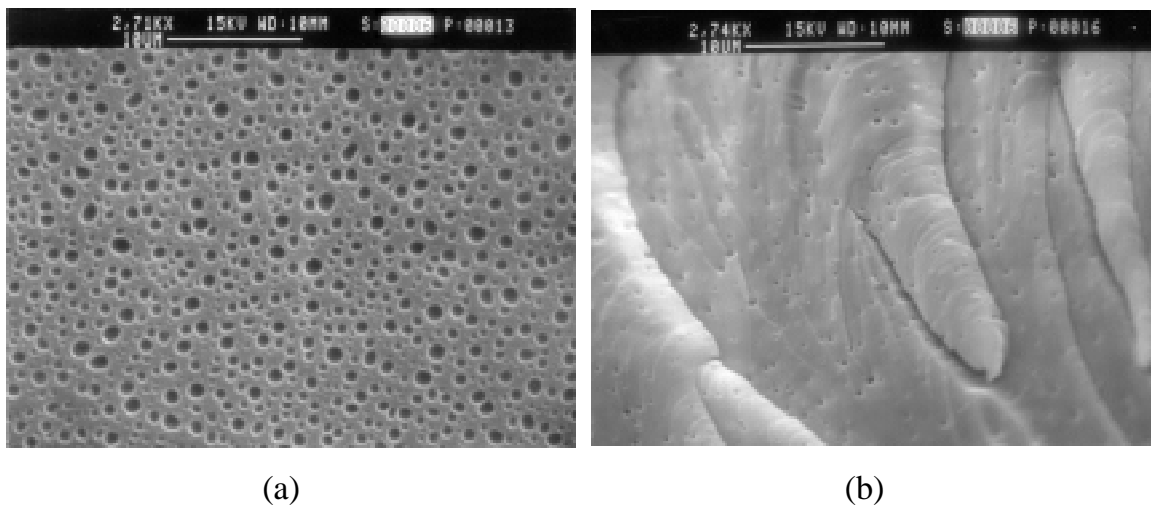


Fig. 6.8. SEM micrographs for gel f-DETA23W33-HAC138 ($r=2.2$) (a) the gel surface; (b) internal fracture surface of the gel.

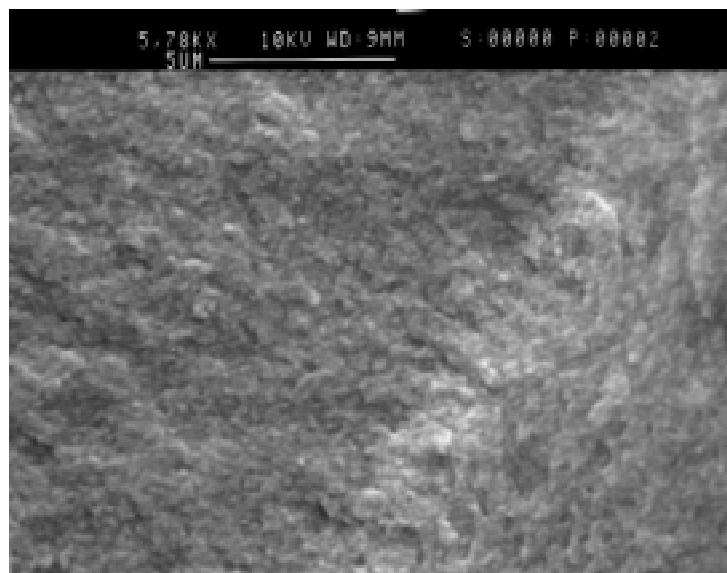


Fig. 6.9. SEM micrograph for the fracture surface of gel f-DETA26TMOS26W19-HCL24 ($r=2.2$)

6.3.4. The Influence of Drying Speed on the Morphology

When a sol is spread on a substrate, it includes high molecular weight clusters or particles, low molecular weight polymers, and non-hydrolyzed or partly hydrolyzed monomers. As the solvent evaporates, all these species aggregate and remain on the surface of the substrate. These clusters or particles gel and interpenetrate each other. At the final stages of drying, the pores between clusters or particles are collapsed by capillary forces and hence a monolithic film is then formed on the substrate^{89,90}.

Pure cluster interpenetration is a diffusion process. As solvent evaporation is typically accompanied by an increase in the condensation rate, so a slow solvent evaporation rate may be beneficial to interpenetration of structurally dense primary clusters, especially for sols developed in basic media. When f-DETA was hydrolyzed using tetramethylammonium hydroxide as the catalyst (ca. pH 12) at $r=14.9$, a transparent sol was formed after ca. 10 hrs. of hydrolysis. As this sol was spread on a bis-A PC substrate, the solvent quickly evaporated and a white powdery material was left on the substrate. However, as the sol was slowly dried slowly in a polystyrene dish, a highly transparent gel was obtained. In this example, the f-DETA sol contained structurally dense primary clusters (a large D_{mass}), which were unable to interpenetrate into each other in a short period. However, interpenetration and collapse of pores became possible if the drying process was sufficiently slow.

On the other hand, if the condensation or microsineresis in a gel is so fast that relatively large changes occur in the gel structure during the drying process, a fast drying rate may be helpful for forming a low porosity film. Recipe f-DETA43W8-HCL38 ($r=1.9$) usually formed a porous gel. However, if the sol was spread and desolvented before big particles had formed, then it was still possible to form transparent films. [Figure 6.10](#) shows a sectional view of a 0.9-mm thick film of this gel. Near the surface shows a structurally compact layer although inside the gel is a bulk porous gel. During the film formation, the surface layer desolvented quickly, thus clusters within this layer collapsed and formed a structurally compact layer. Inside the gel, however, the solvent evaporated at a much slower rate so that clusters or particles continued to

grow, which eventually led to separation of the solvent from the gel and formation of porous structure.

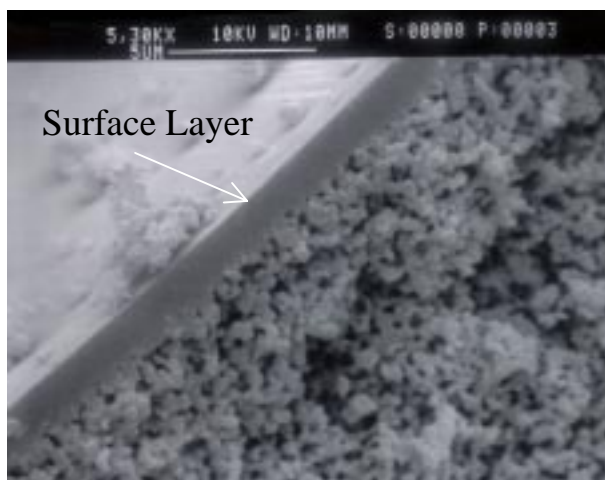


Fig. 6.10. A sectional view of a 0.9-mm thick gel of f-DETA43W8-HCL38 gel showing a structurally compact surface layer.

In general, when prepared at pH 0-2 using a hydrochloric acid catalyst, f-DETA50TMOS50 usually formed a structurally compact gel at a low water concentration ($r < 1$) or a high water concentration ($r > 4$). If acetic acid was used as the catalyst, either pure f-DETA or a mixture of f-DETA with TMOS could form a structurally compact gel at relatively high water concentrations ($r > 4$). The specific surface areas and pore sizes were measured for powders of gels f-DETA31TMOS31W5-HCL27, f-DETA22TMOS22W31-HCL20, f-DETA28W40-HAC166, f-DETA26TMOS31W35-HAC144 and f-DETA22TMOS22W31-HAC166. The results indicated that these samples had a specific surface area of ca. 3-9 m²/g, a pore volume of ca. 0.004-0.007 cm³/g and average pore diameters about 60-100Å. Therefore, f-DETA/TMOS gels derived under appropriate conditions were generally very densely packed. The low pore density of these gels helps to explain why the corresponding coatings are useful in protecting some substrates from the attack of organic solvents and some corrosive chemicals.

6.4. CONCLUSIONS

The morphology of the gels including f-DETA or f-DETA50TMOS50 has been discussed based on the relative reactivities of T and Q. Due to induction effects, the condensation of T was as fast as or even faster than that of TMOS at pH 0-2, but was slower than the latter at pH 4-5. For this reason, systems including f-DETA or both f-DETA and TMOS tended to form relatively large clusters in strong acid media and those clusters are inclined to collapse to relatively dense rigid particles in water abundant conditions. On the other hand, if the sol-gel reactions were carried out at pH 4-5, the condensation of f-DETA was rather slow, so the resulting clusters were structurally more open, and less likely to collapse to dense rigid particles. These loose clusters could well interpenetrate one another during the drying and curing process, thus forming structurally homogeneous films although these gels still showed some particulate features on the surface.

The influence of the water concentration (r) to the morphology has also been discussed. At pH 0-2, the sol-gel reactions of pure f-DETA tended to form gels with morphology changing from mainly a monolithic gel, to porous particles, and to a compact particulate gel as r gradually increased. Similar behavior was observed for f-DETA50TMOS50 systems, however, this system rarely formed porous particulate gels as in the case of pure f-DETA gel. In addition, the particle size in the f-DETA/TMOS system was generally much smaller. The observed phenomena are believed to be due to the blocking of some of the reactive T units by the Q units, which slows cluster growth.

Finally, during the film formation, the solvent evaporation rate with respect to condensation rate could influence the structure of f-DETA/TMOS gels. On the one hand, lengthening aging time may promote interpenetration of primary particles, thus leading to a low porosity. On the other hand, it may also increase the influence of syneresis, hence leading to further particle growth and pore formation. Both phenomena were observed in the f-DETA/TMOS gels. The specific surface areas and pore sizes have been measured for several f-DETA/TMOS gels, and the results indicated these gels were structurally compact, and thus could serve as protective coatings.

CHAPTER 7. INORGANIC-ORGANIC HYBRID MATERIALS AND THEIR POTENTIAL AS ABRASION RESISTANT COATINGS

7.1. INTRODUCTION

Eight years ago, it was found that the compound f-DETA, produced by reaction of diethylenetriamine and 3-isocyanatopropyltriethoxysilane (3-ICPTES), can be processed by a sol-gel approach into abrasion resistant coatings to protect polymeric substrates¹⁵⁰. Since then, the exploration for better abrasion resistant coatings have been proceeding along two directions: 1) incorporation of metal or semi-metal alkoxides into the f-DETA system^{12,13}, and 2) development of new trialkoxysilylated organic compounds^{14,15,152,153}. After several years of continuous research, the abrasion resistance of f-DETA coatings has been significantly improved. New trialkoxysilylated compounds have also been prepared and many of them yield good to excellent abrasion resistant coatings. The structures of these new compounds generally include linkages of urea, urethane, sulfones, phosphine oxide, melamine and bismaleimide. The triethoxysilyl groups are attached to the organic compounds by reaction of amine or hydroxy groups with 3-ICPTES, or by reaction of amine groups with bismaleic anhydride, which later reacts with 3-aminopropyltriethoxysilane by a Michael addition reaction. These compounds are generally hydrolyzed or co-hydrolyzed with tetraalkoxides to form sol-gel coatings. Since this process involves concurrent hydrolysis and condensation of two silane components, it is referred to as a one-step approach. Coatings prepared by this method are very abrasion resistant but the coating recipes usually have a limited pot life.

This chapter continues the previous exploration for new trialkoxysilylated organic compounds that can be potentially used for abrasion resistant coatings. In addition to the one-step approach, a *two-step approach* and a *moisture-curing approach* are also utilized for coating

formation. The two-step approach is introduced to create a microphase-separated gel structure that has more distinct inorganic particles embedded in a matrix that contains more organic component. By doing that, it is hoped that a suitable balance between the hardness and toughness of the material can be established. The moisture-curing method is explored because the process allows formulation of one-part coating recipes. If this approach is successful, the pot life problem plagued in the usual two-part coating recipes can be avoided.

7.2. EXPERIMENTAL

7.2.1. Characterization

^1H , ^{13}C , and ^{29}Si NMR spectra were acquired using a 400 MHz Varian NMR spectrometer. The refractive index was measured at 633 nm via a Metricon 2010 instrument using 0.5-1 mm free sol-gel films. Similar films were also used for UV/Vis and small angle x-ray scattering experiments. UV/Vis spectra were acquired using a Hitachi U-2000 spectrometer.

Small angle x-ray scattering (SAXS) experiments were carried out using $\text{Cu K}\alpha$ radiation from a Philips x-ray generator. The radiation was filtered using a Nickel filter and collimated by a slit. The experiments were carried out in vacuum and a Kratky-Siemens camera and an M Braun positive-sensitive detector was used.

Vickers hardness was measured on a LECO DM-400 hardness tester using a load of 10 g and a loading time of 10 seconds. The coatings were prepared on glass slide substrates and had a thickness of about 25-50 μm . Since the penetration depth was usually less than 3 μm , the influence of substrate should be unimportant. All hardness data were based on the average of ten measurements.

Pencil hardness test (ASTM standard 3363-92a) is a widely used method for evaluation of scratch resistance of organic coatings. Here this test was utilized to rate the scratch resistance of moisture cured coatings. The hardness value was expressed as the hardest pencil that failed to

scratch the coating. The scale of hardness of pencils, arranged in the order of increasing hardness, is 6B, 5B, 4B, 3B, 2B, B, HB, F, H, 2H, 3H, 4H, 5H, 6H, 7H, 8H, and 9H.

Taber abrasion tests were carried out using a pair of CS10 abrading wheels with a 500-gram load per wheel. For transparent substrates, the abrasion resistance was evaluated by the transmittance of the wear tracks after a specified Taber test. The density of scratches in the micrograph of the wear tracks was also used to evaluate abrasion resistance. For opaque substrates, only the reflection microscopy method could be used.

Transmission and reflection optical micrographs were taken using an Olympus DH2-UMA microscopy. For reflection microscopy, a gold layer was sputtered on tested substrates to enhance the image contrast of the wear-induced scratches in Taber wear tracks.

Scratch tests were carried out using a Micro Scratch Tester by Micro Photonics, Inc. During the test, the coating is scratched by a progressively loaded indenter tip. The critical load for the first failure, or the load that causes the first failure of the substrate, can be determined by an optical microscope or an acoustic emission detector.

7.2.2. Chemicals and Preparation

Common chemicals frequently used in this work included 3-isocyanatopropyltriethoxysilane (95%, 3-ICPTES, Aldrich), tetramethoxysilane (99+%, Aldrich), Pt(0)(1,3-divinyldisiloxane) (2% in xylene, Gelest), and 3-glycidoxypropyltrimethoxysilane (98%, 3-GPTMS, Gelest). All these chemicals were used as received.

Silica colloid (Ludox, TM50, DuPont) was purchased from the Aldrich Company, and zirconia (NAYCOL ZrO₂AC) and alumina (NAYCOL AL20) were kindly provided by the PQ Corporation. These materials were used as received.

Bisphenol-A polycarbonate (bis-A PC, Lexan, GE) was purchased from the Atlantic Plastic Company, and pretreated with a 0.5 wt% solution of 3-aminopropyltriethoxysilane (3-APS, 98%, Aldrich) before being coated. Aluminum substrates were purchased from the Q-Panel Company and degreased with 2-propanol before being coated.

[Table 7.1](#) lists the structures and abbreviations of trialkoxysilylated chemicals to be addressed in this chapter. In this work, these chemicals were synthesized and used as starting materials for formulating abrasion resistant coatings.

Table 7.1. Chemical structures and abbreviations of compounds containing multiple trialkoxysilyl groups

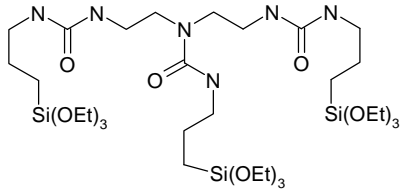
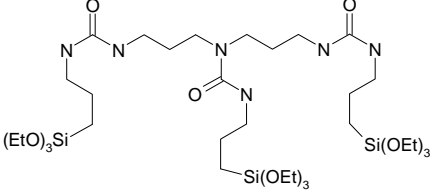
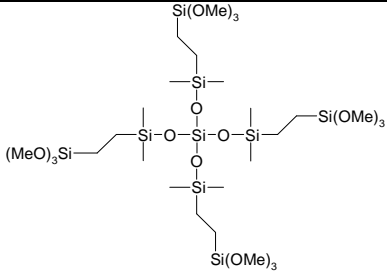
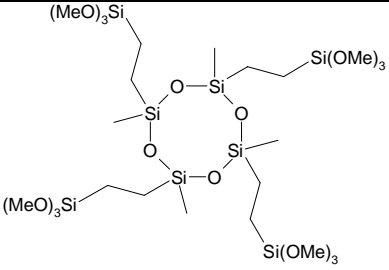
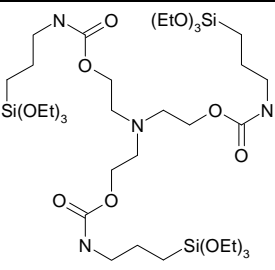
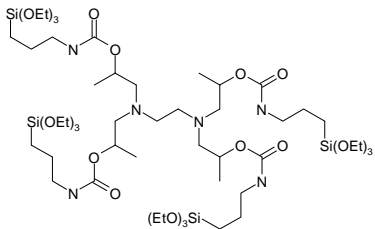
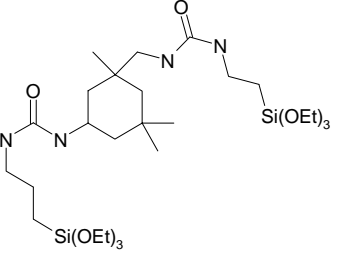
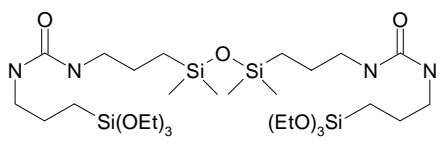
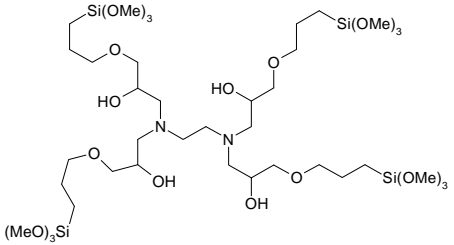
 <p style="text-align: center;">f-DETA Reference</p>	 <p style="text-align: center;">f-BAPI Reference 14</p>	 <p style="text-align: center;">T4M4Q MW = 497.07</p>
 <p style="text-align: center;">MW = 408.84 T4D4</p>	 <p style="text-align: center;">MW = 446.59 f-TEA</p>	 <p style="text-align: center;">MW = 688.96 f-THPDEA</p>
 <p style="text-align: center;">MW = 354.54 f-ISOP</p>	 <p style="text-align: center;">MW = 446.79 f-DISIL</p>	 <p style="text-align: center;">Molecular Weight = 580.85 f-EPXY</p>

Table 7.2. Concentrations and particle sizes of silica, zirconia and alumina

Colloid	Particle Size ^A	Conc. (wt%) ^A	Conc. (wt%) ^B
Silica (Ludox, TM50)	100 nm	50%	52%
ZrO ₂ (NAYCOL ZrO2AC)	100 nm	25%	31%
Al ₂ O ₃ (NAYCOL AL20)	500 nm	20%	25%

A. Information provided by the manufacturer

B. Measured by weight analysis (the colloids were dried at 125°C/4 hrs., which is the usual coating curing condition.)

7.2.2.1. Preparation of F-DETA and F-BAPI (Reference Systems)

7.2.2.1.1. F-DETA

To a 250-ml flask were charged 10 g of diethylenetriamine (99%, DETA, Aldrich) and 37.2 g of anhydrous ethanol. As the mixture was cooled by an ice bath, 78.6 g of 3-ICPTES were gradually added to the stirring mixture via a funnel within a period of ca. 30 min. After all the 3-ICPTES had been added, the flask was capped with a septum and the mixture was stirred for another 12 hrs.

7.2.2.1.2. F-BAPI

The f-BAPI system has a structure very similar to f-DETA (Table 7.1) except that the former has two more methylene groups. The compound was originally introduced by Wen et al and coatings of its binary systems with tetraethoxysilane offered the same level of abrasion resistance as the f-DETA/TMOS system¹⁴.

The preparation of f-BAPI is rather similar to that of f-DETA. A 250-ml flask was charged with 10 g of bis(3-aminopropyl)imine (98%, Aldrich) and 15 g of 2-propanol. As the mixture was cooled by an ice bath, 29.6 g of 3-ICPTES were gradually added to the stirring mixture via a funnel within a period of ca. 30 min. After all the 3-ICPTES had been added, the flask was capped with a septum and mixture was stirred for another 12 hrs.

7.2.2.2. Preparation of T4M8Q and T4D4

The star monomers T4M4Q and T4D4 (Table 7.1) have been introduced by Sharp and Michalczyk in 1996¹⁹², Transparent gels were formed by hydrolyzing these compounds in aqueous or formic acid media, and *the gelation time was reported to be much shorter than that of tetraethoxysilane and alkyltriethoxysilane*. No information about their abrasion resistance has been reported to the author's knowledge.

7.2.2.2.1. T4M4Q

Twenty grams of tetrakis(dimethylsilyl) silicate (Gelest) and 0.020 g of Pt(dvs) (in xylene, Gelest) were added to a 100 ml one-neck flask. While the mixture was stirring, 5 g of vinyltrimethoxysilane (Gelest) were added. As tetrakis(dimethylsilyl) silicate reacted with vinyltrimethoxysilane via a hydrosilylation reaction, the temperature of the mixture would slightly increase. After hydrosilylation had been initiated, another 31 g of vinyltrimethoxysilane were added in aliquots of ca. 5 g at an interval of ~30 min. After the mixture had cooled down, the mixture was stirred at 60°C for another 12 hrs. The compound formed in the reaction was confirmed to be T4M4Q by ¹N NMR and ²⁹Si NMR. This product was stored in a closed container for future use.

7.2.2.2.2. M4D4

To a one-neck flask were charged 34.7 g of 1,3,5,7-tetramethylcyclotetrasiloxane (D^V₄, Gelest), 5 g of vinyltrimethoxysilane (98%, Gelest) and 0.020 g of Pt(dvs). Note the cyclotetrasiloxane starting material included some cyclopentasiloxane (D^V₅) and cyclotrisiloxane (D^V₃). The mixture was heated at 60°C to accelerate the hydrosilylation reaction. After confirming most vinyltrimethoxysilane had been consumed (via FTIR), more vinyltrimethoxysilane was added. Si^D-H is not as reactive as Si^M-H, so the hydrosilylation was carried out at 60°C rather than at room temperature. A total of 36 g of vinyltrimethoxysilane was added in aliquots of ca. 5 g at an interval of ca. 30 min. The product was stored in a closed container for future use. ¹H, ¹³C, and ²⁹Si NMR spectra of the product are given in Figs 7.1-7.3. The NMR spectra indicated the hydrosilylation included ~15% of β-addition (Si-CH(CH₃)-Si) and ~85% of α-addition (Si-CH₂-

CH₂-Si) in the products. Some trimer and pentamer were also revealed by ²⁹Si NMR spectroscopy (Fig. 7.2).

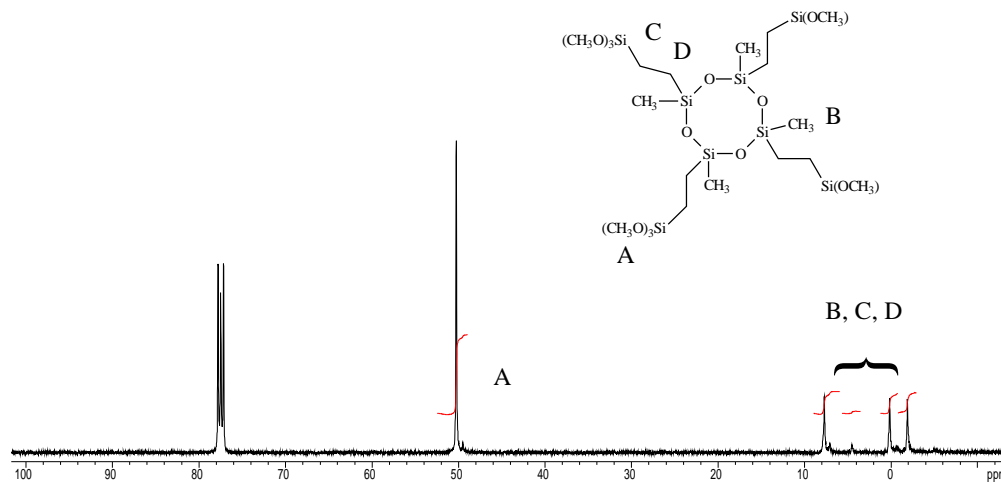


Fig. 7.1. The ¹³C NMR spectrum for tetrakis((2-triethoxysilyl)ethyl)dimethylsilyl)tetramethylcyclotetrasiloxane

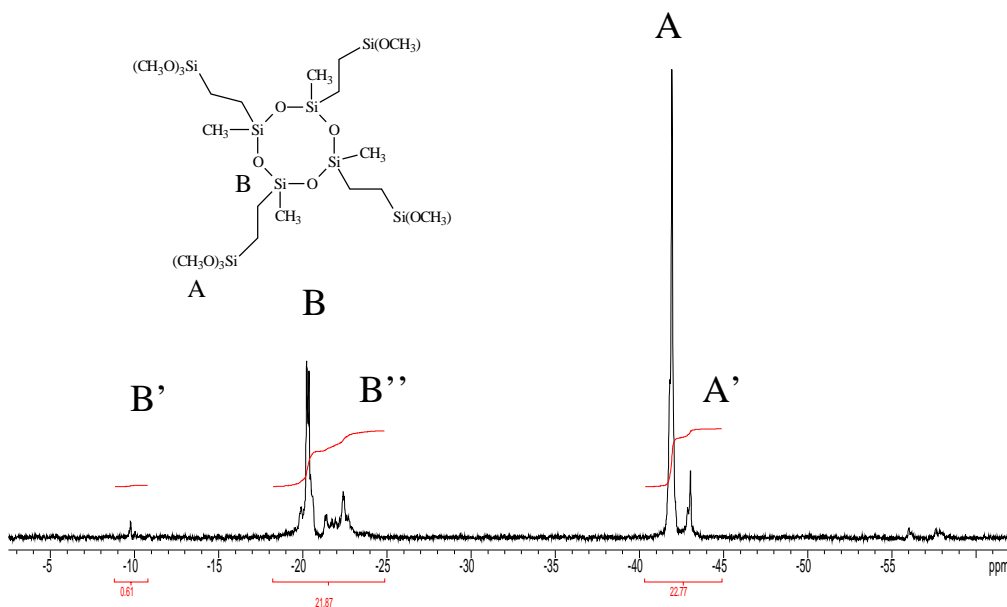


Fig. 7.2. The ²⁹Si NMR spectrum for tetrakis((2-triethoxysilyl)ethyl)dimethylsilyl)tetramethylcyclotetrasiloxane. B'=cyclotrisiloxane, B''=cyclopentasiloxane, and A' is due to β-hydrosilylation.

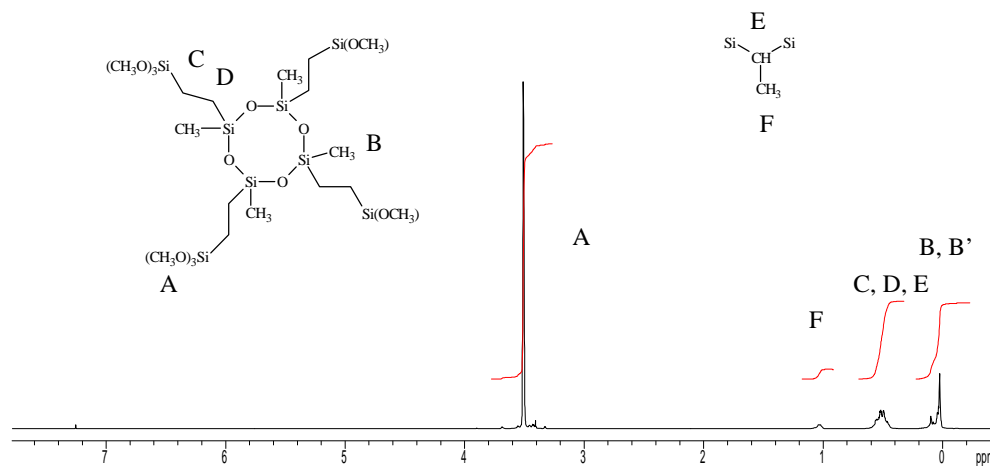


Fig. 7.3. The ¹H NMR spectrum for tetrakis((2-triethoxysilylethyl)dimethylsilyl)tetramethylcyclotetrasiloxane. The Si-CH(CH₃)-Si linkage is caused by β-hydrosilylation

7.2.2.3. Preparation of F-TEA

In a 250-ml round bottle flask were added 10 g of triethanolamine (98%, Aldrich) and 10 g of acetone, and the mixture was stirred until a transparent solution was formed. To the flask were added 52 g (0.210 mol) of 3-ICPTES. The formation of urethane bonds was indicated by a temperature increase of the solution. After the solution cooled down, the mixture was stirred in a closed container at 60°C for another 24 hrs. and then diluted to 70 wt% with acetone. The structure of f-TEA was confirmed by ¹H NMR and FTIR. This compound was stored in a closed container; however, it gradually turned brownish due to an unknown chemical reaction.

7.2.2.4. Preparation of F-THPDEA

A one-neck flask was charged with 10 g of N,N,N',N'-tetrakis(2-hydroxypropyl)ethylene-diamine (98%, Aldrich), 10 g of acetone (as a solvent) and 39 g of 3-ICPTES. The mixture was stirred until a homogeneous solution was formed. About 0.1 g of dibutyltin dilaurate was added as a catalyst. The expected formation of urethane bonds was indicated by a temperature increase of the solution. After the solution (~83 wt%) cooled down, the mixture was stirred for another 12 hrs. This solution was diluted to 70 wt% with acetone and stored at room temperature in a closed

container for future use. The formation of urethane bonds was confirmed by FT-IR. This compound also gradually turned brownish due to an unknown chemical reaction.

7.2.2.5. Preparation of *F-DISIL*

To a 250-ml round bottom flask were added 20 g of 1,3-bis(3-aminopropyl)-1,1,3,3-tetramethyldisiloxane (Gelest) and 26.5 g of 2-propanol (as solvent). As the mixture was cooled by an ice bath, 41.8 g of 3-ICPTES were slowly added to the stirring mixture via a funnel. After all the 3-ICPTES had been added, the flask was capped with a septum and the mixture was stirred for another 12 hrs. The *f-DISIL* was a 70 wt% solution in 2-propanol. It was stored in a closed container and used within a week.

7.2.2.6. Preparation of *F-ISOP*

To a 100-ml round bottom flask were added 20 g of 3-aminopropyltriethoxysilane and 13 g of 2-propanol (as solvent). As the mixture was cooled by an ice bath, 10.0 g of isophorone diisocyanate (98%, Aldrich) was gradually added to the stirring mixture via a funnel. After all the isophorone diisocyanate had been added, the flask was capped with a septum and the mixture was stirred for another ca. 12 hrs. The *f-ISOP* was a 70 wt% solution in 2-propanol. Similarly, it was stored in a closed container and used within a week. This compound formed colorless crystals in 2-propanol during storage and the crystals could be redissolved when the temperature exceeds 60°C.

7.2.2.7. Preparation of *F-EPXY*

A 250-ml round bottom flask was charged with 5 g of ethylenediamine (99 wt%, Alrich), 78 g of 3-glycidoxypropyltrimethoxysilane (98%, Aldrich), and 83 g of methanol. The reaction of amine with epoxy groups is exothermic. The mixture cooled to room temperature within ca. 5-6 hrs., and then it was heated to 60°C for another 10 hrs. The final product was a clear solution in methanol (50 wt%) and it was stored in a closed container.

In cases when no solvent or non-alcoholic solvent was added, the f-EPXY polymerized and even gelled because of intermolecular transesterification between the methoxysilane group with the secondary hydroxy group ($-\text{OCH}_2\text{CH}(\text{OH})\text{CH}_2\text{-N}-(\text{CH}_2)\text{Si}(\text{OMe})_3$) produced by ring-opening of the epoxy rings. The transesterification reaction was confirmed by gel permeation chromatography (GPC). Figure 7.4 shows the GPC scans for f-EPXY solutions (50% in methanol) that had been mixed with chloroform (GPC solvent) for different times. The results indicate that as the mixing time increased, the average molecular weight of this material increased due to transesterification. After 150 min. of mixing, the mixture approached an equilibrium state since no significant increased in molecular weight could be observed.

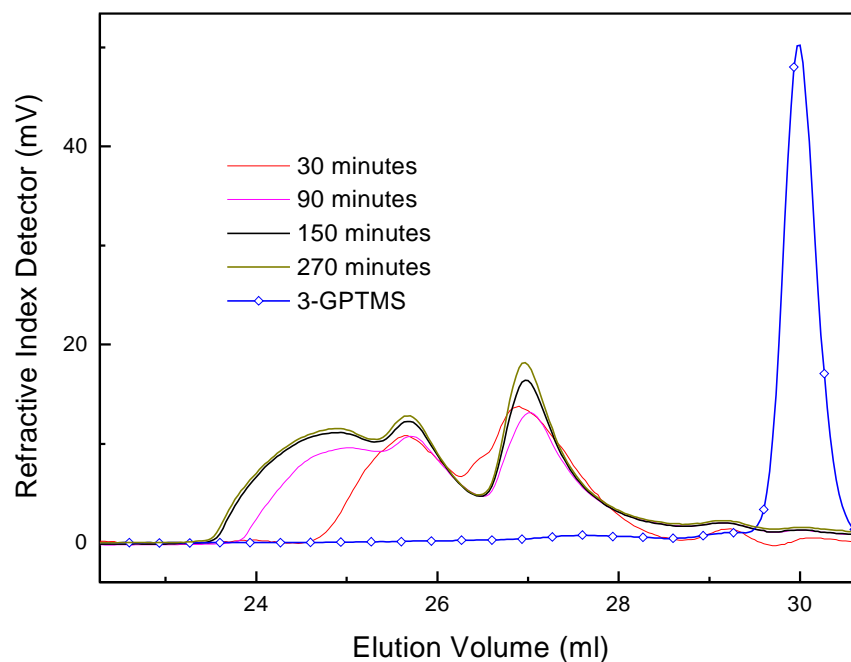


Fig. 7.4. The GPC chromatograms for f-EPXY after the sample was stored in chloroform for the specified time.

7.2.3. Sol-Gel Coatings by One-Step Hydrolysis

The one-step approach generally involves co-hydrolysis and co-condensation of a multi-component system in the presence of an acid catalyst. The resulting sol is spread by dip coating

or spin coating on substrates such as bis-A PC and aluminum substrates, on which it is dried and thermally cured into a hard layer of gel.

F-DETA coatings were prepared by hydrolyzing a mixture of 4 g of f-DETA (70% in 2-propanol), 2.8 g of TMOS, 2 g of 2-propanol, 4 g of water in the presence of 0.1 g of glacial acetic acid. After about six hours of hydrolysis, the resulting sol was dip- or spin-coated on bis-A PC substrates. The coated substrates were dried at room temperature, and thermally cured at 125°C for 4 hrs. *F-BIPA coatings* were prepared similarly by using f-BIPA instead of f-DETA in the procedure. These two recipes are named f-DETA50TMOS50 and f-BIPA50TMOS50, respectively.

Silicone based compounds T4M4Q and T4D4 have rather poor miscibility with water, so their sol-gel reactions were catalyzed by HCl so that the mixture could quickly become homogeneous. Several sol-gel coatings were formulated using T4M4Q and T4D4, along with TMOS and/or dimethyldimethoxysilane (DMDMS). Both T4M4Q and T4D4 coatings were hydrolyzed for 5-10 min. before being coated on bis-A PC substrates.

Table 7.3. Formulation of T4M4Q/TMOS sol-gel coatings

Name	T4M4Q (g)	TMOS (g)	Water (g)	ⁱ PrOH (g)	0.5 N HCl (g)
T4M4Q100	4	0	0	4	0.5
T4M4Q67TMOS33	4	2	0.5	4	0.5
T4M4Q50TMOS50	4	4	0.9	8	0.5
T4M4Q40TMOS60	4	6	1.4	10	0.5

Table 7.4. Formulation of T4D4/TMOS/DMDMS sol-gel coatings

Name	T4D4 (g)	TMOS (g)	DMDMS (g)	THF (g)	ⁱ PrOH (g)	Water (g)	HCl 0.5 N (g)
TD100	6	0	0	0	5	0.25	0.25
TD50TMOS50	2.5	2.5	0	4	5	0.25	0.25
TD83TMOS17	5	0	1	4	5	0.25	0.25
TD67TMOS33	4	0	2	4	5	0.25	0.25

F-THPDEA and f-TEA coating recipes were formulated similar to the f-DETA coating recipe. However, due to the presence of free amine groups in these compounds, sufficient amounts of acid had to be added to neutralize the basic amine groups and to conduct sol-gel reactions in weak acidic media (see Table 7.5 and 7.6). Hydrolysis under basic conditions did not form sols suitable for preparing coatings. Both f-THPDEA and f-TEA coatings were hydrolyzed for 15-30 min. before being applied on bis-A PC substrates.

Table 7.5. Formulation of f-THPDEA/TMOS sol-gel coatings

Name	f-THPDEA (g) (70 % in acetone)	TMOS (g)	ⁱ PrOH (g)	H ₃ PO ₄ 0.5 M (g)
f-THPDEA100	4	0	2	4
f-THPDEA65TMOS35	4	1.5	2	4
f-THPDEA50TMOS50	4	2.8	2	4

Table 7.6. Formulation of f-TEA/TMOS sol-gel coatings

Name	f-TIEDA (g) (70% in acetone)	TMOS (g)	2- ⁱ PrOH (g)	HCl 1N (g)	H ₃ PO ₄ 0.5 M (g)
f-TEA100	4	0	2	2	2
f-TEA65TMOS35	4	1.5	2	2	2
f-TEA50TMOS50	4	2.8	2	2	2

F-DISIL and f-ISOP have two urea linkages in their molecules, and their coating formulation is rather similar to that of f-DETA and f-BIPA. Coatings based on these compounds were formulated according to Table 7.7. The f-DISIL and f-ISOP recipes were hydrolyzed for about 6 hrs. and 15-30 min., respectively, before being applied on bis-A PC substrates.

A series of f-EPXY/TMOS coatings was formulated according to the recipe in Table 7.8. Again, due to the presence of free amine in the system, an excess amount of acid was added to

conduct the sol-gel process in acidic media. These recipes were pre-hydrolyzed for 20-55 min. before being coated, dried, and cured on bis-A PC substrates.

Table 7.7. Formulation of f-DISIL and f-ISOP sol-gel coatings.

Name	f-DISIL (g) (70% in ⁱ PrOH)	TMOS (g)	2- ⁱ PrOH (g)	Water (g)	Glacial HAc (g)
f-DISIL50TMOS50	4	2.8	2	4	0.1
f-DISIL44TMOS56	4	3.5	2	4	0.1
Name	f-ISOP (g) (70% in ⁱ PrOH)	TMOS (g)	2- ⁱ PrOH (g)	Water (g)	0.5 M H ₃ PO ₄ (g)
f-ISOP50TMOS50	4	2.8	2	3.5	0.5 g
f-ISOP44TMOS56	4	3.5	2	3.5	0.5 g

Table 7.8. Formulation of f-EPXY/TMOS sol-gel coatings

Name	f-EPXY (g) (50% in MeOH)	TMOS (g)	H ₃ PO ₄ 0.5 M (g)
f-EPXY100	4	0	4
f-EPXY80TMOS20	4	0.5	4
f-EPXY67TMOS33	4	1	4
f-EPXY50TMOS50	4	2	4

7.2.4. Sol-Gel Coatings by Two-Step Hydrolysis

The two-step approach was carried out by pre-hydrolyzing one or several components before adding the others. By this method, a tetraalkoxysilane or a metal alkoxide such as TMOS was pre-hydrolyzed and discrete inorganic clusters or particles were pre-formed. A trialkoxysilylated organic compound was added later to form a relatively soft and tough continuous gel, which binds the pre-formed hard and brittle inorganic clusters or particles. Since nanometer-scale silica and many metal oxide colloids are commercially available, the pre-preparation of these particles could be omitted. Colloids or sols obtained by the two-step

approach were similarly spin- or dip-coated on bis-A PC or aluminum substrates, dried, and thermally cured into a hard gel layer.

Tetraalkoxysilanes usually form open and extended silica clusters in acidic media, but in basic media, they form more contracted clusters or particles¹⁸. The size and openness of these clusters can be characterized by their radius of gyration and mass fractal dimension, respectively. Since extended clusters can interpenetrate more efficiently, an acid-catalysis process should lead to a more uniform structure than a base-catalysis process.

F-DETA50TMOS50 coatings, with the overall composition corresponding to f-DETA22TMOS22W31-HAC140, were prepared via a two-step acid-catalyzed hydrolysis approach. First, TMOS was pre-hydrolyzed by one eighth of the total amount of water using an acetic acid catalyst. Then f-DETA and the rest of water were added and the mixture was further hydrolyzed. The resulting sols had a slightly longer gelation time than those prepared by the one-step approach, but both offered similar abrasion resistance. However, SAXS experiments indicated that these coatings did not have obvious non-uniformity in structure.

Considering that base-catalyzed sol-gel reactions often yield clusters or particles of a higher mass fraction dimension, if the TMOS component was pre-hydrolyzed using a basic catalyst, the resulting f-DETA/TMOS coating is expected to have a microphase-separated structure. In this research, commercial silica and zirconia colloids were directly used in experiments to form microphase-separated structures with methyltrimethoxysilane (MTMS), f-DETA and f-EPXY.

7.2.4.1. The MTMS/Metal Oxide System

The MTMS/silica system was prepared according to the patents of Clarke^{144,145}, and used as a reference. Commercial alumina and zirconia colloids were also used, but these materials caused quick flocculation of the silane component and hence were not suitable for coating applications. The following is a procedure for the preparation of MTMS60Silica40 coatings.

To a 100 ml beaker were added 20 g of methyltrimethoxysilane (97%, Gelest), 0.4 g of acetic acid and 10 g of water. The mixture was stirred for 30 min. so that the silane was partially hydrolyzed. Then 27 g of colloidal silica (Ludox, TM-50) were added and the mixture was

stirred for 40 hrs. This mixture was directly spin-coated on a bis-A PC substrate, dried at room temperature, and further cured at 125°C for 4 hrs. This system was used as a reference for newly developed systems.

7.2.4.2. The F-DETA/Silica System

F-DETA was pre-hydrolyzed so that it became compatible with silica or metal oxide colloids. Several f-DETA/silica coatings were successfully formulated according to Table 7.9. However, the binary systems of f-DETA with alumina and zirconia were disappointing. Similar to the case of the MTMS system, addition of alumina and zirconia also caused rapid flocculation of the f-DETA component.

Table 7.9. Formulation of f-DETA/Silica coatings

Name	f-DETA (g) (70% in 2-propanol)	2- ¹ PrOH (g)	Water (g)	Glacial HAc (g)	Ludox silica (50%) (g)
f-DETA100	4	2	4	0.1	0
f-DETA74Silica26	4	2	4	0.1	2
f-DETA58Silica42	4	2	4	0.1	4
f-DETA48Silica52	4	2	4	0.1	6

7.2.4.3. The F-EPXY System

F-EPXY is a hexadentate ligand (includes 4 OHs and 2 N), so it is rather compatible with metal oxide colloids. Titanium butoxide could co-hydrolyze with this compound and formed very transparent sol-gel coatings. In addition, transition metal compounds including copper sulfate, copper chloride, nickel chloride, and cobalt chloride can be incorporated into these systems without precipitation of metal salt crystals. WAXS analysis indicated gels of f-EPXY with metal salts were amorphous, and SAXS indicated that the gel structure was microscopically uniform. F-EPXY/ZrO₂ and f-EPXY/Ti(OBu)₄ were formulated according to [Table 7.10](#).

Table 7.10. Preparation of f-EPXY derived sol-gel coatings.

Name	f-EPXY (g) (50% in methanol)	2- ¹ PrOH (g)	Water (g)	Zirconia (20%) (g)	Ti(OBu) ₄ (g)
f-EPXY71ZrO29	4	2		2	
f-EPXY56ZrO44	4	2		4	
f-EPXY45ZrO55	4	2		6	
f-EPXY67TiOBu33	4	2	4		1
f-EPXY50TiOBu50	4	2	4		2

7.2.5. Sol-Gel Coatings By Moisture Vulcanization

Both the one-step approach and the two-step approach involved addition of water into the silane or metal alkoxides systems, which immediately started the hydrolysis and condensation. Therefore, these approaches could only be used to form two-part sol-gel coating formulae. The moisture vulcanization method was used to formulate one-part coating recipes. By this method, the coating recipe usually included silane components and a catalyst, while the water was provided by moisture from the air.

Moisture-curing f-DETA/TMOS coatings were formulated by mixing the silane components with titanium butoxide, which serves as a catalyst as well as a source of the inorganic phase. Moisture from the air is the source of water for hydrolysis and condensation of the silanes in the systems. The TMOS used in the recipe was pre-hydrolyzed ($r \sim 0.5$, acetic acid catalyst) to avoid its evaporation during the curing process. Several f-DETA coatings were prepared according to the formulations in [Table 7.11](#). The moisture-curing recipes were spread on aluminum or bis-A substrates and then the coated substrates were placed in a close chamber (~ 20 - 24°C , humidity $\sim 100\%$) to vulcanize. The coatings generally became nontacky within 4-6 hrs. After 3-4 days of drying at room temperature, the coating reached a pencil hardness of 5-8H depending on the concentrations of TMOS and the catalyst. The system was also cured at room temperature for ca. 24 hrs. and post-vulcanized at 80°C and a humidity of 60% for 2 hrs. After this treatment, the pencil hardness of the coating were typically beyond 9H, the highest rating in pencil hardness. By this way, the curing period can be significantly shortened.

Table 7.11. Formulation of f-DETA derived moisture-curing sol-gel coatings

Name	f-DETA (g) (70 wt% in ethanol)	EtOH (g)	TMOS (40wt %) (g)	Ti(OBu) ₄ (g)
f-DETA97Ti3	4	2		0.1
f-DETA85Ti15	4	2		0.5
f-DETA74Ti26	4	2		1
f-DETA78TMOS22	4	2	2	0.5
f-DETA64TMOS36	4	2	4	0.5
f-DETA54TMOS46	4	2	6	0.5
f-DETA47TMOS53	4	2	8	0.5

7.3. RESULTS AND DISCUSSION

7.3.1. Optical Properties

Sol-gel coatings formulated using the chemicals in [Table 7.1](#) were generally very transparent. If the starting silane-modified compound contained no free amine groups, exposure of these sol-gel coatings at a temperature less than 180°C for a limited time (~4 hrs.) usually did not cause obvious yellowing, which was caused by preferential absorbance of light within visible region of 400-520 nm. F-EPXY series coatings were usually transparent, but they became slightly brownish after being heated at a temperature over 150°C in air likely due to oxidation of the tertiary amine groups in the system. F-TEA and f-THPDEA monomers usually turned brownish after stored for a two-three week period, however, coatings derived from newly prepared monomers were rather transparent. [Figure 7.5](#) shows the UV/Vis/Infrared spectra of sol-gel coatings derived from f-DETA, MTMS, f-TEA, T4M4Q, and f-THPDEA. F-DETA, MTMS and T4M4Q related coatings had no absorbance bands in the visible light region, while f-TEA and f-THPDEA related coatings showed some absorbance in the violet region, thus exhibiting some brownish color. The tested coatings exhibited rather large difference in

transmittance (Fig. 7.5) due to the differences in surface smoothness. T4M4Q and T4Q4 formed extremely smooth and transparent films although these coatings were not abrasion resistant.

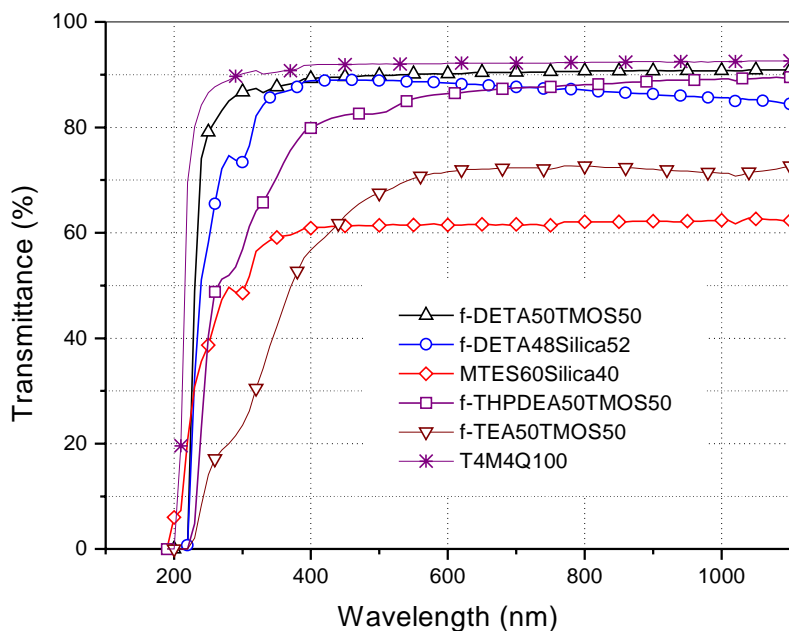


Fig. 7.5. UV/Vis/Infrared spectra of several sol-gel coatings

The refractive index (at 633 nm) was measured for a f-DETA/silica/HAC series, a f-DETA/TMOS/Ti(OBu)₄, and a f-EPXY/ZrO₂ series. HAC, and Ti(OBu)₄ were the catalysts for the first two systems, respectively. In the third system, ZrO₂ served as a catalyst as well as an inorganic component. Generally, the refractive index increased with the concentration of ZrO₂, but decreased with the increase of the silica concentration (Fig. 7.6). Since metal oxide colloids are usually of low density (i.e. low extent of condensation), their addition only leads to a limited increase in refractive index.

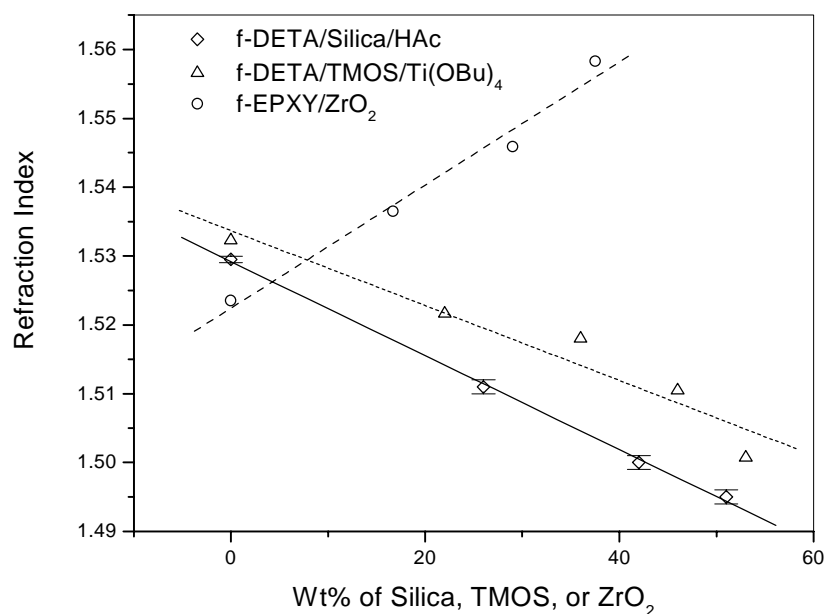


Fig. 7.6. The relationship between the refractive index and the concentration of silica or zirconia.

7.3.2. Morphology

Due to reactivity differences, hydrolysis of multiple component systems often results in non-uniformity in the gel structures. Even in unitary systems, the hydrolysis condition, aging time, and drying process can also cause fluctuations in the structure (i.e. pores and extent of condensation). SAXS experiments indicated that relatively uniform f-DETA/TMOS, f-DISIL/TMOS and f-ISOP/TMOS gels could be developed by *the one-step approach* in water-abundant media using an acetic acid catalyst. However, with the same coating recipe, but a hydrochloric acid catalyst, the resulting gels usually exhibited obvious particulate features (Chapter 6).

The two-step approach is, in principle, more likely to result in non-uniform structures. The structural non-uniformity is related to the fractal dimension of the pre-formed clusters. Clusters of a low fractal dimension can interpenetrate each other, thus leaving few pores and compositional fluctuations. For the f-DETA50TMOS50 coating mentioned in Section 7.2.4,

which were developed by two acid-catalyzed hydrolysis steps using an acetic acid catalyst, no obvious interparticle SAXS correlation peak or shoulder was found in the low angle region ($s=10^{-3}$ - 10^{-1} \AA^{-1}). It is conjectured that the pre-hydrolyzed TMOS was in the form of extended clusters or simple low molecular weight polymers. Both cases could lead to higher structural uniformity.

In contrast, coatings incorporated with a Ludox TM50 silica colloid showed apparent microphase-separated morphologies. Figure 7.7 shows SAXS profiles on both linear-linear (A) and log-log (B) scales for the f-DETA/silica coatings and a MTMS60silica40 coating (Section 7.2.4). These coatings displayed rather strong scattering of x-rays in the low angle region ($s<0.04$ \AA^{-1}). The first and second order correlation Bragg-like peaks are clear in the SAXS profile (Fig. 7.7 a). The correlation distances (ξ) for the f-DETA50Silica48, f-DETA58Silica42 f-DETA574Silica26 gels are estimated to be 290 \AA , 356 \AA and 448 \AA , respectively, which increase, as expected, on the order of reducing the concentration of silica. In addition to the spatial correlation between clusters, the SAXS profiles also show a common feature: a power law region within $s=0.08$ - 0.04 \AA^{-1} (Fig. 7.7 b). After accounting for slit smearing, this region has a Porod slope of ca. -3.1 for all the samples. If the influence of correlation on the Porod slope is negligible in this angular region (generally a reasonable assumption when $\xi \gg R_g$), this Porod slope value suggests that the silica clusters in the system are in the form of surface fractals.

Without a retardant such as acetylacetone, co-hydrolysis of the metal alkoxide with f-DETA usually led to some precipitation of metal oxides. Addition of zirconia and alumina colloids to pre-hydrolyzed f-DETA and MTMS also caused flocculation of the silane component. However, f-EPXY has rather good compatibility with metal oxide colloids because the compound is a hexadentate ligand. Transparent films were prepared by co-hydrolysis of f-EPXY with $\text{Ti}(\text{OBu})_4$ or hydrolysis of f-EPXY in the presence of a zirconia colloid, a metal chloride, or a metal sulfate. Figure 7.8 shows the SAXS profiles of the f-EPXY50TiOBu50 gel and f-EPXY67TiOBu33 gel. The f-EPXY50TiOBu50 gel showed an obvious cluster correlation shoulder at $s=0.024$ \AA^{-1} ($\xi=40$ \AA). The f-EPXY67TiOBu33 did not show an obvious correlation shoulder. It is likely that the former system has included more titanium ions than can be chelated by f-EPXY, so titania particles begin to form in the system.

Figure 7.9 shows SAXS profiles of f-EPXY coatings that include zirconia colloidal particles. Except for f-EPXY100, whose sol-gel reactions were catalyzed by hydrochloric acid catalyst, all others were catalyzed directly by zirconia colloids. As expected, all these coatings showed moderate shoulders in these scattering profiles, which are believed to be caused by correlation of zirconia particles ($\xi \sim 250 \text{ \AA}$).

Mixtures of f-DETA and titanium butoxide can form transparent sol-gel films via moisture vulcanization. Figure 7.10 shows SAXS profiles for the moisture vulcanized pure f-DETA coatings (Table 7.11). Obvious correlation peaks or shoulders are revealed in the SAXS profiles for films f-DETA97Ti3, f-DETA85Ti15, and f-DETA74Ti26 at $s \sim 0.015$, 0.02, and 0.03 \AA^{-1} ($\xi \sim 67$, 50, and 33 \AA), respectively. This suggests that the titanium butoxide had hydrolyzed and condensed into dispersed particles in the matrix of f-DETA gel. The moisture cured f-DETA48TMOS46 gels in Table 7.11 were also investigated by SAXS. However, due to a low $\text{Ti}(\text{OBU})_4$ concentration, no obvious correlation peak or shoulder was revealed by SAXS experiments.

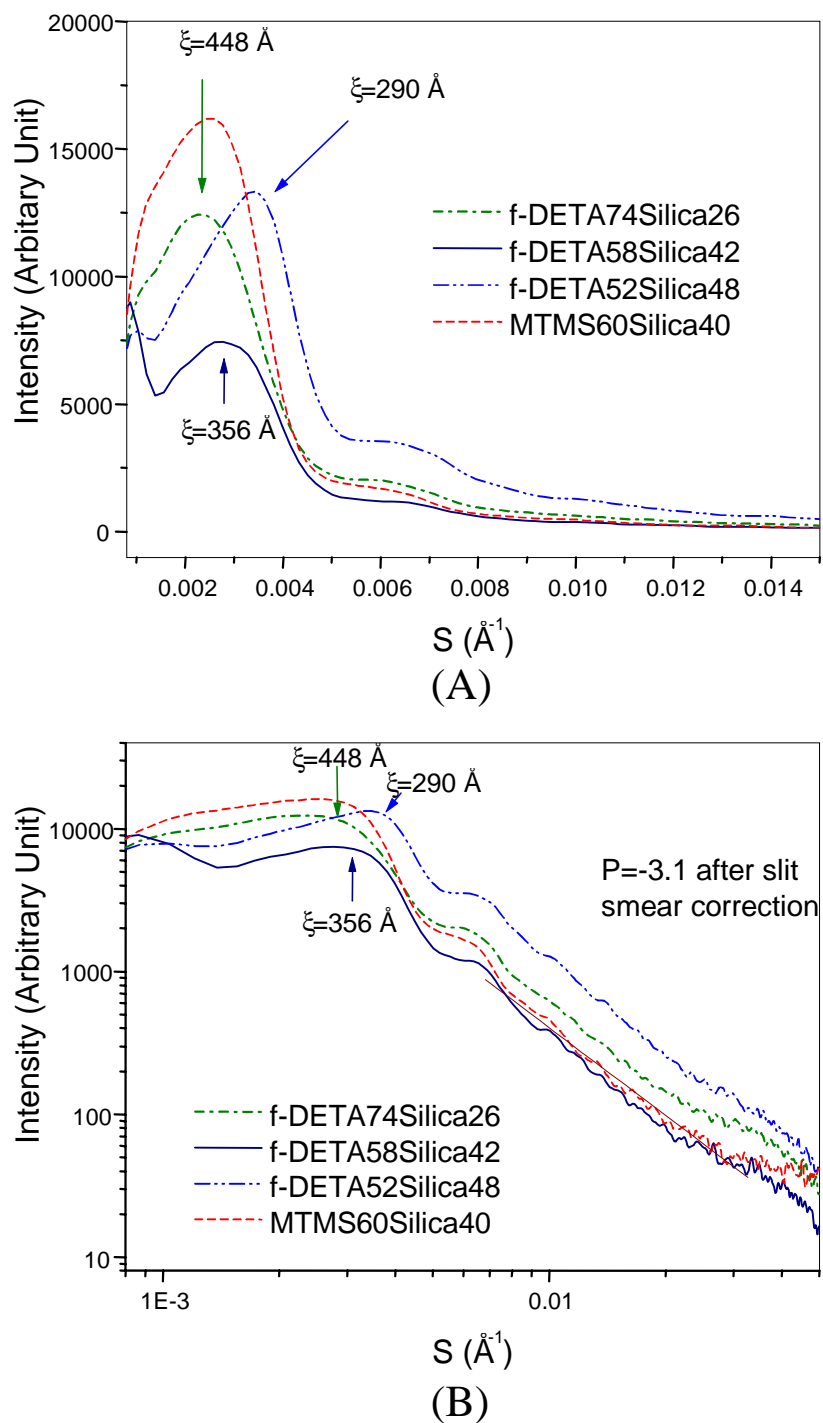


Fig. 7.7. SAXS profiles for sol-gel coatings containing Ludox TM-50 silica. (A) Linear plot, (B) Double logarithm plot.

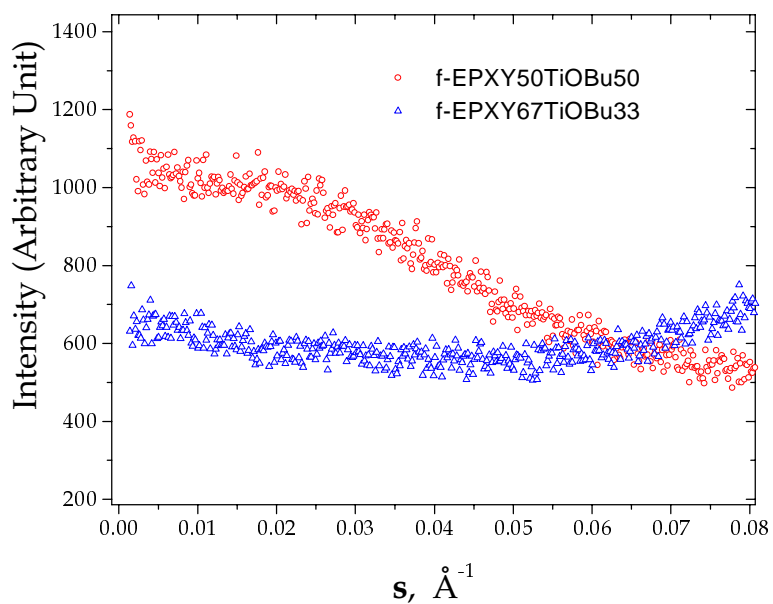


Fig. 7.8. SAXS profiles for sol-gel coatings involving f-EPXY and titanium butoxide

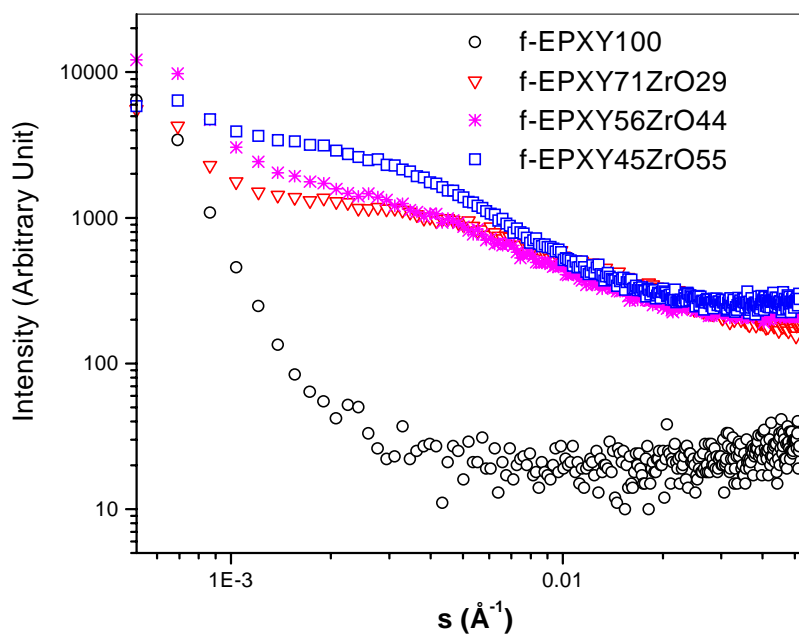


Fig. 7.9. SAXS profiles for the f-EPXY coatings containing titanium butoxide.

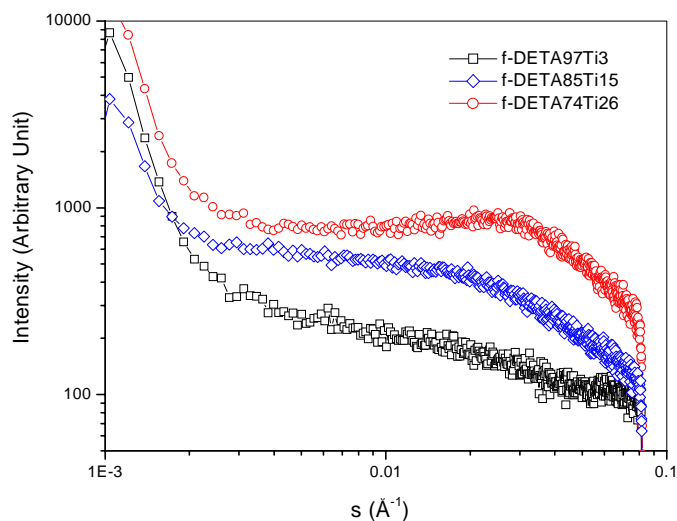


Fig. 7.10. SAXS profiles for RT moisture vulcanized f-DETA sol-gel coatings

7.3.3. Hardness and Abrasion Resistance

Sol-gel coatings derived from compounds in [Table 7.1](#) were tested for their potential as abrasion resistant coatings. Taber abrasion tests were widely used to compare the abrasion resistance, and Vickers hardness was also measured for several series of coatings. The test results are listed in [Table 7.12](#).

[Figures 7.11-7.13](#) reveal surface features of Taber tracks on coatings (with bis-A PC substrate) based on systems f-TEA/TMOS, f-THPDEA/TMOS, and f-DETA/silica. Wide deep scratches as well as fine shallow scratches occurs as a “X “ type pattern can be observed in the Taber wear tracks. It is generally believed that the majority of the transparency loss of the optical coatings and substrates is caused by the presence of only a few wide and deep scratches. By comparing the hardness value to the abrasion resistance in f-DETA/silica, f-TEA/TMOS, and f-THPDEA /TMOS coatings systems ([Table 7.12](#)), it can be easily concluded that a moderate increase in the concentration of the inorganic hard component can lead to significant increases in hardness and abrasion resistance. However, the increase in hardness may often be offset by increases in brittleness and poor adhesion, which are harmful to the abrasion resistance. The

balance between the hardness and brittleness of the coating should eventually lead to a proper concentration of the hard inorganic component(s) to provide best abrasion resistance. For the f-DETA/TMOS system, the suitable ratio of TMOS to f-DETA was around 1:1.

Figure 7.14 shows micrographs of Taber tracks on moisture cured f-DETA coatings containing different amounts of titanium butoxide. The moisture-cured coatings were prepared on aluminum substrates and cured at room temperature for about 4 weeks. The Taber tests involved a pair of CS10 wheels, a 500-gram load per wheel and 50 cycles of abrasion. The course faint fringe patterns in these micrographs are due to the surface features of the aluminum substrate formed during its manufacturing, while the “X” pattern scratches are due to Taber abrasion. As indicated Table 7.12 and Fig. 7.14, the abrasion resistance of moisture vulcanized f-DETA increases with the concentration of $\text{Ti}(\text{OBu})_4$. The presence of $\text{Ti}(\text{OBu})_4$ is believed to promote the abrasion resistance by increasing the extent of condensation as well as the concentration of the inorganic component. Titanium butoxide is a catalyst, so increasing its concentration undoubtedly raises the extent of condensation. On the other hand, as an inorganic component, increasing its concentration can also raise the hardness. According to Table 7.12, the f-DETA₅₄TMOS₄₆ coating vulcanized at 80°C and a humidity of 60% can maintain a transmittance of ~95% transmittance after 500 cycles of abrasion (CS10 wheels and a 500-gram load per wheel). Although it is less abrasion resistant than coatings prepared by the two-part coating formulae previously described, it still significantly improves the abrasion resistance of both the bis-A PC and aluminum substrates.

The abrasion resistance of the T4M4Q and T4D4 coating systems is unexpectedly low. These coatings suffered from an immediate severe surface damage as soon as the abrasion test was initiated. Even films derived from methyltrimethoxysilane could offer much better abrasion resistance than these coatings. It is believed that the high concentration of Si-CH₃ groups in these systems decreased the cohesion of the material, thus leading to a poor performance. In addition, the short organic arms (only two -CH₂- groups) between the siloxane core to the triethoxysilyl groups might not provide sufficient flexibility for the coating to exhibit reasonable toughness.

The f-EPXY/TMOS coating had an abrasion resistance not inferior to a similarly formulated f-DETA/TMOS coating. F-EPXY₅₀TMOS₅₀ had a transmittance of 98.7% after 500

cycles of abrasion and f-EPXY65TMOS35 also showed a transmittance of 98.1%. However, this coating series seemed to be more brittle than its f-DETA counterpart at the same TMOS concentration. For example, a slight bending of a polycarbonate substrate with a f-EPXY50TMOS50 coating caused cracking of the coating; while under the same conditions, f-DETA50TMOS50 coatings, however, remained undamaged. As the TMOS concentration was reduced to 35%, then the f-EPXY coating could sustain some substrate bending and still had excellent abrasion resistance. Alumina, zirconia and titanium butoxide were incorporated into f-EPXY gels and formed coatings of good optical quality and moderate abrasion resistance. In general, the abrasion resistance of these coatings was inferior to their counterparts prepared using TMOS rather than the metal oxide colloids.

As indicated by [Table 7.12](#) and [Fig. 7.15](#), sol-gel coatings derived from compounds that include urea, urethane and epoxy residual linkages usually have rather good abrasion resistance. Coating MTMS60Silica40 also showed abrasion resistance that was only slightly inferior to that of coating f-DETA50TMOS50. However, the MTMS/silica coating was more brittle and even slight bending of the substrates could lead to serious cracking of the coating. Bis-A PC substrates with the f-DETA50TMOS50 and MTMS60Silica40 coatings ([Table 7.12](#)) were also submitted to Micro Photonics Inc. for quantitative scratch tests. The average critical load for the first failure in two scratch tests was found to be 123.5 mN and 71 mN for the two coatings, respectively. The results suggested that the f-DETA50TMOS50 coating could withstand a higher cutting force without failure than the MTMS60Silica40 coating.

Table 7.12. Sol-gel coatings and their curing conditions, hardness and abrasion resistance

Coatings	Curing Conditions	Vickers Hardness (kgf/mm ²)	Abrasion Resistance (%)
PC-Control	N/A	~22	84 ± 0.6 ^A
f-DETA50TMOS50	125°C/4 hrs.	93 ± 7	98.5 ± 0.5
f-DETA100		42 ± 7	89 ± 1
f-DETA74Silica26		68 ± 3	97.3 ± 0.1
f-DETA58Silica42		149 ± 5	98.0 ± 0.1
f-DETA48Silica52		Break	97.6 ± 0.8 ^C
f-DETA74Ti26		RT moisture Ca. 4 weeks	N/A
f-DETA54TMOS46	~ 90 ^B		
f-DETA54TMOS46	80°C moisture humidity 60%, 2 hrs.		95.4 ± 0.6
T4M4Q100	125°C/4 hrs.	N/A	~75
T4M4Q67TMOS33			~52
T4M4Q50TMOS50			~81
T4M4Q40TMOS60			~84
T4D4-100	125°C/4 hrs.	N/A	Extremely Poor
T4D4-50TMOS50			
T4D4-83TMOS17			
T4D4-67TMOS33			
MTMS60TMOS40	125°C/4 hrs.	Break	96.6 ± 0.4 ^C
f-IMPA50TMOS50	125°C/4 hrs.	N/A	98.0 ± 0.4
f-TEA100	125°C/4 hrs.	60 ± 1	93.8 ± 0.3
f-TEA65TMOS35		80 ± 4	97.6 ± 0.4
f-TEA50TMOS50		126 ± 3	97.6 ± 0.2
f-THPDEA100	125°C/4 hrs.	50 ± 3	86.8 ± 1.3
f-THPDEA65TMOS35		59 ± 4	94.6 ± 1.0
f-THPDEA50TMOS50		82 ± 4	97.0 ± 0.2
f-DISIL50TMOS50	125°C/4 hrs.	N/A	96.4 ± 0.9
f-DISIL44TMOS56			98.0 ± 0.4
f-ISOP50TMOS50			96.3 ± 0.5
f-ISOP44TMOS56			97.6 ± 0.3
f-EPXY67TMOS33	125°C/4 hrs.	N/A	98.1 ± 0.3
f-EPXY50TMOS50			98.7 ± 0.1 ^C

Taber Test: CS10 wheels, 500-gram load per wheel, and 500 cycles of abrasions

(A) 20 cycles of abrasions, (B) 50 cycles of abrasions.

(C) The coating cracked when the substrate was bent.

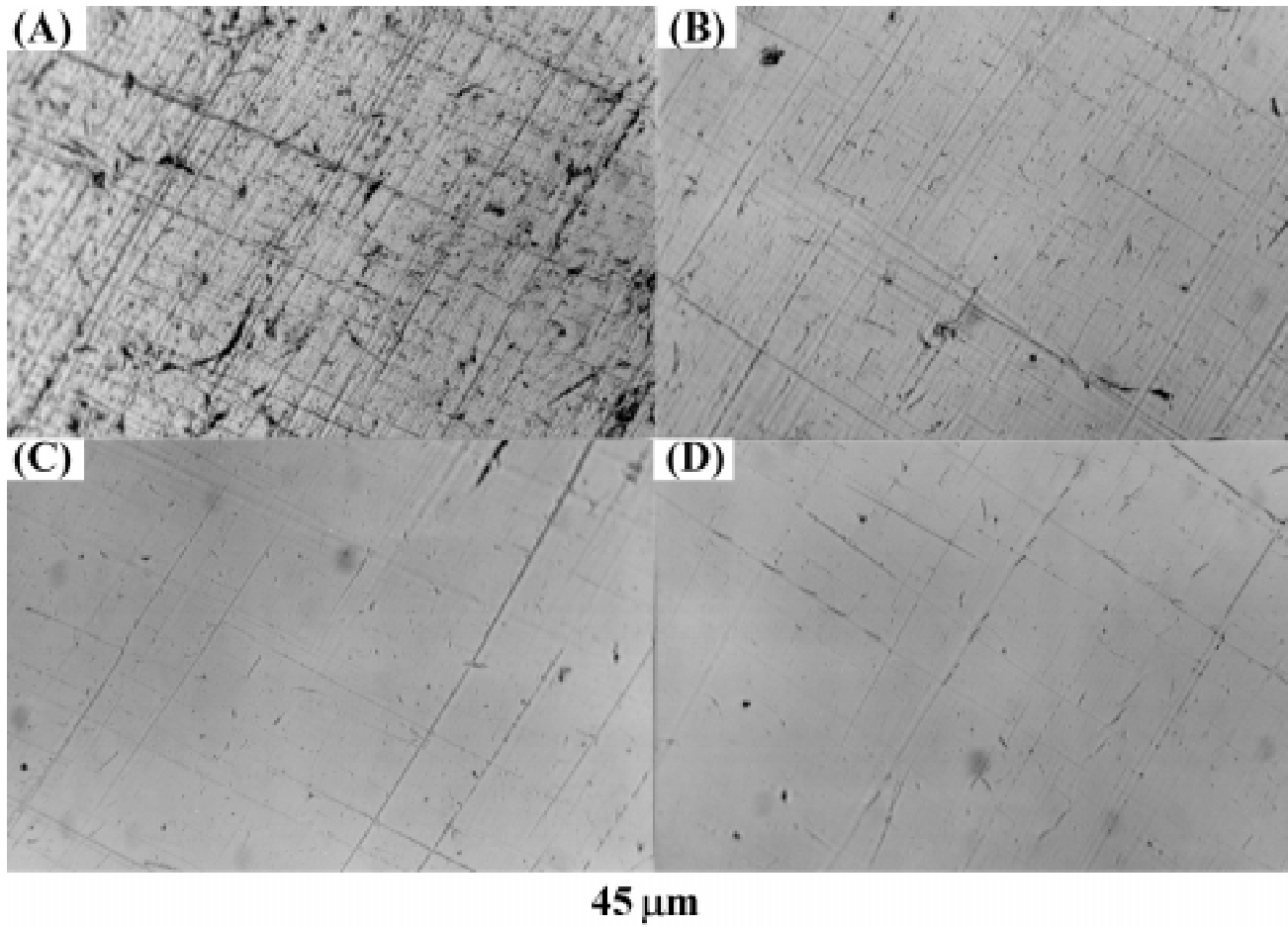


Fig. 7.11. Transmission optical micrographs of Taber wear tracks for bis-A PC substrates: (A) Uncoated (20 cycles), (B) coated with f-TEA100 (500 cycles), (C) coated with f-TEA65TMOS35 (500 cycles), (D) coated with f-TEA50TMOS50 (500 cycles). Taber tests utilized CS10 wheels and a 500-gram load per wheel.

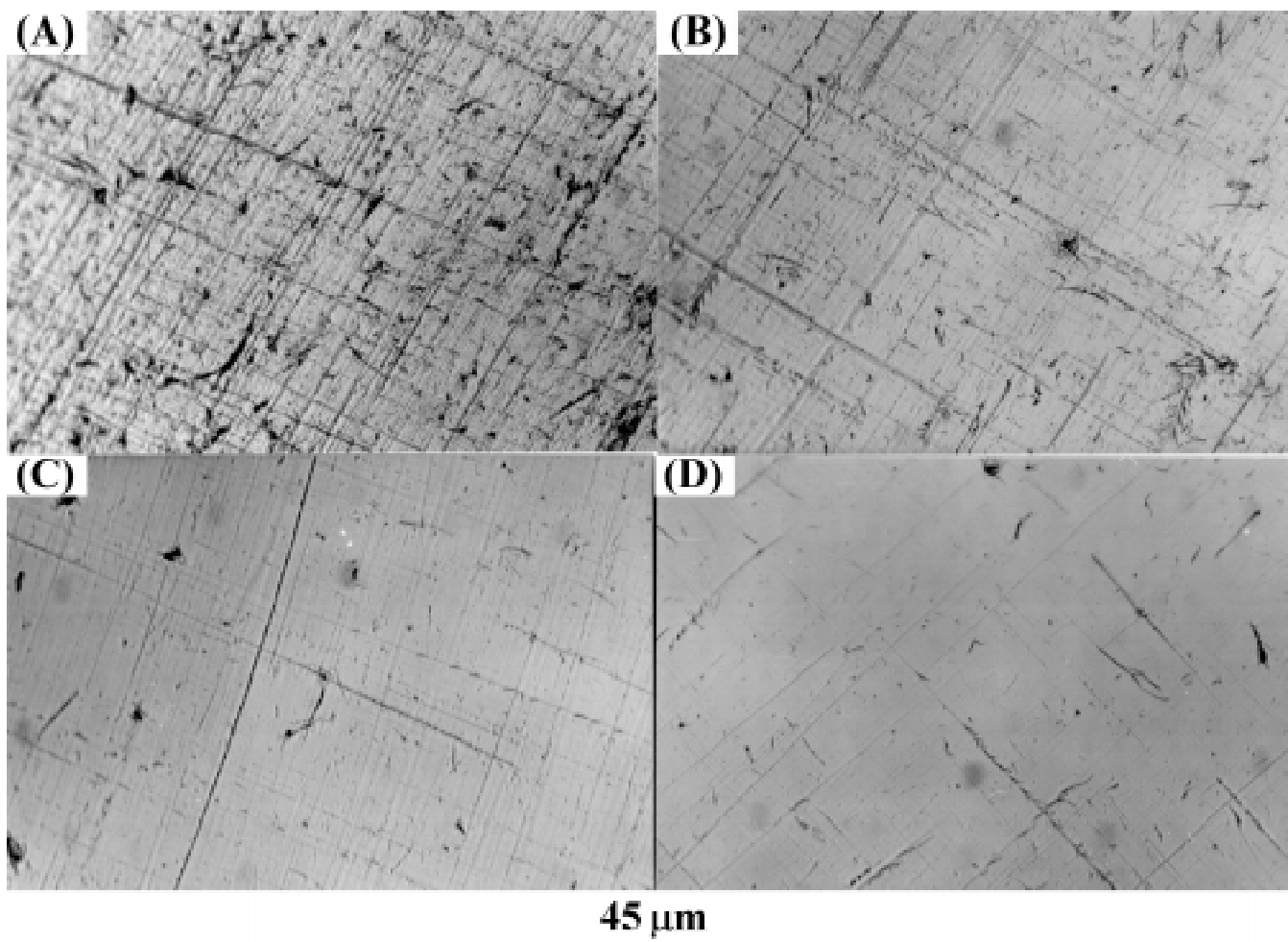


Fig. 7.12. Transmission optical micrographs of Taber wear tracks on bis-A PC substrates: (A) Uncoated (20 cycles), (B) coated with f-THPDEA100 (500 cycles), (C) coated with f-THPDEA65TMOS35 (500 cycles), (D) coated with f-THPDEA 50TMOS50 (500 cycles). Taber tests utilized a pair of CS10 wheels and a 500-gram load per wheel.

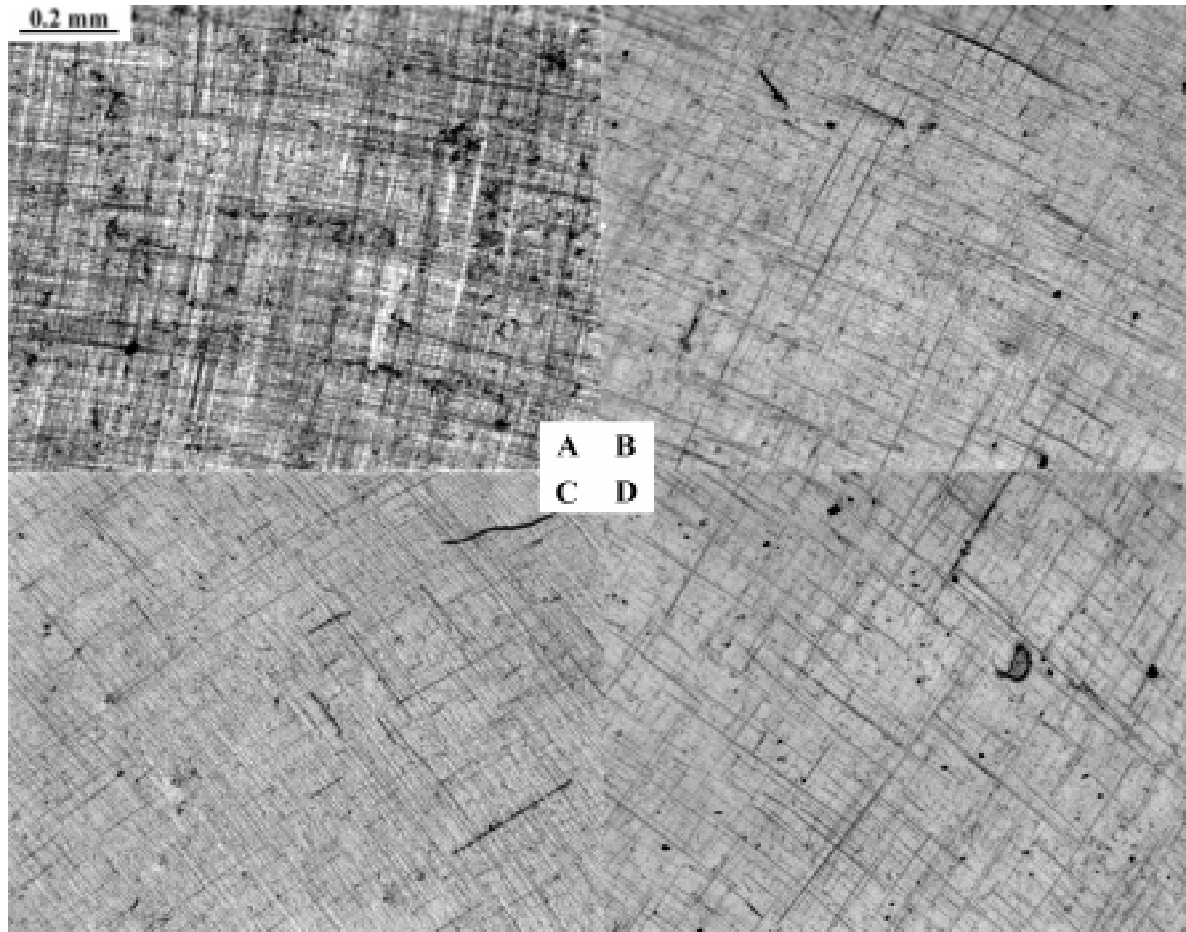


Fig. 7.13. Reflection optical micrographs (contrast intensified by gold coatings) of Taber wear tracks on bis-A PC substrates: (A) Uncoated (20 cycles), (B) coated with f-DETA74Silica26 (500 cycles), (C) coated with f-DETA58Silica42 (500 cycles), (D) coated with f-DETA48Silica52 (500 cycles). Taber tests utilized a pair of CS10 wheels and a 500-gram load per wheel.

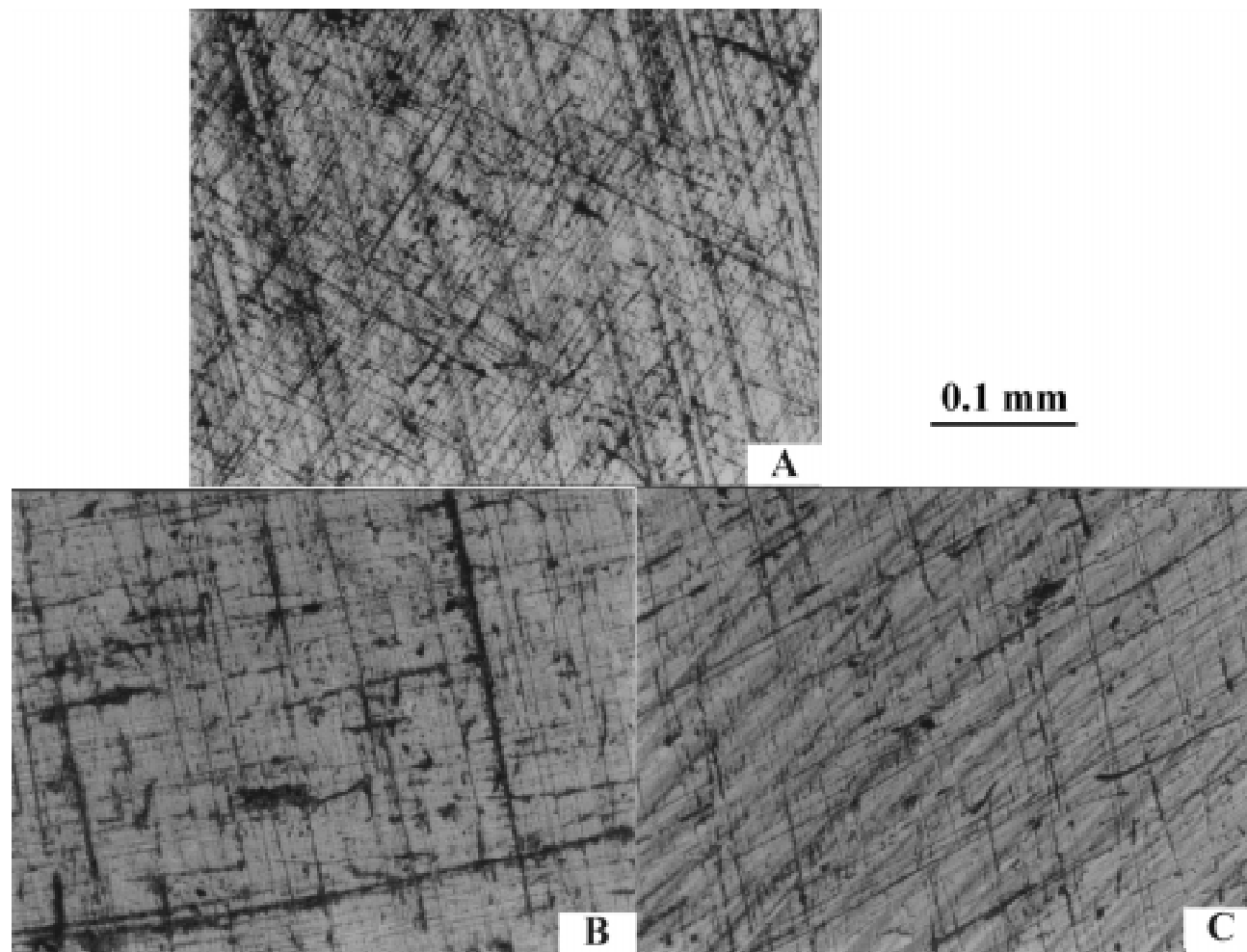


Fig. 7.14. Reflection optical micrographs (contrast intensified by gold coatings) for Taber wear tracks on aluminum substrates: (A) coated with f-DETA97Ti3 (B) coated with f-DETA85Ti15, (C) coated with f-DETA74Ti26. Coatings were cured by RT moisture vulcanization for ca. 4 weeks. Taber tests consisted of 50 cycles of abrasion with a pair of CS10 wheels and a 500-gram load per wheel.

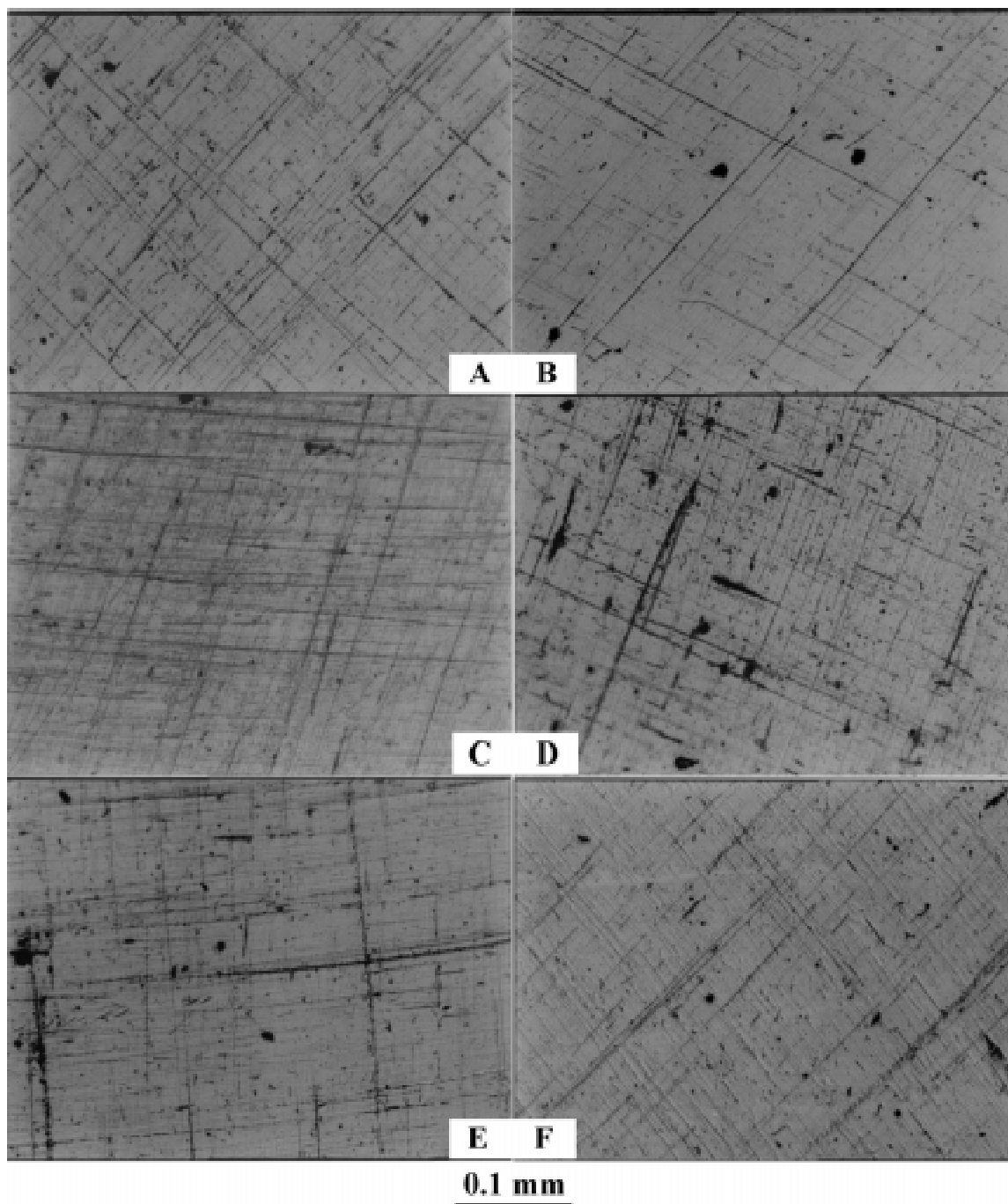


Fig. 7.15. Reflection optical micrographs (scratch contrast intensified) for Taber tracks on bis-A PC substrates coated with: (A) f-DETA50TMOS50, (B) f-BIPA50TMOS50, (C) MTMS60Silica40, (D) f-ISOP44TMOS66, (E) f-THPDEA50TMOS50, (F) f-DISIL50 TMOS50. Taber tests utilized 500 cycles of abrasion with a pair of CS10 wheels and a 500-gram load per wheel.

7.4. CONCLUSIONS

Many trialkoxysilylated organic compounds have been synthesized and used to prepare sol-gel derived coatings. The sol-gel process was carried out via the one-step approach, two-step approach or moisture vulcanization approach. The two-step approach usually involves a pre-hydrolysis step of TMOS or a metal alkoxide, followed by a second hydrolysis step of trialkoxysilylated silane along with the pre-formed clusters of silica or a metal oxide. In the experiments, commercial silica, alumina, and zirconia were directly used so the first hydrolysis step was generally omitted. Coatings containing these colloidal particles usually showed microphase-separated structures. By moisture vulcanization, if the catalyst $\text{Ti}(\text{O}i\text{Bu})_4$ concentration is sufficiently high, the resulting coatings also show some form of microphase-separated morphologies.

Sol-gel coatings derived from all compounds were usually colorless. Storage of monomers f-TEA and f-THPDEA could lead to some brownish color, However, if freshly prepared monomers were used, gels derived from were usually colorless. The refractive index increased with the concentration of metal oxide or metal alkoxide, but decreased with the increase of silica or tetraalkoxysilane concentration. However, since these inorganic components were in a lower density state, their incorporation only leads to a limited increase in refractive index.

Trialkoxysilylated organic compounds containing urea groups, urethane, and epoxy residual groups formed very good abrasion resistant coatings. Siloxane based monomers such as T4M4Q and T4D4 could form high quality coatings or films but these coatings or films usually had extremely poor abrasion resistance. The coatings based on colloidal silica usually had good abrasion resistance comparable to those based on TMOS. Titania and alumina colloids were added to hydrolyzates of f-DETA and methyltrimethoxysilane, however, they resulted in flocculation of these silanes. Due to its chelating ethylenediamine structure, f-EPXY was quite compatible with titania, alumina and titanium butoxide, it formed very transparent sol-gel coatings with these compounds. These metal oxide-containing coatings offered good abrasion resistance although they are usually inferior to the TMOS or silica-containing coatings.

CHAPTER 8. COATINGS DERIVED FROM SPHEREOSILICATES

8.1. INTRODUCTION

Polyhedral oligosilsesquioxanes (POSSes) and sphereosilicates are structurally derived from polyhedral silicate ions by substituting hydrogen, alkyl or trialkylsilyloxy groups for the corner oxygen ions (Fig. 8.1). The term “silsesquioxane” refers to siloxane resins resulting from alkyltrialkoxysilanes and alkyltrichlorosilanes. POSSes and sphereosilicates with small or symmetrical corner groups are usually crystalline solids, and their solubility in organic solvents depends on the nature of the corner organic substituents. In the presence of an acid or base catalyst, these polyhedrals can polymerize to random network polysiloxane resins. The equilibrium mixture of a silsesquioxanes may also include some POSSes and their concentrations are dependent on the alkyl group and the concentration of the silsesquioxane. The equilibria between polyhedral and random silsesquioxanes are quite similar to those between cyclic and linear siloxanes. Many synthetic methods of cyclic siloxanes can be similarly used for polyhedral silsesquioxanes¹⁹³⁻¹⁹⁵. Polyhedral silicates can be derived from polyhedral silsesquioxanes or directly prepared by trialkylsilylation of polyhedral silicates^{196,197}. A comprehensive review addressing POSSes and sphereosilicates has been given by Feher¹⁹⁸.

During the past few years, inorganic-organic hybrid materials based on POSSes and sphereosilicates have received much attention. Such new materials include these polyhedrals in polymer backbones or side chains, thus forming molecular level hybridization. Since these cages are fully condensed, the polymerization or curing process can be performed in a way that yields no low molecular weight by-product, and hence principally avoids the shrinkage problem that plagues the sol-gel process of metal alkoxides. Hybrids with POSS in side chains have also been prepared via free radical co-polymerization of an olefin (PMMA) with a cyclopentyl or

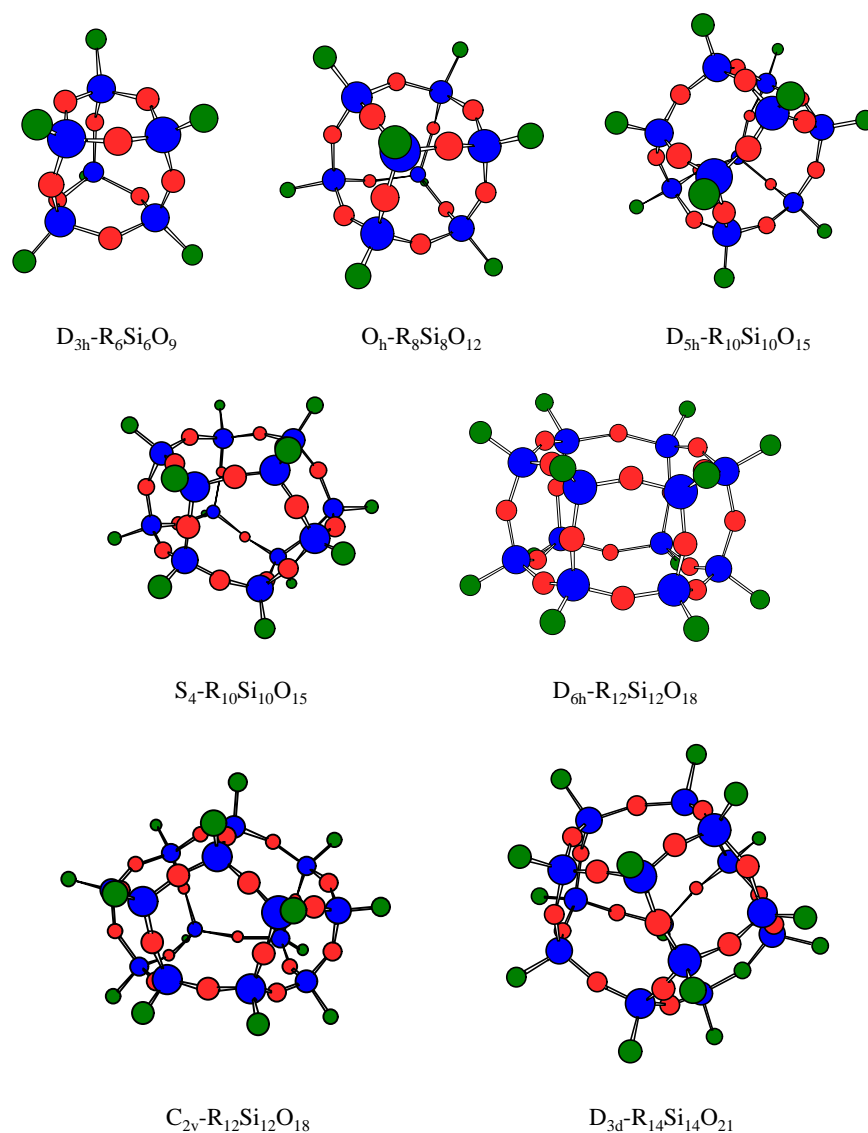


Fig. 8.1. Molecular structures of POSS and spherosilicates. The red, blue, and olive balls represent oxygen atoms, silicon atoms, and corner substituents, respectively, and the point group refers to the molecule structure.

cyclohexyl cubic POSS that has one of its eight corners capped with an olefin substituent^{199,200}. The incorporation of these cubic compounds is reported to increase the decomposition temperatures of the polyolefin. POSSes and spherosilicates may also be functionalized at more than one corner^{201,202}, and these monomers can be polymerized into thermosetting resins via reactions of the functional groups.

This chapter attempts to make some preliminary exploration of POSS or sphereosilicate-containing hybrids for their potential as abrasion resistant coatings. The research focuses on sphereosilicate resins derived from octakis(dimethylsilyl) cubic octasilicate (M^H8Q8) and octakis-(vinyl dimethylsilyl) cubic octasilicate (M^V8Q8), which can be easily prepared by trialkylsilylation of tetramethylammonium cubic octasilicate (Fig. 8.2)^{196,197,203}. M^H and M^V represent $-\text{SiH}(\text{CH}_3)_2$ and $-\text{Si}(\text{CH}_3)_2\text{CH}=\text{CH}_2$, respectively.

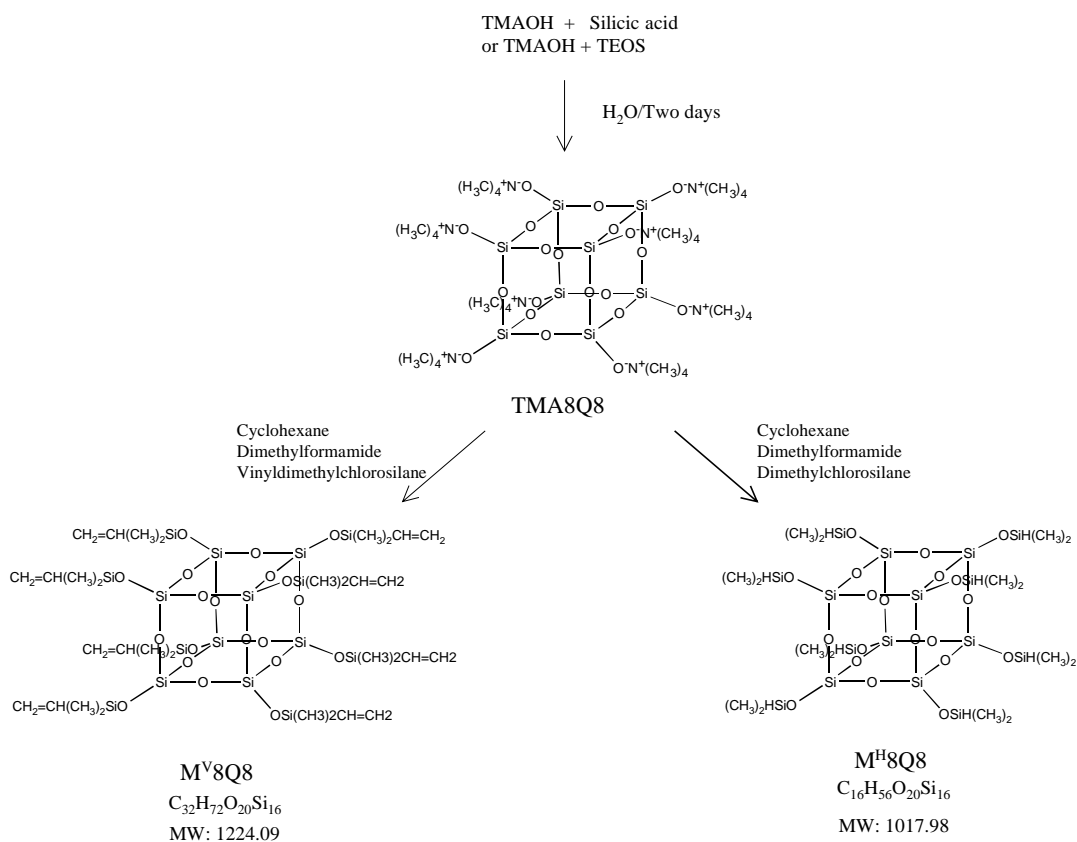


Fig. 8.2. Synthetic approaches for TMA8Q8, M^V8Q8 and M^H8Q8

8.2. EXPERIMENTAL

8.2.1. Characterization

Solution ^1H , ^{13}C and ^{29}Si NMR spectra were acquired on a 400 MHz Varian NMR spectrometer. ^{29}Si CPMAS NMR spectra were acquired on a Bruker MSL 300 MHz spectrometer using a 7 mm rotor, a 90° proton pulse angle and a contact time of 2 ms. GPC experiments were carried out in a chloroform solvent using a Waters 490 instrument with a set of 500 Å, 10^3 Å, 10^4 Å and 10^5 Å ultrastryragel column operated at 30°C . TG/DTA and DSC experiments were carried out using a Seiko system with an air flow of $20\text{ cm}^3/\text{min}$. FTIR spectrum was acquired on a Nicolet 50XB spectrometer with a Harrick reflectance attachment. Pencil hardness test (ASTM standard 3363-92a) was utilized to rate the scratch resistance of moisture cured coatings. The hardness value was expressed as the hardest pencil that failed to scratch the coating. The scale of hardness of pencils, arranged in the order of increasing hardness, is 6B, 5B, 4B, 3B, 2B, B, HB, F, H, 2H, 3H, 4H, 5H, 6H, 7H, 8H, and 9H.

8.2.2. Chemicals and Preparation

8.2.2.1. Tetramethylammonium Cubic Octasilicate (TMA8Q8)

A 1000 ml flask was charged with 71 g of tetramethylammonium hydroxide ($\text{TMAH} \cdot 5\text{H}_2\text{O}$, Aldrich), 22.8 g of silicic acid (Aldrich), and 348 g of water. The mixture in the flask was stirred at room temperature for 24 hrs. After 24 hrs. of reaction, most of the silicic acid was dissolved but the solution remained slightly milky due to the presence of unreacted silicic acid. The mixture was heated at 65°C for another 24 hrs. and the solution eventually became transparent. The solution was evaporated to about 100 ml using a vacuum evaporator. The remaining solution was slowly cooled to the room temperature, and TMA8Q8 gradually crystallized from the solution. The silicate crystals were filtered and dried at room temperature under reduced pressure (yield 90%) for 48 hrs. During the drying process, the primary crystals

underwent dehydration and broke down into fine crystals (ca. 1 mm in diameter). According to the literature, TMA8Q8 has a formula of $\text{Si}_8\text{O}_{20}[\text{N}(\text{CH}_3)_4] \cdot 116\text{H}_2\text{O}$ or $\text{Si}_8\text{O}_{20}[\text{N}(\text{CH}_3)_4] \cdot \sim 69\text{H}_2\text{O}$ ^{204,205}. ^{29}Si Solid State NMR spectroscopy indicated the TMA8Q8 prepared by the above method was exclusively a salt of cubic octasilicate (Fig. 8.3).

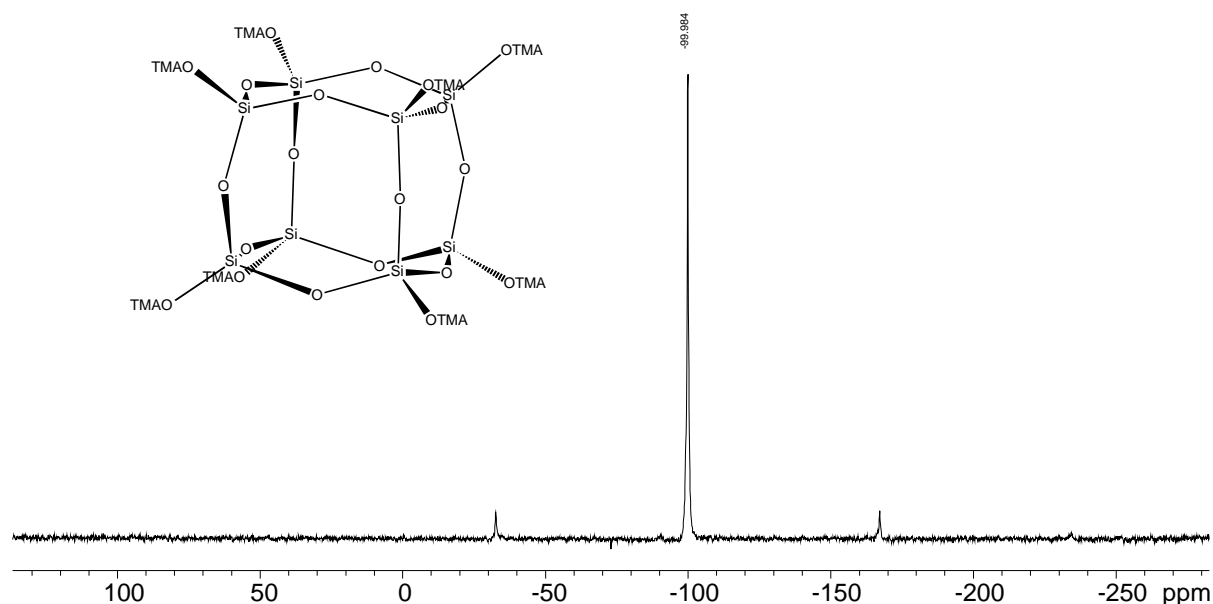


Fig. 8.3. The solid state ^{29}Si NMR spectrum for TMA8Q8 crystals. Peaks at -32 ppm and 168 ppm are side bands.

8.2.2.2. Vinyltrimethylsilyl Cubic Octasilicate ($\text{M}^{\text{V}}8\text{Q8}$)

Twelve grams of TMA8Q8 (slightly soluble in DMF) were added to 250 ml of dry DMF (Fisher) and 150 ml of cyclohexane. As the mixture was stirred, 100 ml of chlorodimethylvinylsilane were slowly added, and the vinyltrimethylsilylated cubes were extracted into the cyclohexane layer. After 30-60 min., the cyclohexane layer was separated and the DMF layer was extracted with another 100 ml of cyclohexane. The second cyclohexane layer was separated and combined with the first cyclohexane layer. The combined cyclohexane phase was washed

with deionized water three times to remove DMF and tetramethylammonium chloride and then pre-dried with anhydrous magnesium sulfate. After separating the magnesium sulfate, the cyclohexane phase was evaporated to 20 ml, and about 30 ml of ethanol were added to crystallize M^V8Q8. Vinyl cubic silicate crystals were filtered (about 4.5 g), and recrystallized in a small amount of cyclohexane (3.2 g). The final product was a white crystalline solid, which was soluble in chloroform, toluene, acetone and cyclohexane, but insoluble in methanol and ethanol. The structure of this compound was confirmed by its ¹H and ²⁹Si NMR spectra in Figs. 8.4 and 8.5.

8.2.2.3. Dimethylsilyl Cubic Octasilicate (M^H8Q8)

M^H8Q8 was prepared and separated by the same method used for M^V8Q8 unless vinyltrimethylchlorosilane was replaced by dimethylchlorosilane. The final product was also a white crystalline solid soluble in chloroform, toluene, acetone and cyclohexane, but not soluble in methanol and ethanol. The structure of this compound was confirmed by its ¹H and ²⁹Si NMR in Figs. 8.6 and 8.7.

In general, due to the presence of a large amount of water in the TMA8Q8 crystals, only a small fraction of chlorosilane was effectively used. The rest was consumed by the water in the crystals and became a disiloxane by-product.

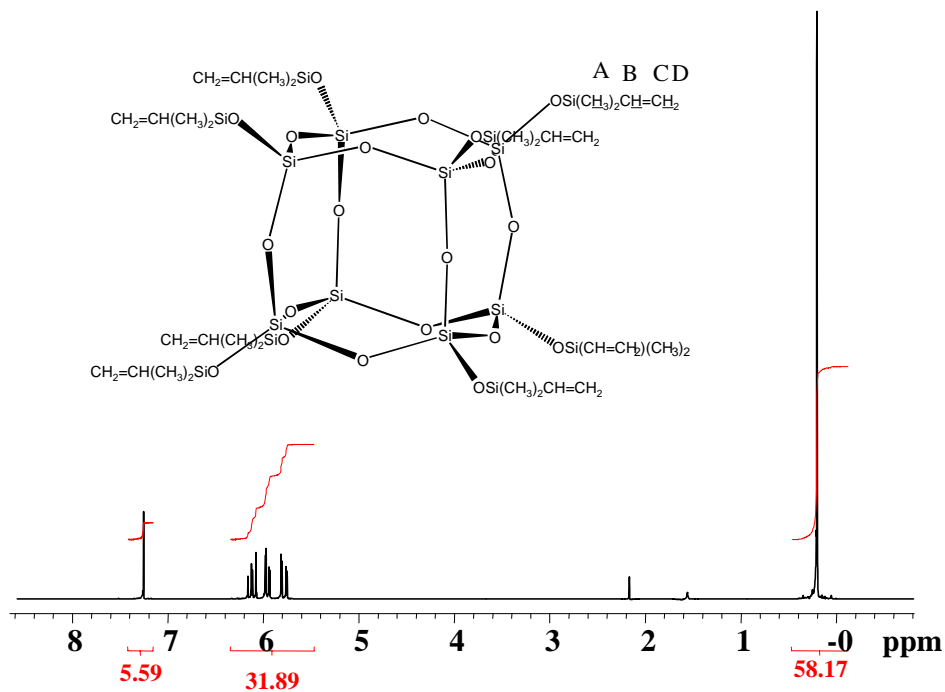


Fig. 8.4. The ^1H NMR spectrum for octakis(vinyl dimethylsilyl) cubic octasilicate

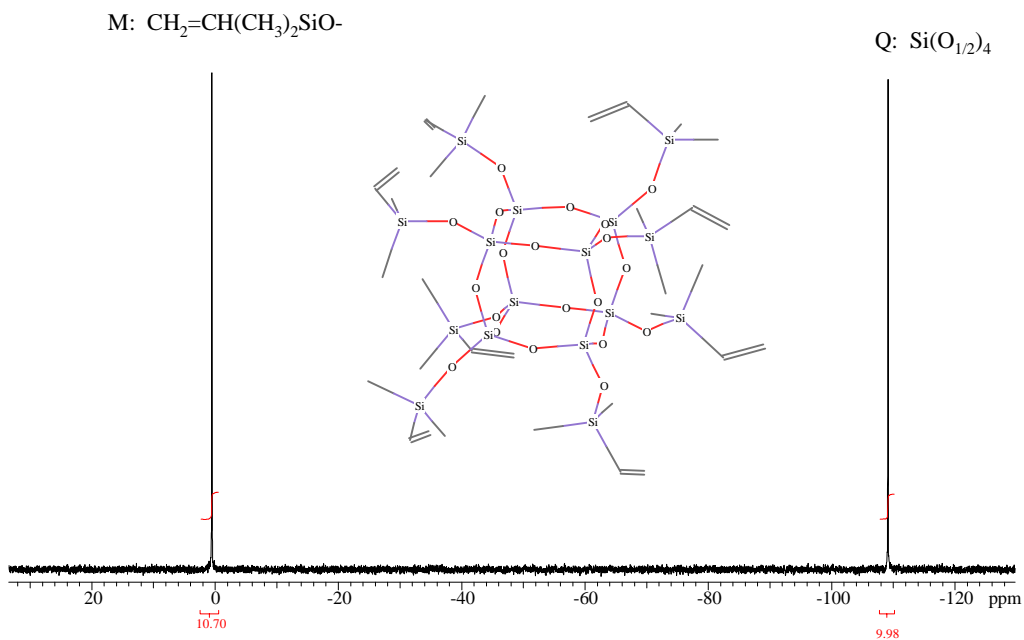


Fig. 8.5. The ^{29}Si NMR spectrum for octakis(vinyl dimethylsilyl) cubic octasilicate

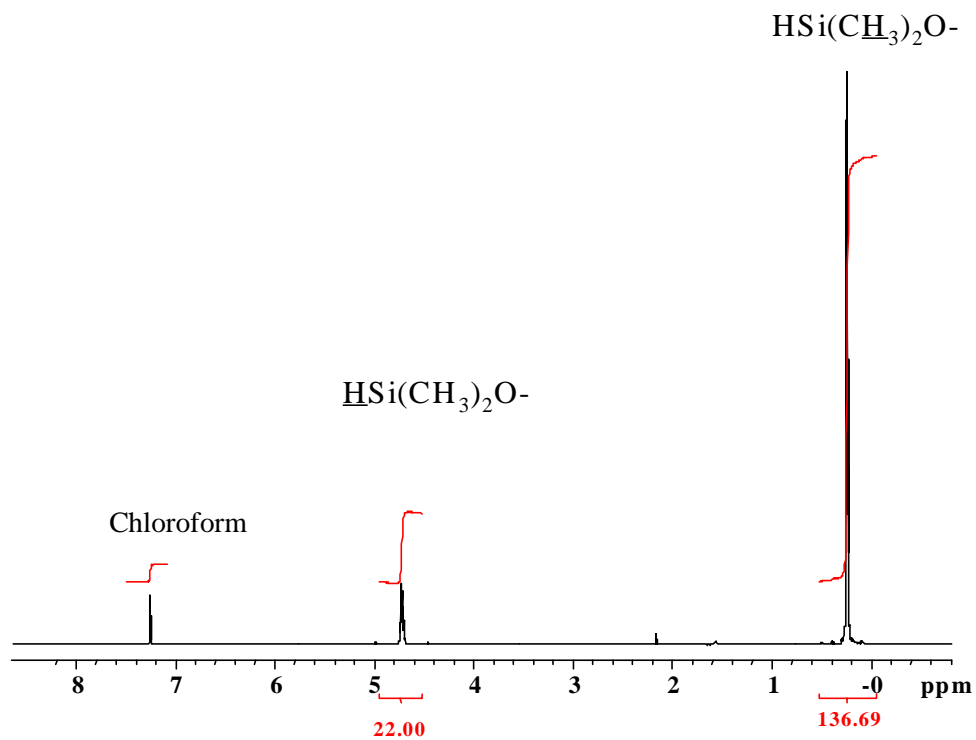


Fig. 8.6. The ^1H NMR spectrum of octakis(dimethylsilyl) cubic octasilicate

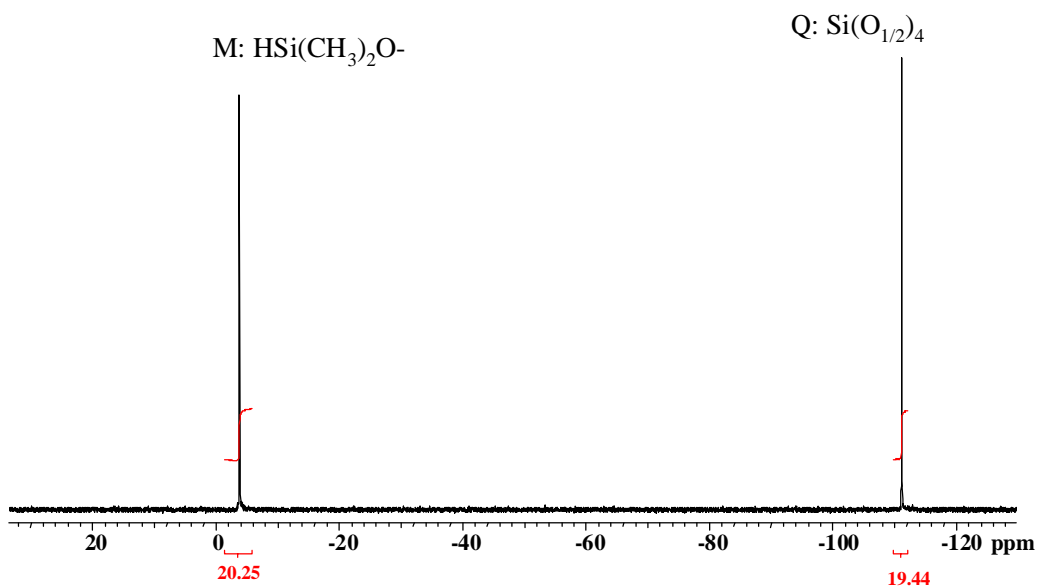


Fig. 8.7. The ^{29}Si NMR spectrum of octakis(dimethylsilyl) cubic octasilicate

8.3. COATINGS THROUGH HYDROSILYLATION

Cubic silicate containing hybrids were prepared by hydrosilylation of vinyl dimethylsilyl silicate (M^V8Q8), 1,3-divinyltetramethyldisiloxane (M^V-O-M^V) with tetradimethylsilylsilicate (M^H4Q) (Fig. 8.8). The reaction yields no low molecular weight by-products, so it is expected that monolithic materials can be prepared. M^V8Q8 is a crystalline material and has a limited solubility in the other reactants, so the reaction had to be carried out in cyclohexane. After the corners of the polyhedral had been partially functionalized, the solvent could be removed without causing crystallization of cubic compounds.

To a vial were added 0.153 g of M^V8Q8 , 0.186 g of M^VOM^V and 0.246 g of M^H4Q (EQ ratio = 1: 2: 3). Then 2 g of cyclohexane was added to dissolve the M^V8Q8 crystals. 50 mg of Pt(0)(1,3-divinyltetramethyldisiloxane) (Pt(dvs), 2% in xylene) were diluted to 10 g with cyclohexane, and 100 mg of this diluted Pt(dvs) were added to the silane mixture as a catalyst. The mixture was stirred for 10 hrs. before being cast on an aluminum substrate (treated with an acidified 3-methacryloxypropyltrimethoxy-silane solution). After the solvent evaporated, the material was further cured at 80°C for 4 hrs. and a colorless insoluble transparent coating was obtained. As expected, the material showed little shrinkage and relatively thick crack-free films were formed without cracking. Unfortunately, the coatings had rather weak mechanical properties, even after further curing at 125°C for 24 hrs. The abrasion of the coating surface occurred by an obvious micro-chipping mechanism. The pencil hardness (ASTM D3363-92a) for this material was about B-2B, close to that of polycarbonate. In fact, the surface of this material could be damaged easily by one's fingernail.

The $M^V8Q8/M^H8Q/M^VOM^V$ silicon resin behaves just like an unfilled polydimethylsiloxane resin, which often has very poor mechanical properties. It is believed that the poor mechanical properties of this silicone resin is due to the presence of large amounts of Si-CH₃ groups, which should result in a reduction in the molecular cohesion of the material.

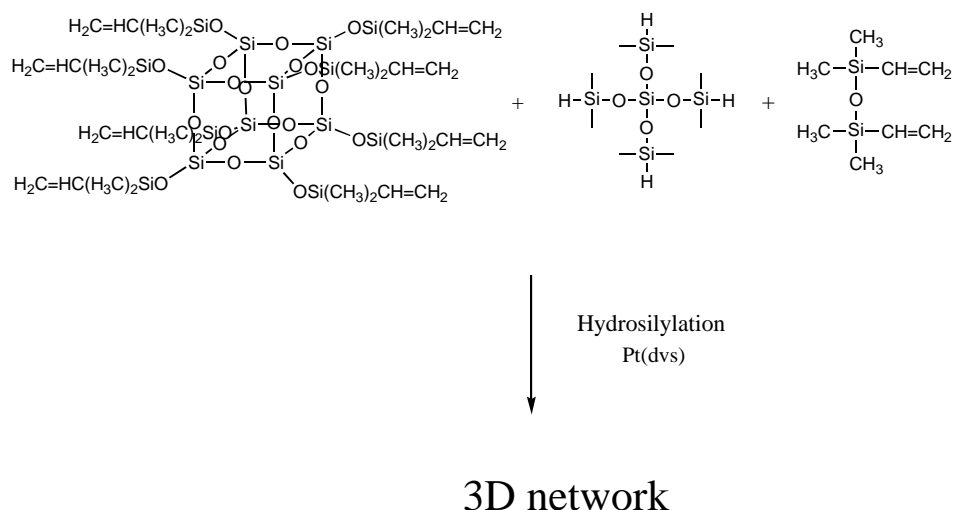


Fig. 8.8. Preparation of a $\text{M}^{\text{V}}8\text{Q8}/\text{M}^{\text{H}}4\text{Q}/\text{M}^{\text{V}}\text{OM}^{\text{V}}$ silicone resin by hydrosilylation.

Figure 8.9 shows the TGA curve for the silicone polyhedral silicate hybrid material. During the experiment, the material began to decompose at 300°C and showed a 5 % loss of weight at 370°C when the temperature was ramped at $10^\circ\text{C}/\text{min}$. The weight loss is expected to be due to the decomposition of $\text{Si}-\text{CH}_3$ and $\text{Si}-\text{CH}_2\text{CH}_2-\text{Si}$ groups. Figure 8.10 shows the DSC curve for the silicone polyhedral silicate hybrid material. No obvious transition can be detected in the temperature range of $25\text{--}280^\circ\text{C}$.

Figure 8.11 shows the dispersion IR spectrum for the compound after being treated at 80°C for 4 hrs. The M^{V} and M^{H} groups have absorbance bands at ca. 3100 cm^{-1} ($-\text{CH}=\text{CH}_2$) and at ca. 2100 cm^{-1} ($\text{H}-\text{Si}$). According to the IR spectrum, only small amounts of M^{V} groups and trace amounts of M^{H} remained unreacted after curing, so the hydrosilylation reaction was quite complete.

Figure 8.12 shows the CPMAG ^{29}Si NMR spectrum for the compound. Peaks at ca. -110 ppm and ca. -106 ppm correspond to Q from $\text{M}^{\text{V}}8\text{Q8}$ and $\text{M}^{\text{V}}4\text{Q}$. Peak at ca. -7 ppm is expected to be from unreacted $\text{Si}-\text{CH}=\text{CH}_2$ species in $\text{M}^{\text{V}}\text{OM}^{\text{V}}$ according to the NMR spectrum of $\text{M}^{\text{V}}8\text{Q8}$. Based on the ^{29}Si NMR spectrum of a gel derived from $\text{T}^{\text{OET}}8\text{M8Q8}$, the peak at ca. 13 ppm can be assigned to the M silicon from $\text{M}^{\text{V}}8\text{Q8}$. According to the relative abundance of

silanes in the formulation, the peaks at ca. 9 ppm and 8 ppm can be assigned to the M silicon atoms from M^H4Q and M^VOM^V , respectively.

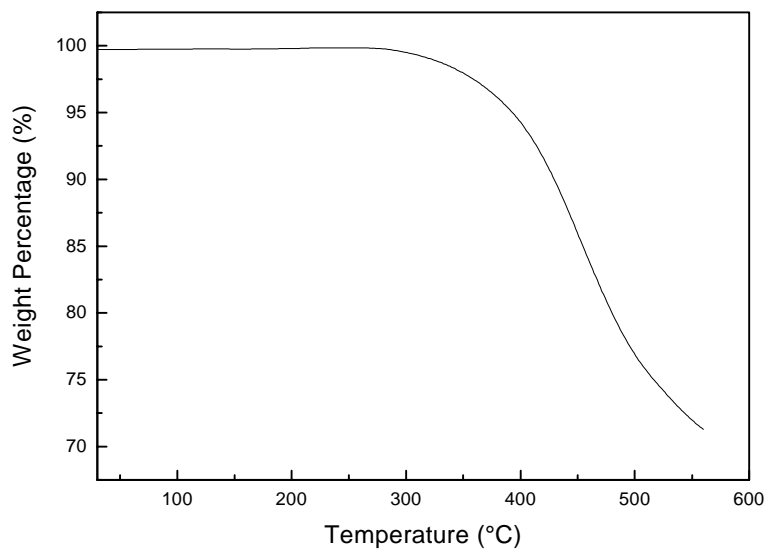


Fig. 8.9. TGA curve (10°C/min) for the $M^V8Q8/M^H4Q/M^VOM^V$ silicone resin.

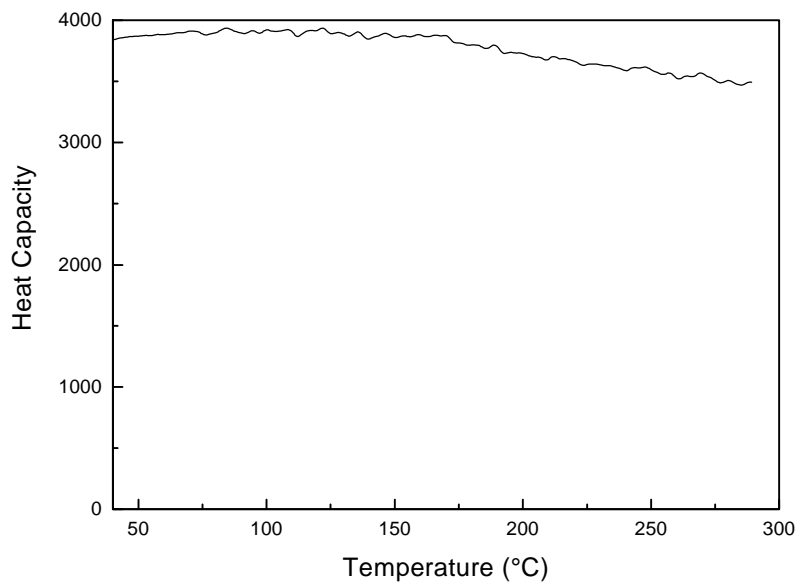


Fig. 8.10. DSC curve (10°C/min) for the $M^V8Q8/M^H4Q/M^VOM^V$ silicone resin.

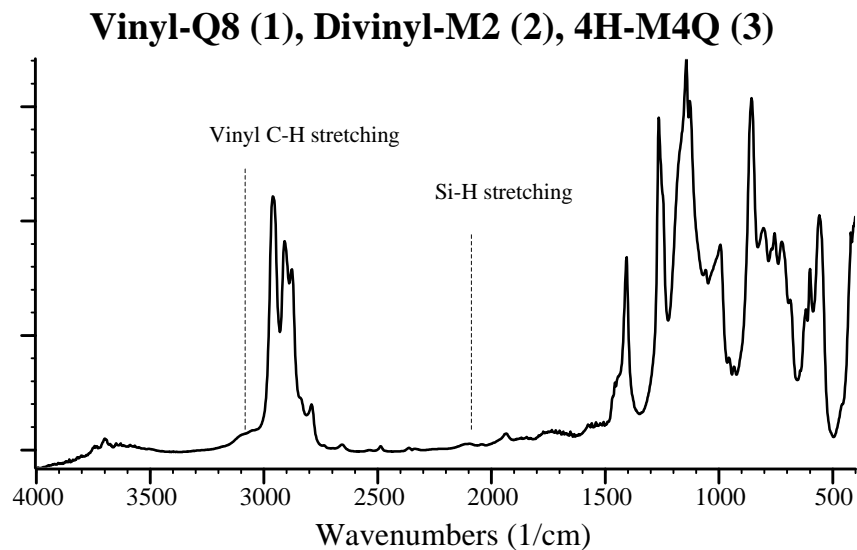


Fig. 8.11. Dispersion IR spectrum for the $M^V8Q8/M^H4Q/M^VOM^V$ silicone resin.

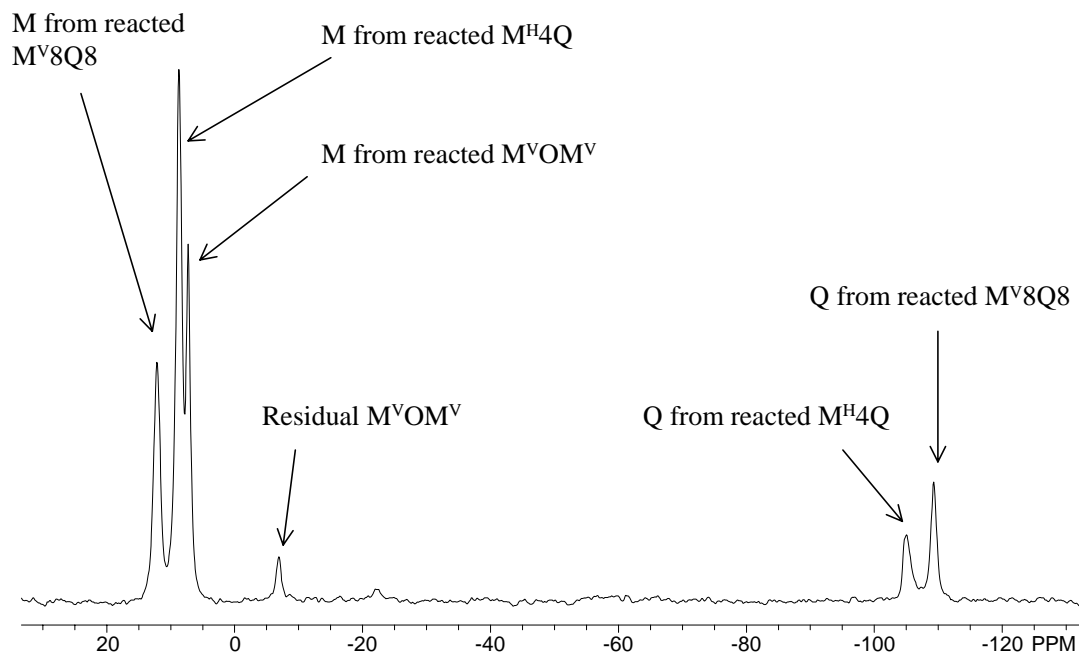


Fig. 8.12. ^{29}Si CPMAG NMR spectra for the $M^V8Q8/M^H4Q/M^VOM^V$ silicone resin. The spectra show residual vinyl groups at -7.5 ppm

8.4. COATINGS THROUGH THE SOL-GEL APPROACH

8.4.1. Octakis(2-triethoxysilylethyldimethylsilyl) Cubic Octasilicate ($T^{OEt}8M8Q8$)

Two g of M^V8Q8 , 3.0 g of triethoxysilane and 5 μ l of Pt(dvs) catalyst were dissolved in 5 g of cyclohexane. The hydrosilylation reaction (Fig. 8.13) was indicated by an increase in the reaction mixture. After 24 hrs., the solvent and unreacted triethoxysilane were removed by vacuum distillation, and a pale brownish oily liquid was obtained. The liquid was re-dissolved in 5 ml of cyclohexane, and the solution was filtered using a 4.5- μ m filter. The filtered solution was pre-dried with a vacuum evaporator and further dried in a vacuum oven at 80°C for 12 hrs. The product was a transparent oily liquid, and it was pale brownish due to the presence of colloidal platinum from the catalyst. The structure of this compound was confirmed by 1H NMR and ^{29}Si NMR spectra in Figs. 8.14 and 8.15. GPC (Fig. 8.16) also indicated that after the hydrosilylation, the hydrodynamic volume of the product $T8M8Q8$ (eluted at 25.5 ml) was much larger than that of the reactant M^V8Q8 (eluted at 27 ml). Some unreacted triethoxysilane and the solvent (eluted at 29-30 ml) were also detected by the GPC scan of the compound $T8M8Q8$.

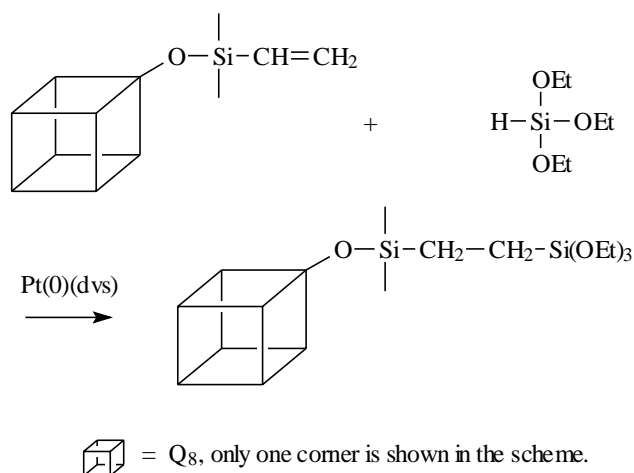


Fig. 8.13. A synthetic approach for Triethoxysilylation of octakis(vinyldimethylsilyl) cubic octasilicate

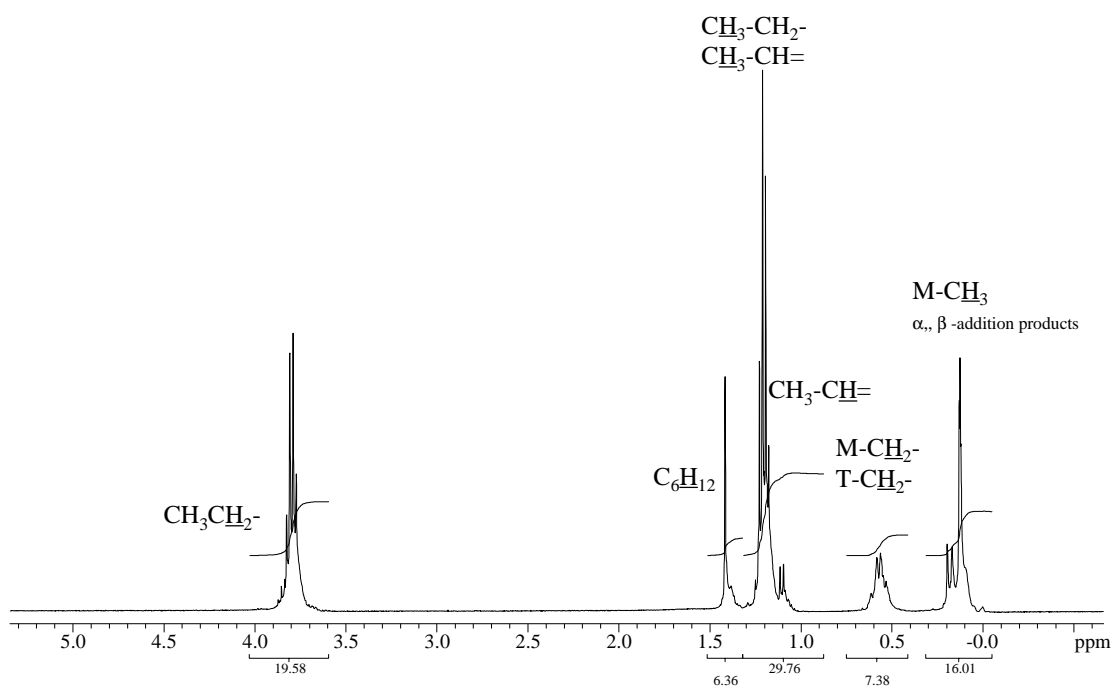


Fig. 8.14. The ^1H NMR spectrum for $\text{T}_8\text{M}_8\text{Q}_8$

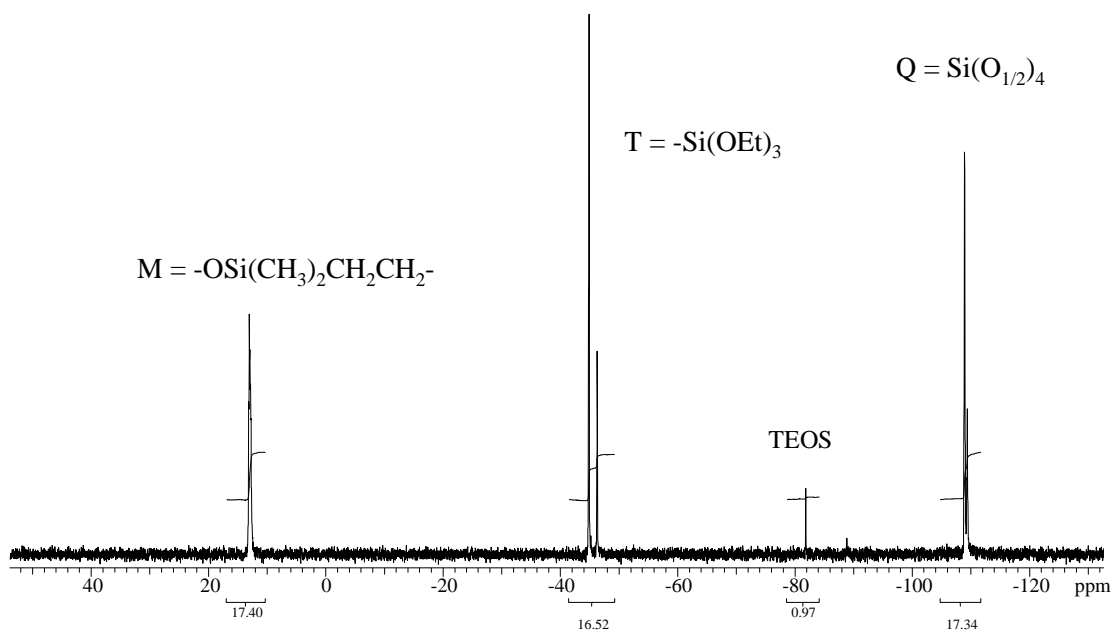


Fig. 8.15. The ^{29}Si NMR spectrum for $\text{T}^{\text{OEt}}_8\text{M}_8\text{Q}_8$

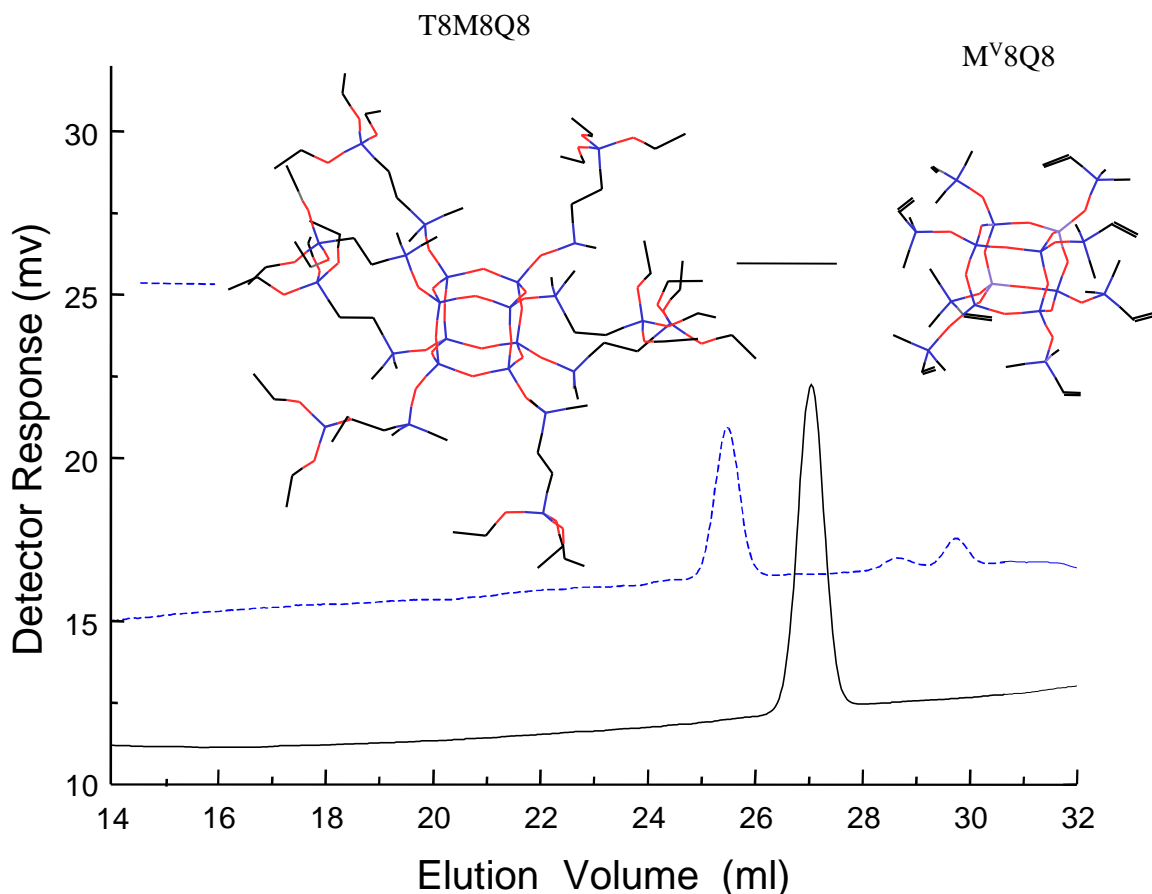


Fig. 8.16. The GPC curves for M^V8Q8 (before reaction) and $T^{OEt}8M8Q8$ (after reaction)

8.4.2. Sol-gel Coatings Derived from $T^{OEt}8M8Q8$

Two grams of $T^{OEt}8M8Q8$ were dissolved in 2 g of 2-propanol, and the mixture was hydrolyzed using 0.085 g of 0.5 N hydrochloric acid ($r=0.5$). Alternatively, the mixture was also hydrolyzed using 0.05 g of glacial acetic acid and 0.340 g of water ($r=2$). The resulting sols were spread on aluminum substrates, dried at room temperature and thermally cured at 125°C for 4 hrs. The resulting films were usually optically transparent, but very brittle and not abrasion resistant compared to many of the inorganic-organic hybrid coatings mentioned in the earlier chapters. Under the Taber test (CS10 wheels, 500-gram load per wheel), the coatings became severely damaged after just a few cycles of abrasion. Figure 8.17 shows the ^{29}Si CPMAS NMR

spectra for the gels prepared using hydrochloric acid and acetic acid catalysts. With hydrochloric acid as the catalyst, the extents of hydrolysis and condensation were much higher than the case of the acetic acid catalyst, in which a large amount of T^0 remained unhydrolyzed or uncondensed. Although the hydrochloric acid catalyst led to a higher extent of condensation in T, it also resulted in “cage-opening” of a considerable amount of the silicate cubes. In the opened cages, some silicon atoms became Q^3 -OH, which has a chemical shift of ca. -102 ppm. The opened cages also had some other Q^4 silicon atoms, which may have a chemical shift slightly different from that of Q^4 in a cube, thus leading to slight widening of the peak Q^4 at -110 ppm and the peak M at 12 ppm. The cage-opening was not observed by ^{29}Si NMR spectroscopy in case of the acetic acid catalyst (Fig. 8.17).

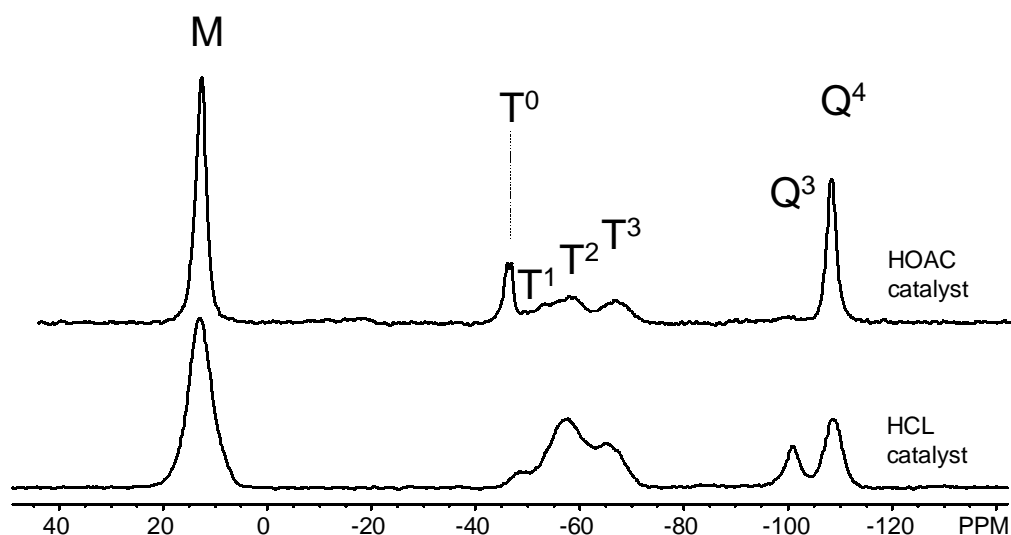


Fig. 8.17. ^{29}Si CPMAS NMR spectra for $T^{\text{OEt}}_8\text{M}_8\text{Q}_8$ gels cured by hydrochloric acid and acetic acid catalysts.

8.5. CONCLUSIONS

Coatings have been prepared using cubic octasilicate via hydrosilylation and sol-gel reactions. The hydrosilylation approach yields no condensation by-product and can form thick crack-free coatings. However, these films are not suitable for protective coatings due to their poor abrasion resistance. The T8M8Q8 monomer yields some condensation by-product during the sol-gel process, but much less than the cases of tetraalkoxysilanes. Sol-gel reactions of T8M8Q8 also lead to brittle transparent coatings that lacked abrasion resistance compared to other inorganic-organic hybrid coatings mentioned earlier. The poor abrasion resistance of these materials is conjectured to be due to large amounts of Si-CH₃ bonds and/or poor packing of the cubic units. The former usually lower the cohesion of the material. The organic chain (only 2 carbons in T8M8Q8) between T and the rigid cube may also be too short to improve the flexibility of the system.

CHAPTER 9. RECOMMENDATIONS FOR FUTURE WORK

Many inorganic-organic hybrid materials have been derived from sol-gel reactions of binary systems such as the f-DETA/TMOS systems and demonstrated excellent abrasion resistance. A next desirable step would be to scale up one or more of these systems to meet the requirements of various industrial coating requirements. Currently, these coatings may be applied as protective coatings for polymer lenses and glazing materials for buildings and automobiles. The current two-part f-DETA/TMOS system has a pot life between 10 to 24 hrs. at ca. 20°C depending on its concentration, which could meet the requirements for a small scale coating process. Of course, an increase in the pot life would be more convenient and economical.

To apply this coatings on plastic lenses, future work should focus on improving the coating smoothness and decreasing the haze of the coating surfaces. The coating itself has excellent transparency, so the major tasks are to control surface porosity and eliminate dust particles. Since the viscosity of the coating recipe increases with the hydrolysis time, it is necessary to establish the dependence of viscosity on the environmental temperature and hydrolysis time. With these relationships, it is possible to obtain coatings of uniform thickness during different stages of hydrolysis by adjusting coating processing variables.

Coating automobile plastic windows requires relatively large dip coating or spray coating processes, which usually require the coating recipe to have a pot life of about six months. Otherwise, the cost of the process may be very high and less controllable. As coatings for plastic materials, the f-DETA/TMOS coating so far has exhibited excellent abrasion resistance and met the abrasion resistant requirement of automobile rear windows. The next objective should be, of course, to increase the pot life or develop a new processing method to reduce the cost. In addition, the weatherability of bisphenol-A polycarbonate with f-DETA/TMOS coatings, which is also a major issue for the automobile coatings, should be considered in future studies.

Although attempts have been made to optimize the f-DETA/TMOS system, the current recipe is still not the best because incorporation of additional components can provide more

opportunities for future development. For example, a UV absorber may be incorporated into the system so that the resulting coating is not only abrasion resistant but also can protect the substrate from radiation damage¹⁷. Sol-gel coatings usually have poor compatibility with most commercial UV absorbers (water-insoluble), but a small amount of UV absorber (~0.5wt%) has already been incorporated into the sol-gel system without causing a serious increase in haze of the coating. The UV resistance and abrasion resistance can also be provided by multiple-layer coatings which include an inner layer of UV resistant coating and an outer layer of abrasion resistant coating. However, a stable coating that is resistant to both UV and would be the most desirable.

Currently, only a few results have been reported about the self- and cross-condensation of the T and Q alkoxy silanes. However, these studies did not consider the dependence of condensation rates on pH. In fact, pH has a significant influence over the relative values of the rate constants of these condensation reactions. The establishment of the pH-dependence of these condensation rates of simple systems like methyltriethoxysilane/ tetraethoxysilane would be very meaningful to the understanding of the gel structures consisting of both T and Q species.

To date, there are still no chemicals that can retard solution sol-gel condensations but do not affect later thermal curing. The only method to increase the pot life is to dilute the recipe so silanol/ alkoxy silane groups have fewer chances to collide. The two-step approach may reduce the silanol/ alkoxy silane concentrations and hence can increase the pot life. For this reason, to increase the pot life, the two-step approach should represent the direction of the future development.

Moisture curing provides f-DETA/TMOS coatings with slightly poorer abrasion resistance compared with coatings prepared by direct hydrolysis methods, but it usually have a very long pot life. Room temperature moisture curing is rather time-consuming, so the future research should focus on higher temperature moisture curing.

Finally, developing new trialkoxysilylated organic compounds is always a future research direction. Generally, gels derived by hydrolysis and condensation contains more or less porosity unless they are fully sintered at a high temperature, these pores are believed to result in poorer mechanical strength of the gel. Incorporation of some flexible organic components can help to

relax the internal stress that are formed during the drying and curing processes, thus hopefully leading to improved mechanical properties. Ideal organic components should include groups or linkages that can improve the toughness and flexibility of the sol-gel materials.

BIBLIOGRAPHY

- (1) http://www.ge.com/plastics/americas/press/press_release/03_09_98.htm
- (2) <http://www.ge.com/plastics/americas/press/npe/press/pr6397.htm>
- (3) <http://www.bayerus.com/new/1997/7.16.2.htm>
- (4) Schmidt, H.; Krug, H. In *Inorganic and Organometallic Polymers II Advanced Materials and Intermediates*; Wisian-Neilson, P., Allcock, H. R., Wynne, K. J., Eds.; American Chemical Society: Washington DC, 1994; Vol. 572.
- (5) Schmidt, H. *J. Sol-Gel Science and Technology* **1994**, *1*, 217.
- (6) Schmidt, H. In *Sol-Gel Optics Processing and Applications*; Klein, L. C., Ed.; Kluwer Academic Publishers: Boston, 1994.
- (7) Schmidt, H.; Seiferling, B.; Philipp, G.; Deichmann, K. In *Ultrastructure of Processing of Advanced Ceramics*; Mackernzie, J. D., Ulrich, D. R., Eds. New York, 1988.
- (8) Schmidt, H.; Seiferling, B. In *Better Ceramics through Chemistry II*; Brinker, C. J., Clark, D. E., Ulrich, D. R., Eds.; Pittsburgh, PA., 1986; Mat. Res. Soc. Symp. Proc. Vol. 73. 739
- (9) Schmidt, H. In *Better Ceramics through Chemistry*; Brinker, C. J., Clark, D. E., Ulrich, D. R., Eds.; Wiley, New York:, 1984. Mat. Res. Soc. Symp. Proc. Vol. 32 327
- (10) Schmidt, H.; Kasemann, R.; Burkhart, T.; Wagner, G.; Arpac, E.; Geiter, E. In *Hybrid Organic-Inorganic Composites*; Mark, J. E., Lee, C. Y.-C., Bianconi, P. A., Eds.; Amer. Chem. Soc.: Washington DC, 1995; Mat. Res. Soc. Symp. Proc. Vol. 585. 331
- (11) Wang, B.; Gungor, A.; Brennan, A. B.; Rodrigues, D. E.; McGrath, J. E.; Wilkes, G. L. *Polym. Prepr.* **1991**, *32*, 521.
- (12) Wang, B.; Wilkes, G. L. *J. Macromol. Sci., Pure Appl. Chem.* **1994**, *A31*, 249.
- (13) Wang, B.; Wilkes, G. L. In *US Patent*; Virginia Tech Intellectual Properties, Inc.: United States, 1994.

- (14) Wen, J.; Vasudevan, V. J.; Wilkes, G. L. *J. Sol Gel Sci. Technol.* **1995**, *5*, 115.
- (15) Wen, J.; Wilkes, G. L. *J. Inorg. Organomet. Polym.* **1995**, *5*, 343.
- (16) Wen, J.; Wilkes, G. L. *Polym. Mater. Sci. Eng.* **1995**, *73*, 429.
- (17) Wen, J.; Jordens, K.; Wilkes, G. L. *Mater. Res. Soc. Symp. Proc.* **1996**, *435*, 207.
- (18) Brinker, C. J.; Scherer, G. W. *Sol-Gel Science : The Physics and Chemistry of Sol-Gel Processing*; Academic Press: Boston, 1990.
- (19) Egelhardt, V. G.; Altenburg, W.; Hoebbel, D.; Wieker, W. Z. *Anorg. Allg. Chem.* **1977**, *418*, 43.
- (20) Kay, B. D.; Assink, R. A. *J. Non-Crystalline Solids* **1988**, *104*, 112.
- (21) Assink, R. A.; Kay, B. D. *J. Non-Crystalline Solids* **1988**, *99*, 359.
- (22) Assink, R. A.; Kay, B. D. In *Better Ceramics through Chemistry*; Brinker, C. J., Clark, D. E., Ulrich, D. R., Eds.; North Holland: New York, 1984. *Mat. Res. Soc. Symp. Proc. Vol.* 32 301.
- (23) Clarson, S. J.; Semlyen, J. A. *Siloxane Polymers*; PTR Prentice Hall: New York, 1993.
- (24) Carey, F. A.; Sundberg, R. J. *Advanced Organic Chemistry, Part A: Structure and Mechanism*; 3 ed.; Plenum Press: New York, 1990. 261
- (25) Corrius, R. J. P.; LeClercq, D.; Vioux, A.; Pauthe, M.; Phalippou, J. In *Ultrastructure Processing of Advanced Ceramics*; Mackenzie, J. D., Ulrich, D. R., Eds.; Wiley: New York, 1988.
- (26) Aelion, R.; Leobel, A.; Eirich, F. *J. Am. Chem. Soc.* **1950**, *72*, 5705.
- (27) Schmidt, H. *J. Non-Crystalline Solids* **1985**, *73*, 681.
- (28) Pohl, E. R.; Osterholtz, F. D. In *Molecular Characterization of Composite Interfaces*; Ishida, H., Kumar, G., Eds.; Plenum: New York, 1985.
- (29) Sommer, L. H.; Frye, C. L. *J. Am. Chem. Soc.* **1960**, *82*, 3796.
- (30) Sommer, L. H.; Frye, C. L.; Musolf, M. C.; Parker, G. A.; Rodewald, P. G.; Michael, K. W.; Okaya, Y.; Peplinski, P. *J. Am. Chem. Soc.* **1961**, *83*, 2210.
- (31) Voronkov, V. P.; Mileshkevich, V. P.; Yuzhelevski, Y. A. *The Siloxane Bond*; Consultant Bureau, New York: New York, 1978.
- (32) Schmidt, H.; Scholze, H.; Kaiser, A. *J. Non-Crystalline Solids* **1984**, *63*, 1.

- (33) Klemperer, W. G.; Mainz, V. V.; Millar, D. M. In *Better Ceramics through Chemistry II*; Brinker, C. J., Clark, D. E., Ulrich, D. R., Eds.; Pittsburgh, PA., 1986; Mat. Res. Soc. Symp. Proc. Vol. 73 3
- (34) Iler, R. K. *The Chemistry of Silica : Solubility, Polymerization, Colloid and Surface Properties, and Biochemistry*; Wiley: New York, 1979.
- (35) Thomas, D. R. In *Siloxane Polymers*; Clarson, S. J., Semlyen, J. A., Eds.; PTR Prentice Hall: New York, 1993.
- (36) Pkabakar, S.; Assink, R. A. Mat. Res. Soc. Symp. Proc., 1996; 45.
- (37) Grubbs, W. T. *J. Am. Chem. Soc.* **1954**, 76, 3408.
- (38) Artaki, I.; Sinha, S.; Irwin, A., D.; Jonas, J. J. *J. Non-Crystalline Solids* **1985**, 72, 391.
- (39) Swain, C. G.; Esteve, R. M.; Jones, R. H. *J. Am. Chem. Soc.* **1949**, 11, 965.
- (40) Okkerse, C. In *Physical and Chemical Aspects of Absorbents and Catalysts*; Linsen, B. G., Ed.; Academica Press: New York, 1970.
- (41) Davis, L. P.; Burggraf, L. W. In *Ultrastructure Processing of Advanced Ceramics*; Mackenzie, J. D., Ulrich, D. R., Eds.; Wiley: New York, 1988.
- (42) Brinker, C. J. *J. Non-Crystalline Solids* **1988**, 100, 30.
- (43) Doughty, D. H.; Assink, R. A.; Bruce, D. K. In *Silicon-Based Polymer Science*; Zeigler, J. M., Gordon Fearon, F. W., Eds.; American Chemical Society: Washington DC, 1990); Adv. Chem. Series Vol. 222 241.
- (44) Pouxviel, J. C.; Boilet, J. P.; Beloeil, J. C.; Lallenmand, J. Y. *J. Non-Crystalline Solids* **1987**, 89, 345.
- (45) Van der Weij, F. W. *Makromol. Chem.* **1980**, 181, 2541.
- (46) Severnyi, V. V.; Minasyan, R. M.; Makarenko, I. A.; Bizyuakova, N. M. *Vysokomoh Soedin. Ser. A (Eng. Trans.)* **1976**, 18, 1464.
- (47) Mandelbrot, B. B. In *The Fractal Approach to Heterogeneous Chemistry, Surfaces, Colloids, Polymers*; Avnir, D., Ed.; John Wiley & Sons: Chichester, 1989 3
- (48) Schmidt, P. W. In *The Fractal Approach to Heterogeneous Chemistry*; Avnir, D., Ed.; John Wiley & Sons Ltd.: Chichester, 1989 67.

- (49) Schaefer, D. W.; Keefer, K. D. In *Better Ceramics through Chemistry*; Brinker, C. J., Clarke, D. E., Ulrich, D. R., Eds.; Elsevier North Holland: New York, 1984. Mat. Res. Soc. Symp. Proc. Vol. 32 1
- (50) Schaefer, D. W. *MRS Bulletin* **1988**, 8, 22.
- (51) Schaefer, D. W.; Martin, J. E.; Keefer, K. D. In *Physics of Finely Divided Matters*; Bocarra, N., Daoud, M., Eds.; Springer-Verlag: Berlin, 1985.
- (52) Kim, H. C.; Song, J. H.; Wilkes, G. L.; Smith, S. D.; McGrath, J. E. *Polym. Prepr.* **1987**, 28, 242.
- (53) Beaucage, G.; Ulibarri, T. A.; Black, E. P.; Schaefer, D. W. In *Hybrid Organic-Inorganic Composites*; Mark, J. E., Lee, C. Y.-C., Bianconi, P. A., Eds.; Amer. Chem. Soc.: Washington DC, 1995; ACS Symp. Series Vol. 585 97.
- (54) Williams, C. E.; Roland, P. M.; Guinier, A. In *Characterization of Materials*; Lifshin, E., Ed.; VCH: Weinheim, 1993; Vol. 2.
- (55) Hurd, C. B. *Chem. Rev.* **1938**, 22, 403.
- (56) Colby, M. W.; Osaka, A.; Mackenzie, J. D. *J. Non-Crystalline Solids* **1988**, 99, 129-139.
- (57) Mackenzie, J. D. In *Science of Ceramic Chemical Processing*; Hench, L. L., Ulrich, D. R., Eds.; Wiley: New York, 1986.
- (58) Chen, K. C.; Tsuchiya, T.; Mackenzie, J. D. *J. Non-Crystalline Solids* **1986**, 81, 227-237.
- (59) Betchtold, M. F.; Mahler, W.; Schunn, R. A. *J. Polym. Sci.: Polym. Chem. Ed.* **1980**, 18, 2823.
- (60) Gottardi, V.; Guglielmi, M.; Bertoluzza, A.; Fagnano, C.; Morelli, M. A., *J. Non-Crystalline Solids* *J. Non-Crystalline Solids* **1984**, 63, 71.
- (61) Debsikdarr, J. C. *Adv. Ceram. Mater.* **1986**, 1, 93.
- (62) Klein, L. C. *Ann. Rev. Mater. Sci.* **1985**, 15, 227.
- (63) Harris, R. K.; Knight, C. T. G.; Hull, W. E. In *Soluble Silicates*, ACS Symp. Series; Falcone Jr., J. S., Ed.; American Chemical Society: Washington D.C., 1982; Vol. 194.
- (64) Carmen, P. C. *Trans, Faraday Soc.* **1940**, 36, 964.
- (65) Flory, P. J. *Principles of Polymer Chemistry*; Cornell Univ. Press: Ithaca, NY, 1953.
- (66) Zallen, R. *The Physics of Amorphous Solids*; Wiley: New York, 1983.

- (67) Chandrasekhar, S. *Rev. Mod. Phys.* **1943**, *15*, 5269.
- (68) Ernst, M. In *Fractal Physics*; Pietronero, L., Tosatti, E., Eds.; North Holland: New York, 1986.
- (69) Meakin, P. In *The Fractal Approach to Heterogeneous Chemistry*; Avnir, D., Ed.; John Wiley & Sons: Chichester, 1989 131.
- (70) Sakka, S. In *Better Ceramics through Chemistry*; Brinker, C. J., Clarke, D. E., Ulrich, D. R., Eds.; North Holland: New York, 1984. Mat. Res. Soc. Symp. Proc. Vol. 32 91
- (71) Sakka, S.; Kamiya, K.; Makita, K.; Yamamoto, Y. *J. Non-Crystalline Solids* **1984**, *63*, 223.
- (72) Sakka, S.; Kamiya, K. *J. Non-Crystalline Solids* **1982**, *48*, 31.
- (73) Kamiya, K.; Yoko, T.; Suzuki, H. *J. Non-Crystalline Solids* **1987**, *93*, 407.
- (74) Meakin, P. In *One Growth and Form*; Stanley, H. E., Ostrowsky, N., Eds.; Martinus-Nijhoff: Boston, 1986.
- (75) Keefer, K. D. In *Better Ceramics through Chemistry II*; Brinker, C. J., Clarke, D. E., Ulrich, D. R., Eds.; Mater. Res. Soc.: Pittsburgh, PA, 1986. Mat. Res. Soc. Symp. Proc. Vol. 73 295
- (76) Coltrain, B. K.; Melpolder, S. M.; Salva, J. M. Proceeding of the Ivth Int'l. Conference on Ultrastructure Processing of Ceramics, Glass and Composites, New York, Feb, 19-24 1989.
- (77) Cihlar, J. *Colloids and Surfaces A: Physicochemical and Engineering Aspects* **1993**, *70*, 253.
- (78) Iler, R. K. *The Colloid Chemistry of Silica and Silicates*; Cornell University Press: Ithaca, N.Y., 1955.
- (79) Kelts, L. W.; Effinger, N. J.; Melpolder, J. *J. Non-Crystalline Solids* **1986**, *83*, 353-374.
- (80) Brinker, C. J.; Keefer, K. D.; Schaefer, D. W.; Ashley, C. S. *J. Non-Crystalline Solids* **1982**, *48*, 47.
- (81) Brinker, C. J.; Keefer, K. D.; Schaefer, D. W.; Assink, R. A.; Kay, B. D.; Ashley, C. S. *J. Non-Crystalline Solids* **1984**, *63*, 45.
- (82) Boonstra, A. H.; Bernardis, T. N. M. *J. Non-Crystalline Solids* **1988**, *105*, 207.

- (83) Assink, R. A.; Kay, B. D. *Mat. Res. Soc. Sym. Proc.* **1984**, 32, 301.
- (84) Lierop, J. G. V.; Huizing, A.; Meerman, W. C. P. M.; Mulder, C. A. M. *J. Non-Crystalline Solids* **1986**, 82, 265.
- (85) Boonstra, A. H.; Mulder, C. A. M. *J. Non-Crystalline Solids* **1988**, 201, 105.
- (86) Schaefer, D. W.; Keefer, K. D. In *Fractals in Physics*; Pietronero, J., Tosatti, E., Eds.; North Holland: Amsterdam, 1986.
- (87) Fortes, M.; Okos, M. R. In *Advances in Drying*; Mujumdar, A. S., Ed.; Hemisphere: New York, 1980; Vol. 1.
- (88) Moore, F. *Trans. Brit. Ceram. Soc.* **1961**, 60, 517.
- (89) Brinker, C. J.; Hurd, A. J.; Schunk, P. R.; Frye, G. C.; Ashley, C. S. *J. Non-Crystalline Solids* **1992**, 147&148, 424.
- (90) Brinker, C. J.; Raman, N. K.; Logan, M. N.; Sehgal, R.; Assink, R. A.; Hua, D.-W.; Ward, T. L. In *Inorganic and Organometallic Polymers II: Advanced Materials and Intermediates*; Wisian-Neilson, P., Allock, H. R., Wyanne, K. J., Eds.; American Chemical Society: Washington DC, 1994; ACS Symp. Series Vol. 572. 104
- (91) Dwivedi, R. K. *J. Mater. Sci. Lett.* **1986**, 5, 373.
- (92) Mandelbrot, B. B. *The Fractal Geometry of Nature*; Freeman: San Francisco, 1982.
- (93) Brinker, C. J.; Scherer, G. W. *J. Non-Crystalline Solids* **1985**, 70, 301-322.
- (94) Scherer, G. W. *J. Non-Crystalline Solids* **1986**, 87, 199.
- (95) Scherer, G. W. *J. Non-Crystalline Solids* **1987**, 89, 217.
- (96) Scherer, G. W. *J. Non-Crystalline Solids* **1987**, 91, 83.
- (97) Scherer, G. W. *J. Non-Crystalline Solids* **1987**, 91, 101.
- (98) Scherer, G. W. *J. Non-Crystalline Solids* **1987**, 92, 122.
- (99) Scherer, G. W. *J. Non-Crystalline Solids* **1987**, 92, 375.
- (100) Scherer, G. W. *J. Non-Crystalline Solids* **1988**, 99, 324.
- (101) Scherer, G. W. *J. Non-Crystalline Solids* **1989**, 107, 135.
- (102) Wallace, S.; Hench, L. L. In *Better Ceramics through Chemistry*; Brinker, C. J., Clark, D. E., Ulrich, D. R., Eds.; North Holland: New York, 1985; Mat. Res. Soc. Symp. Proc. Vol. 32. 47

- (103) Orcel, G.; Gould, R. W.; Hench, L. L. In *Better Ceramics through Chemistry II*; Brinker, C. J., Clark, D. E., Ulrich, D. R., Eds.; Material Research Society: Pittsburgh, PA, 1986; Mat. Res. Soc. Symp. Proc. Vol. 73 289.
- (104) Orcel, G.; Hench, L. L.; ArtaKi, I.; Jonas, J.; Zerda, T. W. *J. Non-Crystalline Solids* **1988**, *105*, 223.
- (105) Adachi, T.; Sakka, S. *J. Non-Crystalline Solid* **1988**, *99*, 118.
- (106) Hench, L. L. In *Science of Ceramic Chemical Engineering*; Hench, L. L., Ulrich, D. R., Eds.; Wiley: New York, 1986.
- (107) Wolfrum, S. M. *J. Mater. Sci. Lett.* **1987**, *6*, 706.
- (108) Tewari, P. H.; Hunt, A. J.; Lufftus, K. D. *Mater. Lett.* **1985**, *3*, 363.
- (109) Woignier, T. Thesis, Univ. des Sciences et Techniques du languedoc, 1984.
- (110) Abramoff, B.; Covino, J. J. A. P. S.-. *J. Appl. Polym. Sci.* **1992**, *46*, 1785.
- (111) Abramoff, B.; Klein, L. C. *SPIE Proc.* **1990**, *1328*, 241.
- (112) Pope, E. J. A.; Asami, M.; Mackenzie, J. D. *J. Mater. Res.* **1989**, *4*, 1018.
- (113) Schmidt, H. K. In *Inorganic and Organometallic Polymers with Special Properties*; Laine, R. M., Ed.; Kluwer Academic Publisher: Dordrecht, The Netherlands, 1992; Vol. 206.
- (114) Philipse, A. P.; Vrij, A. J. *Colloid Interface Sci.* **1988**, *128*, 121.
- (115) Sunkara, H. B.; Jethmalani, J. M.; Ford, W. T. In *Hybrid Organic-Inorganic Composites*; Mark, J. E., Lee, C. Y.-C., Bianconi, P. A., Eds.; Amer. Chem. Soc.: Washington DC, 1995; ACS Symp. Series Vol. 585.
- (116) Novak, B. M.; Ellsworth, M. W.; Verrier, C. In *Hybrid Organic-Inorganic Composites*; Mark, J. E., Lee, C. Y.-C., Bianconi, P. A., Eds.; Amer. Chem. Soc.: Washington DC; ACS Symp. Series Vol. 585. 86
- (117) Bourgeat-Lami, E.; Espiard, P.; Guyot, A.; Briat, S.; Gauthier, C.; Vigier, G.; Perez, J. In *Hybrid Organic-Inorganic Composites*; Mark, J. E., Lee, C. Y.-C., Bianconi, P. A., Eds.; Amer. Chem. Soc.: Washington DC, 1995; ACS Symp. Series Vol. 585. 112

- (118) Wilkes, G. L.; Huang, H.-H.; Glaser, R. H. In *Silicon-Based Polymer Science, A Comprehensive Resource*; Zeigler, J. M., Fearon, F. W. G., Eds.; American Chemical Society: Washington DC, 1990; Adv. Chem. Series Vol. 225 207.
- (119) Wen, J.; Wilkes, G. L. *Chem. Mater.* **1996**, *8*, 1667.
- (120) Pope, E. J. A.; Mackenzie, J. D. *MRS Bull.* **1988**, *12*, 29.
- (121) Jiang, C. Y.; Mark, J. E. *Macromol. Chem.* **1984**, *18*, 2609.
- (122) Silverra, K. F.; Valeria, I.; Yoshida, P.; Nunes, S. P. *Polymer* **1995**, *36*, 1425-1434.
- (123) Rabinowicz, E. *Friction and Wear of Materials*; 2 ed.; John Wiley & Sons: New York, 1995.
- (124) *Metal Handbook*; 8 ed.; ASM: Metals Park, Novelty, OH, 1961.
- (125) *The Handbook of Chemistry and Physics*; 43 ed.; Chemical Rubber Publishing Co.: Cleveland, OH, 1962.
- (126) Tabor, D. *The Hardness of Metals*; Oxford University Press: Oxford, 1951.
- (127) Barker, R. E. *J. Appl. Phys.* **1963**, *34*, 107.
- (128) Lee, L.-H. In *Polymer Wear and Its Control*; Lee, L.-H., Ed.; Amer. Chem. Soc.: Washington DC, 1985. ACS Symp. Series Vol. 287 77
- (129) Friedrich, J. K. *Friction and Wear of Polymer Composites* **1984**, *18*.
- (130) Lancaster, J. K. In *Polymer Science*; Jenkins, A. D., Ed.; North Holland: London, 1972; Vol. 2.
- (131) Ratner, S. B.; Farberova, I. I.; Radyukevich, O. V.; Lure, E. G. *Soviet Plastics* **1964**, *7*, 37.
- (132) Hornbogen, E. *Wear* **1975**, *33*, 251.
- (133) Briscoe, B. J.; Tabor, D. In *Fundamental Tribology, Proceedings of International Conference*; MIT Press: Cambridge, MA, 1980.
- (134) Lee, L. H. In *Adhesion Joints-Formation, Characterization and Testing*; Mittal, K. L., Ed.; Plenum: New York, 1984; Vol. 1.
- (135) Ratner, S. B.; Klitenik, G. S. *Zav Lab.* **1959**, *25*, 1357.
- (136) Champ, D. H.; Southern, E.; Thomas, A. G. In *Advances in Polymer Friction and Wear*; H., L. L., Ed.; Plenum: New York, 1974; Vol. 3A.

- (137) Coghill, M. D. E. *Surface and Coating Technology* **1990**, *41*, 135.
- (138) Briscoe, B. J.; Pelillo, E.; Sinha, S. K. *Polym. Eng. & Sci.* **1996**, *36*, 2996.
- (139) Briscoe, B. J.; Evans, P. D.; Lancaster, J. K. *J. Phys. D: Appl. Phys.* **1987**, *20*, 346.
- (140) Briscoe, B. J.; Briggs, D.; Rance, D. G. In *Comprehensive Polymer Science*, Pergamon Press, Pergamon Press: Oxford, United Kingdom, 1988.
- (141) <http://boa106.bo.inf.it/intercast/charact.html>
- (142) Jain, V. K.; Bahadur, S. *Wear* **1982**, *79*, 241.
- (143) Wrobel, A. M.; Kryszewski, M. In *Plasma Polymerization*; American Chemical Society: Washington D.C., 1979; ACS Symp. Series Vol. 108 237.
- (144) Clark, H. A. In *U. S. Patent*, 1976.
- (145) Clark, H. A. In *U. S. Patent*, 1977.
- (146) Vincent, H. L.; Kimball, D. J.; Roundy, R. R. In *Polymer Wear and Its Control*; Lee, L.-H., Ed.; American Chemical Society: Washington D.C., 1985. ACS Symp. Series Vol. 287 129
- (147) Philipp, G.; Schmidt, H. *J. Non-Crystalline Solids* **1984**, *63*, 283.
- (148) Schmidt, H.; Wolter, H. *J. Non-Crystalline Solids* **1990**, *121*, 428.
- (149) Kasemann, R.; Schmidt, H. *New J. Chem.* **1994**, *18*, 1117.
- (150) Wang, B.; Wilkes, G. L. In *PCT International*; Virginia Tech Intellectual Properties, Inc., 1992.
- (151) Wang, B.; Wilkes, G. L. In *PCT International*; Virginia Tech Intellectual Properties, Inc., 1991.
- (152) Tamami, B.; Betrabet, C.; Wilkes, G. L. *Polym. Bull.* **1993**, *30*, 293.
- (153) Tamami, B.; Betrabet, C.; Wilkes, G. L. *Polym. Bull.* **1993**, *30*, 39.
- (154) Betrabet, C. S. Ph. D. Thesis, Virginia Polytechnic Inst. and State University, 1993.
- (155) Betrabet, C. S.; Wilkes, G. L. *J. Inorg. Organomet. Polym.* **1994**, *4*, 343.
- (156) Betrabet, C. S.; Wilkes, G. L. *Polym. Prepr.* **1992**, *33*, 286.
- (157) Wen, J.; Wilkes, G. L. *PMSE Prepr.* **1995**, *73*, 429.
- (158) Jordens, K.; Wilkes, G. *J. Adhes. Sealant Comm.* **1997**, *1997*, 345.
- (159) Jordens, K.; Wilkes, G. L. *Polym. Mater. Sci. Eng.* **1995**, *73*, 290.

- (160) Jordens, K.; Wilkes, G. L. *PMSE Prepr.* **1995**, 73, 290.
- (161) Jordens, K.; Wilkes, G. L. *Proc. Annu. Meet. Adhes. Soc.* **1996**, 19th, 154.
- (162) McNeil, K. J.; DiCaprio, J. A.; Walsh, D. A.; Pratt, R. F. *J. Am. Chem. Soc.* **1980**, 102, 1859.
- (163) Li, C.; Wilkes, G. L. *J. Inorg. Organometallic Polym.* **1998**, 8, 33.
- (164) Bornside, D. E.; Macosko, C. W.; Scriven, L. E. *J. Imaging Tech.* **1987**, 13, 122.
- (165) Scriven, L. E. In *Better Ceramics Through Chemistry III*; Brinker, C. J., Clark, D. E., Ulrich, D. R., Eds.; Pittsburgh, PA, 1988. Mat. Res. Soc. Symp. Proc. Vol. 121 717
- (166) Meyerhofer, D. *J. Appl. Phys.* **1978**, 49, 3993.
- (167) Landau, L. D.; Levich, B. G. *Acta Physiochim, U.R.S.S* **1942**, 17, 42.
- (168) http://www.taberindustries.com/test_meas/abrasers/abtestsp.html
- (169) Gahr, K. H. Z. *Microstructure and Wear of Materials, Tribology Series*; Elsevier: Amsterdam, 1987.
- (170) Lee, L.-H. In *Polymer Wear and Its Control*; Lee, L.-H., Ed.; Amer. Chem. Soc.: Washington DC, 1985. ACS Symp. Series Vol. 287 27
- (171) Plueddemann, E. P. *Silane Coupling Agents*; Plenum Pub. Corp: New York, 1991.
- (172) Plueddemann, E. P. Int. Conf. Composite Interfaces II, 1988; p17.
- (173) Kim, J.-K.; Mai, Y.-M. In *Material Science and Technology, A Comprehensive Treatment* VCH, Weinheim, Germany and VCH New York, USA, 1992; Vol. 13.
- (174) Antoon, M. K.; Koenig, J. L. *J. Polym. Sci. Polym. Phys.* **1981**, 19, 197.
- (175) Koenig, J. L.; Shih, P. Y. K. *J. Colloid. Interf. Sci.* **1971**, 36, 247.
- (176) Ishida, H.; Koenig, J. L. *J. Polym. Sci. Polym. Phys.* **1979**, 17.
- (177) Sung, N. H.; Kahl, A.; Ni, S.; Sung, C. S. P.; Chin, I. J. 36th Ann. Tech. Conf. Reif. Plast. Comp., Washington DC, 1981.
- (178) *The Aldrich Library of ¹³C and ¹H FT NMR Spectra*; Pouchert, C. J.; Behnke, J., Eds.; Aldrich Chemical Inc., 1994.
- (179) Advanced Chemistry Development Inc.; 2.51 ed. Toronto, Canada, 1997.
- (180) *High Resolution XPS of Organic Polymers, The Scienta ESC300 Database*; Beamson, G.; Briggs, D., Eds.; John Wiley and Sons Ltd.: New York, 1992.

- (181) *Handbook of X-Ray Photoelectron Spectroscopy, A Reference Book of Standard Data for Use in X-Ray Photoelectron Spectroscopy*; Wagner, C. D.; Riggs, W. M.; Davis, L. E.; Moulder, J. F., Eds.; Perkin-Elmer Corporation, Physical Electronics Division: Eden Prairie, Minnesota, 1979.
- (182) Mehring, M. *Principles of High Resolution NMR in Solids*; 2 ed.; Springer-Verlag: Berlin, 1983.
- (183) Glaser, R. H.; Wilkes, G. L.; Bronnimann, C. E. *J. Non Cryst. Solids* **1989**, *113*, 73.
- (184) Knight, C. T. G.; Kirkpatrick, R. J.; Oldfield, E. *J. Mag. Reson.* **1988**, *78*, 31.
- (185) Marsman, H. C. *Chem. Zeitung* **1973**, *97*, 128.
- (186) Lippert, J. L.; Melponder, S. B.; Kelts, L. W. *J. Non-Crystalline Solids* **1988**, *104*, 139.
- (187) Williams, E. A. In *Annual Reports on NMR Spectroscopy*; Webb, G. A., Ed.; Academic Press: London, 1983; Vol. 15.
- (188) Peace, B. W.; Mayhan, K. G. *Polymer* **1973**, *14*, 420.
- (189) Sacks, M.; Sheu, R. *J. Non-Crystalline Solids* **1987**, *92*, 383.
- (190) Keefer, K. D.; Schaefer, D. W. *Phys. Rev. Lett.* **1986**, *57*, 637.
- (191) Barrett, E. P.; Joyner, L. G.; Halenda, P. P. *J. Amer. Chem Soc.* **1951**, *73*, 373.
- (192) Sharp, K. G.; Michalczyk, M. J. *Mater. Res. Soc. Symp. Proc.* **105**, 435, 105.
- (193) Brown, J. F. J.; Vogt, L. H. *J. Am. Chem. Soc.* **1965**, *87*, 4313.
- (194) Brown, J. F. J. *J. Amer. Chem. Soc.* **1965**, *87*, 4318.
- (195) Feher, F. J. *J. Am. Chem. Soc.* **1986**, *108*, 3850.
- (196) Hasegawa, I.; Motojima, S. *J. Organometallic Chem.* **1992**, *441*, 373.
- (197) Majors, I.; Marsalko, T. M.; Kennedy, J. P. *Polym. Bull.* **1997**, *38*, 15.
- (198) Feher, F. J. In *Silanes, Silicones, and Metal Organics*; 2nd ed.; Arkles, B., Ed.; Gelest Inc.: Tullytown, PA, USA, 1998.
- (199) Lichtenhan, J. D.; Otonari, Y. A.; Carr, M. J. *Macromolecules* **1995**, *28*, 8435.
- (200) Lichtenhan, J. D.; Noel, C. J.; Bolf, A. G.; Ruth, P. N. *Mater. Res. Soc. Symp. Proc.* **1996**, *435*, 3.
- (201) Sellinger, A.; Zhang, C.; Laine, R. M. *Polym. Prepr.* **1995**, *36*, 282.
- (202) Sellinger, A.; Laine, R. M. *Macromolecules* **1996**, *29*, 2327.

- (203) Hasegawa, I. *Mater. Res. Symp. Proc.* **1998**, 519, 3.
- (204) Hoebbel, D.; Wieker, W. *Z Anorg. Allg. Chem.* **1971**, 384, 43.
- (205) Wiebcke, M.; Hoebbel, D. *J. Chem. Soc., Dalton Trans.* **1992**, 2451.

VITA

Chenghong Li

Chenghong Li was born in a middle school teachers' family on September 18, 1964 in Ningxiang, Hunan, the People's Republic of China. He finished his high school in the First Middle School of Ningxiang in 1980. Mr. Li received his B.S. in Chemistry in 1985 from East China Normal University, Shanghai. In the same year, Mr. Li was enrolled in Institute of Ceramics, Chinese Academy of Science and he received his M.S. in Material Science and Engineering in 1988. After graduation, Mr. Li joined the Advanced Materials Research Institute, Wuhan University of Technology, and worked as a research scientist in the area of metal-ceramic composites. In May 1991, Mr. Li joined the Research and Development Group in Donghu Corporation of Advanced Technologies of hybrid materials, Wuhan, and worked as a major research scientist, co-leading the development of several new polymer-related projects. During this period, Mr. Li developed strong interests in macromolecules. In August 1993, he entered Department of Chemistry at Virginia Polytechnic Institute and State University to receive systematic training in polymer sciences. He joined Dr. Judy S. Riffle's group to develop polysiloxane block polymers in the next year and received his second M.S. in Chemistry in 1996. Immediately, Mr. Li joined Dr. Garth L. Wilkes's group and he received his Ph.D. in Chemistry in Aug. 1999.